ULTRASONOGRAPHY FOR THE ASSESSMENT OF CONTRACTILE PROPERTIES OF FRESH AND FATIGUED DIAPHRAGM MUSCLE IN HEALTHY HUMANS

A Thesis Submitted for the Degree of Doctor of Philosophy

By

Camilla Rønn Illidi

Department of Life Sciences, Brunel University London

April 2021

Abstract

Contractile function of the diaphragm is characterised by its ability to shorten, generate force, produce power and perform work. Due to the diaphragm's inaccessibility, these attributes are typically measured as the pressure difference across the diaphragm in response to twitch stimulation of phrenic nerves (i.e., twitch transdiaphragmatic pressure [$\Delta P_{di,tw}$]). This technique, however, provides limited information concerning the muscle's ability to shorten under load and to produce power. The overarching aim of this thesis was to determine whether ultrasound imaging could be used to elucidate the *in vivo* contractile properties of *fresh* and *fatigued* diaphragm muscle in healthy humans. Chapter 4 and 5 evaluated the feasibility, validity and intra-observer reliability of ultrasound-derived measures of crural diaphragm excursion, excursion velocity and power (i.e., kinetics) and costal diaphragm shortening in response to nerve stimulation, sniffs and hypercapnic hyperpnoea. Diaphragm kinetics and shortening exhibited good-to-excellent within-day reliability, with ultrasound acquisition during hyperpnoea unaffected by increasing tidal volume. Chapter 6 compared diaphragm contractile properties during CO_2- vs. exercise-induced hyperpnoea, thereby elucidating the mechanisms that underpin postural-ventilatory modulation of the diaphragm. Compared to CO_2-rebreathe, exercise evoked greater P_{di} (17 ± 9 vs. 20 ± 8 cmH_2O, $p = 0.03$; mean ± *SD*) but less diaphragm excursion (3.4 ± 1.1 vs. 2.5 ± 1.2 cm, $p < 0.001$), despite similar levels of ventilation. Thus, the diaphragm may be constrained during exercise due to quasi-isometric contractions required for modulating postural and ventilatory tasks. Chapter 7 assessed the effect of external loading (pressure and flow) on diaphragm kinetics and force to elucidate the mechanisms that underpin task-dependency of diaphragm fatigue. Pressure-loading, but not flow-loading, elicited a decline in $\Delta P_{di,tw}$ (–13%, $p = 0.013$) and excursion velocity (–39%; $p = 0.043$) with a subsequent decline in diaphragm power (–46%, $p = 0.033$). Chapter 8 was an exploratory study to assess the effect of external loading (pressure and flow) on costal diaphragm thickening. Despite a reduction in $\Delta P_{di,tw}$ (–11 ± 3%) after pressure loading, diaphragm thickening remained well-preserved in response to evoked contractions (fresh: 54 ± 27%; fatigued: 50 ± 33%), sniffs (fresh: 65 ± 25; fatigued: 78 ± 70%) and hypercapnic hyperpnoea (fresh: 130 ± 55%; fatigued: 86 ± 22%). Because measures of diaphragm thickening were highly variable, they may not be adequately sensitive to capture acute changes with fatigue. This body of work supports the use of subcostal ultrasonography in the assessment of *in vivo* diaphragm force-velocity-power relations, and suggests that ultrasound may be a useful tool to explore the effects of training interventions and healthy ageing on dynamic contractile properties of the human diaphragm.

Acknowledgements

The completion of this thesis would not have been possible without the support of Dr. Lee Romer and Dr. Siân MacRae. Lee, although your attention to detail and strive for perfection have undoubtedly made my life hard at times, your diligence, patience and enthusiasm is truly inspiring, and I thank you for patiently guiding me through this process. Siân, in a new and foreign country, I have found solace in knowing that your door was always open whenever I needed support and guidance, and I thank you for making me feel so welcome.

I would also like to express my gratitude to the chief technician of the physiology laboratory at Brunel, Tom Howes. You have revived dead magnetic stimulators, corrected catheter drifts and been a true friend to me – thank you. To Dr. Richard Godfrey, I will forever be grateful for your advice on how 'to survive' a PhD, and I thank you for your constant support and positive encouragements when I found this process to be particularly challenging.

To Hannah and Fabio, with whom I shared office and house for three years: thank you for all the talks, laughs and coffees we shared on and off campus. Hannah, whether we were analysing bloods, moving goldfish across town, or climbing the walls of Harrow, you made our time together at Brunel enjoyable and memorable.

Finally, to my dearest friends and most ardent supporters, Nick and Nina: I'm unable to express the full extent of my gratitude towards you both. You have always been unwavering in your support of me, and I'm so very grateful to have had you with me on this journey. And to my three parents, thank you for showing your support the only way Italian-Danish-Norwegian parents can do; namely through food and creating 'hygge' whenever I needed. Lastly, to my grandfather, Luigi, whose work ethic and diligence inspired me to complete this work to the best of my ability. This thesis is dedicated to you.

List of Contents

List of Figures

List of Tables

List of Abbreviations

AM-mode	Angle-independent, anatomic motion-mode ultrasound
B-mode	Brightness-mode ultrasound
BMI	Body mass index
BTPS	Body temperature and pressure saturated
CMAP	Compound muscle action potential
CV	Coefficient of variation
EELV	End-expiratory lung volume
EEPga	End-expiratory gastric pressure
EEPoe	End-expiratory oesophageal pressure
EILV	End-inspiratory lung volume
EMG_{di}	Diaphragm electromyogram
F_ECO_2	Fractional concentration of carbon dioxide in expired gas
FEV_1	Forced expiratory volume in 1 second
F_EO_2	Fractional concentration of oxygen in expired gas
FPS	Frames per second
f_R	Respiratory frequency
FRC_{pleth}	Functional residual capacity by whole-body plethysmography
FVC	Forced vital capacity
HFF	High-frequency fatigue
IC	Inspiratory capacity
IRL	Inspiratory resistive loading
ISI	Inter-stimulus interval
LFF	Low-frequency fatigue
M-mode	Conventional motion-mode ultrasound
MEP	Maximum expiratory mouth pressure
MIP	Maximum inspiratory mouth pressure
MVV_{12}	Maximal voluntary ventilation over 12 seconds
η_p^2	Partial eta squared
$\int P_{di}$	Time integral of transdiaphragmatic pressure
P_{di}	Transdiaphragmatic pressure
$\bar{P}_{di}$	Mean inspiratory transdiaphragmatic pressure

$\bar{P}_{di,a}$	Active component of mean inspiratory transdiaphragmatic pressure
$P_{di,max}$	Maximum transdiaphragmatic pressure
$\Delta P_{di,sn}$	Sniff transdiaphragmatic pressure
$\Delta P_{di,tw}$	Twitch transdiaphragmatic pressure
$P_{ET}CO_2$	End-tidal partial pressure of carbon dioxide
P_{ga}	Gastric pressure
$\bar{P}_{ga}$	Mean inspiratory gastric pressure
$\bar{P}_{ga,a}$	Active component of mean inspiratory gastric pressure
$\Delta P_{ga,sn}$	Sniff gastric pressure
$\Delta P_{ga,tw}$	Twitch gastric pressure
P_{mo}	Mouth pressure
P_{oe}	Oesophageal pressure
$\bar{P}_{oe}$	Mean inspiratory oesophageal pressure
$\bar{P}_{oe,a}$	Active component of mean inspiratory oesophageal pressure
$\Delta P_{oe,sn}$	Sniff oesophageal pressure
$\Delta P_{oe,tw}$	Twitch oesophageal pressure
PTI_{di}	Transdiaphragmatic pressure-time index
ρ	Spearman's rank correlation coefficient (rho)
RER	Respiratory exchange ratio
RPE	Ratings of perceived exertion
RV	Residual volume
SD	Standard deviation
SpO_2	Peripheral oxygen saturation
T_I	Inspiratory time
T_{TOT}	Total breath time
TLC	Total lung capacity
$\dot{V}_I$	Inspired minute ventilation
VIH	Voluntary isocapnic hyperpnoea
$\dot{V}O_2$	Oxygen uptake
V_{TI}	Inspiratory tidal volume
V_{TI}/T_I	Mean inspiratory flow

Chapter 1

Thesis Introduction

The diaphragm is the primary muscle of inspiration (Grimby et al., 1976). As with other striated skeletal muscles, its role is to shorten, generate force, produce power and perform work. Clinically, an inability of the diaphragm muscle to generate power and perform work has been suggested to occur with exercise-induced fatigue in healthy humans (Johnson et al., 1993). Force development across the diaphragm is assessed objectively by measuring the difference between the gastric and oesophageal pressures induced by electrical or magnetic stimulation of the phrenic nerves as (quasi-)isometric twitch transdiaphragmatic pressure ($\Delta P_{di,tw}$) (Mills et al., 1996). Application of these nerve stimulation techniques has shown a decrement in $\Delta P_{di,tw}$ in response to various conditions, including inspiratory resistive loading (IRL), voluntary increases in ventilation (hyperpnoea) and dynamic whole-body exercise (Romer & Polkey, 2008). A major limitation of this technique, however, is that isometric twitch force is a relatively poor index of *in vivo* diaphragm function, providing no information concerning the muscle's ability to shorten and generate power. Because previous research has focused on understanding force development of the fresh and fatigued diaphragm, the muscle's ability to shorten and produce power has been invariably ignored (Gibson et al., 2002). For this reason, little is known about the dynamic, contractile properties of the human diaphragm, and how these properties may be impaired with fatigue. Accordingly, the overarching aim of this thesis was to evaluate the usefulness of ultrasonography for the assessment of *in vivo* contractile properties of fresh and fatigued diaphragm in healthy humans.

Ultrasonography was first developed in the late 1940s, and the imaging tool has since been referred to as the most 'elegant diagnostic approach in clinical medicine' (European Respiratory Society, 2018, p. 4). In recent decades, ultrasonography has become an important method in the biomechanical sciences for assessing skeletal muscle contractile properties, and has provided information to form our current understanding of muscle-tendon properties and the influence of architectural attributes, such as muscle thickness, stiffness and fascicle length, on force development (Hodges et al., 2003). In addition, ultrasonography has been used to better understand how these architectural attributes may change with fatigue, disuse atrophy and systematic training interventions (Pillen, 2010). Diaphragm ultrasonography specifically, is an established tool in the intensive care unit (ICU). Here, in patients undergoing mechanical ventilation, ultrasound is used to monitor atrophy- and weakness-related changes in costal

diaphragm thickness and thickening, and crural diaphragm kinetics (i.e., craniocaudal excursion and excursion velocity) that may contribute to weaning failure, respiratory distress and potential reintubation (Goligher et al., 2018).

Despite the abovementioned applications, diaphragm ultrasonography is still an undervalued tool in the study of respiratory mechanics (e.g., shortening, contractile velocity and power) in healthy humans. Diaphragm force-velocity-power relations have been thoroughly described *in vitro* and *in situ* (e.g., Coirault et al., 1995, 1997), but have yet to be quantified for the *in vivo* human diaphragm. Like other striated skeletal muscles, the fatigued diaphragm is likely to exhibit decrements in force (e.g., $\Delta P_{di,tw}$) *and* shortening velocity; both of which are expected to compromise the muscle's ability to produce power and perform work. To date, however, this postulate has primarily been derived from *in vitro* preparations (e.g., Ameredes et al., 2006; Coirault et al., 1995; Mardini & McCarter, 1987). In this thesis, ultrasound is proposed as a means of directly quantifying diaphragm contractile properties in the fresh and fatigued state.

To evaluate the usefulness of ultrasonography for the assessment of *in vivo* contractile properties of fresh and fatigued human diaphragm, five experimental studies were performed with the following aims: *i*) to determine the feasibility, validity, and within-day reliability of ultrasound-derived measures of diaphragm kinetics and thickening (shortening) in response to stimulation-evoked twitch contractions, maximal sniffs and hypercapnic hyperpnoea (Chapters 4 and 5); *ii*) to evaluate the feasibility of ultrasonography for the assessment of diaphragm kinetics during exercise-induced hyperpnoea, and to compare diaphragm kinetics across non-exercise-induced and exercise-induced hyperpnoea to elucidate the mechanisms that underpin postural-ventilatory modulation of the diaphragm (Chapter 6); and *iii*) to assess the effect of external loading on diaphragm kinetics and thickening to elucidate the mechanisms that underpin task-dependency of diaphragm fatigue (Chapters 7 and 8).

The following section is a literature review that contains the background theory and rationale for the thesis, followed by a detailed outline of the thesis aims. Thereafter, a thorough description of the apparatus and procedures used in the five experimental chapters is presented. The thesis concludes with a general discussion that outlines the implications of the findings and explores the future of respiratory muscle imaging.

Chapter 2

Literature Review

2.1 Introduction

The aim of this literature review is to provide the background theory and rationale for the five experimental chapters presented in this thesis. The first section provides a general overview of the human diaphragm muscle, including its anatomical characteristics and functional roles. The main body of the literature review will then discuss the contractile properties of *fresh* and *fatigued* diaphragm muscle. To contextualise the physiologic and mechanistic features of the human diaphragm, each section will initially provide a generic overview of the physiologic principles discussed (e.g., force-velocity relationship) before discussing how this principle pertains to the human diaphragm specifically. Finally, the review will discuss the literature related to the use of ultrasonography for the assessment of skeletal muscle contractile properties, with specific emphasis on how ultrasound may offer novel insight into the contractile properties of the fresh and fatigued diaphragm muscle in healthy adults.

2.2 The diaphragm muscle

Anatomically, the *in vivo* mammalian diaphragm muscle can be seen as two large, dome-shaped membranes – or muscle sheets – originating from a non-contractile central tendon between the pleural and abdominal cavity. From the central tendon, which encircles the oesophageal and caval hiatus, muscle fibres project peripherally in two main directions: *i)* to the xiphoid process and the anterior part of the 7-12th ribs (costal diaphragm); and *ii)* to lumbar vertebrae 1-3 (L1-3) posteriorly (crural diaphragm) (De Troyer & Boriek, 2011). Upon contraction, the crural diaphragm descends and flattens, whereas the costal diaphragm acts with insertional and appositional forces that rotate and lift the lower five ribs outward. As a result of diaphragm contraction, intraabdominal increases and causes the ribcage to expand. As per Boyle's law, expansion of the pleural cavity causes a decrease in pleural pressure, which, in turn, drives inspiratory airflow (De Troyer & Boriek, 2011).

Beyond its role in ventilating the lungs, the diaphragm serves a number of non-respiratory roles. For instance, the increased intraabdominal pressure generated upon crural diaphragm descent stabilises the lumbar spine and torso and positions the spinal segments in a biomechanically neutral position (Hodges et al., 1997, 2005). Thus, the diaphragm serves as an internal abdominal binder that optimises the lumbar spine under load such as heavy lifting (Hemborg et al., 1985; Panjabi et al., 1989). In other instances, like vomiting, both costal and crural diaphragm contract phasically alongside the abdominal muscles and external and internal intercostals during the retching phase, before culminating in expulsion (Miller, 1990).

Interestingly, in order to eject gastric content through the oesophageal hiatus during vomiting, the crural diaphragm must relax while costal diaphragm, abdominal muscles and external intercostals contract forcefully during the expulsion (Miller et al., 1988; Miller, 1990). Electromyogram (EMG) studies of diaphragm have also revealed activation and subsequent changes in intrathoracic and intraabdominal pressure before and during rapid arm movements, suggesting that the diaphragm also plays a role in anticipatory postural adjustments (Hodges & Gandevia, 2000b).

Despite the complex anatomical structure and functional roles of the diaphragm, the muscle is a regular skeletal muscle, composed of striated muscle fibres and innervated by the phrenic nerves that originate from the phrenic motor nucleus in the cervical spinal cord (Seeley et al., 2011). Accordingly, diaphragm contraction is elicited by the excitation-contraction coupling as described for limb locomotor muscles, encompassing the propagation of actional potentials along the sarcolemma, signal transmission to the sarcoplasmic reticulum and calcium (Ca^{2+}) binding to the contractile apparatus. Moreover, diaphragm contractile function is characterised mechanically by the ability to shorten, generate force and power, and perform physiological work (Green et al., 2002). There are, however, two unique aspects about the human diaphragm: first, diaphragm force cannot be measured directly at the level of the muscle, and must instead be estimated as transdiaphragmatic pressure (P_{di}); that is, the pressure difference across the pleural and abdominal cavities. Because the diaphragm is the only muscle that simultaneously lowers pleural pressure while also increasing abdominal pressure, contraction of the diaphragm results in an increase in P_{di}. Second, diaphragm neural control originates from two distinct, but finely-coordinated neural pathways: the *automatic* and rhythmic neural activation from the medullary respiratory centres during spontaneous breathing, and the *voluntary* activation via corticospinal pathways of the motor cortex (Butler, 2007). Neural drive from the two pathways must be finely coordinated to meet the current demand, be it ventilatory, postural, physiological (e.g., vomiting) and/or behavioural (e.g., eating, swallowing, speaking, or laughing).

2.2.1 Defining the contractile properties of skeletal muscle

At the cellular level, the contractile properties of a muscle fibre comprise the cross-bridge cycling of contractile proteins (i.e., actin and myosin myofilaments), the rate of cross-bridge cycling and the hydrolysis of adenosine triphosphate (ATP) for fibre shortening and generation of force (Fitts et al., 1991). These physiologic mechanisms are also called *muscle contractility* (Clausen, 2003). For the human diaphragm muscle *in vivo*, contractility has often been used to describe the muscle's ability to generate force, or pressure, in response to stimulation-evoked

contractions (Laghi et al., 1998; Similowski et al., 1989; Wragg et al., 1994). However, this use of the term does not consider the extent to which the force (pressure) is generated with active fibre shortening, or the rate at which fibre shortening occurs. In this thesis, therefore, the term muscle *contractility* will be used when referring to the cellular mechanisms of a muscle contraction, as defined by Fitts et al. (1991) and Clausen (2003). For the *in vivo* human diaphragm, the term *contractile properties* will be used to describe "the relationships between fibre length, velocity of shortening, force development, and time" (Finucane & Singh, 2009, p. 1392), thereby encompassing the muscle's ability to shorten under load while generating force.

2.3 Contractile properties of *fresh* skeletal muscle

Skeletal muscle function is characterised mechanically as the ability to generate force, shorten, produce power and perform work. These mechanical characteristics are determined by the structural organisation, substrate utilisation, and metabolic environment of individual muscle fibres. The first part of this literature review will discuss the determinants of the contractile properties of *fresh* skeletal muscle generally, and later how these determinants are reflected in the human diaphragm *in vivo*.

2.3.2 Cross-bridge interaction and muscle morphology

The sarcomere and cross-bridge interaction

H. Huxley and J. Hanson in 1954 (Huxley & Hanson, 1954) acquired the first definite images showing that the muscle comprised an interdigitating array of myosin and actin filaments that slid relative to each other during a contraction. Also in 1954, Sir A. Huxley and R. Niedergerker showed similar results (Huxley & Niedergerke, 1954), referring to the phenomenon as *the sliding filament theory*. Specifically, the myosin (thick) filament comprises two myosin heavy chains (MHC) and four myosin light chains (two regulatory, two alkali; MLC). The MHC contain the myosin head that interact with the actin filament, and also contain the enzyme adenosine-triphosphatase (ATPase) for ATP hydrolysis that provides the energy necessary for muscle contraction (Calderón et al., 2014). The actin (thin) filament contains two regulatory proteins, troponin and tropomyosin, which are intertwined with the actin filament and occupy the myosin binding sites on the actin filament. It is only when intracellular Ca^{2+} is released from sarcoplasmic reticulum, secondary to depolarisation of the muscle fibre membrane, that tropomyosin exposes the actin binding sites for the myosin heads to bind (Seeley et al., 2011). In the presence of ATP, the myosin heads will attach and release from binding sites on the actin filament (cross-bridge cycling), allowing the fibre to shorten. The rate of cross-bridge cycling

is primarily determined by the rate at which myosin ATPase can hydrolyse ATP during the contraction, which, in turn, is determined by the MHC isoform expressed by the specific muscle fibre (Pette & Staron, 2000). As discussed in detail below, muscle fibres are, therefore, classified according to the ATPase activity and MHC isoforms content.

Morphology of skeletal muscle

The fundamental, contractile properties of skeletal muscles are defined by the fibre type composition (morphology) of muscle fascicles (Fitts et al., 1991). Fibre types vary in size, their contractile properties (i.e., ability to generate force and the rate at which force can be generated) and their substrate utilisation. Muscle fibre types can therefore be described using histochemical, biochemical, morphological, or physiologic characteristics, using several classification systems. In this literature review, classification of fibre types will be defined by myosin ATPase histochemical staining and identification of MHC isoforms.

Originally, muscle fibre types were defined as either type I or type IIA and IIB fibres based on their myosin ATPase activity (e.g., Mizuno, 1991; Mizuno & Secher, 1989a). However, recent advances in staining techniques have identified four additional fibre types in human skeletal muscles: IC, IIC, IIAC, and IIAB (Scott et al., 2001). Fibres are classified solely on the intensity and characteristics of the histochemical staining (not the hydrolysis rates of ATPase), and the order from slowest to fastest staining are: fibre types I, IC, IIC, IIAC, IIA, IIAB, IIB (Scott et al., 2001). It is worth noting that because this classification based on the qualitative characterisation of histochemical staining at different pH levels, different researchers may classify fibre types differently than above. As an example, depending on histochemical analysis previously utilised, some classify fibre types in type I, IIA, IIB and IIC (Larsson et al., 1978), while others have used the original three fibre types (i.e., type I, IIA and IIB) (Mizuno, 1991; Mizuno & Secher, 1989b).

Muscle fibres may also be classified by their distribution of MHC isoforms (Scott et al., 2001). In fact, the MHC isoform classification corresponds well with the ATPase activity (above), simply because the MHC is the molecular structure that hold the site that serves as the ATPase (Seeley et al., 2011). Although the human genome contains the genes for 10 different MHC isoforms, there are only three types of MHC isoforms expressed in human skeletal muscles: MHC-I, MHC-IIa and MHC-IIx (Canepari et al., 2010). These three isoforms correspond with ATPase staining types I, IIA and IIB, respectively (Table 2.3.1) (Scott et al., 2001). It is worth noting that, although all mammals carry the gene for the myosin isoform MHC-IIb, the isoform is only expressed in smaller mammals, and not in humans (Canepari et al., 2010). The third

classification of muscle fibre types refer to slow- and fast-twitch fibres based to their enzymatic activity and metabolic pathways (Zierath & Hawley, 2004), and is included in Table 2.3.1 for contextualisation.

Table 2.3.1 Skeletal muscle fibre type classification: histochemical ATPase staining, identification of MHC isoforms and biochemical identification of enzymatic activity of metabolites.

Histochemical ATPase staining	Myosin heavy chain identification	Biochemical and enzymatic activity
I	MHC-I	Slow-twitch, oxidative
IC		
IIC		
IIAC		
IIA	MHC-IIa	Fast-twitch, oxidative
IIAB		
IIB	MHC-IIx	Fast-twitch, glycolytic

Adapted from "Human skeletal muscle fibre type classifications", by W. Scott et al., 2001, *Physical Therapy*, 81(11), p.1810-1816.

The rate and efficiency of ATPase activity and distribution of MHC isoforms determine the rate of ATP hydrolysis, and therefore also the rate of fibre shortening (Fitts et al., 1991). Specifically, MHC-I isoforms in type I fibres contain a form of ATPase that breaks down ATP slowly, consequently driving a slow cross-bridge cycle. Conversely, MHC-IIa or IIx isoforms in type IIA and IIB fibres contain faster, more efficient forms of ATPase that drive rapid cross-bridge cycling (Pette & Staron, 2000). Thus, there are significant differences in the contractile properties of the various muscle fibre types. As an example, the time to peak tension in type IIA and IIB fibres is half the time measured in slower type I fibres (Zierath & Hawley, 2004). Similarly, maximal shortening velocity is five- to six times faster in type IIB fibres compared to type I fibres (Fitts et al., 1991).

Muscle fibre types also differ in the maximum force they can generate. For instance, the *peak force* of a muscle fibre is strongly dependent on fibre diameter to allow for more cross-bridges to be organised in parallel (Fitts et al., 1991). Generally, type IIB muscle fibres have greater diameter and greater cross-sectional area compared to type I and IIA fibres (Mizuno, 1991; Zierath & Hawley, 2004), which suggests that muscles with a dominant distribution of type IIB

fibres contain more cross-bridges organised in parallel, and can ultimately generate higher maximum force compared to muscles with lower proportion of type IIB fibres. It is also worth noting that sensitivity for Ca^{2+} differs between fibre types. For instance, type I fibres have a markedly lower activation threshold for free Ca^{2+} to bind to tropomyosin compared to type IIA and IIB fibres (Fitts et al., 1991). This means that type I fibres contract more readily when exposed to free Ca^{2+}, albeit with slower velocity and less force than type II fibres.

Morphology of the human diaphragm

In human skeletal muscle, fibre composition is remarkably heterogeneous. For instance, there are intra- and inter-muscle variability as well as inter-individual variability (Zierath & Hawley, 2004). Moreover, muscle fibres are plastic, meaning that metabolic and mechanical stimuli can convert MHC isoforms in fast-to-slow or slow-to-fast conversions, and thereby produce hybrid muscle fibres (e.g., type I-IIA and type II-AX) as a way of adapting to physiologic and pathologic conditions (Canepari et al., 2010; Pette & Staron, 2000).

Our current understanding of human diaphragm morphology is shaped by the findings from animal studies *in vitro* (Ameredes et al., 2006; Coirault et al., 1995, 1997; Mardini & McCarter, 1987) or – at best – from human autopsy studies (Meznaric & Cvetko, 2016; Mizuno, 1991; Mizuno & Secher, 1989b). In a post-mortem study of human costal diaphragm preparations, Mizuno & Secher (1989b) reported a fibre type distribution of 49% type I, 28% type IIA and 23% type IIB, which is similar to that reported by others (Sánchez et al., 1985). One report has also suggested that the diaphragm contains a small percentage of hybrid fibres ($2.6 \pm 0.8\%$); that is, fibres with both MHC-I and MHC-IIa isoforms (Meznaric & Cvetko, 2016). This report also compared the morphology of the left and right hemi-diaphragms, but no difference was observed between the two sides ($51.3 \pm 2.9\%$ *vs*. $49.3 \pm 1.3\%$; $p > 0.05$). Similarly, there appears to be no difference in fibre type distribution between costal and crural diaphragm in humans (Sánchez et al., 1985). Thus, the almost equal distribution of type I and type II fibres in the human diaphragm clearly reflects the muscle's functional role: to contract continuously and rhythmically during an entire lifespan, but also rapidly and forcefully when necessary.

2.3.3 Force-frequency relationship of skeletal muscle

The contraction of a muscle fibre must be evoked by an electrical potential that has the intensity to depolarise the muscle fibre membrane, and thereby initiate cross-bridge cycling as described above. These rapid electrical events, from depolarisation to initiation of contraction, are referred to as *excitation-contraction coupling* (Sandow, 1952). The electrical potential starts as a

'graded' potential, and it is only when the electrical charge reaches a certain threshold (–55 mV) that it becomes an action potential that will depolarise the membrane surface via the transverse tubular (t-) system (Seeley et al., 2011). Specifically, upon depolarisation, voltage-gated sodium (Na^+) channels in the fibre membrane open. This results in a rapid influx of Na^+ to the sarcoplasm, which quickly makes the intra-cellular environment positive from resting membrane potential (typically –70 to –90 mV) to +20-30 mV (Clausen, 2003). Depolarisation of the fibre membrane is, however, quickly counteracted by the closing of voltage-gated Na^+ channels, abruptly causing the influx to stop. Voltage-gated potassium (K^+) channels in the fibre membrane then open, and K^+ diffuses down the concentration gradient out of the sarcoplasm, ultimately returning the membrane to its resting potential (Clausen, 2003). The effect of strenuous muscle activity on the Na^+-K^+-pump is discussed further in section 2.4.10 in this Literature Review.

Action potentials are generated as equally-sized impulses, or bursts, of electrical potential. Thus, the only way to increase the neural input to a muscle is by increasing the frequency with which action potentials are generated and transmitted (Seeley et al., 2011). The higher the action potential frequency, the stronger the excitatory drive to the muscle fibre membrane, and the higher the force output (MacIntosh & Willis, 2000). The relationship between stimulation frequency (i.e., from action potential or peripheral nerve stimulation) and force output is therefore referred to as the *force-frequency relationship* (Cooper & Eccles, 1930).

The force-frequency relationship is also strongly related to the *force-pCa^{2+} relationship*: when the stimulation frequency is low, the prolonged inter-stimulus interval allows for a rapid release and reuptake of Ca^{2+} by sarcoplasmic reticulum in-between each stimulus. This results in an immediate drop in force before a new stimulus is imposed (MacIntosh & Willis, 2000). Conversely, when the stimulation frequency increases, the inter-stimulus interval becomes shorter than the time needed for reuptake of free Ca^{2+} into sarcoplasmic reticulum, causing free Ca^{2+} to accumulate in the myoplasm and the force to increase. Figure 2.3.1 illustrates the effect stimulation frequencies of 5 Hz (panel *A*) and 20-80 Hz (panel *B*) on muscle force. In panel *A),* the long inter-stimulus interval allows free Ca^{2+} to return only partially to sarcoplasmic reticulum before a new stimulus is imposed, which, in turn, results in a summation of force. In panel *B,* five repeated stimulations of increasing frequency (20-80 Hz) result in various force responses.

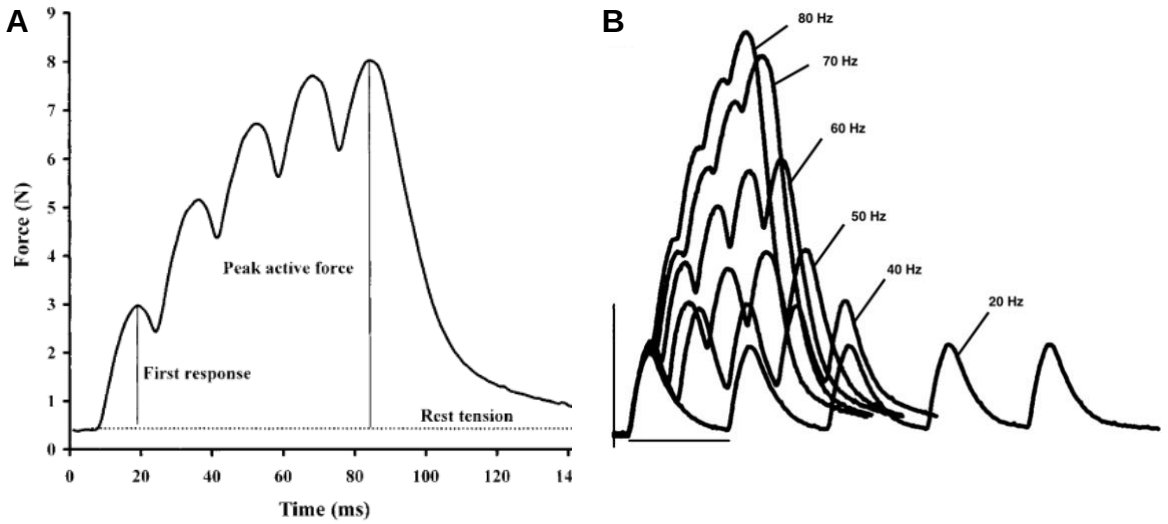

Figure 2.3.1 Muscle force-frequency relationship. *A*) incompletely fused contraction in response to 5 Hz stimulation over 100 ms. *B*) incompletely fused contractions by five repetitive stimuli of 20- 80 Hz. *X*-axis represents time (ms) and *y*-axis represents force (N) in both panels. Adapted from "Force-frequency relationship and potentiation in mammalian skeletal muscle", by B. MacIntosh & J. Willis, 2000, *Journal of Applied Physiology*, 88(6), p. 2088-96.

It has been estimated that type I muscle fibres require a stimulus frequency of ~100 Hz to reach a completely fused, tetanic contraction, whereas type II fibres require stimuli frequency of ~200 Hz (Fitts et al., 1991). It is worth noting, however, that firing frequencies of this rate are rare under physiologic conditions, and that stimulus frequencies of 40 and 80 Hz are normally adequate to develop near-maximum force in type I and II fibres, respectively (Fogarty et al., 2018).

Force-frequency relationship of in vivo human diaphragm: discharge frequencies of single motor neurons

As stated above, neural activation of muscle is only possible if the graded potential reaches threshold, by which the fibre membrane is depolarised. One of the few ways to increase the force output is therefore to increase the frequency of stimulation. At the level of the motor unit, this stimulus frequency is referred to as discharge frequency, and is typically assessed using intra-muscular EMG electrodes (Butler, 2007; Butler & Gandevia, 2008). Studies of discharge frequency in human inspiratory muscles demonstrate a heterogeneous pattern that is strongly influenced by ventilatory drive, breathing pattern and chemical stimuli to breathe (Fogarty et al., 2018). During quiet breathing, discharge frequency measured in the human diaphragm range from ≤5 Hz to 30 Hz (mean ~11-12 Hz) (Butler, 2007; Butler et al., 2001). Under hypoxic and hypercapnic stimuli, discharge rates are generally higher (30-50 Hz) due to the increased

ventilatory drive to breathe (Seven et al., 2014). Deep breathing and expulsive manoeuvres, such as coughing and sneezing, elicit discharge rates of 30-80 Hz (Fogarty et al., 2018). Combined, studies demonstrate that the human diaphragm exhibits the same force-frequency relationship as seen isolated preparations *in vitro* and *in situ*.

Force-frequency relationship in response to motor nerve stimulation

The classical force-frequency relationship seen isolated muscle preparations is analogous to *the pressure-frequency relationship* seen for the human diaphragm *in vivo*. The pressure-frequency relationship of human diaphragm was duly demonstrated by Aubier et al. (1981) by electrically stimulating the right phrenic nerve at 10, 20, 50 and 100 Hz. In line with the classical force-frequency relationship, the authors showed that $\Delta P_{di,tw}$ increased as a function of stimulation frequency: by ∼38% from 10 to 20 Hz; by ∼20% from 20 to 50 Hz; and then only negligibly (∼2%) from 50 to 100 Hz (Figure 2.3.2), which is similar to that reported by others (Farkas & Rochester, 1988; Moxham et al., 1981).

Some discussion is warranted regarding the stimulation frequency required for a completely fused (tetanic) contractions of the diaphragm. An interesting point was made by Bellemare & Poirier (2005), who reasoned that, despite a partial fusion between successive stimuli starting at 7-8 Hz, a complete fusion of successive stimuli occurs at stimulation frequencies of 50-100 Hz in the human diaphragm. Like limb locomotor muscles, the force-frequency relationship of the diaphragm appears to be similar to other skeletal muscles with mixed fibre type composition, such as quadriceps and sternocleidomastoids (Moxham et al., 1981). Our current understanding of the pressure-frequency relationship of the diaphragm has also been applied to the distinction between high- and low-frequency fatigue, which will be discussed in detail in section 2.4.10. The pressure-frequency relationship, and the effect of increasing stimulation frequency on ultrasound-derived diaphragm kinetics will be the focus in Chapter 4 (*Part 1*).

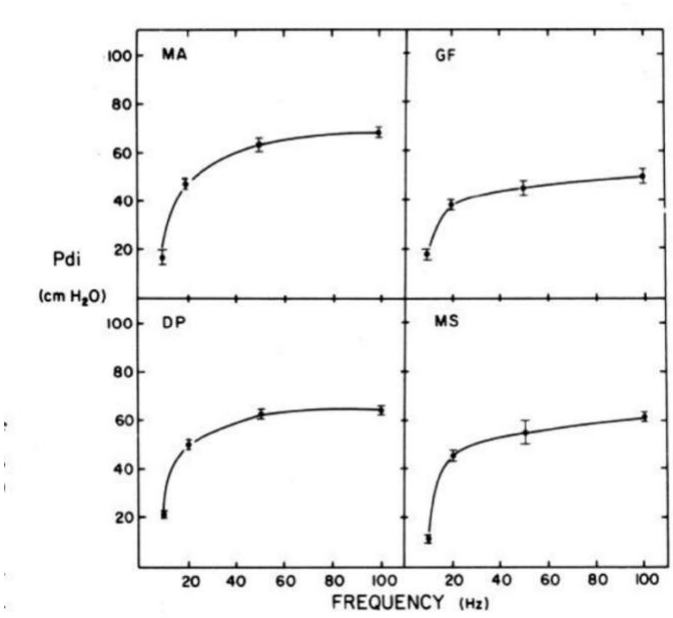

Figure 2.3.2 Force-frequency relationship of human diaphragm in four subjects. From "Detection of diaphragmatic fatigue in man by phrenic stimulation", by M. Aubier et al., 1981, *Journal of Applied Physiology*, 50(3) p. 538-544.

2.3.4 Length-tension relationship of skeletal muscle

In line with the sliding filament theory (Huxley & Niedergerke, 1954; Huxley & Hanson, 1954), the ability of a cross-bridge interaction to generate force is determined by the degree of overlap between actin and myosin myofilaments. The *length-tension relationship* states that all muscle fibres have a length at which there is an optimal overlap between actin and myosin myofilaments (L_O), and at which point maximum (isometric) tension can be generated (Gordon et al., 1966). At fibre lengths below L_O, the myosin filaments will touch the Z-disks; that is, the network of filamentous protein holding the structure of the contractile apparatus, and thereby limit further shortening of the fibre. At fibre lengths exceeding L_O, there is little overlap between the two filaments, resulting in fewer cross-bridges formed (Seeley et al., 2011). Accordingly, the tension generated falls significantly at fibre lengths below or exceeding L_O.

Length-tension relationship of human diaphragm in vivo

The length-tension relationship of mammalian diaphragm fibres in isolated preparations is shown in Figure **2.3.3**. The figure demonstrates that, in isolated preparations, the mammalian diaphragm exhibits similar length-tension relations as seen in other striated skeletal muscles (McCully & Faulkner, 1983). For the human diaphragm *in vivo*, however, the classical length-tension relationship is analogous to the *volume-pressure relationship*. Specifically, the pressure-volume relationship is based on the assumption that any change in lung volume during

inspiration is elicited by the shortening of inspiratory muscle fibres (Braun et al., 1982). Further, the isometric force (pressure) generated at a given lung volume is determined by the muscle fibre length at which force (pressure) is generated, as per the classical length-tension relationship (D'Angelo & Milic-Emili, 2005).

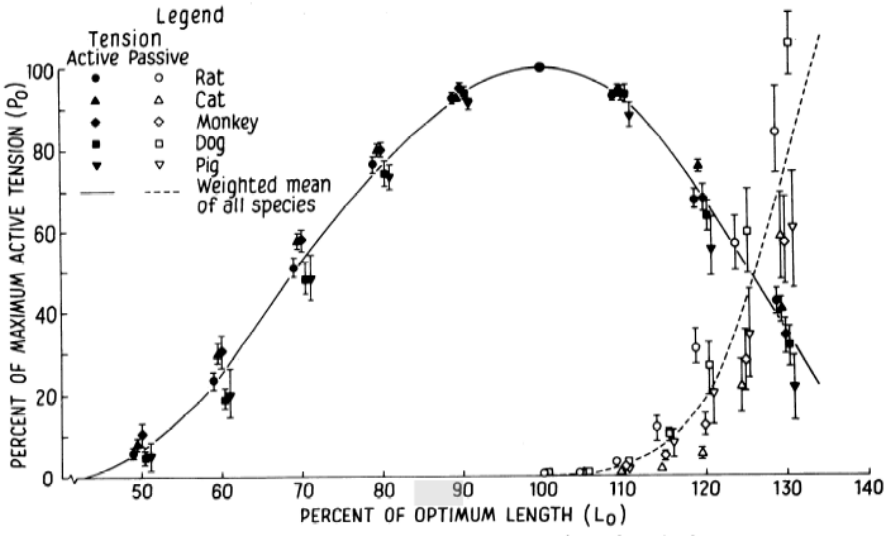

Figure 2.3.3 Length-tension relationship of isolated diaphragm fibres from five mammalian species (solid line and closed symbols). Isometric, active tension was generated with tetanic stimulation at fibre lengths ranging from 50 to 130% of optimum length (L_O). Broken line and open symbols represent passive tension generated at fibre lengths $\geq L_O$. From "Length-tension relationship of mammalian diaphragm muscles", by K. McCully & J. Faulkner, 1983, *Journal of Applied Physiology*, 54(6), p.1681-1686.

The pressure-volume relationship of human respiratory muscles (inspiratory and expiratory) were first demonstrated by Agostoni & Rahn (1960), who showed that maximal inspiratory pressures decreased with increasing lung volume. Conversely, maximal expiratory pressures increased with increasing lung volume. Combined, these results were the first characterisation of the length-tension relationship for all the respiratory muscles working simultaneously. Moreover, the results demonstrated that L_O of inspiratory and expiratory respiratory muscles were at, or around, the lowest and highest lung volumes, respectively. These observations lead the authors to conclude that the respiratory muscle pressure-volume relationships were indeed analogous to the length-tension relationship as seen isolated preparations. Some discussion is, however, warranted regarding the limitations of the study by Agostoni & Rahn (1960), because the authors did not have the means to measure inspiratory muscle fibre length. Instead, the

experimental study design was based purely on the theoretical assumption that any change in lung volume during inspiration was elicited by the shortening of inspiratory muscle fibres.

To circumvent this methodological limitation, Braun, Arora & Rochester (1982) used chest x-ray (roentgenogram) to estimate human diaphragm fibre length while participants held four lung volumes (TLC, FRC + ½ IC, FRC, and RV), and generated maximum (static) inspiratory pressures (MIP and $P_{di,}$) at each of the four lung volumes. Expectedly, both MIP and P_{di} were inversely related to lung volume, with the highest inspiratory pressures generated at RV (mean ± *SD* MIP: –112 ± 25 cmH_2O; P_{di} 121 ± 20 cmH_2O) and FRC (MIP: –91 ± 21 cmH_2O; P_{di}: 114 ± 19 cmH_2O), and the lowest inspiratory pressures generated at TLC (MIP: –8 ± 7 cmH_2O; P_{di}: 35 ± 15 cmH_2O). In addition to measuring lung volumes, the authors were able to use the x-ray films to estimate the fibre lengths at which these inspiratory efforts were performed (Braun et al., 1982). A limitation of this study was, however, that inspiratory pressures were generated using volitional manoeuvres. Accordingly, the findings by Braun et al. (1982) were later expanded by Hubmayr et al. (1989), who electrically stimulated phrenic nerves at various lung volumes from FRC to TLC. As shown in Figure 2.3.4, the authors demonstrated that $\Delta P_{di,tw}$ was inversely related to lung volume, declining by ~8 cmH_2O per litre above FRC. Collectively, these studies have demonstrated the influence of lung volume (i.e., fibre length) on static force output of inspiratory muscles generally, but also of the diaphragm muscle specifically. Moreover, these studies underline the importance of monitoring lung volume when quantifying respiratory pressures, particularly when performing maximal manoeuvres (e.g., maximal sniffs) and stimulation-evoked contractions.

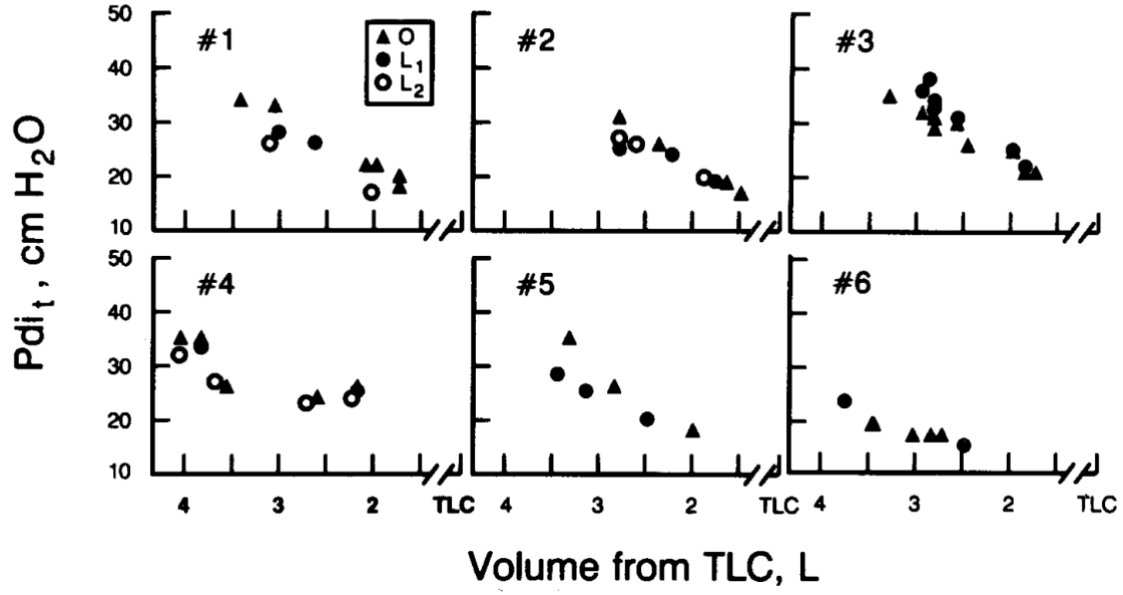

Figure 2.3.4 Volume-pressure relationship of the human diaphragm *in vivo*, as demonstrated by the linear relationship between pressure ($\Delta P_{di,tw}$; here: $P_{di,t}$) and lung volume from TLC. Open and closed, circled and triangled show various external loads applied to the rib cage during stimulation, although these did not affect the volume-pressure relationship. From "Transdiaphragmatic Twitch Pressure: Effects of Lung Volume and Chest Wall Shape", by R. Hubmayr et al., 1989, *American Review of Respiratory Disease*, 139(3), p.647-652.

2.3.5 Force-velocity relationship of skeletal muscle

The force output of a contraction is not only determined by the degree of overlap between myofilaments (length-tension relationship), but also the rate of fibre shortening. After the initial work of Hill (1938) and Fenn & Marsh (1935), it was established that there is a hyperbolic relationship between force and velocity of fibre shortening in concentric contractions. The force-velocity relationship is also the basis of skeletal muscle power; that is, the dot product of force and shortening velocity (power = force × velocity), which forms a parabolic relationship relative to force and shortening velocity. The force-velocity relationship, and the concavity of the parabolic power curve, differ between muscle fibre types (Jones, 2010). Moreover, force-velocity-power relations appear vastly different depending on whether fibres are studied in isolated preparations *in vitro*, in dissected preparations *in situ*, or for the whole muscle *in vivo* (Alcazar et al., 2019). Generally, however, peak power of skeletal muscles is usually found around 25-30% of maximum force and ~50% of maximum shortening velocity (Fitts et al., 1991).

Physiologically, shortening velocity is determined by the rate of ATP hydrolysis, and the rate at which ADP can be dissociated from the myosin head during the 'power stroke' in the cross-bridge cycle (Fitts, 2008). Because type IIA and IIB fibres predominantly contain MHC isoforms with fast ATPase activity (MHC-IIa and IIx), these fibre types shorten faster and exhibit greater peak force compared to type I fibres (Zierath & Hawley, 2004). In turn, type IIA and IIB fibres produce greater power compared to type I fibres. The force-velocity relationship of the intact muscle is, therefore, determined by the specific fibre type composition (morphology) of each muscle.

Force-velocity relationship of human diaphragm in vivo

The classical force-velocity-power relationship described *in vitro* and *in situ*, has traditionally been depicted as analogous to the *pressure-flow relationship* for the *in vivo* human diaphragm. The close relationship between flow and shortening velocity has been assumed on the basis that inspiratory muscles must shorten a rate proportional to inspiratory flow (Fitting et al., 1985). Indeed, the pressure-flow relationship of human diaphragm was first documented in the early studies of Hyatt & Flath (1966) and Agostoni & Fenn (1960), who concluded – based on *in vivo* measurements of inspiratory flow and oesophageal pressure – that *in vivo* inspiratory muscles exhibit similar force-velocity characteristics as seen in isolated preparations. Unlike isolated fibre preparations, however, the pressure-flow relationship appeared to be linear; not hyperbolic, as *in vitro* and *in situ* (Figure 2.3.5) (e.g., Ameredes et al., 2006; Coirault et al., 1997). The linear relationship between inspiratory flow and pressure has later been attributed to the complexity of inspiratory muscle recruitment during maximum inspiratory efforts, and the fact that the various inspiratory muscles operate under sub-optimal fibre lengths during these maximal efforts (Nava et al., 1993). Inspiratory flow measured at the level of the mouth should, therefore, be considered only an approximation of inspiratory muscle shortening velocity because it does not take into account the resistance to airflow in the airways (Agostoni & Fenn, 1960), nor does it take into account the fact that inspiratory airflow can occur without diaphragm shortening (Goldman et al., 1978).

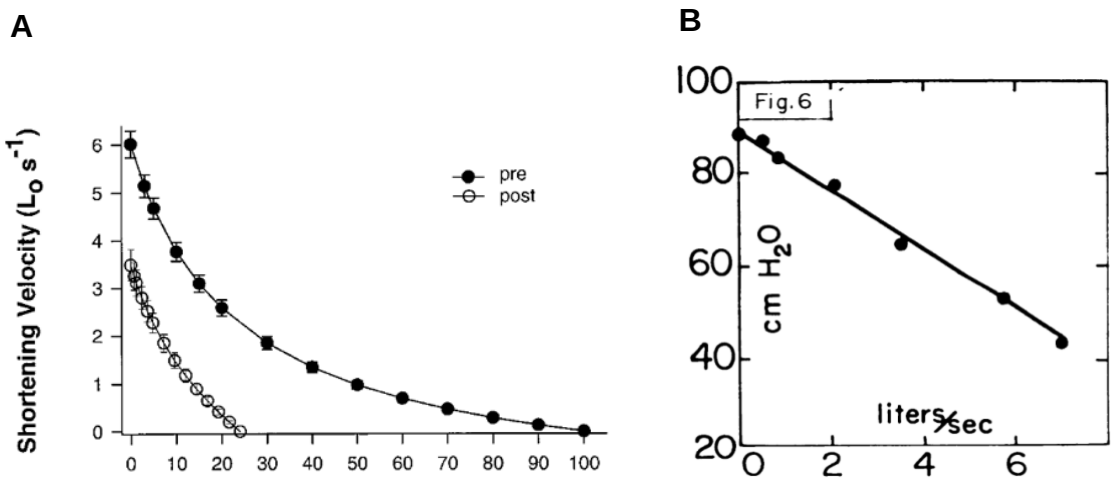

Figure 2.3.5 Hyperbolic force-velocity relationship in rat diaphragm pre- and post-fatigue *in vitro*. *X*-axis is force (% of maximum; panel *A*); Linear pressure-flow relationship in human inspiratory muscles *in vivo*. Inspiratory pressure (*y*-axis) was measured as P_{mo} (panel *B*). *A*) from "Power fatigue of the rat diaphragm muscle", by B. Ameredes et al, 2006, *Journal of Applied Physiology*, 89(6), p.2215-2219. *B*) from "Velocity of muscle shortening as a limiting factor in respiratory air flow", by E. Agostoni & W. Fenn, 1960, *Journal of Applied Physiology*, 15, p.349-353.

The development of sonomicrometry; that is, the measurement of displacement of piezoelectric transducers attached to muscle tissue during contractions, has since enhanced our understanding of the pressure-flow relationship of the mammalian diaphragm muscle. Although sonomicrometry is not appropriate in humans, the advantage of sonomicrometry is that it provides a direct measure of fibre shortening at the level of the muscle. Moreover, whereas inspiratory flow is the result of the global contribution from several inspiratory muscles, sonomicrometry can be used to assess shortening of the diaphragm (Easton et al., 1993; Newman et al., 1984; Road et al., 1986), external intercostals (Fitting et al., 1985), scalenes and/or sternocleidomastoids (De Troyer et al., 1994). Thus, sonomicrometry circumvents the limitations associated with approximating fibre shortening velocity from inspiratory flow.

There have been multiple studies investigating the relationship between inspiratory flow and diaphragm shortening velocity, with some arguing that flow is a poor estimate of *in vivo* diaphragm shortening velocity after finding no relationship between instantaneous flow and shortening velocity in canine diaphragm (Newman et al., 1984). On the other hand, Fitting et al. (1985) found that the mean (not instantaneous) shortening velocity of canine costal and crural diaphragm were strongly related to mean inspiratory airflow (costal diaphragm: $r = 0.95$; crural diaphragm: $r = 0.94$) during hypercapnic hyperpnoea.

This being said, beyond the work of Agostoni & Fenn (1960) and Hyatt & Flath (1966), little is still known about the force-velocity-power relationship of the *in vivo* human diaphragm. Although inspiratory airflow is merely an approximation of inspiratory muscle shortening velocity, the consensus is still that inspiratory muscles shorten at the same rate of inspiratory flow. Because direct methods of quantifying fibre shortening velocity, such as sonomicrometry, are appropriate in humans, our current understanding of shortening velocity of human diaphragm is founded on isolated preparations of diaphragm fibres of other mammals (e.g., canine). Based on these considerations, it is evident that the force-velocity-power relationship of the *in vivo* human diaphragm is methodologically difficult assess. In line with the overarching aims of this thesis (see section 2.6), ultrasonography will be proposed as a novel method to quantify the shortening and shortening velocity of the *in vivo* human diaphragm. Moreover, the influence of skeletal muscle fatigue on force-velocity-power relations will be discussed in section 2.4.10. In addition, the effect of external loading (flow- and pressure-loading) on diaphragm force-velocity-power relations will be the focus in Chapter 7.

2.3.6 Post-activation potentiation of skeletal muscle

Post-activation potentiation is an acute, short-term increase in force following prior muscle activity (Kufel et al., 2002). Post-activation potentiation (referred to as 'potentiation' hereafter) has traditionally been characterised by an increase in force following prior activity (e.g., tetanic stimulation or voluntary contraction) in response to subsequent twitch stimulation (Hodgson et al., 2005). Physiologically, the effect of potentiation is attributed to the increased sensitivity of Ca^{2+} due to phosphorylation of regulatory MLC (MacIntosh & Willis, 2000). MLCs are essential in attaching the myosin heads to the actin filament during cross-bridge cycling, and phosphorylation of MLCs causes the molecule to undergo a structural change that rotates the myosin heads closer to the actin (Yu et al., 2016). Myosin heads are restructured to a more favourable position that exposes the Ca^{2+} binding site on troponin, thereby increasing Ca^{2+} sensitivity and the number of active cross-bridges during a contraction (Hodgson et al., 2005; MacIntosh & Willis, 2000). Because slow-twitch type I fibres are already highly sensitivity to Ca^{2+}, the effect of potentiation on muscles with high distribution of type I fibres is small. Conversely, the effect of potentiation on fast-twitch type II fibres is usually more pronounced (Abbate et al., 2000; Bárány et al., 1983).

The effect of potentiation on muscle contractile properties are determined by the activation strategy (i.e., short- or long-lasting contractions; electrical stimulation or volitional contractions; isometric or concentric contractions), and, as indicated above, by the muscle fibre

distribution (Abbate et al., 2000; MacIntosh & Bryan, 2002). For instance, stimulation-evoked twitch force can increase by 30-110% in mammalian muscles when the fibre composition is dominated by fast-twitch fibres (Bárány et al., 1983; Hodgson et al., 2005). On the other hand, skeletal muscles like the soleus – a muscle dominated by type I fibres (~80%) – has little to no effect of potentiation (Bárány et al., 1983; MacIntosh & Willis, 2000). Interestingly, MacIntosh & Bryan (2002) have also demonstrated that shortening velocity may increase with potentiation. Those authors reported a 51% increase in shortening velocity (61 to 92 mm/s) in rat gastrocnemius preparations after potentiation by electrical stimulation. Accordingly, both force *and* shortening velocity may be affected by potentiation, ultimately increasing skeletal muscle power.

Post-activation potentiation of human diaphragm

As for isolated preparations, potentiation may also affect human diaphragm. However, the effect of potentiation appears to be less marked in the diaphragm compared to that seen in other respiratory and airway muscles, such as the sternohyoids (Van Lunteren & Vafaie, 1993). This discrepancy is likely due to the high distribution of type II fibres in the sternohyoids compared to the diaphragm, measuring ~1% type I fibres, ~23% type IIA fibres and ~76% type IIB fibres *versus* the diaphragm's 49% type I fibres, 28% type IIA fibres and 23% type IIB fibres (Dick & Van Lunteren, 1990; Mizuno & Secher, 1989b; Van Lunteren & Vafaie, 1993). Yet, a number of studies have established that prior activation of the diaphragm may increase $\Delta P_{di,tw}$ with as much as 46% to 63% (Laghi et al., 1995; Mador, Magalang, et al., 2000). Although most previous studies have used maximal inspiratory efforts to induce potentiation (Geary et al., 2019; Guenette et al., 2010; Laghi et al., 1995; Man et al., 2002), some evidence suggest that inspiratory efforts of only 33% of $P_{di,max}$ (Mador, Magalang, et al., 2000) or 50% of $P_{di,max}$ (Wragg et al., 1994) are needed to induce potentiation of the human diaphragm.

It is worth noting that potentiation and skeletal muscle fatigue can coexist; that is, an enhancement *and* impairment of the muscle's contractile properties. This means that fatigue can be hidden, or 'masked', behind potentiation. A common practice is, therefore, to induce potentiation before performing magnetic stimulation phrenic nerves, and thereby to use potentiated twitch pressures as an index of twitch force (Kufel et al., 2002). Some argue that potentiated twitches may be even more sensitive for detecting diaphragm fatigue compared to non-potentiated twitches (Kufel et al., 2002; Laghi et al., 1995, 1998). For instance, by inducing potentiation before performing magnetic stimulation of phrenic nerves, Laghi et al. (1998) found that only potentiated twitches showed a consistent decline in $\Delta P_{di,tw}$ during and after the

completion of an inspiratory resistive loading (IRL) task, with a mean decrement in potentiated $\Delta P_{di,tw}$ of –26% *versus* –14% in non-potentiated $\Delta P_{di,tw}$.

Because potentiation may have a significant effect on muscle contractile properties, a discussion is warranted regarding the recovery time of potentiation. This is particularly important to consider when multiple perturbations (e.g., external loading tasks, stimulation of phrenic nerves and maximal efforts) are performed within a short space of time. While some have found that effect of potentiation is diminished already within 8-10 min post-activation (Mador, Magalang, et al., 2000), others claim that potentiation may persist for up to 20 min post-activation; particularly if the activity was of high force (P_{di} ≥75% of $P_{di,max}$) and long duration (≥10 s) (Wragg et al., 1994). Understanding the time course for recovery from potentiation is particularly important when using non-potentiated twitches pre- and post-loading tasks in order to avoid potentiation 'masking' fatigue-induced decrements in $\Delta P_{di,tw}$. It is important to carefully consider the timing of twitch contractions to let potentiation dissipate before measurements are made. Further discussion regarding the effect of potentiation on diaphragm contractile properties is provided in Chapter 4. The coexistence of potentiation and diaphragm muscle fatigue is discussed in greater detail in Chapter 7.

2.3.7 Influence of structural attributes on diaphragm contractile properties

For limb locomotor muscles, it has traditionally been assumed that muscle cross-sectional area is strongly related to the maximal force capacity under the premise that a muscle with large cross-sectional area can hold more sarcomeres in parallel, and thereby generate greater force compared to a muscle with smaller cross-sectional area (Fitts et al., 1991; Hodgson et al., 2005). Despite critique of this of this assumption (Jones et al., 2008), a number of studies have proposed that a similar relationship exists between costal diaphragm thickness and maximal diaphragm force (pressure). For instance, McCool et at (1997) found strong positive relationship between costal diaphragm thickness, assessed with ultrasonography, and MIP (r^2 = 0.58) and $P_{di,max}$ (r^2 = 0.89). Similarly, a loss of diaphragm thickness due to disuse and atrophy during mechanical ventilation has been associated with diaphragm weakness, dysfunction and weaning failure (Dres et al., 2018; Goligher, Laghi, et al., 2015). The relative thickening of the diaphragm during both static and dynamic manoeuvres has further been associated with breathing effort during assisted ventilation (Bellani et al., 2013) and MIP in healthy individuals (Ueki et al., 1995). Combined, these studies confirm the close relationship between structural attributes of the human diaphragm and its ability to generate force.

The structural attributes of the human diaphragm, such as thickness and volume are determined by multiple factors. For example, body mass is positively correlated with costal diaphragm thickness (McCool, Benditt, et al., 1997) and muscle mass (Arora & Rochester, 1982). Diaphragm area; that is, the area over which the diaphragm spans within the thorax, is also positively correlated with body mass and stature (Arora & Rochester, 1982; McCool, Benditt, et al., 1997). Moreover, physical activity levels seem to play an important role in diaphragm structural attributes, with individuals undertaking regular weight-training exhibiting thicker diaphragms and higher inspiratory pressures compared to sedentary counterparts, even when corrected for body mass and stature (McCool, Benditt, et al., 1997). Targeted respiratory muscle training also appears to have an effect on diaphragm thickness and inspiratory pressures, with Souza et al. (2014) showing an 13% increase in diaphragm thickness at FRC alongside a 24% increase in MIP in healthy, older women (age 68.3 ± 5.2 y).

2.4 Contractile properties of *fatigued* skeletal muscle

As outlined above, the contractile properties of skeletal muscles are primarily determined by the molecular, chemical, neural and structural factors controlling the neuromuscular recruitment; the number of interacting cross-bridges, and the rate at which this interaction occurs. Excessive muscle activity may impair contractile properties to the extent that task failure may be inevitable. For the respiratory muscles specifically, this task failure may adversely affect exercise tolerance and sensation of dyspnoea, as well as promote early exercise cessation (Romer & Polkey, 2008). The sum of these impairments in the healthy muscle constitutes the definition of fatigue as "the loss in the capacity for developing force and/or velocity of a muscle, resulting from muscle activity under load and which is reversible by rest" (Respiratory Muscle Fatigue Workshop Group, 1990, p. 474). Skeletal muscle fatigue (referred to as *fatigue* hereafter), is therefore different from muscle weakness, in which the contractile properties of the rested muscle are impaired and not reversible by rest (Laveneziana et al., 2019).

A more contemporary definition of fatigue has been provided by Enoka & Duchateu (2016). Those authors argue that fatigue should be defined as "a disabling symptom in which physical and cognitive function is limited by interactions between performance fatigability and perceived fatiguability" (Enoka & Duchateau, 2016, p. 1). This two-domain concept (i.e., objectively-determined decline in contractile properties *and* perceived fatigability) encompasses the physiologic mechanisms underlying the development of fatigue and task failure, but also acknowledges the psychological factors mediating the perception of fatigue and exercise tolerance. Although the second part of this literature review will primarily operate under the classic definition of fatigue provided by the Respiratory Muscle Fatigue Workshop Group (1990), it is necessary to acknowledge the contemporary definition of fatigue when discussing the mechanisms that underpin fatigue-related activity cessation (e.g., perceived breathing discomfort).

The second part of this literature review will provide an overview of the physiologic mechanisms that underpin fatigue of skeletal muscles generally, and of the diaphragm specifically. More importantly, there will be a discussion concerning the implications of diaphragm fatigue as well as the strengths and limitations of current methodologies in the assessment of diaphragm contractile properties.

2.4.8 Central and peripheral fatigue of skeletal muscle

Fatigue can be central and/or peripheral in origin. More specifically, central fatigue is the failure of central nervous system to generate appropriate central command for a given task, resulting in a suboptimal (voluntary) activation of the muscle relative to the demand (Enoka, 1995). Central fatigue can be explained by factors at spinal and supraspinal sites, and includes altered intrinsic behaviour of the motoneuron, recurrent inhibition, altered output of descending paths to motoneurons, and concentration changes in neurotransmitters (Boyas & Guével, 2011). Peripheral fatigue occurs at sites at or distal to the neuromuscular junction, and includes disturbances of excitation-contraction coupling and metabolic changes within the muscle (Allen et al., 2008). To contextualise the forthcoming discussion of skeletal muscle fatigue, and diaphragm muscle fatigue specifically, a brief overview of central and peripheral factors governing fatigue will be provided in the following sections.

2.4.9 Central fatigue of *in vivo* human diaphragm

Central fatigue is defined as the disparity between the maximal voluntary force *generated* and the *true* maximal force of the muscle (Gandevia, 2001). For the muscle *in vivo*, central fatigue can be identified by superimposed twitch contractions, whereby an evoked twitch contraction is superimposed on a maximal voluntary contraction (MVC). If the superimposed twitch amplitude is undetectable in the voluntary contraction, causing no further increase in force, the MVC is a true maximal contraction. Conversely, if the superimposed twitch amplitude is visible, and increases relative to the MVC as the task progresses, this suggests the occurrence of central fatigue (Boyas & Guével, 2011).

Superimposed twitch contractions can also be used to detect central fatigue of the human diaphragm by superimposing twitch contractions on maximal inspiratory efforts. For instance, the early study by Bellemare & Bigland-Richie (1984) showed that diaphragm twitches could be superimposed on maximum expulsive efforts and Müller expulsive manoeuvres. The authors superimposed twitch contractions on gradually increasing inspiratory efforts, finding that the twitch amplitude decreased as a function of inspiratory effort. These findings were later expanded by the same authors by superimposing twitches on inspiratory efforts (50% of $P_{di,max}$) before and after the induction of fatigue (Bellemare & Bigland-Ritchie, 1987). As fatigue developed during an inspiratory loading task, the superimposed twitch amplitude increased. Ultimately, the authors concluded that half of the fatigue-induced decrement in P_{di} was of central origin, with the remaining half of peripheral origin (Bellemare & Bigland-Ritchie, 1987).

Fatigue of central origin is characterised by a relatively short recovery time compared to fatigue of peripheral origin. In fact, after a sustained MVC until 'task failure', the largest component of recovery usually occurs within 90 s after exercise cessation, with a full recovery seen within 30 min (Gandevia, 2001). The time course for recovery from central fatigue is determined by exercise modality (e.g., concentric or eccentric contraction, sustained MVC or intermittent shortening), exercise duration and intensity (Carroll et al., 2017). More recent attempts have also been made to better understand within- and between-day reliability of superimposed twitch contractions for the voluntary activation of the diaphragm (Ramsook et al., 2021). Because most literature pertaining to human diaphragm fatigue is dedicated to peripheral, low-frequency fatigue, these techniques may provide novel insight into the presence and implications of central fatigue of this important muscle.

2.4.10 Peripheral fatigue of human diaphragm *in vivo*

As mentioned above, fatigue of peripheral origin occurs at sites at or distal to the neuromuscular junction (Gandevia, 2001). Primarily, these sites include, but are not exclusive to, disturbances of the excitation-contraction coupling, impaired release and reuptake of Ca^{2+} from sarcoplasmic reticulum, or altered sensitivity to Ca^{2+}. The following sections will provide an overview of the physiologic mechanisms that underpin peripheral fatigue followed by a discussion regarding the effect of peripheral fatigue on dynamic diaphragm contractile properties.

High- and low-frequency fatigue

There are two types of disturbances to the excitation-contraction coupling that are associated with peripheral fatigue. The first type results in the loss of force in response to high-frequency stimulations (≥50 Hz; high-frequency fatigue [HFF]), and usually recovers within 60-120 s. The second type results in the loss of force in response to low-frequency stimulations (10-30 Hz; low-frequency fatigue [LFF]), and usually recovers slowly (Carroll et al., 2017; Jones, 1996). The particularly long recovery times from LFF, sometimes ranging from hours to days, are primarily due to excessive eccentric contractions that require structural repair (protein turnover) of the contractile apparatus (Carroll et al., 2017). However, because the diaphragm muscle rarely contracts eccentrically under physiological conditions (Gea et al., 2009), fatigue by eccentric contractions will not be discussed further.

High-frequency fatigue (HFF)

Although HFF can result in substantial decrements in force, there has been doubt as to whether the phenomenon is a 'normal' mechanism of fatigue under physiological conditions given that firing frequency in skeletal muscle rarely exceeds 30 Hz (Jones, 1996). However, when stimulated at 30 Hz at short muscle lengths, there is evidence of fatigue with many of the same features of HFF (Sacco et al., 1994). The decrement in force seen with HFF has been attributed to the release and accumulation of potassium (K^+) in extracellular spaces secondary to altered K^+/Na^+-pump function (Jones, 1996). Specifically during high-frequency stimulation, K^+ accumulates in the lumen of the t-tubules which causes an impairment of action potential propagation along the t-tubular system and fibre membrane (Clausen, 2003). Although the mechanisms behind extracellular accumulation of K^+ and the subsequent loss of force are not entirely clear (Allen et al., 2008), some have suggested that the K^+/Na^+-pump may not have the capacity to adjust to the rapid ionic changes across the muscle membrane during high-frequency stimuli, thus causing an extracellular accumulation of K^+ (Clausen, 2003; Jones, 1996).

To identify HFF of the whole muscle *in vivo*, EMG electrodes can be used to measure the compound muscle action potential (M-wave). More specifically, peripheral stimulation of nerves can evoke an electrical response in the target muscle that can be measured as the M-wave by EMG electrodes positioned in close proximity to the stimulated motor units (Aldrich et al., 2005). M-waves represent the summated electrical activity from the depolarised fibre membranes located within the recording range of the electrode. For decades, it was understood that impaired excitability of fibre membrane reduces the M-wave peak-to-peak amplitude (Bigland-Ritchie & Woods, 1984; Luo et al., 1998, 1999). However, a more recent review has suggested that M-wave shape (i.e., duration, area and amplitude of first and second phases) should instead be evaluated separately (first and second phase independently) and as a whole (the two phases combined) (Rodriguez-Falces & Place, 2018). The authors argue that the first and second phases of the M-wave behave differently depending on details of the fatigue task, the degree of structural damage caused to the muscle during the task, and environmental factors (e.g., pH and temperature) (Rodriguez-Falces & Place, 2018).

Few previous studies have, however, applied the elaborative approach to assess M-wave characteristics as suggested by Rodriguez-Falces & Price (2018). In fact, most authors reporting M-waves only report peak-to-peak amplitude, the amplitude of the first phase or the total area of the M-wave. This is true also for the human diaphragm (Archiza et al., 2018; Guenette et al., 2007; Luo et al., 1999). It is important to note that there are no established reference values for

diaphragm M-wave characteristics beyond latency (phrenic nerve conduction time), central conduction time (i.e., total conduction time minus phrenic nerve latency) and peak-to-peak amplitude (Aldrich et al., 2005; Laveneziana et al., 2019).Thus, the elaborative approach suggested by Rodriguez-Falces & Price (2018) may not be implemented for the analysis of diaphragm M-wave characteristics within the near future.

Low-frequency fatigue (LFF)

There are three theories explaining the decrement in force seen with LFF. The first theory relates to the altered release and reuptake of Ca^{2+} from sarcoplasmic reticulum seen after prolonged muscle activity. Strenuous muscle activity causes an intracellular accumulation of hydrolysis by-products (e.g., H^+ and P_i) which impairs the release and reuptake of Ca^{2+} from sarcoplasmic reticulum (Boyas & Guével, 2011). An intra-cellular accumulation of Ca^{2+} reduces the concentration gradient of Ca^{2+} and diminishes the flux of Ca^{2+} across sarcoplasmic reticulum in response to depolarisation (Enoka & Stuart, 1992).

The second theory relates to reduced troponin sensitivity to Ca^{2+} (Jones, 1996). The increased concentration of P_i at the early stages of intense muscle activity has been found to have an inhibitory effect on cross-bridge kinetics by altering the Ca^{2+} sensitivity of troponin in the actin-myosin interaction (Allen et al., 2008). Some have also suggested that increased concentration of H^+ (acidosis) may have an inhibitory effect on cross-bridge interaction by competing with Ca^{2+} in troponin binding, which will also reduce the overall force output (Sundberg & Fitts, 2019). The third theory relates to sarcomere damage caused by the mechanical stress induced by eccentric contractions (Allen et al., 2008; Jones, 1996). However, this theory is less likely to apply to the diaphragm *in vivo* because the muscle very rarely works eccentrically under applied, physiological conditions (Gea et al., 2009).

For shortening velocity, alterations inn Ca^{2+} release and reuptake appear to have negligible effect (Ameredes et al., 2006). Instead, intracellular accumulation of H^+ (acidosis) increases significantly the cross-bridge attachment times compared to under normal conditions because ATPase activity; that is, the isomerisation and release of ADP in the cross-bridge cycling, is greatly impaired under acid conditions (Sundberg & Fitts, 2019). Based on these considerations, it is evident that any mechanism that impairs force and/or shortening velocity will also greatly impair power of a muscle. The effect of fatigue on shortening velocity and power is discussed in detail in Chapter 7.

High- and low-frequency fatigue of human diaphragm

As with isolated fibre preparations, the human diaphragm is susceptible to both HFF and LFF following external loading. As mentioned previously, diaphragm fatigue has traditionally been defined as a decrement in $\Delta P_{di,tw}$ in response to single, paired or repetitive stimuli by electrical or magnetic stimulation of one or both of the phrenic nerves. Although electrical stimulation is considered more specific than magnetic stimulation, evoking little coactivation of other chest wall muscles, electrical stimulation is painful and requires more precision upon stimulation (Bellemare & Poirier, 2005). Conversely, magnetic stimulation is virtually painless, and has become the preferred method to stimulate phrenic nerves (Green et al., 2002; Similowski et al., 1989). Because phrenic nerve branches are readily accessible around the neck, stimuli can be delivered cervically using a circular coil at the spinous process at C7 for bilateral, cervical stimulation, or anterolaterally with a figure-eight coil over the sternocleidomastoid (Bellemare & Poirier, 2005). Anterolateral stimulation can be performed bilaterally (Mills et al., 1996) or unilaterally (Mills et al., 1995). In unilateral stimulation, it is worth noting that the contralateral phrenic nerve is indirectly stimulated (Mills et al., 1995), and the activated hemi-diaphragm distorts laterally during contraction; not craniocaudally as seen with bilateral stimulation (De Troyer & Boriek, 2011).

A number of different stimulation protocols have been used to identify diaphragm fatigue in humans. This includes single (1 Hz) non-potentiated twitch contractions (Laghi et al., 1995; Tomczak et al., 2011); single (1 Hz) potentiated twitches (Archiza et al., 2018; Geary et al., 2019; Guenette et al., 2010); paired twitches at various frequencies (Polkey, Kyroussis, et al., 1997) and repetitive twitches at various frequencies (Johnson et al., 1993). As previously mentioned, some have also used superimposed twitches to identify the central components of diaphragm fatigue (Bellemare & Bigland-Ritchie, 1987). Accordingly, design of stimulation protocols are determined by study purpose (e.g., peripheral *vs*. central fatigue, or LFF *vs*. HFF), study sample (e.g., healthy adults or patients) and available equipment (e.g., coils and laboratory set-up for repetitive stimulation).

Based on the abovementioned considerations, it is evident that diaphragm HFF can only be assessed using repetitive (paired or tetanic) stimulation at stimulation frequencies ≥50 Hz. For instance, in the first study to clearly demonstrate diaphragm HFF, Aubier et al. (1981) magnetically stimulated right phrenic nerve at 10, 20, 50 and 100 Hz before and after IRL. Although the decline in $\Delta P_{di,tw}$ was greatest at the low frequencies (e.g.,–42 ± 7% at 20 Hz), also the $\Delta P_{di,tw}$ in response 100 Hz was lower (–12 ± 6%) after IRL. Perhaps more interesting

was the rapid recovery of $\Delta P_{di,tw}$ in response to high-frequency stimulations (≤10 min) compared to the slow recovery after low-frequency stimulations (≥60 min) (Aubier et al., 1981). These findings were in line with pattern of recovery seen in isolated preparations after inducing HFF and LFF.

To determine whether HFF was present in the human diaphragm after whole-body exercise, Babcock et al. (1998) used a stimulation protocol of paired twitches at 10, 20, 50, 70 and 100 Hz before and after intense, sustained, whole-body exercise that elicited 93 ± 2% of $\dot{V}O_{2max}$. At exercise cessation, $\Delta P_{di,tw}$ was significantly reduced in response to all stimulation frequencies (mean –28%). However, $\Delta P_{di,tw}$ in response to 70 and 100 Hz recovered to a pre-fatigue state within 30 min, whereas the $\Delta P_{di,tw}$ at 10-50 Hz persisted for up to an hour post-exercise. These findings support the notion that HFF and LFF can coexist in the human diaphragm after resistive breathing and sustained whole-body exercise.

The assessment of LFF in human diaphragm is characterised by a decrement in $\Delta P_{di,tw}$ in response to low-frequency single, paired or repetitive stimulations of phrenic nerves at 10-50 Hz. As stated above, LFF also exhibits a long time course for recovery, ranging from hours to days (Carroll et al., 2017). Although the initial study of Aubier et al. (1981) identified both HFF and LFF following IRL, the most rigorous study of LLF of human diaphragm was performed by Johnson et al. (1993) who first demonstrated LFF after strenuous, whole-body exercise until exhaustion that elicited 95% of $\dot{V}O_{2max}$. In the study by Johnson et al. (1993), phrenic nerves were tetanically stimulated over 400 ms at 10 and 20 Hz. At exercise cessation, the authors reported a decrement in $\Delta P_{di,tw}$ of –21 ± 3% and –13 ± 2% in response to 10 and 20 Hz, respectively, and that it took 60-70 min for $\Delta P_{di,tw}$ to return to pre-fatigue baseline.

A discussion is also warranted regarding the use of volitional tests to assess diaphragm fatigue. Because stimulation of phrenic nerves may not be feasible (e.g., due to lack of equipment) or desirable (e.g., due to invasiveness of gastro-oesophageal catheters for the assessment of P_{di}), some find it necessary to use volitional tests to quantify fatigue-induced changes in inspiratory muscle force (Green et al., 2002; Laveneziana et al., 2019). Such tests include maximal static inspiratory efforts against closed glottis (McCool et al., 1992) or short, sharp inspiratory efforts (sniffs) (Koulouris, Vianna, et al., 1989; Mulvey et al., 1991). If performing these efforts while only measuring mouth pressure (P_{mo}) or sniff nasal pressure, it is important to note that the pressures are not specific the diaphragm, but is rather the global contribution of multiple muscles (Nava et al., 1993; Verin et al., 2001). Moreover, because the tests are volitional, validity and reliability is strongly dependent on subject cooperation and motivation. This is a

particularly important point when assessing inspiratory muscle fatigue after strenuous exercise, because whole-body fatigue and participant weariness may adversely affect motivation to perform maximal respiratory efforts (Laveneziana et al., 2019).

2.4.11 Causes of diaphragm fatigue

The development and severity of muscle fatigue is primarily determined by cumulative inspiratory muscle work and the competition with locomotor muscles for available blood flow (Johnson et al., 1993; Romer & Polkey, 2008). The magnitude of diaphragm work can be quantified as the pressure-time index (PTI_{di}) from the equation $PTI_{di} = \overline{P}_{di}/P_{di,max} \times T_I/T_{TOT}$ (Bellemare & Grassino, 1982). During stable ventilation, changes in PTI_{di} is closely related to changes in respiratory muscle oxygen consumption (Collett et al., 1985) and blood flow (Bellemare et al., 1983). PTI_{di} is therefore considered a good reflection of the work performed by the diaphragm. To examine the influence of diaphragm work (PTI_{di}) on the time course and severity of diaphragm fatigue, Bellemare & Grassino (1982) applied various inspiratory pressures (15-90% of $P_{di,max}$) over a range of inspiratory duty cycles ([T_I/T_{TOT}]; 0.15-1.0, with 1.0 being a continuous static contraction) in order to modify diaphragm work. In this study, each task was performed until the target breathing pattern (T_I/T_{TOT}) or pressure could not be reached ('task failure'). The authors found that PTI_{di} of 0.15-0.18 could be sustained for 45-60 min before task failure, and consequently labelled this the critical PTI_{di}. A PTI_{di} exceeding the critical PTI_{di} would induce diaphragm fatigue rapidly (Bellemare & Grassino, 1982).

During sustained, isometric contractions at moderate-to-high force, evidence shows that blood flow to the diaphragm is partially or fully occluded. In fact, sustained muscle contractions at 70% of maximal force may increase intramuscular pressure and reduce vascular conductance to the extent of full blood flow occlusion (Bellemare et al., 1983; Buchler et al., 1985). In dogs, even intermittent contractions at 18% of $P_{di,max}$ can partially occlude blood flow to the diaphragm (Bellemare et al., 1983). In humans, higher pressures (≥40% of $P_{di,max}$) are likely necessary for full blood flow occlusion (Buchler et al., 1985).The physiologic implications of a partial or full blood flow occlusion to the working muscle are severe. For instance, blood flow occlusion will result in an inadequate O_2-supply to the working muscle, leaving the resynthesis of ATP to depend partially or solely on anaerobic pathways to sustain the force output and mechanical work (Smith-Blair, 2002). This results in an intramuscular accumulation of anaerobic by-products (e.g., H^+ and P_i), further favouring development of fatigue (Boyas & Guével, 2011).

Inadequate O_2-supply is also the major cause of respiratory muscle fatigue induced by whole-body exercise, particularly when exercise intensity is high (Sheel et al., 2018). The metabolic demand of respiratory and locomotor muscles increases with exercise intensity; and so, the competition for blood flow and O_2 increases with work rate (Andersen & Saltin, 1985). Accordingly, respiratory muscles and limb locomotor muscles may receive less O_2 relative to demand during exercise. In fact, from rest to heavy exercise, the $\dot{V}O_2$ of respiratory muscles increases from ~3-6% to ~13-15% of $\dot{V}O_{2,max}$ in well-trained adults, which is a significant proportion of total O_2 uptake (Aaron et al., 1992). Moreover, up to 14-16% of cardiac output is directed to the respiratory muscles during maximal exercise (Harms et al., 1998), again confirming the significant metabolic work done by the respiratory muscles in this condition.

The importance of blood flow limitation on the development of respiratory muscle fatigue during whole-body exercise was demonstrated by Babcock et al. (1995), who showed that *mimicking* the exercise-induced diaphragm work at rest did not induce diaphragm fatigue. It was only when diaphragm work at rest was almost double the magnitude seen during exercise that the authors found evidence of fatigue. A more recent study by Dominelli et al. (2017) investigated whether manipulating the work of breathing during high-intensity exercise at 90% of maximal work rate would alter blood flow to respiratory muscles. In this study, blood flow to respiratory muscles was measured to sternocleidomastoids, and blood flow to limb locomotor muscles was measured to the quadriceps. To manipulate the work of breathing, participants breathed with resistors (increased work), proportional assisted ventilator (decreased work) or without manipulation. The authors found that when increasing the work of breathing, blood flow to respiratory muscles increased whereas blood flow to limb muscles decreased. Conversely, when reducing the work of breathing, blood flow to locomotor muscles increased. During exercise with increased work of breathing, respiratory and locomotor muscles compete for blood flow and O_2 supply to meet the metabolic demand. In turn, this competition may culminate in a scenario in which respiratory and locomotor muscles are mutually fatigued (Dempsey et al., 2006; Sheel et al., 2018).

2.4.12 Fatigue task-dependency

The mechanisms that underpin fatigue of skeletal muscles are determined by the task performed as well as the effort associated with performing this task; that is, fatigue task-dependency (Enoka, 1995). Fatigue task-dependency means that contraction details, such as contraction type (eccentric, isometric or concentric), shortening velocity, external load and/or duration of contraction evoke various physiologic responses that acutely impair the contractile apparatus

(Enoka & Stuart, 1992). For example, tasks that involve isometric contractions of short duration with low-to-moderate force appear to impair force as a result of disturbances at the excitation-contraction (Enoka, 1995). Conversely, sustained isometric contractions with moderate-to-high force impair force as a result of partial or full occlusion of blood flow, intra-cellular accumulation of anaerobic metabolites and reduced Ca^{2+} sensitivity (Allen et al., 2008). Understanding task-dependency of fatigue is important because fatigue, in combination with systematic recovery, represents the acute overload necessary for neuromuscular adaptation and enhanced performance, whether it be endurance or strength (Hunter, 2018).

A major challenge is, however, that fatigue task-dependency is difficult to demonstrate for the muscle *in vivo* because rarely can force- and velocity-tasks be fully isolated. In theory, a task performed with negligible resistance and high shortening velocity would impair primarily shortening velocity while maximal force would remain well-preserved (Enoka & Stuart, 1992). Yet, even in low force-high velocity tasks it is necessary to generate force to overcome resistance to contraction, even when no external load is applied (e.g., intramuscular elastic and viscous stiffness and the force required for limb movement). For the diaphragm, this resistance includes flow-resistive, inertial, and viscoelastic properties that all contribute to an elevated work of breathing (Otis, 1954; Peters, 1969). Accordingly, even tasks of low force-high velocity may impair the muscle's ability to generate force, thereby making it difficult to demonstrate fatigue task-dependency of muscles *in vivo*. The following section will further discuss fatigue task-dependency of the human diaphragm.

Fatigue task-dependency of human diaphragm

Fatigue task-dependency in human diaphragm has rarely been studied. In fact, the first and only study to demonstrate fatigue task-dependency of human diaphragm was done by McCool et al. (1992). Here, participants performed a high force-low velocity task (IRL at P_{oe} of 40-50 cmH_2O) and a low force-high velocity task (voluntary isocapnic hyperpnoea with inspiratory flow of 5-6 L/s) until task failure. The authors found that high force-low velocity task significantly impaired the ability to generate maximal inspiratory pressure ($P_{oe,max}$) with negligible effect on peak inspiratory flow ($P_{oe,max}$: –25 ± 7%; peak inspiratory flow: –3 ± 4%). Conversely, the low force-high velocity task primarily impaired peak inspiratory flow, with negligible effect on $P_{oe,max}$ ($P_{oe,max}$: –8 ± 8%; peak inspiratory flow: –16 ± 3%).

There are, however, a number of limitations in the study by McCool et al. (1992). First, the study did not objectively quantify inspiratory muscle force (e.g., by evoked pressure responses), and did not use objective measures to determine the presence of fatigue. Instead, the authors

used volitional efforts to arrive at their conclusions. Second, the study operated under the assumption that inspiratory airflow is a direct reflection of inspiratory muscle shortening velocity, which is an assumption that includes a number of limitations in itself (see section 2.3.5). Third, the study did not show a direct effect of velocity loading on diaphragm shortening velocity specifically, but only on the surrogate measure of inspiratory flow at the level of the mouth. Thus, future research using objective measures of diaphragm contractile properties is necessary to better understand fatigue task-dependency of human diaphragm.

As previously discussed, force- and velocity-tasks cannot be readily isolated for the muscle *in vivo*. This methodological challenge is particularly evident for the human diaphragm, which may be one of the reasons why little is still known about fatigue task-dependency of human diaphragm. For instance, voluntary isocapnic hyperpnoea (VIH) is frequently used as a low force-high velocity task to induce diaphragm fatigue, whereby the participant maintains voluntary hyperpnoea without external resistance to breathing for a pre-determined duration or until task failure (McCool et al., 1992; Renggli et al., 2008). However, even during 'unloaded' hyperpnoea, there is resistance to diaphragm contraction that requires force to overcome; including elastic and resistive resistance to inspiratory airflow and lung inflation (Otis, 1954; Peters, 1969). In fact, in the study by McCool et al. (1992), the low force-high velocity elicited inspiratory pressure (P_{oe}) of –28 ± 4 cmH_2O, which was more than half (62%) the pressure elicited during high force-low velocity task (–45 ± 5 cmH_2O). This example illustrates that complete isolation of velocity and force tasks may not be feasible for intact muscles *in vivo*.

Nonetheless, because contractile properties of human diaphragm are governed by the same physiologic mechanisms as preparations *in vitro* and *in situ*, it is intuitive that fatigue of the human diaphragm is also task-dependent. The major limitation is that diaphragm shortening velocity is not readily measured at the level of the muscle, and little is thus known about the effect of various loading tasks on diaphragm fatigue. Fatigue task-dependency of diaphragm fatigue will be studied and discussed in Chapter 7.

2.4.13 Assessment of diaphragm fatigue

As previously mentioned, diaphragm fatigue is objectively defined by a decrement in $\Delta P_{di,tw}$ in response to electrical or magnetic stimulation of the phrenic nerves; either by a cervical or anterolateral approach. Diaphragm fatigue is typically considered present when $\Delta P_{di,tw}$ declines twice the typical variation seen in $\Delta P_{di,tw}$, which is usually in the range of –10-20% (Babcock et al., 1996; Green et al., 2002). Some have also used a reduction in MIP to identify inspiratory muscle fatigue (e.g., Lomax & McConnell, 2003), although MIP should be considered a global

measure of inspiratory muscle function rather than a measure of diaphragm function specifically (Green et al., 2002; Laveneziana et al., 2019).

Because stimulation-evoked pressures do not provide information concerning the diaphragm's ability to shorten, generate power and perform work, some have instead used reflexively-driven hyperpnoea to assess respiratory function under more applied conditions. Indeed, various methods have been used to elicit hyperpnoea, including hypercapnic rebreathe methods (Duffin, 2011; Read, 1966; Read et al., 1966), steady-state and progressive hypoxia (Hirschman et al., 1975) and whole-body exercise (Johnson et al., 1993; Mador & Acevedo, 1991). Several of the experimental chapters in this thesis used hypercapnic hyperpnoea (CO_2-rebreathe) to elicit effort-independent increases in ventilation. Thus, the following discussion pertains to hypercapnic rebreathe methods specifically.

Hypercapnic rebreathe methods are useful for the assessment of respiratory muscle function because the tests require minimal co-operation from the subject. In general, hypercapnic rebreathe methods have fewer adverse effects on respiratory muscle function compared to hypoxic methods, which may in itself promote fatigue of diaphragm and abdominal muscles (Verges et al., 2010). Hypercapnic rebreathe methods are based on the premise that metabolic accumulation of CO_2 in a closed system (i.e., rebreathing bag, exhaled gas, lung tissue and arterial and venous blood) gradually increases partial pressure of CO_2 (PCO_2) of the enclosed system, thereby stimulating medullary central chemoreceptors to increase ventilation (Read, 1966; Read et al., 1966; Read & Leigh, 1967). Although the technique was originally intended to quantify the sensitivity of central chemoreceptors and 'chemoreflex threshold' (see Jensen et al., 2010; MacKay et al., 2016; Sahn et al., 1977), the method also provides useful information regarding dynamic respiratory muscle function during hyperpnoea.

As an example of application of hypercapnic rebreathe tests, Yan et al. (1993) evaluated the effect of diaphragm fatigue on intrathoracic pressures and breathing pattern during hypercapnic hyperpnoea using the Read (1966) rebreathe method. Expectedly, the authors found a reduction in $\Delta P_{di,tw}$ (–32%) following IRL, thereby objectively confirming the presence of diaphragm fatigue. In addition, inspiratory pressure swings (P_{di} and P_{ga}) during hyperpnoea were reduced. However, CO_2 sensitivity, minute ventilation (ventilatory slope), inspiratory flow and breathing pattern remained well-preserved during subsequent hypercapnic hyperpnoea. In a later study, Yan et al. (1993) found that inspiratory pressure swings were significantly reduced following the induction of global inspiratory muscle fatigue (not diaphragm fatigue specifically), and that participants adopted a tachypnoeic breathing pattern (i.e., lower V_T and higher f_R). Combined,

these studies demonstrated that hypercapnic methods (e.g., Read rebreathe method) can be used to evaluate dynamic diaphragm function under more applied conditions compared to stimulation-evoked twitch contractions. Moreover, rebreathe methods can reveal fatigue-induced changes to ventilatory indices (e.g., CO_2 sensitivity and breathing pattern) and respiratory mechanics (i.e., intrathoracic pressures and the work of breathing) that cannot be quantified in response to evoked twitch contractions.

As discussed in section 2.3.5, shortening velocity of human diaphragm has been studied to a limited extent. Due to the muscle's inaccessibility as well as methodological and technological limitations, "[diaphragm] length changes and velocity of shortening are invariably ignored and the focus has been on assessing diaphragm force development of pressure" (Green et al., 2002, p. 538). As previously discussed, some have therefore worked under the assumption that inspiratory muscles must shorten at a rate proportional to inspiratory flow (Agostoni & Fenn, 1960; Fitting et al., 1985; Johnson et al., 1993; McCool et al., 1992). Accordingly, this notion assumes that the slowing of inspiratory flow after external loading must be the result of slower shortening velocity of inspiratory muscles (McCool et al., 1992). Despite the clear limitations associated with using inspiratory flow as an indirect estimate of inspiratory muscle shortening velocity, the assessment of airflow is feasible during most perturbations, including whole-body exercise. Furthermore, the assessment of flow requires only basic equipment usually found in physiology laboratories. This is in contrast to more advanced methods that have been used to estimate diaphragm shortening and shortening velocity, such as fluoroscopy (Finucane & Singh, 2009), x-ray (Singh et al., 2003) and optoelectronic plethysmography (Aliverti et al., 1997). Although these methods provide more direct estimates of muscle shortening velocity compared to inspiratory flow, they also require specialty equipment and advanced training. Moreover, fluoroscopy and x-ray imaging do not enable the assessment of respiratory mechanics during whole-body exercise. To overcome these limitations, the experimental chapters in this thesis will focus on the use of ultrasonography for the assessment of dynamic contractile function of the diaphragm (i.e., excursion velocity) and thickening (shortening), as well as the muscle's ability to generate power.

2.4.14 Does task failure imply fatigue?

Historically, some authors have preferred operating with an alternative definition of fatigue to those proposed earlier (section 2.4). This definition implies that that fatigue occurs when a pre-determined task fails to be executed despite verbal encouragement (i.e., task failure; Hunter, 2018) . A major limitation is, however, that this definition does not specify the physiological or

psychological mechanisms that underpin failure, nor does it adequately address the loss of contractile properties associated with fatigue. Indeed, this definition of fatigue has also been applied to the human diaphragm (Bellemare & Grassino, 1982; Roussos et al., 1979; Roussos & Macklem, 1977), whereby task failure from resistive loading tasks has been considered analogous to diaphragm fatigue but without objectively quantifying decrements in contractile properties. Two of the experimental chapters (7 and 8) in this thesis used IRL to induce diaphragm fatigue. Thus, the following discussion was warranted when considering the design of the IRL protocol for this thesis.

Based on the above considerations, a number of studies investigated whether task failure coincides with objectively-determined diaphragm fatigue (e.g., decrement in $\Delta P_{di,tw}$) (Gorman et al., 1999; McKenzie et al., 1997; Rohrbach et al., 2003). Combined, these studies showed that task failure does not necessarily imply diaphragm fatigue. Instead, the authors suggested that there may be other reasons for task failure other than failure of the contractile apparatus. For instance, McKenzie et al. (1997) investigated the prevalence of task failure from IRL at 35-90% of MIP performed for 20 min *or* until task failure (< 20 min). Although 75% of all trials ended prematurely due to task failure, both MIP and $\Delta P_{di,tw}$ remained unchanged (MIP: +9.2%; $\Delta P_{di,tw}$: +6.9%; both $p > 0.05$). The authors also found that the time to task failure during IRL was strongly dependent on subjects' ability to reduce the rate of CO_2 accumulation, with coinciding evidence of hypoxic stimulus in some subjects at the point of task failure. CO_2 accumulation and hypoxia may further exacerbate the perception of 'air hunger' and non-respiratory sensations such as headache, drowsiness and restlessness (Moosavi et al., 2003). Accordingly, the authors concluded that task failure was not due to a contractile failure of the diaphragm, but rather hypoventilation and hypercapnia resulting in increased breathing discomfort. Gorman et al. (1999) later found that CO_2 accumulation and hypoventilation during IRL could be prevented by using protocols that integrate very short periods (e.g., one respiratory cycle every 30 s) without loading in order to relieve breathing discomfort. Another alternative protocol to prevent hypercapnia during resistive loading includes protocols with longer rest periods; that is, five minutes of IRL repeated three times (3 × 5 min), with each bout of loading separated by 10 min of rest (Luo et al., 2001).

2.4.15 Implications of diaphragm fatigue

In healthy, young adults, the respiratory system – including the respiratory muscles – is thought to have ample capacity relative to the demand for gas exchange, even during heavy-to-severe exercise (Johnson et al., 1992; Romer & Polkey, 2008). As previously mentioned, the

diaphragm contains an almost-equal distribution of slow- and fast-twitch muscle fibres. This means that the muscle has high oxidative capacity and short capillary-to-mitochondrial diffusion distance, but with an ability to contract rapidly under load when necessary (Meznaric & Cvetko, 2016). Thus, under normal physiologic conditions, inspiratory muscles have the capacity to meet the demand evoked by every-day activities without fatiguing. Yet, strenuous whole-body exercise may still impair the contractile properties of the muscle when blood flow and O_2 supply are compromised (Dempsey et al., 2006; Sheel et al., 2018).

Although the diaphragm is the principal muscle of inspiration at rest, the contribution from other inspiratory muscles increases with increasing ventilatory drive. This includes contribution from muscles such as the external intercostals, sternocleidomastoids and scalenes (Grimby et al., 1976). Accordingly, during strenuous exercise, the diaphragm and accessory inspiratory muscles are coordinated to meet the ventilatory demand by sharing the work of breathing (Dempsey et al., 2006; Haverkamp et al., 2005). An important question is, however, whether the recruitment of accessory inspiratory muscles is a protective mechanism to *delay* the onset of diaphragm fatigue (e.g., by reducing the absolute workload on the diaphragm), or a *consequence of* diaphragm fatigue (i.e., accessory inspiratory muscles are recruited at the onset of diaphragm fatigue to compensate for reduced diaphragm capacity). For instance, Johnson et al. (1993) showed that subjects who exhibited a progressive decline in diaphragm contribution relative to accessory muscles during maximal exercise also exhibited less severe diaphragm fatigue at exercise cessation. This study suggested that the onset of diaphragm fatigue, even at an early stage of exercise, may trigger the recruitment of accessory muscles. In endurance-trained athletes, Guenette et al. (2010) found that male athletes experienced a progressive decrease in diaphragm contribution (–12%) with a concurrent increase in accessory muscle contribution during incremental exercise compared to their female counterparts. Female athletes, on the other hand, experienced only a negligible reduction in diaphragm contribution (–3%). Interestingly, there was a greater reduction in $\Delta P_{di,tw}$ in males athletes compared to the female athletes (–20 *vs*. –13%; $p < 0.05$). Accordingly, male athletes exhibited a greater reliance on accessory inspiratory muscles compared to female athletes, but still exhibited a greater severity of diaphragm fatigue at exercise cessation. In line with the findings by Johnson et al. (1993), these results suggested that the recruitment of accessory inspiratory muscles may be an early response at the onset of diaphragm fatigue in an attempt to prevent or delay further fatigue.

The recruitment of accessory inspiratory muscles during exercise may, however, evoke adverse effects on ventilatory capacity. For instance, a higher contribution and dependence on accessory

muscles may distort the chest wall (Goldman et al., 1976; Grimby et al., 1976), and thereby reduce the efficiency of breathing and increase the work of breathing (Hart et al., 2002). This response would further increase the demand for blood flow and O_2 to the respiratory muscles (Dempsey et al., 2006). Global fatigue of inspiratory muscles have also been found to increase the intensity of dyspnoea (Gandevia et al., 1981; Supinski et al., 1987), although this phenomenon does not appear to be specific to diaphragm fatigue alone (Ward et al., 1988).

Another implication of global inspiratory muscle fatigue is the change in breathing pattern. Specifically, global fatigue of inspiratory muscles appears to alter breathing pattern significantly during subsequent hypercapnic hyperpnoea (Gallagher et al., 1985; Yan, Sliwinski, et al., 1993), but diaphragm fatigue specifically does not (Yan, Lichros, et al., 1993). This appears to be true also during exercise-induced hyperpnoea, because only global fatigue of inspiratory muscles appears to adversely affect breathing pattern (Mador & Acevedo, 1991), not diaphragm fatigue specifically (Welch et al., 2018). Global fatigue of inspiratory muscles has usually been manifested as a tachypnoeic breathing pattern, whereby ventilatory demand is met with lower V_T and higher f_R at the same level of ventilation (Gallagher et al., 1985; Yan, Sliwinski, et al., 1993). When V_T declines, less intrathoracic pressure is required per breath, which reduces inspiratory muscle workload and avoids further development of fatigue.

Perhaps a more important implication of diaphragm fatigue is the respiratory muscle fatigue-induced metaboreflex; that is, a systemic, cardiovascular phenomenon that accelerates fatigue of limb locomotor muscles and consequently limits exercise tolerance (Romer & Polkey, 2008). Evidence suggest that rhythmic diaphragm contractions and accumulation of metabolites (e.g., H^+) evoke afferent feedback from metaboreceptors in the diaphragm via group III and IV phrenic afferents (Hill, 2000; Rodman et al., 2003). The afferent feedback is projected to supraspinal centres in the brainstem, resulting in increased sympathetic tone and systemic vasoconstriction that reduce limb blood flow and vascular conductance, and that elevates mean arterial pressure (Hill, 2000; Rodman et al., 2003).

Conclusively, the implications of inspiratory muscle fatigue generally, and diaphragm fatigue specifically, may increase the sensation of breathing effort and perceived exertion during exercise; both of which reduce exercise tolerance and promote exercise cessation (Romer & Polkey, 2008; Welch et al., 2018). At least in healthy adults, diaphragm fatigue does not appear of adversely affect alveolar ventilation (Babcock et al., 1995, 1996; Johnson et al., 1993) or breathing pattern (Welch et al., 2018) during exercise. However, the redistribution of blood flow from limb locomotor muscles to respiratory muscles via the respiratory muscle fatigue-

induced metaboreflex may limit exercise tolerance in healthy adults (Dempsey et al., 2006; Sheel et al., 2018).

2.5 Ultrasonography of skeletal muscle contractile properties

Supposedly one of the most 'elegant diagnostic approaches in clinical medicine' (European Respiratory Society, 2018, p. 4), ultrasonography has become an important tool in clinical diagnostics since it was first developed in the late 1940s (Scatliff & Morris, 2014). Moreover, within the area of biomechanics, ultrasonography as become a tool for the assessment of skeletal muscle architectural features and contractile properties (Pillen, 2010). For instance, ultrasonography has shaped our current understanding of muscle-tendon properties (Cronin & Lichtwark, 2013) and the influence of architectural attributes (e.g., pennation angle, thickness and fascicle length) on force development (Hodges et al., 2003). Ultrasound studies of skeletal muscle anatomical features, such as thickness and cross-sectional area, have also demonstrated the plasticity of skeletal muscles with disuse, atrophy and weakness (Bunnell et al., 2015; Goligher, Fan, et al., 2015).

To explore intramuscular processes involved in fatigue, a number of ultrasound studies have assessed the acute architectural changes in skeletal muscle induced by fatigue. For instance, following fatigue induced by (single) leg press exercise at maximum power (mean ± *SD* 91 ± 19 kg with maximal shortening velocity), Csapo et al. (2011) found that ultrasound-derived thickness and pennation angle of vastus lateralis increased by 7% and 10%, respectively (both $p < 0.05$ vs. baseline). Conversely, fascicle length decreased by 2% ($p < 0.05$ vs. baseline). The physiologic mechanisms that underpin these acute changes in muscle architecture are not entirely clear. Some have attributed these acute changes to increased vascular perfusion during and immediately after exercise (Brancaccio et al., 2008), while others have suggested that muscle tonic activity may remain elevated well into recovery, causing muscle thickness and pennation angle to remain elevated into recovery (Csapo et al., 2011).

It is necessary, however, to discuss to what extent these architectural changes can occur within the fatigued human diaphragm. The existing literature on acute architectural changes with fatigue pertains specifically to unipennate or bipennate muscles, in which fascicles are oriented obliquely to the aponeuroses. Thus, fascicles and pennation angle can be readily measured using ultrasound (Hodges et al., 2003). Conversely, diaphragm muscle fibres radiate from the central tendon and inserts at the ventrolateral aspect of L1-3 and the aponeurotic arcuate ligaments (crural diaphragm), and the xiphoid process and upper margins of the lower six ribs (costal diaphragm) (De Troyer & Boriek, 2011). There are two ways to perform diaphragm ultrasonography: using a *subcostal* approach to image the posterior crural diaphragm dome, or an *intercostal* approach to image the costal diaphragm at the zone of apposition (Ferrari et al.,

2018). Neither of the two approaches can image the diaphragm at the level of the fascicles. This is due to the anatomical structure and fibre orientation of the muscle, its depth within the thorax and the angles from which the muscle can be imaged (see section 3.10). Thus, ultrasound assessment of the diaphragm is not necessarily comparable to ultrasound assessment of pennate limb locomotor muscles.

Diaphragm ultrasonography was originally developed for use in the intensive care unit (ICU). Understanding diaphragm function is particularly important in patients undergoing invasive mechanical ventilation due to the rapid rate of diaphragm atrophy seen in this population (Bunnell et al., 2015; Goligher, Fan, et al., 2015). Specifically, diaphragm ultrasonography is used to measure the thickness and thickening (or the lack thereof) of costal diaphragm during quiet tidal breathing in order to detect muscle weakness, and thereby to mitigate implications associated with weaning failure, respiratory distress and potential reintubation (Goligher et al., 2018). Because the costal diaphragm thickens upon inspiration, and this thickening is measurable using an intercostal approach (see Figure 3.10.1 and Figure 3.10.2 for examples), ultrasound-derived diaphragm thickening serves as an estimates of costal diaphragm shortening *in vivo* (Ferrari et al., 2018; Wait et al., 1989). Moreover, the use of intercostal ultrasonography to assess costal diaphragm thickening appears to be feasible in most populations, and exhibit high levels of intra- and inter-rater reliability in healthy adults (Cohn et al., 1997; Harper et al., 2013; Oppersma et al., 2017; Ueki et al., 1995) and critically ill patients (Dubé et al., 2017; Goligher, Laghi, et al., 2015; Santana et al., 2016; Vivier et al., 2012).

Subcostal ultrasonography enables the assessment of crural diaphragm craniocaudal excursion (descent) during quiet breathing and various manoeuvres, such as maximal inspiratory and expiratory efforts (Testa et al., 2011) and IC manoeuvres (Corbellini et al., 2018; Santana et al., 2016). Originally, diaphragm excursion was measured using fluoroscopy, but due to the ionising radiation associated with fluoroscopy, the method was replaced by ultrasonography in the mid-1990s (Houston et al., 1992, 1995; Scatliff & Morris, 2014). The subcostal ultrasound approach is unique because it images *posterior* crural diaphragm from the *anterior* view at a depth of 20-30 cm (see Figure 3.10.3 and Figure 3.10.6 for examples). From this view, the crural diaphragm dome can be seen as moving closer to the ultrasound transducer during inspiration by moving vertically in the B-mode ultrasound. Further, diaphragm excursion can be readily measured with digital calliper tools in specialised ultrasound software packages in motion (M-) mode ultrasound; that is a real-time motion capture along a single scan line. Because M-mode ultrasound captures diaphragm excursion as a function of time, it is also

possible to measure diaphragm excursion time. In turn, the rate of diaphragm decent (excursion velocity) can be calculated as the quotient of excursion divided by excursion time (Kocis et al., 1997; Testa et al., 2011). Moreover, because skeletal muscle power is the dot product of force and shortening velocity, diaphragm power can be estimated by multiplying diaphragm force (i.e., mean inspiratory $\overline{P}_{di}$ or $\Delta P_{di,tw}$) by excursion velocity. Because diaphragm excursion (displacement), velocity, force and power are fundamental elements within the field of dynamics and kinetics, these ultrasound-derived indices will from hereon be referred to as *diaphragm kinetics*.

Because subcostal ultrasonography of is feasible in most individuals (Boussuges et al., 2009; Gerscovich et al., 2001), a number of studies have assessed diaphragm excursion during spontaneous breathing (Dres et al., 2017; Umbrello et al., 2015; Vivier et al., 2012), deep breathing (Boussuges et al., 2009; Santana et al., 2016; Umbrello et al., 2015), or other manoeuvres. This includes maximal sniff manoeuvres (Boussuges et al., 2009; Fayssoil et al., 2019), and forced expiratory efforts (Testa et al., 2011). There are, however, few studies that have used ultrasonography to better understand the contractile velocity of mammalian diaphragm; and even fewer have attempted to use ultrasonography to estimate diaphragm power.

Compared to other imaging techniques, such as x-ray and fluoroscopy, two-dimensional ultrasound requires little equipment beyond a commercially available ultrasound machine. Moreover, sonographers performing diaphragm ultrasonography require little training to produce reliable measures of diaphragm movement (Testa et al., 2011). To further promote the use of diaphragm ultrasonography in clinical populations, the European Respiratory Society (ERS) in 2018 included diaphragm ultrasonography in the ERS Monograph for thoracic ultrasound (European Respiratory Society, 2018). In their latest statement on thoracic ultrasound (Laursen et al., 2021), ultrasound of the diaphragm and intercostals are both included. By including normative reference values of diaphragm excursion and thickening, as well as detailed instructions on image acquisition, the ERS is continuously promoting the implementation of diaphragm ultrasonography internationally and across respiratory pathologies.

2.5.16 Ultrasonography for the assessment of diaphragm fatigue

Despite the well-established application of ultrasound in the area of biomechanics and in the ICU, the technology has rarely been used to assess the contractile properties of fresh and fatigued diaphragm muscle in healthy humans. Albeit in piglets, Kocis et al. (1997) performed

what is likely the only study to have used ultrasonography for the assessment of diaphragm contractile velocity after external loading. As mentioned above, M-mode ultrasound captures diaphragm descent as a function of time (time-capture), enabling the calculation of excursion velocity. Because diaphragm excursion velocity is the rate at which the diaphragm contracts and descents, the measure is used an *in vivo* estimate of shortening velocity (Kocis et al., 1997; Testa et al., 2011). Briefly, Kocis et al. (1997) measured diaphragm force (P_{di}) and diaphragm excursion velocity during hypercapnic hyperpnoea before and after inducing fatigue by electrical phrenic nerve pacing. Expectedly, the authors reported a decrement in P_{di} tidal swings (–46%; $p < 0.05$ relative to baseline) after the induction of fatigue. However, diaphragm fatigue also resulted in a marked slowing of inspiratory excursion velocity (–38%; $p < 0.05$), which was attributed to a decline in craniocaudal excursion (–39%) while excursion time remained unaffected by fatigue. The authors ultimately concluded that the fatigued diaphragm moves less and slower than compared to fresh state (Kocis et al., 1997).

The findings by Kocis et al. (1997) are in line with the number of studies showing that isolated diaphragm fibres *in vitro* exhibit a decline in force and slowing of shortening velocity with fatigue (e.g., Ameredes et al., 2006; Coirault et al., 1995). Because the human diaphragm exhibits similar force-velocity-power, length-tension and force-frequency relations as seen in other skeletal muscles, it is intuitive that shortening velocity of the diaphragm *in vivo* is also impaired with fatigue. However, as pointed out repeatedly in this literature review, it has not been feasible to measure directly human diaphragm shortening or shortening velocity for the human diaphragm *in vivo*. Being able to quantify diaphragm shortening and shortening velocity in humans will facilitate a greater understanding of dynamic contractile properties of this unique muscle. Moreover, it will facilitate a greater understanding of how dynamic contractile properties may be impaired in fatigue. In order to achieve this, however, diaphragm ultrasonography must first be shown to be feasible, valid and reliable in response to standardised perturbations (e.g., phrenic nerve stimulation and hypercapnic hyperpnoea) in healthy adults. It may then be possible to use ultrasonography to quantify the dynamic diaphragm contractile properties during various modes of hyperpnoea to better understand diaphragm function during increasing ventilatory drive. Finally, ultrasonography may be used to assess the potential loss of dynamic diaphragm contractile properties with external loading and fatigue.

2.6 Thesis aims

Based on the abovementioned considerations, the overarching aim of this thesis was to evaluate the usefulness of ultrasonography for the assessment of *in vivo* contractile properties of fresh and fatigued diaphragm in healthy humans. This was achieved in five experimental chapters with the specific aims as follows:

i. To determine the feasibility, validity, and within-day reliability of ultrasound-derived measures of crural diaphragm kinetics (i.e., excursion, excursion time, excursion velocity and power) and costal diaphragm shortening in response to stimulation-evoked contractions and maximal inspiratory efforts (sniffs) (*Chapter 4*)

ii. To determine the feasibility, validity, and within-day reliability of ultrasound-derived measures of crural diaphragm kinetics and costal diaphragm shortening during hypercapnic hyperpnoea (*Chapter 5)*

iii. To evaluate the feasibility of subcostal ultrasonography for the assessment of crural diaphragm kinetics during exercise- and non-exercise-induced hyperpnoea, and to compare diaphragm kinetics across the two modes of hyperpnoea to elucidate the mechanisms that underpin postural-ventilatory modulation of the diaphragm (*Chapter 6*).

iv. To assess the effect of external loading (pressure- and flow-loading) on diaphragm kinetics and force output to elucidate the mechanisms that underpin task-dependency of diaphragm fatigue (*Chapter 7*).

v. To assess the effect of external loading (pressure- and flow-loading) on costal diaphragm shortening and force to better understand the effect of loading on the muscle's ability to shorten. (*Chapter 8*).

Chapter 3

General Methods

3.1 Introduction

This chapter provides a detailed description of the methods, techniques and equipment used in this thesis. In addition, this chapter includes a detailed description of calibration procedures as well as the analysis procedures used to generate the data presented in each experimental chapter.

3.2 Ethics approval and participant recruitment

The studies included in this thesis received ethical approval from Brunel University Research Ethics Committee. Minor changes were made to some of the study protocols and amendment forms were submitted and approved (letters of approval in Appendix 1). All studies conformed to the most recent standards of the Declaration of Helsinki (World Medical Association, 2013). For three of the studies, financial support was provided to participants in the form of Amazon vouchers.

During recruitment, eligible volunteers received a study-specific participant information sheet (Appendix 3), and verbal information about the study: volunteers were informed that they could withdraw from the study at any given time without subsequent penalty or prejudice. Student volunteers were reassured that potential withdrawal would not affect their university grades. Volunteers were further required to complete a standardised health questionnaire, confirming that she/he had no medical history of cardiovascular, respiratory or neuromuscular disease, and no known allergy/hypersensitivity to latex or local anaesthetics (Appendix 2). Finally, volunteers provided written informed consent (Appendix 2).

3.3 Participant information

Participants were recruited from the university student population and the surrounding area (London Borough of Hillingdon). Participants were required to be healthy, recreationally active, non-smoking adults with BMI within normal range (18-30 kg/m^2). Moreover, participants were required to have pulmonary function within normal limits (see section 3.5). Specific inclusion and exclusion criteria for each study are shown below.

Chapters 4 (Part 1) and 6:

Male and female volunteers between ages of 18-30 y were recruited. Biological sex was self-reported as per the standardised health questionnaire (Appendix 2), and an equal number of male and female participants were recruited (n = 5 of each sex). Due to the use of latex-rubber rebreathe bags used for hypercapnic hyperpnoea, individuals with allergy or hypersensitivity to latex were not included.

Chapters 4 (Part 2), 5, 7 and 8:

Male volunteers between ages of 18-40 y were recruited. Only participants of (self-reported) male sex were included in this study due to the limited resources and time available to include female participants and to control for menstrual cycle phase in multi-visit studies. Given that these studies were considered exploratory and hypothesis-generating, a study sample including only one biological sex enhanced the homogeneity of the study sample. Due to the use of intercostal ultrasonography to quantify diaphragm thickness during spontaneous breathing, participants had to demonstrate diaphragm thickening during spontaneous breathing at rest (Harper et al., 2013).

Participant preparations

Prior to all experimental visits, participants were asked to refrain from strenuous exercise for ≥24 h to avoid the potential influence of exercise-induced respiratory muscle fatigue on dyspnoea and exercise tolerance (Gandevia et al., 1981; Ward et al., 1988), breathing pattern during subsequent hypercapnic hyperpnoea (Gallagher et al., 1985; Mador & Acevedo, 1991), and diaphragm force (e.g., $\Delta P_{di,tw}$) (Babcock et al., 1996; Johnson et al., 1993). Because respiratory muscle fatigue may persist up to 24 h (Laghi et al., 1995), it was considered reasonable to ask participants to refrain from strenuous exercise for ≥24 h prior to all laboratory visits.

Participants were asked to refrain from caffeine for >12 h due to the effects of caffeine and theophylline on pulmonary function and diaphragm contractility. Theophylline, found alongside caffeine in tea and cocoa, increases fresh diaphragm contractility by increasing the efflux of Ca^{2+} from sarcoplasmic reticulum, thereby increasing contractility at the cross-bridge level (Aubier, 1986). Theophylline may also delay the onset of diaphragm fatigue and reduce fatigue recovery time (Murgiano et al., 1984). Similarly, caffeine prolongs the time to exhaustion during loaded breathing and reduces the sense of breathing effort (Supinski et al., 1986), and may also increase sensitivity to CO_2 during hypercapnic rebreathing (D'Urzo et al., 1990). The mean half-life of caffeine and theophylline in blood is 4-6 h (Benowitz, 1990) and ~8 h (Jilani et al., 2019), respectively. It was therefore considered reasonable to ask participants to refrain from caffeine (and theophylline) for >12 h prior to all laboratory visits. Lastly, participants were asked to refrain from eating ≥3 h prior to all laboratory visits due to postprandial effects on abdominal compliance, which increases $\Delta P_{di,tw}$ via an increased gastric component (Man et al., 2002).

It must be noted that neither day nor phase of menstrual cycle, or the use of contraceptives, were controlled for in female participants (Chapters 4 and 6). Indeed, within-cycle fluctuations in female reproductive hormones (oestrogen and progesterone) may alter CO_2 sensitivity during hypercapnic rebreathing (Dutton et al., 1989). Also, resting ventilation and end-tidal partial pressure for CO_2 ($P_{ET}CO_2$) appear to be lower during early follicular phase and mid-luteal phase compared to late follicular phase, although ventilatory responses to normoxic exercise do not appear to differ between phases of menstrual cycle (MacNutt et al., 2012). Despite these considerations, it was concluded that it was not necessary to control for menstrual cycle due to the within-day (not between-day) designs used in these studies.

3.4 Anthropometric measurements

For screening purposes, semi-nude body mass and erect stature were measured using an electronic measuring station (Seca 798, Hamburg, Germany). The participant stood erect with heels, buttocks and shoulders touching the stadiometer and head positioned in the Frankfort plane. Chest depth and width were measured using an anthropometer (Harpenden, Holtain Ltd., Crymych, UK) at the level of the xiphoid process at relaxation volume. Chest circumference was measured with a circumference measuring tape (Seca 201, Hamburg, Germany) at the xiphoid process, again at relaxation volume.

3.5 Pulmonary function tests

3.5.1 Whole-body plethysmography

As per the definitions from the European Respiratory Society (Wanger et al., 2005), the term ‘lung volume’ refers to the volume of gas within the lungs measured with whole-body plethysmography, gas dilution or nitrogen washout. In this thesis, absolute lung volumes were measured for screening purposes using whole-body plethysmography to ensure that all participants exhibited absolute lung volumes within normal limits.

Principles of plethysmography

Plethysmography is based on the principles of Boyle’s law (1660): ‘For a fixed amount of gas in a closed compartment the relative changes in the compartment’s volume are always equal in magnitude but opposite in sign to the relative changes in pressure’ (from Criée et al., 2011). In a whole-body plethysmograph, this means that the box and subject are both ‘closed compartments’ and, assuming isothermal conditions and no leaks, that any change in pressure in the closed compartments equals a change in volume of similar, but opposite, magnitude. Moreover, the compartments’ volumes (i.e., subject and box volumes) are known: the subject

volume is calculated from body mass, and the box volume is measured during box calibration (Criée et al., 2011). In addition, one pressure transducer is positioned inside the box to measure box pressure (P_{box}), and one pressure transducer is positioned in the mouthpiece to measure mouth pressure (P_{mo}) as an estimate of alveolar pressure (P_A) (Goldman et al., 2005).

During the standardised series of 'linked' manoeuvre for the assessment of absolute lung volumes (see below), airways are occluded at EELV by a shutter in the mouthpiece. Despite airway occlusion, the volume of gas remaining in the lungs ('shift volume', $\dot{V}$) can still be compressed and decompressed during the well-established 'panting manoeuvre' by movement of the thoracic wall (Criée et al., 2011). Although this is a compression and decompression of thoracic gas *volume*, it is recorded as a change in *pressure* by the pressure transducer at the mouth (ΔP_{mo}). In turn, ΔP_{mo} is used in the calculation of thoracic gas volume (TGV), also referred to as functional residual capacity (FRC), with the equation:

$$TGV = \frac{\Delta \dot{V}}{\Delta P_{mo}} \times \Delta P_{BOX},$$

where $\Delta \dot{V}$ is the 'shift volume', and ΔP_{box} is the pressure in the box (Goldman et al., 2005). FRC can then be calculated by subtracting the dead space of the apparatus ($\dot{V}_{d,app}$) and the volume of air inspired above EELV ($\dot{V}_{r,occ}$) from the equation:

$$FRC_{pleth} = TGV - \dot{V}_{d,app} - \dot{V}_{r,occ}$$

Accordingly, FRC is the volume of gas present in the lung at EELV during tidal breathing (Wanger et al., 2005). Once FRC is established, the additional lung volumes are measured by asking the participant to exhale maximally to quantify expiratory reserve volume (ERV), which is volume of gas that can be exhaled from FRC (Figure 3.5.1). From here, a slow inspiratory manoeuvre is performed to quantify inspiratory capacity (IC) and inspiratory reserve volume (IRV). IRV is the maximum volume of gas that can be inhaled from FRC (Wanger et al., 2005). Residual volume, which is the volume of gas remaining in the lung after maximal exhalation, is calculated as the difference between ERV and FRC. Total lung capacity (TLC) is calculated as the sum of all volume compartments.

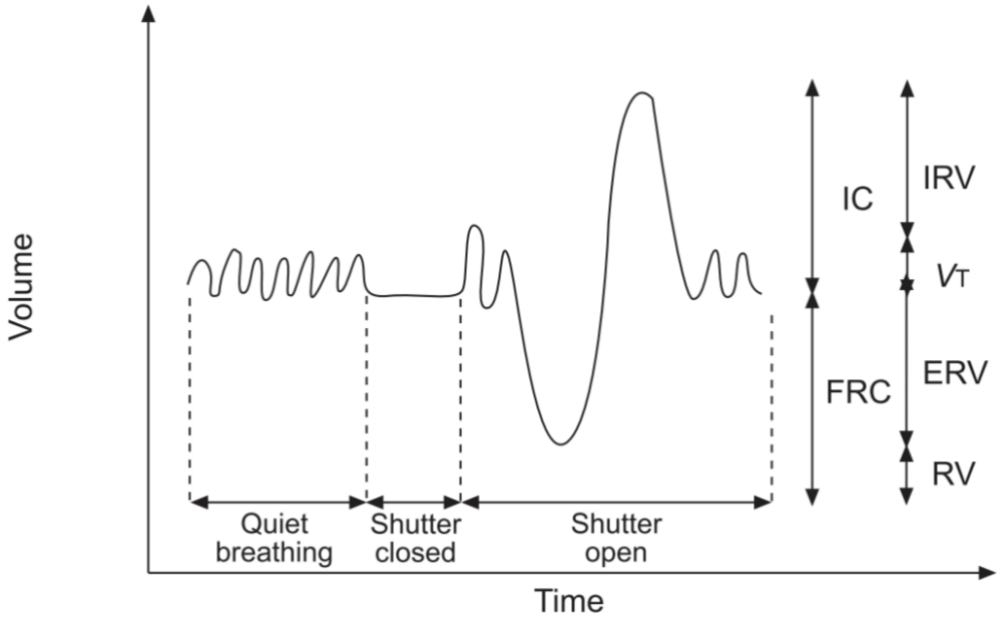

Figure 3.5.1 Volume-time display of 'linked' manoeuvres to measure absolute lung volumes during whole-body plethysmography. From "Standardisation of the measurement of lung volumes", by Wanger et al., 2005, *European Respiratory Journal*, 26(3), p.511-522.

Procedures

Whole-body plethysmography was performed using a calibrated volume-displacement plethysmograph box (1110 L) and a Lilly type pneumotachograph (MasterScreen PFT system, CareFusion, Basingstoke, UK). The Lilly type pneumotachograph determines the pressure drop across a fine metal mesh, which offers and fixed, known resistance to the exhaled and inhaled breath (de Jongh, 2008). Flow is calculated by dividing the pressure drop by the known resistance of the mesh, which is then used to calculate volume by time integration (Milanzi et al., 2019). To avoid contamination of the pneumotach by sputum or moisture, participants breathed through low-resistance, disposable filters (MicroGard IIC, CareFusion) attached to the mouthpiece assembly.

In line with current guidelines (Wanger et al., 2005), absolute lung volumes were measured in the series of 'linked' manoeuvres described above. The participant was seated upright and wore a nose-clip throughout the test. The series of 'linked' manoeuvres was always initiated with the participant breathing quietly for 5-10 breaths for the assessment of tidal volume (V_T). The 'linked' manoeuvres were performed until at least three FRC values, derived from satisfactory manoeuvres, were within 5% (Wanger et al., 2005). The mean FRC value from these three manoeuvres was reported.

Calibration

The plethysmograph and pneumotachograph were calibrated immediately prior to use. The calibration comprised three steps: first, ambient temperature, barometric pressure, relative humidity, and altitude were manually input into the system (JLAB, v5.72.1.77, CareFusion, Hoechberg, Germany) to adjust for body temperature and the pressure of saturated water vapour (BTPS correction). Second, the pneumotachograph was volume calibrated by manually delivering a defined volume of air (3 L) via a certified syringe (T604, CareFusion) at constant flow. Third, the box pressure and box leak (half-value time of the box) were determined through automatic box calibration. Immediately prior to testing, the box underwent equilibration of temperature and humidity with the subject seated inside the box for one minute (Goldman et al., 2005).

Participant considerations

Because participants were asymptomatic lifelong non-smokers with BMI within normal range, predicted values for TLC, RV and FRC were calculated based on the reference equations of Stocks & Quanjer (1995). For screening purposes, absolute lung volumes were compared to lower- and upper-limits of normal (LLN and ULN, respectively), defined as the 5^{th} and 95^{th} percentile (±1.64 *SD*) of predicted values, respectively (Pellegrino et al., 2005). The regression equations were specific to Caucasian ethnic group and included corrections for sex, stature and age. For Black and Asian participants, predicted values for FRC and TLC were multiplied by 0.88, and the predicted value for RV was multiplied by 0.93 (Pellegrino et al., 2005).

3.5.2 Spirometry

As with whole-body plethysmography, spirometry was used as a screening tool to ensure participants' pulmonary function was within normal limits.

Principles of spirometry

Spirometry is a standard pulmonary function test that measures inhalation and exhalation of volumes of air as a function of time (Miller et al., 2005). Thus, spirometry determines the dynamic volumes and flows associated with inspiration and expiration. In this thesis, spirometry was performed using a Lilly type pneumotachograph (MasterScreen PFT system, CareFusion), as described under *whole-body plethysmography* above.

Spirometry is performed in a series of 'linked' manoeuvres that comprises three distinct phases: the first phase is a maximal inhalation to TLC, immediately followed a forceful exhalation, or 'blast (phase two; Figure 3.5.2). The third phase is a continuation of this forceful exhalation,

and is continued for 6 s *or* until further expiration cannot be achieved (Graham et al., 2019). This series of 'linked' manoeuvres produces the maximum flow-volume loop, from which dynamic lung volumes, capacities and flows can be derived. One of these indices is the forced vital capacity (FVC), which is the maximum volume of air exhaled with maximally forced effort from the maximal inspiration. The forced expiratory volume in one second (FEV_1) is the volume of air delivered in the first second of the forced expiration (Miller et al., 2005).

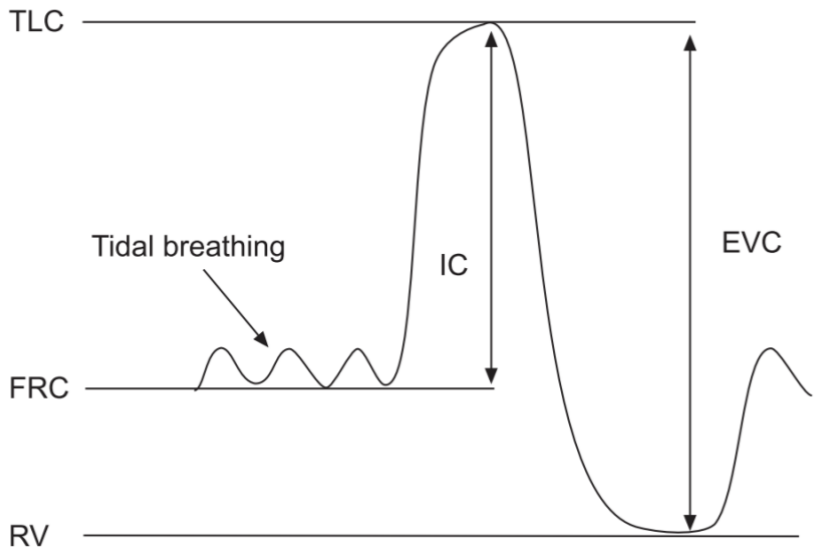

Figure 3.5.2 Volume-time display of 'linked' manoeuvres to assess dynamic capacities, volumes and flows during spirometry. EVC: expiratory vital capacity. From "Standardisation of spirometry", by Miller et al., 2005, *European Respiratory Journal*, 26(2), p. 319-338.

Procedures

In line with established guidelines (Graham et al., 2019; Miller et al., 2005), spirometry was performed as the series of 'linked' manoeuvres with three distinct phases described above. The participant was seated upright and wore a nose-clip throughout the test. Maximal forceful exhalation ('blast') lasted for 6 s *or* until further expiration could not be achieved (≤0.025 L change in volume for at least 1 s), and efforts were repeated until three successful efforts had been performed, with the total number of efforts not exceeding eight (Graham et al., 2019). The two largest measures of FVC and FEV_1 within 150 mL were recorded.

After publication of the updated guidelines on spirometry (Graham et al., 2019), minor adjustments were made to the execution of the test. For instance, the pause between full inspiration and maximal inspiration (phase one and two) was limited to ≤2 s and the acceptable

within-manoeuvre variability of FVC was reduced from 150 mL to 100 mL (Graham et al., 2019).

Calibration

The spirometer was calibrated immediately prior to use. The calibration process comprised two steps: first, ambient temperature, barometric pressure, relative humidity and altitude were manually inserted into the system software (JLAB, v5.72.1.77, CareFusion) for BTPS correction. Second, volume calibration of the pneumotach was performed by delivering a known volume of air (3 L) via a certified syringe (T604, CareFusion) at constant flow. Ambient temperature was measured by an internal thermistor (Ambient Unit, Jaeger, CareFusion) and confirmed by an independent, external thermometer (Graham et al., 2019).

Participant considerations

Measurements of FVC, FEV_1 and their ratio (FEV_1/FVC) were expressed as absolute values and as percent of predicted reference values based on the reference equations of Quanjer et al. (2012). For screening purposes, absolute values were compared to age-dependent LLN and ULN, calculated as the 5^{th} and 95^{th} percentile (±1.64 *SD*) of predicted values, respectively (Pellegrino et al., 2005). The reference equations of Quanjer et al. (2012) included adjustment factors for non-Caucasian participants (i.e., Black and Asian).

3.5.3 Maximal voluntary ventilation

Maximal voluntary ventilation over 12 s (MVV_{12}) was used for descriptive purposes. Assuming maximal effort from the participant, the test can provide important information regarding ventilatory capacity and breathing reserve during exercise (Wasserman et al., 2012).

MVV_{12} was measured using the Lilly type pneumotachograph (MasterScreen PFT system, CareFusion), as described for *spirometry* above. Prior to testing, the protocol was explained to the participant and correct breathing pattern was demonstrated by the investigator. The participant was seated upright and wore a nose-clip throughout the test. As per established guidelines (Miller et al., 2005), the participant was instructed to breathe maximally (deeply and rapidly) throughout the duration of the test, with verbal encouragement to promote maximal effort. It was ensured that respiratory frequency (f_R) was within 90-110 breaths/min, and the values from at least two acceptable manoeuvres with ≤10% between-manoeuvre variability were recorded. The highest of the two values retained for subsequent analysis (Miller et al., 2005). Predicted MVV_{12} was calculated as $FEV_1 \times 40$ (Miller et al., 2005).

3.6 Assessment of respiratory pressures

3.6.4 Maximal respiratory mouth pressures

Maximal respiratory mouth pressures were assessed to ensure that participants exhibited global respiratory muscle strength above age-specific LLN (Evans & Whitelaw, 2009). For this thesis, it was important to ensure that maximal inspiratory mouth pressure (MIP) was greater than the LLN because of the close relationship between MIP and diaphragm anatomical characteristics, such as diaphragm thickness and cross-sectional area (McCool, Conomos, et al., 1997), and diaphragm thickening during inspiratory efforts (Ueki et al., 1995).

Procedures

MIP was measured before maximal expiratory mouth pressure (MEP), with the participant seated upright wearing a nose-clip (Evans & Whitelaw, 2009; Green et al., 2002). Maximal inspiratory and expiratory efforts were generated against a semi-occluded (1.5 mm ID), flanged mouthpiece at RV (MIP) and TLC (MEP) using a hand-held, digital pressure meter (MicroRPM, CareFusion). Maximal pressures were measured as the most negative [MIP] and most positive [MEP] plateau mouth pressure generated over 1 s. For the assessment of MEP specifically, participants' cheeks were supported by the investigator to avoid activation of buccal muscles. A minimum of three and a maximum of eight efforts were performed at each lung volume, and the maximum value of three efforts that varied ≤10% was recorded (Green et al., 2002). Predictive reference values and LLN for maximal respiratory mouth pressures were calculated using the equations of Evans & Whitelaw (2009), accounting for sex and age.

3.6.5 Intrathoracic pressures

Intrathoracic pressures were assessed in all experimental chapters. Specifically, in Chapters 4 (*Part 1*) and 6, single-use balloon-tipped catheters (86 cm, Cooper Surgical, Trumbull, US) were used to measure oesophageal (P_{oe}) and gastric (P_{ga}) pressures. In Chapters 4 (*Part 2*), 5, 7 and 8, a multi-pair, gastro-oesophageal electrode catheter (Gaeltec Devices Ltd., Isle of Skye, Scotland) was used for the assessment of P_{oe} and P_{ga}.

Balloon-Tipped Catheters

The balloon-tipped catheters each comprised a guide wire and a polyethylene balloon (Figure 3.6.1), and were connected to a very low-pressure differential transducer (range ±0.6 to 225 cmH_2O, DP45, Validyne Engineering Corp., Northridge, CA, US). Prior to instalment, participants were offered ≤1 mL of topical anaesthetic (Instillagel, CliniMed Ltd., High Wycombe, UK) to ease insertion. Additional anaesthetic was applied to the catheter for

lubrication. Each catheter was carefully inserted into the preferred nostril and swallowed via peristalsis. Participants sipped water through a straw until the catheter was in the stomach.

Once in the stomach, the guide wires were removed, and the balloons were deflated from any air. The balloons were then filled with 1 mL (P_{oe}) and 2 mL (P_{ga}) of ambient air using a 10 mL glass syringe (Figure 3.6.1) (Zin & Milic-Emili, 2005). The volume of 1 mL in the oesophageal balloon was the minimal volume that ensured that pressure could be recorded, while the volume of 2 mL in the gastric balloon was sufficient to stop the balloon from collapsing when intraabdominal pressure was high, but still within the linear (balloon volume-intraballoon pressure) range reported for balloon-tipped catheter systems (Cross et al., 2015). The oesophageal balloon was then withdrawn from the stomach until a negative deflection in P_{oe} was seen in response to a sniff (~35-45 cm distal from the nostril, depending on erect stature).

Figure 3.6.1 Balloon-tipped catheters used for intrathoracic pressure measurements with 10 mL glass syringe used for balloon inflation.

The correct catheter position was confirmed by monitoring the agreement between P_{oe} and P_{mo} swings while the participant performed the 'dynamic occlusion test' (Baydur et al., 1982), whereby the seated participant performed graded inspiratory efforts against an occluded mouthpiece while wearing a nose-clip. Unity between changes in P_{oe} and P_{mo} confirmed that the oesophageal catheter was positioned in the optimal position to reflect pleural pressure (Baydur et al., 1982; Gibson et al., 2002). The catheters were then taped securely at the nose to ensure that their positions did not change throughout the course of the trial. All balloon-tipped catheters were checked for leaks prior to placement by soaking the inflated balloons in ultrapure water. Moreover, the volume of air in the balloons was checked frequently during the experimental trials to ensure that no leaks had occurred

Data acquisition

The analogue signals of intrathoracic pressures were passed through a signal amplifier (1902, Cambridge Electronic Design Ltd. [CED], Cambridge, UK) at a gain of 1000 Hz, digitised using an analogue-to-digital converter (1401mk-II, CED), and recorded at a frequency of 200 Hz. Mouth pressure (P_{mo}) was also recorded with this resolution, but derived from a side-port of the mouthpiece valve.

Calibration

Prior to use, each pressure transducer (incl. for P_{mo}) was calibrated by manually applying pressure to the transducer and a digital electromanometer (C9553, JMW, Harlow, UK) connected via rigid plastic tubing of 100 cm. Pressures were applied in increments of 10 cmH_2O across the physiological range (±225 cmH_2O) using a plastic syringe. Calibration curves and linear equations were then calculated and input into the data acquisition software (Figure 3.6.2). Linearity of the transducers was always ≥0.995 (r^2), and hysteresis was always within the manufacturer's pressure excursion limits of ≤0.25% (Validyne Engineering, 2020).

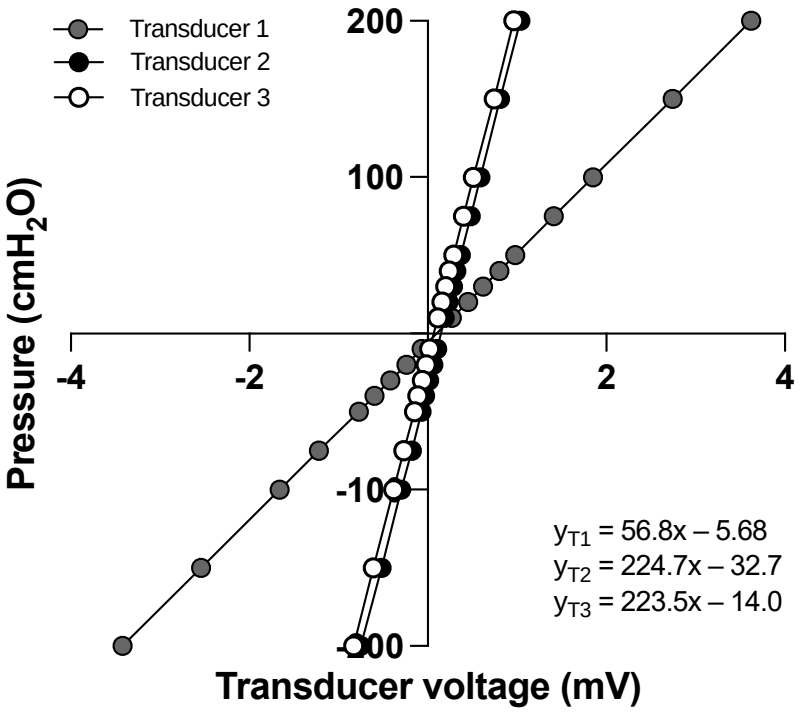

Figure 3.6.2 Calibration curves and linear equations for the three low-pressure differential transducers (T1-3). In this example, the transducers were calibrated across the range of ±200 cmH_2O.

Multi-pair gastro-oesophageal electrode catheter

The multi-pair gastro-oesophageal electrode catheter comprised silicone shaft (2.7 mm × 100 cm) with two integrated pressure transducers for the assessment of P_{oe} and P_{ga}, plus seven platinum electrodes for crural diaphragm electromyography (EMG_{di}; section 3.7) (Figure 3.6.3A). Again, topical anaesthetic was applied to the nostrils and the catheter to ease instalment. Both pressure transducers were first positioned in the stomach before the catheter was slowly withdrawn until a negative deflection was seen in P_{oe} in response to a sniff, indicating that the upper pressure transducer was positioned above the crural diaphragm (Figure 3.6.3B). Correct catheter position was confirmed by monitoring the agreement between P_{oe} and P_{mo} swings while the participant performed the "dynamic occlusion test", as described above (Baydur et al., 1982). Once in position, the catheter was taped securely at the nose to ensure that their positions did not change throughout the course of the trial.

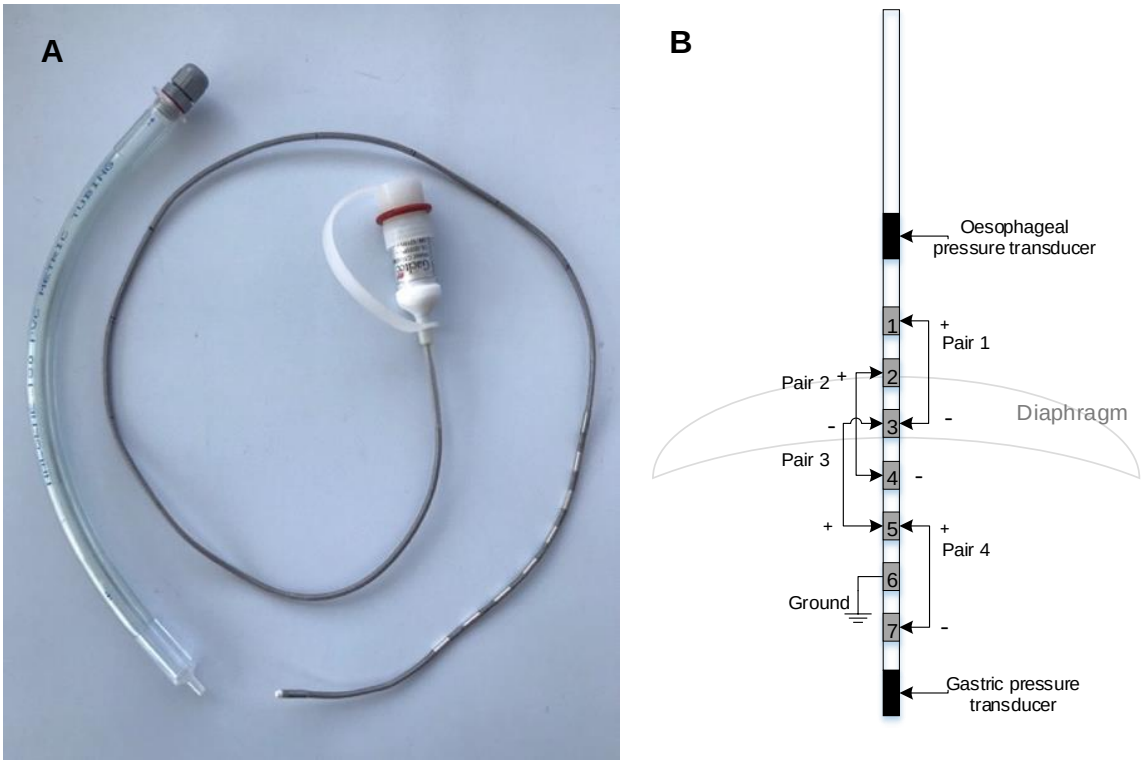

Figure 3.6.3 *A*) Multi-pair gastro-oesophageal catheter system with calibration tube (left). *B*) multi-pair oesophageal electrode catheter position in thorax. Two pressure transducers (black) were at the proximal and distal ends of the catheter and positioned on each side of diaphragm. Between pressure transducers, seven electrodes (grey) were paired (indicated by arrows), with one positive and one negative input terminal. The sixth electrode was ground.

Data acquisition

The analogue signals of intrathoracic pressure and EMG_{di} were passed through a signal amplifier (1902, CED) at a gain of 1000 Hz; digitised using an analogue-to-digital converter (1401mk-II, CED), and recorded at 200 Hz.

Calibration

To avoid systematic baseline drift, the catheter was soaked in ultrapure water for 2 h prior to use (Stell et al., 1999). The pressure transducers were then calibrated across the physiological range (±200 cmH_2O) using a calibration tube (Gaeltec Devices Ltd.; Figure 3.6.3A;). The catheter was sealed in the air-tight calibration tube which, in turn, was connected via a 50 mL plastic syringe to an electromanometer (C9553, JMW, Harlow, UK). Pressures were manually applied to the system, as described above. See Figure 3.6.4 for examples of calibration curves.

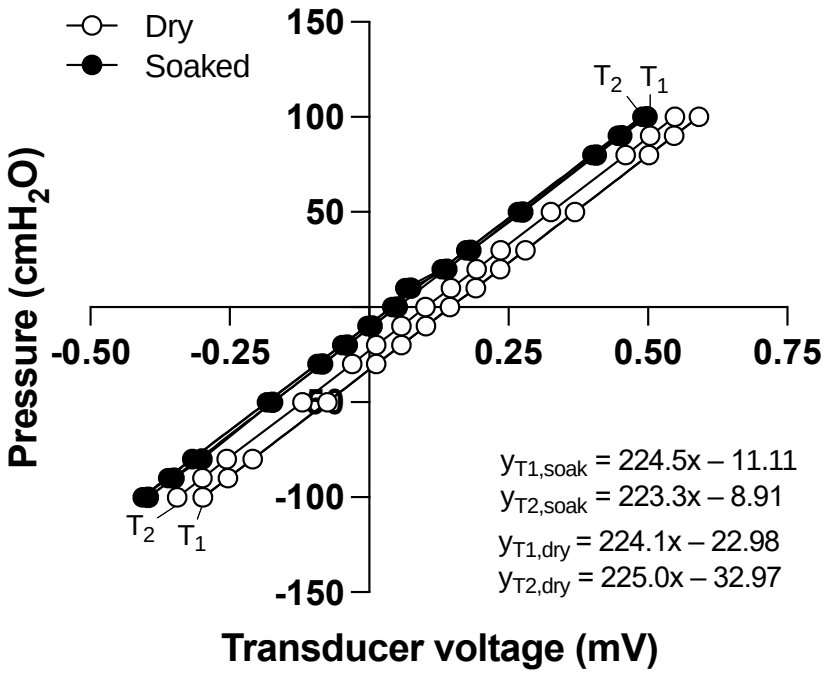

Figure 3.6.4 Calibration curve for the two pressure transducers in a dry and soaked state. Although data acquisition was performed only with soaked transducers (y_{1soak} and $y_{2,soak}$), the effect of soaking on pressures was evaluated by calibrating the dry transducers. In this example, the transducers were calibrated over ±100 cmH_2O.

Cleaning and sterilisation procedures

After each use, the catheter was cleaned and sterilised using a three-step procedure in line with manufacturer recommendations: first, the catheter was soaked in advanced tri-enzymatic formulation (40 mL, Sonozyme 3, Ultrawave Ltd., Cardiff, Wales) mixed with 8 L of tap water for 15 min. Next, the catheter was soaked in ortho-phthalaldehyde (Cidex Opa Solution, Cilag GmbH International, Zug, Switzerland) for another 15 min. Finally, the catheter was soaked in ultrapure water for three intervals of 15 min. Between each interval, the ultrapure water was discarded and replaced with a fresh quantity. After the final soak, the catheter was removed from the ultrapure water and left to dry in ambient room air before being sealed in a sterile bag until next use.

Service and control testing

Prior to project start, the multi-pair oesophageal catheter underwent service and control testing at the manufacturer's headquarters (Isle of Skye, Scotland). All EMG electrodes were refurbished and one pressure transducer was re-calibrated before the catheter was resealed. The hysteresis error of the pressure transducers was measured at 0.4-0.5%, which was within the range for low-range pressure transducers, as recommended by the manufacturer.

Partitioning active and passive pressures during spontaneous breathing

During spontaneous breathing, intrathoracic pressures were recorded breath-by-breath as waveforms. Tidal pressures were calculated as mean inspiratory pressures (i.e., $\overline{P}_{di}$, $\overline{P}_{ga}$ and $\overline{P}_{oe}$), using the equation of Barnard and Levine (1986), with $\overline{P}_{di}$ as example:

$$\bar{P}_{di} = \Sigma_0^n \, (P_{di}/n),$$

where *0* was the absolute P_{di} at the onset of inspiration, and *n* was equal to the number of data points during inspiration (Figure 3.6.5A). Because $\overline{P}_{di}$ included both passive ($\overline{P}_{di,p}$) and active ($\overline{P}_{di,a}$) components of inspiratory pressures, the two pressure components were distinguished by subtracting the lowest pressure during any given respiratory cycle from the instantaneous $\overline{P}_{di}$, as shown in Figure 3.6.5B. Accordingly, $\overline{P}_{di,a}$ was the mean pressure generated during tidal inspiration based on tidal pressure swings, whereas $\overline{P}_{di,p}$ was the pressure generated passively (e.g., isometric contractions, such as 'bracing' and trunk stabilisation with elevated intraabdominal pressure).

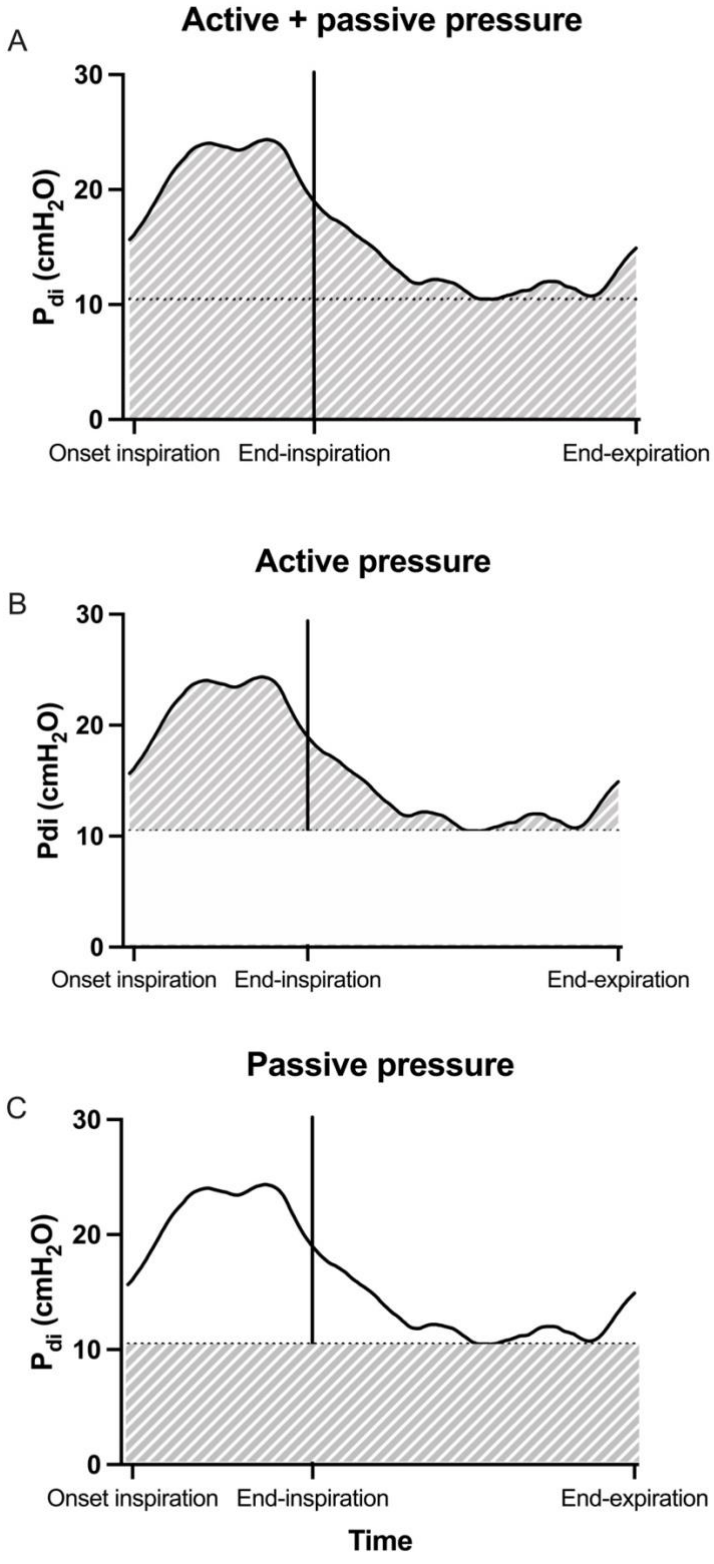

Figure 3.6.5 Tidal swing of transdiaphragmatic pressure (P_{di}). *A*) $\overline{P}_{di}$ was the mean inspiratory pressure using absolute pressure values, thereby including both active and passive components (grey-shaded area under curve). *B*) The active component of $\overline{P}_{di}$ ($\overline{P}_{di,a}$) was calculated by subtracting the lowest pressure during a given respiratory cycle from $\overline{P}_{di}$, thereby excluding the passive component of inspiratory pressure. *C*) The passive component of $\overline{P}_{di}$ ($P_{di,p}$) was pressure remaining when $\overline{P}_{di,a}$ had been subtracted (grey-shaded area).

3.7 Diaphragm electromyography

Diaphragm electromyogram (EMG_{di}) was assessed in Chapters 4, 5, 7 and 8. Specifically, compound muscle action potentials (M-waves) were assessed to determine the neuromuscular activation of diaphragm muscle in response to phrenic nerve stimulation, and the influence of external loading on M-wave characteristics.

Principles of electromyography

Electromyography is the assessment of myoelectric signals in the muscle caused by a propagating action potential along the muscle fibre membrane (depolarisation). To record the summated electrical activity of the depolarised muscle fibre membrane, electrodes are strategically positioned in close proximity to the specific muscle (Rodriguez-Falces & Place, 2018). Because only the electrical activity of motor units within close proximity to the electrodes is recorded, electrodes must be positioned as close to the muscle as possible. Thus, electrodes are usually placed directly *on* the skin over the evoked muscle (surface EMG) or by needle/wire electrodes inserted directly *in* the muscle (intramuscular EMG).

For the assessment of costal diaphragm EMG specifically, surface electrodes are most common, but are susceptible to signal contamination from accessory and non-respiratory muscles (Luo et al., 1998, 1999, 2008). For the assessment of crural diaphragm EMG, electrodes mounted on a gastro-oesophageal catheter are swallowed (Aldrich et al., 2005). Catheter-mounted EMG electrodes are less susceptible to signal contamination from other muscles but may instead be affected by cardiac artefacts (Luo et al., 1998, 1999).

Procedures

As described above (section 3.6.5), the multi-pair electrode catheter (Gaeltec Devices Ltd.) comprised a silicone shaft with two integrated pressure transducers for the assessment of P_{oe} and P_{ga}, plus seven platinum electrodes spaced by 3 cm for the assessment of EMG_{di}. As shown in Figure 3.6.3B, the seven platinum electrodes formed four sequential, bipolar electrode pairs plus an electrode for reference (ground). The benefit of using bipolar electrodes rather than monopolar electrodes is that the same action potential is captured twice when the electrical signal propagates along the muscle membrane, making the signal less susceptible to crosstalk from surrounding tissues (Aldrich et al., 2005). With bipolar electrodes, signal differential-amplification; that is, the subtraction of the signal at one electrode from that at the other electrode, and then an amplification of that difference, reduces the common noise for both

electrodes while the differential summed muscle action potential is recorded (Rodriguez-Falces & Place, 2018).

Data acquisition

The raw EMG_{di} underwent signal differential-amplification using an electrode adaptor (VED1902-11/4, CED), which was fed into the signal amplifier (1902, CED). The analogue signal was then digitised (Micro1401-3, CED) and recorded in the data acquisition software (Spike2, v9.0, CED) at a frequency of 4 kHz (Sinderby et al., 1998). Raw EMG_{di} was further processed with a notch filter (50 Hz) to remove power line artefacts and filtered with a band-pass filter of 10-1000 Hz (Luo et al., 1999). Each bipolar electrode pair represented one channel in the data acquisition software, meaning that four separate EMG_{di} channels were recorded. However, only the channel that produced the largest EMG_{di} amplitude was used for analysis (Luo et al., 1999; Luo et al., 2008). Specific analysis processes for EMG_{di} are outlined in respective experimental chapters.

Removal of ECG artefacts

Oesophageal catheter-mounted EMG electrodes are particularly susceptible to electrical interference from cardiac cross-talk. The electrical power of cardiac activity can be up to ten times stronger than that of EMG_{di}, with frequencies ranging from 25 to 250 Hz (Aldrich et al., 2005; Schweitzer et al., 1979). Thus, cardiac artefacts need to be removed with bespoke signal processing script to process EMG_{di}.

The script used in this thesis (Horseman, 2020b) removes a manually-determined number of data points comprising each QRS complex. Specifically, the user must identify the peak-to-peak amplitude and duration of a single QRS complex. The script algorithms then use linear interpolation to predict future QRS complexes of equivalent size and duration, assuming that future (and past) QRS complexes have similar characteristics. For instance, if a hypothetical QRS complex has a total duration of 80 ms and is recorded at a rate of 4 kHz, a total of 320 data points will be removed at each QRS complex throughout the data ((4000 Hz ÷ 1000 ms) × 80 ms = 320 data points), and replaced by the mean of surrounding data points.

3.8 Assessment of ventilatory- and gas-exchange indices

In Chapters 5, 6, 7 and 8, ventilatory and pulmonary gas-exchange indices were measured during hypercapnic hyperpnoea (CO_2-rebreathe), incremental cycling exercise and external-loading tasks.

Principles and procedures

Ventilatory and pulmonary gas-exchange indices were measured breath-by-breath using an online metabolic cart comprising a gas analysis system and a turbine flow-meter (Oxycon Pro, Jaeger, Viasys Healthcare, Hoechberg, Germany). The turbine flow-meter consisted of a low-resistance (<0.1 kPa/L/s), high-resolution (100 Hz) turbine with a bidirectional vane that span as a function of the airflow that passed through. The speed of airflow was detected by a beam of light that was broken each time the vane span (Dominelli & Sheel, 2012). The bidirectional vane used in this thesis had a flow and volume range of 0-15 L/s and 0-10 L, respectively. Expired gas composition was measured by drawing a gas volume of 320 mL/min through a rigid tube connected to the flow-meter for analysis with an ultra-fast, electrochemical (potassium hydroxide) fuel cell (O_2) and an infrared sensor, measuring absorption of infrared light by the gas sample (CO_2).

Calibration

The online system was calibrated immediately prior to each test within an experimental trial. This frequency of calibration was deemed important as accurate monitoring of $P_{ET}CO_2$ was a prerequisite for termination hypercapnic hyperpnoea (section 3.11). The calibration process comprised three steps: first, ambient temperature, barometric pressure, relative humidity and altitude were input into the system for BTPS correction. Second, volume calibration of the flow turbine was performed by delivering a known volume of air (3 L) via a certified syringe (T604, CareFusion) at constant flow. Third, gas analysers were calibrated using a certified gas (5.16% CO_2, 15.15% O_2, 79.7% N; BOC, Guildford, UK). All calibrations were repeated until there was ≤1% difference between the current calibration and the former calibration (Wasserman et al., 2012). The accuracy of the Oxycon Pro volume sensor is 50 mL (2%), with a resolution of 3 mL. The accuracy of the CO_2 infrared sensor is 0.05% with a resolution of 0.01%, whereas the accuracy of the O_2 high-speed analyser is 0.05-0.2% with a resolution of 0.01% (Viasys Healthcare, 2004).

Data acquisition and processing

To integrate ventilatory indices with intrathoracic pressures, the digital signals of volume, flow, and fractional end-tidal O_2 and CO_2 (F_EO_2 and F_ECO_2) were exported into the online data acquisition system via a digital-to-analogue signal converter (USB-30A16, μDAQ, Eagle Technology, Cape Town, South Africa), before being re-digitised using an analogue-to-digital converter (Micro1401-3, CED). The digital signals were recorded as waveforms in the data acquisition system at a frequency of 100 Hz, which was the highest frequency possible.

Once recorded, the digital signals were processed offline using bespoke scripts (Horseman, 2020a). Because the data were already BTPS corrected, it was not necessary to apply further corrections. However, because the raw volume signal was affected by incorrectable drift, inspired and expired tidal volumes were derived by numerical integration of the flow signal then corrected for minor drift with DC offset removal. Moreover, a virtual channel was created to convert F_ECO_2 to $P_{ET}CO_2$ (mmHg) in order to accurately determine the cut-off value for CO_2-rebreathe (55 mmHg); this conversion was based on the principles of Dalton's law, where $P_{ET}CO_2 = barometric\ pressure - 47 \times (F_ECO_2/100)$ (Wasserman et al., 2012).

Measurement of gas sample volume

Because hypercapnic hyperpnoea was performed in a closed circuit, the gas sample drawn for analysis of expired gas composition could deflate the closed-circuit rebreathe bag prematurely, particularly if the test duration was long. It was therefore necessary to measure the rate at which volume was extracted from the closed circuit. Briefly, the sample line of the gas analyser was connected to a manual dry-gas flow-meter (series FR4000, Key Instruments, Trevose, PA, US). When the gas analysers were on, the extraction of gas generated a negative pressure inside the manual flow-meter, causing a float inside the flow-meter to move on a visual scale ranging from 0.1 to 1.5 L/min (Figure 3.8.1). As stated above, the volume of gas extracted for gas analysis was 320 mL/min.

Figure 3.8.1 Manual dry-gas flow-meter. The black float indicated the rate at which air was extracted via the black sample tube. Note that the angle from which the picture was taken does not accurately show the flow rate.

Calculation and correction for signal delays

There were two delays in the online gas analysis system: first, there was the inevitable delay time from the transport of expired gases sampled at the mouth, transported via the sample line to the gas analysers, then to the online representation in the computer software. The delay time was determined by the gas calibration process (range 1.18-1.21 s), and was automatically corrected by the online software (JLAB, v5.72.1.77, CareFusion).

The second time delay was caused by the multi-step process of exporting volume, flow, F_ECO_2 and F_EO_2 from the online gas analysis system (JLAB, CareFusion) to the data acquisition system (Spike2, CED). The digital-to-analogue-to-digital conversion via an external signal converter resulted in a delay of ventilatory and gas-exchange signals relative to other signals sampled (e.g., intrathoracic pressures and EMG_{di}). This delay (~1.28 s) was measured by manually applying signal artefacts to the flow-meter, and then corrected with offline time-shift processing in the data acquisition software.

3.9 Magnetic stimulation of phrenic nerves

In Chapter 4, unilateral and bilateral magnetic stimulation of the phrenic nerve(s) were used to assess the feasibility, validity and reliability of diaphragm contractile responses to stimulation-evoked contractions. In Chapters 7 and 8, bilateral magnetic stimulation was used to identify changes from baseline in transdiaphragmatic twitch pressure ($\Delta P_{di,tw}$) and diaphragm kinetic and contractile responses following external loading.

Principles of magnetic stimulation

Magnetic stimulation is based on the principles of Faraday's law of induction, which states that the voltage evoked in a circuit is proportional to the rate of change of the magnetic flux through that circuit (in Matsumoto et al., 2013). Thus, the faster the change of electric current in the circuit, the greater will be the voltage of the magnetic field generated. Magnetic stimulators comprise a capacitor that holds static, electric energy that is rapidly transferred to coils of insulated wires upon triggering (Bellemare & Poirier, 2005). Magnetic stimulators can generate intense, and rapidly changing magnetic fields that penetrate clothing and soft tissue in order to stimulate the motor cortex and peripheral nervous tissue. However, because magnetic stimulation does not cause a direct depolarisation of nervous tissue by penetrating skin with electrical current (i.e., electrical stimulation), but instead creates magnetic pulses parallel to the coil in the body, the technique is virtually painless (Matsumoto et al., 2013; Similowski et al., 1989).

It is important to note, however, that depolarisation of nervous tissue can only occur if the current is of sufficient intensity (amplitude and duration). Moreover, the mechanical response (e.g., force or M-wave) can only reach a maximum when the current successfully depolarises all motor units innervated by the stimulated nerve (Man et al., 2004). To ensure that motor units are maximally stimulated it is necessary to increase stimulator intensity until increasing the stimulator intensity elicits no further increase in mechanical response (Bellemare & Poirier, 2005). It is therefore necessary to stimulate with currents greater than maximal stimulation intensity, thereby applying the principle of 'supramaximality' of stimulation which ensures consistency of maximal stimulation (Bellemare & Bigland-Ritchie, 1984).

It is also important to note that different insulated coils hold distinctive characteristics, and may serve different purposes. For instance, figure-eight coils (as used in this thesis) are more selective compared to circular coils used for cervical stimulation of phrenic nerves (Bellemare & Poirier, 2005; Mills et al., 1996). This difference stems from the faster transmission of

magnetic flux through and across small-surfaced coils, which ultimately generates stronger magnetic fields compared to larger coils. Nonetheless, figure-eight coils positioned at the posterior border of the sternocleidomastoids still evokes minor co-activation of sternocleidomastoids, brachial plexus and upper rib cage muscles. During unilateral stimulation of phrenic nerves, there may also be contralateral activation of opposite phrenic nerve (Mills et al., 1995).

Procedures

In Chapter 4 (*Part 1*), the right phrenic nerve was stimulated *unilaterally* by positioning an insulated figure-eight coil (D70 Alpha B.I, Magstim Company Ltd., Whitland, Wales) on the posterior border of the right sternocleidomastoid (Figure 3.9.1A) (Mills et al., 1995). In Chapter 4 (*Part 2*), 7 and 8, phrenic nerves were stimulated *bilaterally* by positioning two insulated figure-eight coils on the posterior borders of the left and right sternocleidomastoids (Figure 3.9.1B) (Mills et al., 1996). Coils were connected to two commercially-available magnetic stimulators (Magstim 200, Magstim Company Ltd.) connected to a paired-pulse stimulator module (BiStim, Magstim Company Ltd.). During unilateral stimulation, the paired-pulse stimulator module enabled the use of paired or repetitive stimuli with various inter-stimulus intervals to the common coil. During bilateral stimulation, the paired-pulse module enabled the triggering of both coils simultaneously with single (1 Hz) stimuli.

The correct coil positions were located by moving each coil systematically around the participant's neck area while stimulating 1 Hz at 70% of stimulator maximum power until the highest $\Delta P_{di,tw}$ was identified. The skin was then marked with a water-soluble skin-marking pen to ensure that subsequent stimulations were delivered at the same site. All stimulations were performed at relaxation volume against closed glottis by asking the participant to breathe quietly before closing the mouth at the end of a tidal expiration and raising the thumb to signal readiness. Participants were always seated in the semi-recumbent position (30° hip angle) wearing a nose-clip during stimulation.

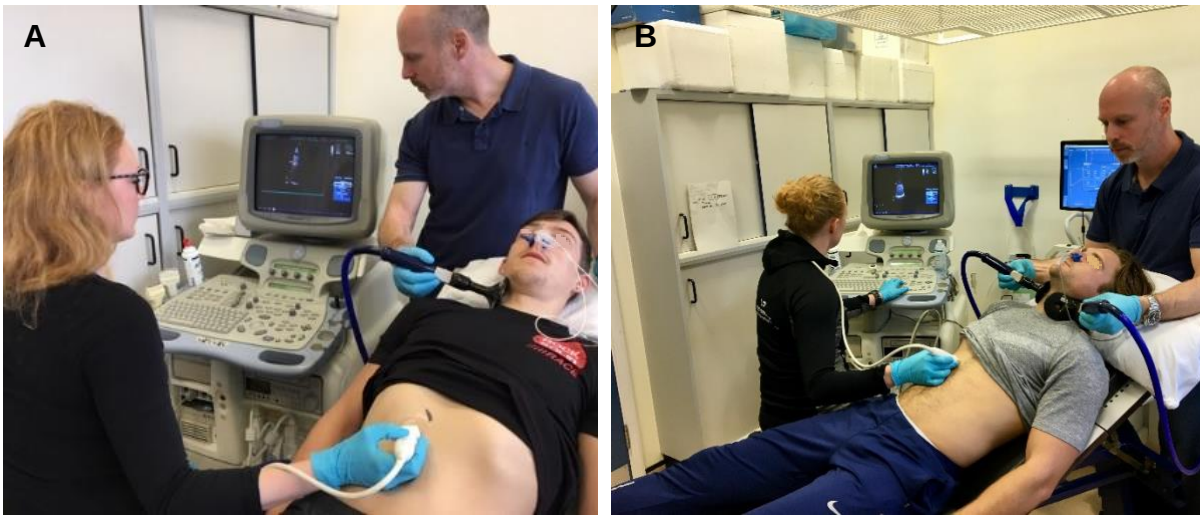

Figure 3.9.1 Unilateral (*A*) and bilateral (*B*) anterolateral magnetic stimulation of phrenic nerves.

Supramaximal stimulation of phrenic nerves

To check for supramaximal stimulation of phrenic nerves, participants underwent an incremental stimulation protocol comprised of 1 Hz stimuli at stimulator power ranging from 50 to 100% of maximum. Starting at 50%, stimulator power was increased by increments of 10% between 50 and 80%, and then by increments of 5% between 80 and 100%, with three twitches performed at each stimulator power. A plateau of $\Delta P_{di,tw}$ suggested that further increase of stimulation power would not result in further increase in diaphragm mechanical output, and was defined when mean $\Delta P_{di,tw}$ at submaximal and maximal stimulation intensities were equal to or less than the coefficient of variation (CV) for all twitches within an individual participant (Geary et al., 2019; Man et al., 2004).

3.10 Diaphragm ultrasonography

Ultrasonography was performed in all five experimental chapters. Ultrasound scans were conducted using a commercially-available ultrasound system (Vivid 7 Pro, GE Medical, Horten, Norway), with the participant in a semi-recumbent position (30° hip angle) and the sonographer on the participant's right side.

Principles of ultrasound

Unlike other imaging techniques, such as fluoroscopy and x-ray imaging, ultrasound uses sound waves instead of ionising radiation to produce images of tissues within the body. An ultrasound machine usually comprises a monitor, keyboard, data processor, data storage and the ultrasound transducer. Upon use, the ultrasound machine sends electrical signals to the transducer, which then produces the sound waves that penetrate the skin via acoustic transmission gel (Jacobsen, 2018). When sound waves interact with soft tissue structures (e.g., muscle, membranes and blood vessels), some of these sound waves are reflected back to the transducer and converted into electrical current for the monitor to produce the characteristic ultrasound image. The reflection of sound waves is especially prominent at soft tissue interfaces; that is, where two soft tissues intersect. Wave reflection is particularly prominent if the two tissues have different impedance, which produces a bright (white) echo that is characteristic of ultrasound images (Ng & Swanevelder, 2011). Sound waves are, however, also absorbed by soft tissue. Combined, the reflection and absorption of sound waves makes it possible to distinguish between two points that are in parallel (axial resolution) and perpendicular (lateral resolution) relative to the transducer and ultrasound waves (Ng & Swanevelder, 2011).

Perhaps the most important consideration in ultrasound is the choice of transducer. There are multiple ways of categorising ultrasound transducers, such as categories based on body region (e.g., abdominal ultrasound transducers specific for deep tissues), or on the sound wave frequency they can generate (with the unit of megahertz; MHz). For instance, high-frequency transducers can produce images of high resolution (both axial and lateral), but at the expense of wave penetration depth, while low-frequency transducers produce images of poorer resolution, but can image deeper tissues. This is because low-frequency sound waves are less prone to absorption and can, therefore, penetrate deeper (Ng & Swanevelder, 2011). The shape of the transducer head further dictates how ultrasound waves are propagated. For instance, a linear transducer (see example Figure 3.10.1A), propagates waves linearly and in parallel with the transducer head. Conversely, a curvilinear transducer (see example Figure 3.10.3)

propagates waves in a fan-shaped fashion, and is used to image deeper, larger structures in the abdomen (e.g., the diaphragm muscle or foetus in the uterus).

In this thesis, ultrasound was performed using a high-frequency, linear transducer and two low-frequency transducers (one curvilinear transducer and one phased-array transducer). Although both curvilinear and phased-array transducers project ultrasound waves in a fan-like fashion (and are readily confused by the untrained eye), the phased-array transducer has a squared footprint that makes the ultrasound waves project more narrowly proximal to the transducer and can capture ultrasound videos (cine-loops) with a high frame rate (Jacobsen, 2018; Ng & Swanevelder, 2011). This being said, phased-array transducers produce images inferior resolution compared to curvilinear transducers. Accordingly, the sonographer must decide to prioritise resolution and image quality at the expense of frame rate.

3.10.6 Procedures of *intercostal* ultrasonography of costal diaphragm

In all experimental chapters, intercostal ultrasonography was used to measure costal diaphragm thickness and thickening to ensure that values were within normal range reported for healthy adults (Carrillo-Esper et al., 2016). In Chapter 4 and 8, the intercostal approach was also used to measure costal diaphragm thickening in response to stimulation-evoked twitch contractions and maximal sniffs. The approach was also used to assess diaphragm thickening during hypercapnic hyperpnoea in Chapter 5 and 8.

A high-frequency linear transducer (4.0-11.0 MHz, 10L, GE Medical) was positioned on the right, anterior or mid-axillary line at the 8-10th intercostal space (Figure 3.10.1). The ideal intercostal space for scanning was determined by asking the participant to perform an IC manoeuvre to evaluate the degree of lung tissue obscurity at high lung volumes. The intercostal space with least obscurity was chosen. The transducer was held perpendicularly on the lower ribs, angled medially to image costal diaphragm as a three-layered structure: the hyperechoic, non-contractile peritoneal and pleural membranes bordering the less-hyperechoic diaphragm (Figure 3.10.2). Depending on the depth of subcutaneous fat, the diaphragm was imaged at a depth of 15-30 mm with transducer penetration depth set at 30-40 mm. To keep the transducer firmly in position during scanning, a step stool was used to rest the arm and wrist on the sonographer's knee while holding the transducer. This was of particular importance during high levels of ventilation, as the associated rib cage distortion was likely to cause the transducer to 'roll' on the ribs.

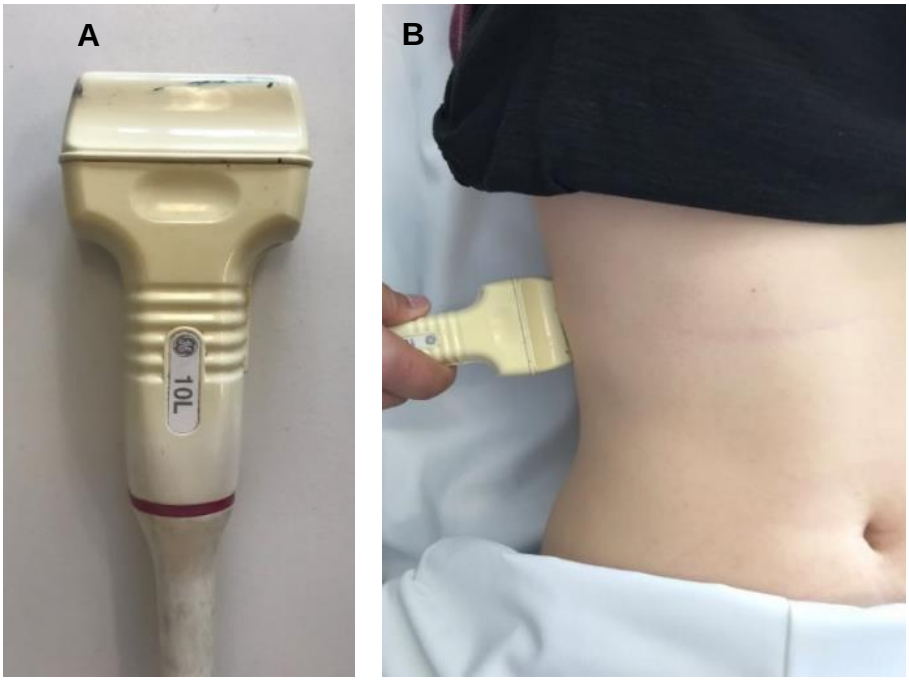

Figure 3.10.1 *A*) Linear, high-frequency ultrasound transducer used for intercostal ultrasonography. *B*) The transducer was positioned on the 8-10th intercostal space to image costal diaphragm thickness and thickening at the zone of apposition.

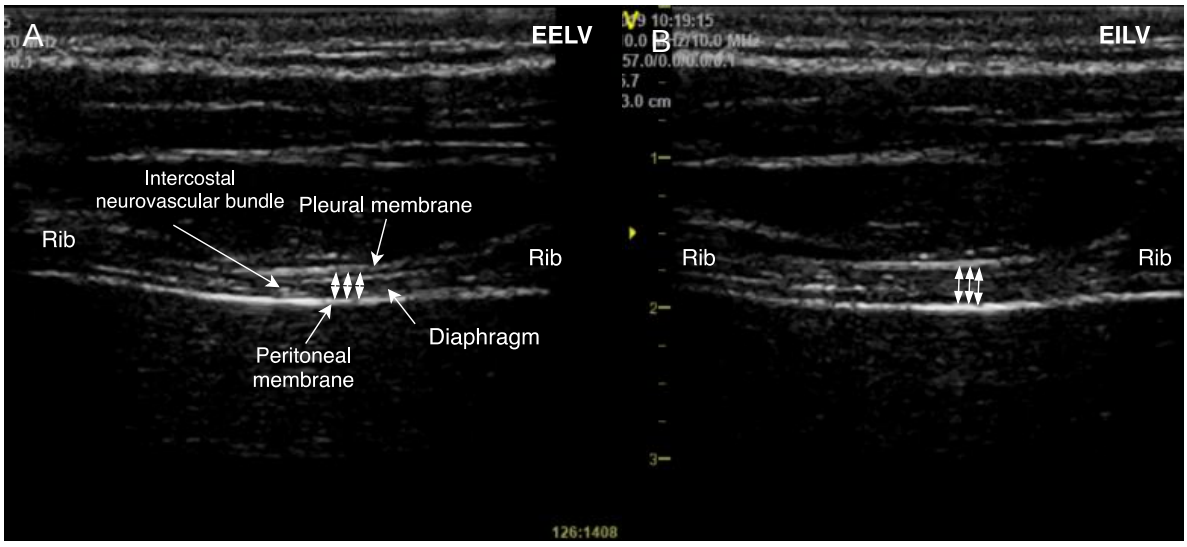

Figure 3.10.2 Costal diaphragm thickness during hyperpnoea, measured at EELV (*A*) and EILV (*B*). Costal diaphragm is a less-echoic tissue with signs of intercostal neurovascular bundles (white lines) between the pair of ribs. Costal diaphragm thickness was measured as indicated by vertical arrows.

There are no established guidelines for operating frequency and ultrasound beam width when assessing costal diaphragm thickness and thickening with the intercostal approach. These parameters were therefore set to best distinguish the three-layered hyperechoic structure of the diaphragm and surrounding tissues (e.g., ribs). Moreover, one focal point was set at the depth of the hyperechoic diaphragm to enhance lateral resolution of the target tissue (see yellow triangle in Figure 3.10.2B). Although adding a focal point reduces temporal resolution and, consequently, maximum frame rate, it significantly improves lateral resolution by creating a dynamic focal region around the target tissue (Ng & Swanevelder, 2011). By shifting the narrowest point of the ultrasound beam – and also the point with the best lateral resolution – to the target tissue (diaphragm), the focal point optimised image quality in the area of interest. The capture rate (frames per second [FPS]) was set automatically as a result of the optimised resolutions (range 69-75 FPS).

To help distinguish between inspiration and expiration, particularly during hyperpnoea, the respiratory function on the ultrasound system was used. ECG electrodes (3M, Berkshire, UK) were placed on the right and left mid-axillary lines for the ultrasound system to monitor changes in rib cage volume via changes in distance between the two electrodes. The waveform signal of rib cage distortion was shown online during scanning and offline during analysis.

Assessment of diaphragm thickness and thickening

Ultrasound cine-loops were recorded as B-mode ultrasound and analysed offline using specialty software (EchoPac v6.1, GE Medical). Diaphragm thickness was measured in triplicate using a digital calliper tool between the inner edges of the peritoneal and pleural membranes, and medially between the two adjacent ribs (Figure 3.10.2). Although diaphragm thickness is typically measured from the *outer* edges of the peritoneal and pleural membranes (Cohn et al., 1997), it was decided that only the contractile tissue was relevant in context of this thesis.

For screening purposes, diaphragm thickness was measured at FRC and TLC during a slow IC manoeuvre (Cohn et al., 1997; Ferrari et al., 2018). The participant was asked to breath-hold at TLC to ensure that the diaphragm could be adequately imaged despite potential lung tissue obscuration. In response to stimulation-evoked contractions and maximal sniffs (Chapter 4 and 8), costal diaphragm thickness was measured at relaxation volume (immediately prior to the perturbation), and when the diaphragm was at its thickest during contraction. During spontaneous breathing (Chapter 5 and 8), thickness was measured at EELV and EILV, as shown in Figure 3.10.2. Diaphragm thickness was measured to the nearest 0.1 mm, which was the highest resolution provided by the software.

Diaphragm thickening was calculated using equations recommended by the ERS (Ferrari et al., 2018; Laursen et al., 2021):

$$Thickening\ fraction = \frac{thickness\ at\ TLC - thickness\ at\ FRC}{thickness\ at\ FRC}$$

$$Thickening\ ratio = \frac{thickness\ at\ TLC}{thickness\ at\ FRC}$$

In response to stimulation-evoked contractions and maximal sniffs, the abovementioned variables were substituted *by diaphragm thickness at relaxation volume* [thickness at FRC] and *peak diaphragm thickness during contraction* [thickness at TLC]. During spontaneous breathing, the variables were substituted by *thickness at EILV* [thickness at TLC] and *thickness at EELV* [thickness at FRC].

3.10.7 Procedures of *subcostal* ultrasonography of crural diaphragm

The subcostal ultrasound approach was used in all experimental chapters to measure maximal diaphragm excursion (mobility). In Chapters 4 (*Part 1*) and 7, the approach was used to measure diaphragm kinetics in response to stimulation-evoked contractions and maximal sniffs. In Chapters 5 (*Part 1*),6 and 7, the approach was used to measure diaphragm kinetics during spontaneous breathing during hyperpnoea.

The ultrasound transducer (either phased-array transducer or curvilinear transducer; see details below) was positioned firmly on the right mid-clavicular line, directly under the costal margin, and angled cranially using the gallbladder and liver as acoustic windows to reach the posterior portion of crural diaphragm (Figure 3.10.3 and Figure 3.10.4) (Boussuges et al., 2009; Ferrari et al., 2018). The right hemi-diaphragm dome was imaged as a bright hyperechoic line, arching from the costophrenic angle laterally to inferior vena cava (IVC) medially. The bright hyperechoic features of the diaphragm dome stem from the soft tissue interfaces of diaphragm, visceral pleura and air-filled lung. It is worth noting, therefore, that what is commonly perceived as diaphragm excursion is in fact pleural line displacement during inspiration. Due to the noticeable appearance of the IVC, imaged as a dark, pulsating circle medial to the hemi-diaphragm, this structure was used as an anatomical landmark (Block, 2004; Testa et al., 2011; Ye et al., 2013).

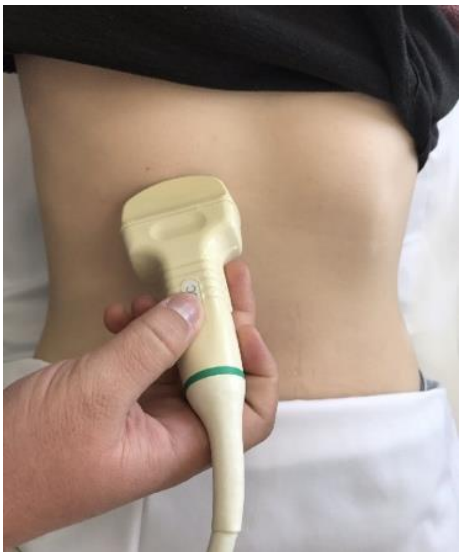

Figure 3.10.3 Subcostal ultrasonography of crural diaphragm. In this example, subcostal ultrasonography was performed with a curvilinear transducer.

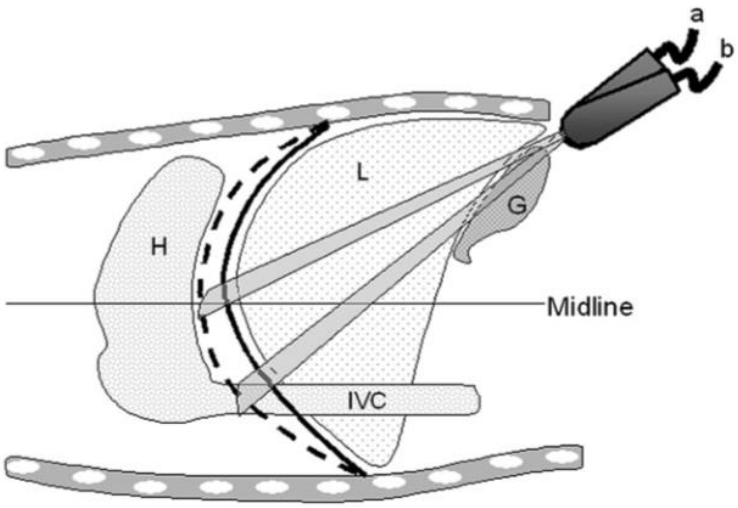

Figure 3.10.4 Subcostal ultrasonography of crural diaphragm from the sagittal plane. Gallbladder (G) and liver (L) were used as acoustic windows to image the posterior portion of right diaphragm (black solid and dashed line). H, heart; IVC, inferior vena cava. From "Ultrasound m-mode assessment of diaphragmatic kinetics by anterior transverse scanning in healthy subjects", by A. Testa et al., 2011, *Ultrasound in Medicine & Biology*, 37(1), p.44-52.

Ultrasound acquisition

Because the human diaphragm is wider and positioned deeper than most other anatomical structures within the human body, the transducers used to image the crural diaphragm with the subcostal approach were low-frequency transducers with sufficient resolution at depths of 150-250 mm. Seeing as diaphragm contraction time ranged from 0.1 s (twitch contraction) to quiet tidal breathing at rest (2-4 s), it was necessary to use two different transducers based on the type of muscle contraction to be imaged in order to avoid temporal alias while still maintaining acceptable beam projection and depth (Ng & Swanevelder, 2011):

A *phased-array transducer* (1.5-4.0 MHz, M4S, GE Medical) was used to image crural diaphragm excursion in response to stimulation-evoked twitch contractions and maximal sniffs because this transducer could achieve a frame rate of ≥200 FPS (Figure 3.10.5A). To achieve the highest possible frame rate to capture the rapid twitch contractions while still maintaining beam depth, it was necessary to use a narrow field of view (Figure 3.10.5B). The standard anatomical landmarks were, therefore, not visible during these rapid contractions. To compensate for this, it was ensured that the skin was adequately marked; that the hemi-diaphragm apex was always in the centre of the B-mode image, and that a focal point was set at the depth of the hyperechoic diaphragm at relaxation volume (yellow triangle in Figure 3.10.5B).

For slower diaphragm contractions (e.g., spontaneous breathing), a low-frequency, curvilinear transducer (2.4-5.0 MHz, 3.5C, GE Medical) was used (Figure 3.10.6A). Although this transducer could only achieve a frame rate of 35-40 FPS, this transducer had a footprint of 18 × 64 mm and 58° field of view (compared to 20 × 28 mm footprint for M4S), enabling us to capture a larger portion of diaphragm excursion over a greater distance compared to the phased-array transducer. This feature was important when tidal volume was of significant magnitude (e.g., during hyperpnoea). Moreover, as shown in Figure 3.10.6B, anatomical landmarks were readily identified, thereby enhancing validity and reliability of the scan. To improve lateral resolution, one focal point was set at the hyperechoic diaphragm structure at relaxation volume (yellow triangle in Figure 3.10.6B).

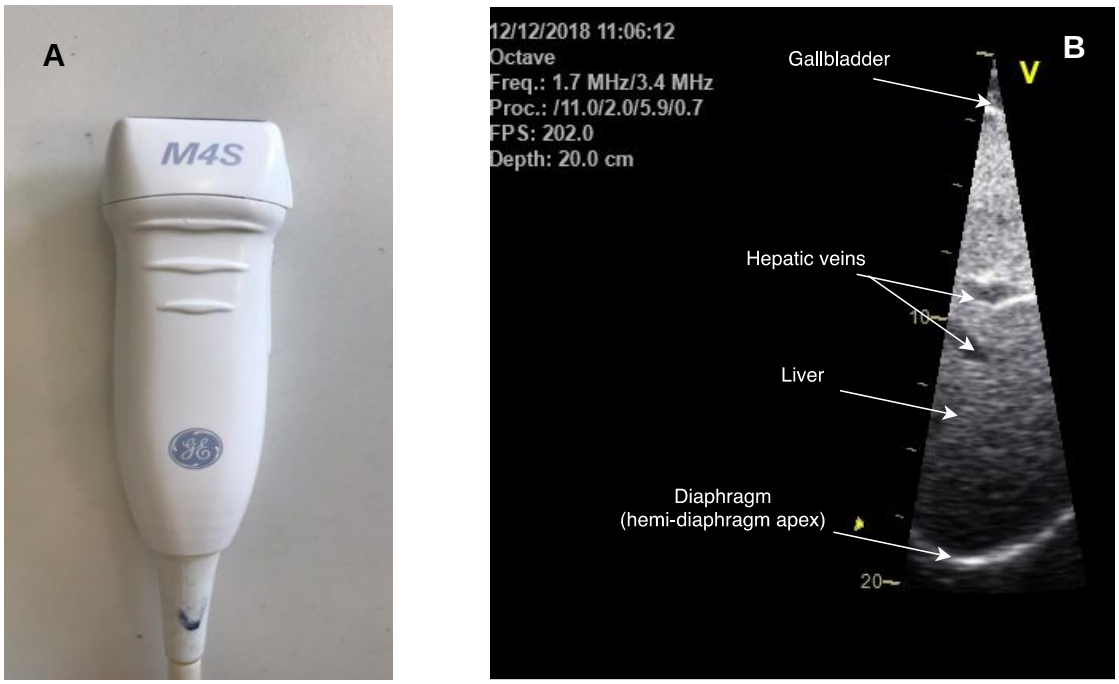

Figure 3.10.5 *A*) Phased-array transducer to assess crural diaphragm excursion during evoked twitch contractions and maximal sniffs. *B*) B-mode of right crural diaphragm using phased-array transducer. Here, crural diaphragm was imaged in a female participant at a depth of 170-200 mm when at relaxation volume.

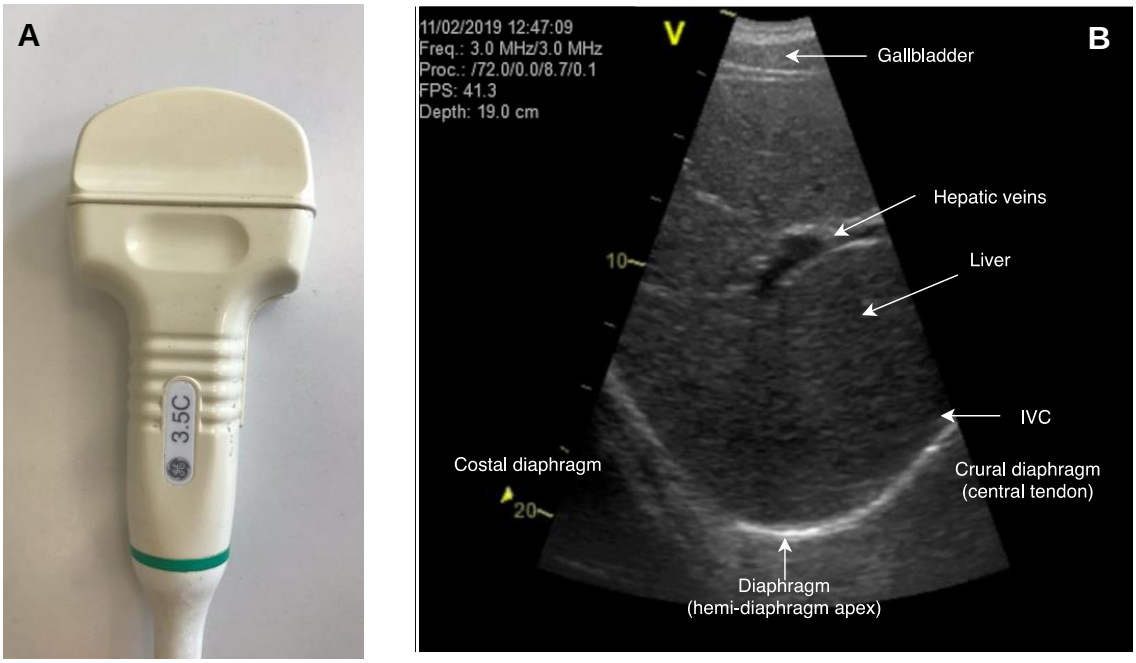

Figure 3.10.6 *A*) Curvilinear transducer to assess crural diaphragm excursion during spontaneous breathing. *B*) B-mode ultrasound of crural diaphragm with curvilinear transducer. IVC was readily identified in all subjects due to pulsating motion (not visible on still-image). In this example, crural diaphragm was imaged in the same female participant as above.

Assessment of crural diaphragm excursion and excursion velocity (kinetics)

Ultrasound cine-loops were recorded in B-mode, and then exported for offline analysis in specialty software (EchoPac v6.1, GE Medical). In this thesis, diaphragm excursion and excursion time were measured using three different analysis techniques: *i*) conventional M-mode ultrasound (Chapters 4 and 5); *ii*) angle-independent AM-mode ultrasound (Chapters 4 to 7); and *iii*) speckle-tracking algorithms (Chapter 4).

Conventional M-mode ultrasound

Conventional M-mode ultrasound is a time-motion display of a single scan-line, and is presented with the ordinate as the distance from the transducer with the abscissa as time (Figure 3.10.7). Cine-loops can be recorded directly as M-mode, or as B-mode that can later be converted to M-mode using specialty software; the latter of which was done for this thesis. The single scan-line for M-mode is represented by a vertical, static cursor, and movement of bright echoic structures are imaged as they move along this static axis. For the diaphragm specifically, the bright echoic structure seen with B-mode ultrasound is shown as a white line moving vertically (craniocaudally) upon inspiration and expiration. Diaphragm craniocaudal excursion and excursion time were measured with a digital calliper tool as the absolute excursion amplitude (cm) and the time (s) from onset of excursion to peak excursion (Testa et al., 2011).

Diaphragm excursion velocity (cm/s) was then calculated as the quotient of diaphragm excursion divided by excursion time.

Angle-independent AM-mode ultrasound

Like conventional M-mode, AM-mode ultrasound is a time-motion capture of a single scan-line, and is also presented with the ordinate as the distance from the transducer and the abscissa as time (Figure 3.10.7). However, the single scan-line (cursor) in AM-mode ultrasound is dynamic (not static), and can be oriented along any axis chosen by the operator. AM-mode ultrasound is, therefore, considered a more accurate technique compared to M-mode because the scan-line can be oriented to follow the true movement of the target tissue. Accordingly, when assessing diaphragm excursion with AM-mode, the cursor was oriented along the true axis of diaphragm (Orde et al., 2016b). As with conventional M-mode, diaphragm excursion and excursion time were measured with a digital calliper tool as the absolute excursion amplitude (cm) and the time (s) from onset of excursion to peak excursion (Testa et al., 2011). Diaphragm excursion velocity (cm/s) was again calculated as the quotient of diaphragm excursion divided by excursion time.

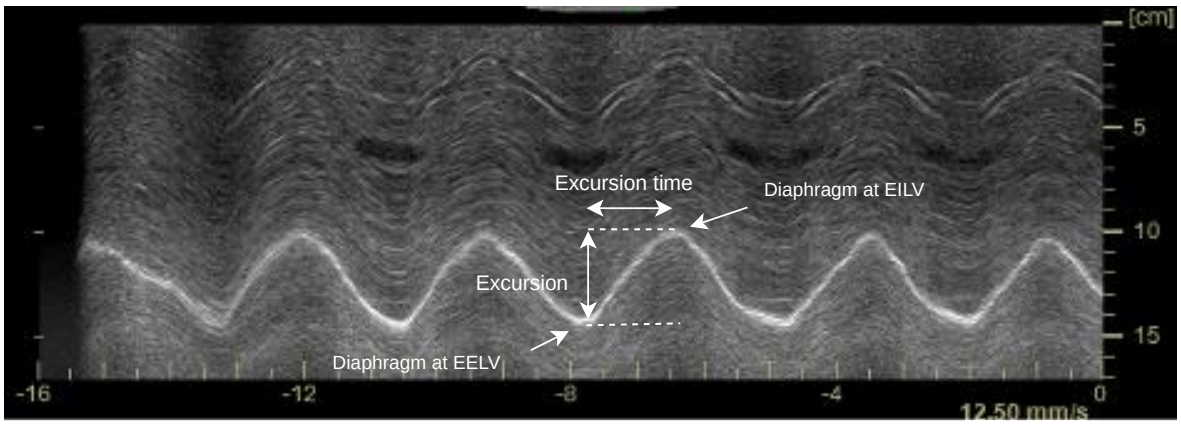

Figure 3.10.7 Conventional M-mode and AM-mode ultrasound of crural diaphragm excursion. The ordinate is the distance (cm) from the transducer, and abscissa is shown time (s). Using a digital calliper tool, diaphragm excursion was measured as the absolute excursion amplitude from onset of excursion (e.g., at EELV) to peak excursion (e.g., at EILV), as indicated by arrows. In this example, diaphragm excursion was ~4.8 cm and excursion time was ~2 s during hyperpnoea in a female participant.

Speckle-tracking algorithms

Unlike M-mode and AM-mode, speckle-tracking is a set of algorithms that track the displacement of ultrasound image pixels (speckles) during tissue movement (Teske et al., 2007). Speckle-tracking algorithms were originally developed for the non-invasive assessment of regional and global myocardial function; that is, the electro-mechanical activation and subsequent displacement and three-dimensional deformation of myocardium during a cardiac cycle (Teske et al., 2007). Recent studies have, however, applied speckle-tracking algorithms to better understand the contractile properties of the human diaphragm, which includes crural diaphragm displacement (Goutman et al., 2017) and deformation (strain) (Ye et al., 2013), as well as costal diaphragm strain (Oppersma et al., 2017; Orde et al., 2016a).

Speckle-tracking was performed on the ultrasound B-mode images using the Quality Analysis (Q-Analysis) tool in EchoPac (v6.1) by drawing a region of interest (ROI) with the apical long axis (APLAX) drawing tool on the hyperechoic diaphragm structure (see coloured ROI in Figure 3.10.8A). Because the software did not allow for the analysis of an entire 15 s cine-loop, each respiratory cycle or perturbation had to be manually identified by visual inspection and analysed separately. Following an automated speckle-tracking analysis, the operator was given the option of accepting or rejecting the speckle-tracking analysis of each sub-region after reviewing how well the software tracked the deformation/displacement of the tissue.

As shown in Figure 3.10.8B, the output from speckle-tracking analysis is a time-motion capture of diaphragm excursion ('displacement') over a single respiratory cycle. Diaphragm excursion was measured as the absolute displacement of speckles of the hemi-diaphragm apex (blue subregion in Figure 3.10.8) in the transverse *and* longitudinal plane. The decision to primarily track the hemi-diaphragm apex was that this approach was most comparable to the excursion measured with M-mode and AM-mode. In line with the method described Goutman et al. (2017), the diagonal diaphragm excursion was manually calculated as the length of the hypotenuse of a right-angle triangle:

$$Diagonal\ excursion = \sqrt{longitudinal\ excursion^2 + \ transverse\ excursion^2}$$

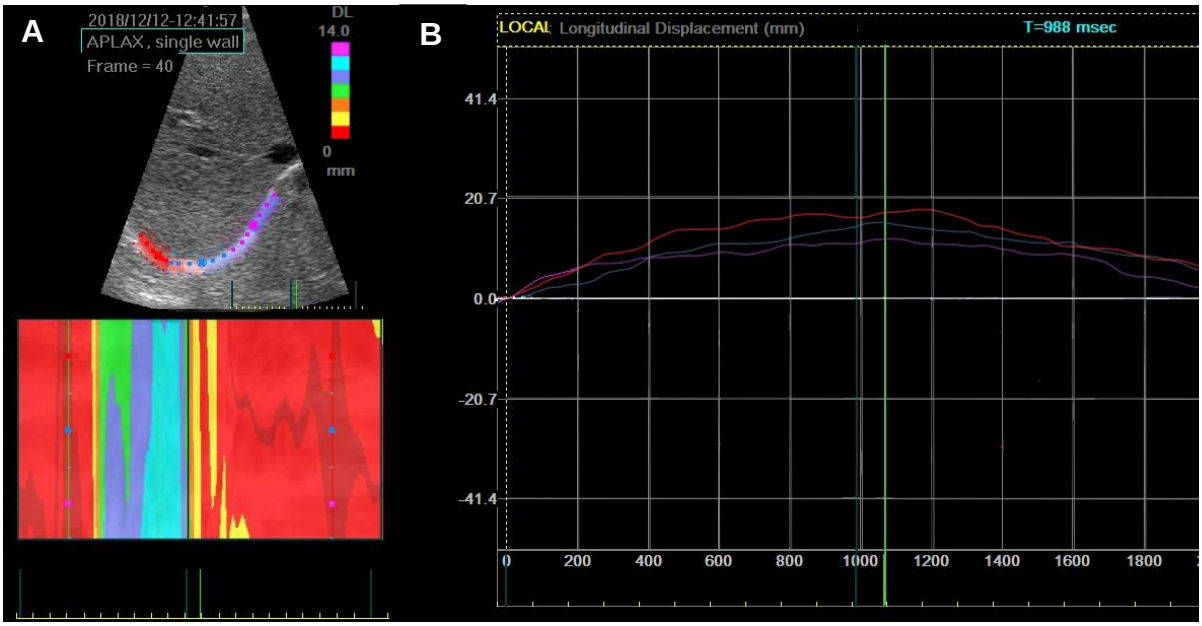

Figure 3.10.8 Speckle-tracking analysis of diaphragm excursion ('displacement') during a respiratory cycle. *A*) The region of interest (ROI) was drawn on the B-mode ultrasound and automatically divided into three sub-regions, distinguished by colours red, blue and pink. *B)* Diaphragm excursion expressed time-motion capture, with the ordinate representing excursion (mm) and the abscissa as time (ms). In this example, the excursion of crural diaphragm apex (blue sub-region) was 1.87 cm with an excursion time of 1.06 s in a female participant during quiet breathing.

3.11 Hypercapnic hyperpnoea (CO_2-rebreathe)

CO_2-rebreathe was performed in Chapter 5 to 8. In Chapter 5, the purpose was to evaluate the feasibility, validity and reliability of ultrasonography for the assessment of diaphragm kinetics and shortening during hypercapnic hyperpnoea. In Chapter 6, CO_2-rebreathe was used alongside exercise to compare diaphragm kinetic responses to reflexively-induced hyperpnoea with or without postural adjustments. Lastly, in Chapter 7 and 8, CO_2-rebreathe was performed to determine the effect of external loading on CO_2 sensitivity, breathing pattern and diaphragm kinetics and shortening during hyperpnoea.

Principles of hypercapnic hyperpnoea (CO_2-rebreathe)

For the purpose of this thesis, the original Read CO_2-rebreathe method was adopted and slightly modified to fit the purpose(s) and equipment available (Read, 1966; Read & Leigh, 1967). CO_2-rebreathe is based on the premise that breathing in a closed circuit that initially contains 93-95% O_2 and 5-7% CO_2 will return expired CO_2 to the lungs via inspiration. As the test progresses, accumulated CO_2 in the closed circuit increases PCO_2 in arterial blood and tissues, resulting in a progressive stimulus to central chemoreceptors and a subsequent increase in ventilation. There is an assumption that peripheral chemoreceptors are 'silenced' by the hyperoxic inspirate because the carotid bodies primarily respond to hypoxia and/or changes in blood pH, not hypercapnia (Read, 1966; Read & Leigh, 1967; Seeley et al., 2011).

Procedures

CO_2-rebreathe was performed using a closed-circuit, three-way valve (2110, Hans Rudolph, Shawknee, KA, US) connected to a rebreathe bag filled with a certified gas containing 95% O_2 and 5% CO_2 (BOC, Guildford, UK). In Chapters 5 (*Part 1*) and 6, the rebreathe bag was a latex-rubber, reusable bag (5 and 6 L, P3 Medical, Bristol, UK) (see Figure 3.11.1). However, due to the tendency for the heavy material of the rubber-latex bag to increase resistance to inflation, these rebreathe bags were replaced by disposable plastic bags in Chapters 5 (*Part 2*), 7 and 8 (Figure 3.11.2). The bag volume was based on the participant's vital capacity plus one litre (VC + 1 L), as this volume was 'as small as possible' (Read, 1966, p. 53) without encroaching on tidal volume. The dead space of the mouthpiece-valve assembly was 53.5 mL (incl. side ports; excl. rebreathe bag).

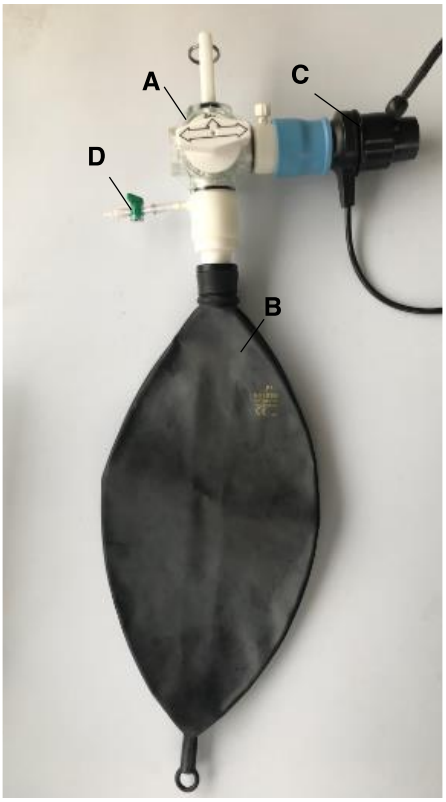

Figure 3.11.1 *A*) Mouthpiece-valve assembly with three-way valve; *B*) latex-rubber rebreathe bag; *C*) valve port for turbine flow-meter for assessment of flow and volume; *D*) side-port to inflate bag with hyperoxic gas.

Figure 3.11.2 Laboratory set-up for hypercapnic hyperpnoea. Support was provided to the mouthpiece-valve assembly so that the participant remained relaxed. Here, a disposable, plastic rebreathe bag was used.

Prior to initiating the test, participants breathed quietly from ambient room air for ~10 min without a mouthpiece to ensure that the test was initiated from a relaxed, wakeful state. To prevent fluctuations in arousal level and the influence of participant-experimenter interaction, the laboratory was kept silent with stable temperature and lights before, during and after (3 min) each test (Spengler & Shea, 2001). Upon initiating the test, participants exhaled to RV, at which point the three-way valve was twisted and the circuit closed. Next, three deep, rapid breaths were taken to equilibrate PCO_2 between arterial blood, oxygenated mixed venous blood, gas in the lungs and the now-closed rebreathe circuit. At this point, participants were instructed to relax and breathe as needed with eyes closed. The test was terminated when one of the following criteria was met: *i*) $P_{ET}CO_2$ = 55 mmHg [7.33 kPa]; *ii*) the rebreathe bag deflated; *iii*) the maximum test duration of 15 min was reached; or *iv*) the participant terminated the test prematurely (MacKay et al., 2016).

Great effort was made to prevent fluctuations in CO_2 sensitivity, particularly when participants were required to perform multiple CO_2-rebreathe tests within- and between-days. For instance, all participants practiced the CO_2-rebreathe test during familiarisation (first visit), and were asked to refrain from caffeine for ≥12 h prior to testing (D'Urzo et al., 1990). Moreover, for between-day trials (e.g., Chapters 7 and 8), it was ensured that rebreathe tests were performed at the same time of day to reduce the influence of circadian rhythm on ventilatory response to CO_2 (Spengler & Shea, 2001).

Cleaning procedures of rebreathe bag

After each use, the latex-rubber rebreathe bag was cleaned and sterilised in line with manufacturer guidelines: first, the bag was washed in tap water before being soaked in 5 L of sterilising solution for 15 min (Milton Pharmaceuticals Ltd., Ceuta Healthcare Ltd., Bournemouth, UK). The rebreathe bag was then left to dry in ambient, room air, and then stored in a sealed, sterile bag until next use. The plastic bags used in Chapters 5, 7 and 8 were disposed after each experimental visit.

3.12 Incremental cycling exercise

Incremental cycling exercise was performed in Chapter 6 alongside CO_2-rebreathe to compare diaphragm kinetics during reflexively-driven hyperpnoea with and without postural adjustments. The exercise test was performed on a calibrated electromagnetically-braked, semi-recumbent (30° hip flexion) cycle ergometer (Angio Imaging, Lode, Groningen, Netherlands) that accommodated for ultrasound acquisition (Figure 3.12.1).

Procedures

Prior to initiating the incremental cycling test, participants warmed-up for 3 min at a work rate of 10 W and a cadence of 55-60 rpm. This pedal cadence was chosen specifically to limit lateral motion of the torso and hips that might cause motion artefacts during ultrasound acquisition. Following warm-up, work rate was increased as a ramp by 15-30 W/min. The specific ramp slope was calculated on a participant-by-participant basis by estimating the predicted peak oxygen uptake ($\dot{V}O_{2peak}$) and predicted maximal work rate (W_{max}) using equations proposed by Hansen et al. (1984) and Wasserman et al. (2012). More specifically, the estimation assumed a work efficiency ($\Delta\dot{V}O_{2peak}/\Delta W$) of 10.0 mL/min/W (Wasserman & Whipp, 1975) over a test duration of 8 min, whereby the increase in work rate (ΔW) was related to the energy equivalent to the increase in $\dot{V}O_2$ required to perform the given work (see Table 3.12.1 for full set of equations). The work efficiency of Wasserman & Whipp (1975) was derived from 'normal', healthy men during upright cycling exercise, as it was only recently that Wehrle et al. (2021) published a full set of cardiorespiratory and metabolic indices for semi-recumbent cycling exercise. As such, this project was completed before the work efficiency for semi-recumbent cycling could be accounted for. The effect of using this set of equations should, however, be considered only negligible and should not have unduly compromised our ability to test the research question. The duration of 8 min was chosen on the basis that it was near the expected duration for CO_2-rebreathe (~2-3 min), yet still at the lower end of the range expected to elicit peak physiological responses (Buchfuhrer et al., 1983). The exercise test was terminated when the pedal cadence dropped below 50 rpm for >5 s despite verbal encouragement.

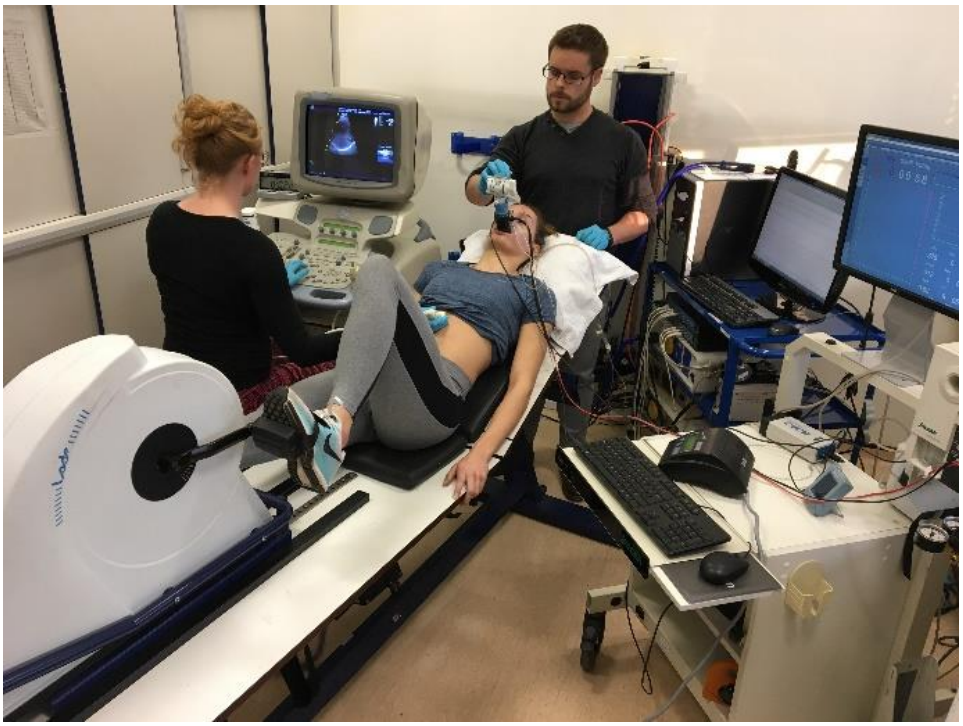

Figure 3.12.1 Laboratory set-up for incremental cycling exercise. Support was provided to the mouthpiece-valve assembly to ensure that the participant was relaxed.

Table 3.12.1 Equations to calculate ramp slope for incremental exercise.

Males	**Females**
Calculation of ideal body mass: Ideal body mass (kg) = 0.79 × stature (cm) – 60.7	**Calculation of ideal body mass:** Ideal body mass (kg) = 0.65 × stature (cm) – 42.8
Estimation of $\dot{V}O_{2,peak}$: *If actual body mass ≥ideal body mass:* $\dot{V}O_{2,peak}$ (L/min) = 0.0337 × stature – 0.000165 × age[a] × stature – 1.963 + 0.006 × body mass (actual – ideal) *If actual body mass is <ideal weight:* $\dot{V}O_{2,peak}$ (L/min) = 9.0337 × stature × 0.000165 × age[a] × stature – 1.963 + 0.014 × body mass (actual – ideal)	**Estimation of $\dot{V}O_{2,peak}$:** $\dot{V}O_{2,peak}$ (L/min) = 0.001 × stature × (14.783 – 0.11 × age[a]) + 0.006 × body mass (actual – ideal)
Estimation of peak work rate (W_{peak}): W_{peak} (W) = $\dot{V}O_{2,peak}$ (L/min) ÷ 10 mL/kg/min*	**Estimation of peak work rate (W_{peak}):** W_{peak} (W) = $\dot{V}O_{2,peak}$ (L/min) ÷ 10 mL/kg/min*
Calculation of ramp slope: Slope (W/min) = W_{peak} (W) ÷ test duration (min)	**Calculation of ramp slope:** Slope (W/min) = W_{peak} (W) ÷ test duration (min)

$\dot{V}O_{2,peak}$, estimated peak oxygen uptake; W_{peak}, estimated peak work rate. [a] use age of 30 y for adults younger than 30 y; *assumed work efficiency ($\Delta\dot{V}O_{2peak}$ /ΔW) derived from Wasserman & Whipp (1975). Adapted from "Principles of Exercise Testing and Interpretation: Including Pathophysiology and Clinical Application", by K. Wasserman et al., 2012.

Chapter 4

Feasibility, Validity and Reliability of Ultrasonography for the Assessment of Diaphragm Kinetics and Thickening in Response to Non-Volitional and Volitional Perturbations

4.1 Introduction

Force development across the diaphragm is assessed objectively by measuring the difference between the gastric and oesophageal pressure evoked by electrical or magnetic stimulation of the phrenic nerves, and is quantified as the quasi-isometric twitch transdiaphragmatic pressure ($\Delta P_{di,tw}$) (Moxham et al., 1981). Application of these nerve stimulation techniques to humans has shown a decrement in $\Delta P_{di,tw}$ in response to various conditions, including inspiratory resistive loading (IRL) and dynamic whole-body exercise (Romer & Polkey, 2008). A major limitation of these techniques, however, is that quasi-isometric twitch force is a relatively poor index of diaphragm function *in vivo*, providing no information regarding the muscle's ability to shorten and generate power. For this reason, little is known about the dynamic contractile properties of the human diaphragm, and how these attributes may be affected by loading and fatigue. Accordingly, the overarching aim of this study was to explore the use of ultrasound to directly quantify the dynamic, contractile properties of the fresh human diaphragm in response to stimulation-evoked twitch contractions and maximal inspiratory efforts (sniffs).

In the area of biomechanics, ultrasound is considered a useful tool for assessing skeletal muscle architectural properties (e.g., thickness, fascicle length and pennation angle) as well as muscle-tendon properties (Cronin & Lichtwark, 2013; Hodges et al., 2003). Moreover, ultrasound has been used to better understand how these architectural attributes may change with fatigue (Morel et al., 2019; Pillen, 2010). For the diaphragm muscle specifically, ultrasound is primarily used in the ICU as a non-invasive, non-ionising tool to quantify crural diaphragm kinetics and costal diaphragm thickness and thickening (Laursen et al., 2021). In patients undergoing mechanical ventilation, ultrasound of the diaphragm has also been used to detect muscle paralysis (Gottesman & McCool, 1997), to monitor disuse atrophy (Goligher, Fan, et al., 2015), and to identify patient-ventilator asynchrony (Vivier et al., 2020) with the overarching aim of avoiding weaning failure and a potential reintubation (Goligher et al., 2018).

Measures of crural diaphragm kinetics can be obtained from a subcostal ultrasound approach, and measured using three different analysis techniques: *i*) conventional M-mode ultrasound, whereby craniocaudal diaphragm descent (excursion) is derived from a time-motion capture in which the hemi-diaphragm dome moves along a static, vertical scan line (cursor) during inspiration (Gerscovich et al., 2001); *ii*) angle-independent AM-mode ultrasound, whereby diaphragm descent (excursion) is also derived from a time-motion capture, but along a dynamic scan line (cursor), which can be oriented along the true axis of diaphragm descent regardless of

anatomical direction (Orde et al., 2016b); and *iii*) speckle-tracking algorithms, whereby the dislocation of image speckles is tracked and measured in an automated analysis process (Goutman et al., 2017). On the other hand, costal diaphragm thickness and thickening can be measured from an intercostal approach at the zone of apposition in B-mode ultrasound (Cohn et al., 1997). With the intercostal approach, it is possible to measure costal diaphragm thickness and thickening during inspiration. Ultrasound-derived diaphragm thickening may, therefore, serve as an estimate of costal diaphragm shortening *in vivo* (Ferrari et al., 2018; Wait et al., 1989).

Despite these established applications, ultrasound has not yet been used to measure the diaphragm's ability to shorten and produce power in response to stimulation-evoked twitch contractions and maximal inspiratory efforts (sniffs). Based on these considerations, this study sought to explore the feasibility, validity and reliability of ultrasonography for the assessment of diaphragm kinetics and thickening in response to stimulation-evoked twitch contractions and maximal inspiratory efforts.

4.1.1 Aims and hypotheses

In *Part 1* of this study, the aim was to determine the feasibility, concurrent validity and within-day, intra-observer reliability of ultrasound-derived measures of crural diaphragm kinetics (i.e., excursion, excursion time, excursion velocity and power) by *subcostal* ultrasonography in response to stimulation-evoked twitch contractions and maximal inspiratory efforts (sniffs). It was hypothesised that the assessment of diaphragm kinetics would be feasible in response to both perturbations; that ultrasound-derived measures of diaphragm kinetics would be strongly correlated with conventional measures of diaphragm contractile properties ($\Delta P_{di,tw}$ and $\Delta P_{di,sn}$), and that the measures would exhibit acceptable within-day reliability.

In *Part 2*, the aim was to determine the feasibility, concurrent validity and within-day, intra-observer reliability of ultrasound-derived measures of costal diaphragm thickening by *intercostal* ultrasonography in response to stimulation-evoked twitch contractions and maximal sniffs. It was hypothesised that the assessment of costal diaphragm thickening would be feasible in response to both perturbations; that ultrasound-derived measures of costal diaphragm thickening would be strongly correlated with conventional measures of diaphragm contractile properties ($\Delta P_{di,tw}$ and $\Delta P_{di,sn}$) and that the measures would demonstrate acceptable within-day reliability.

4.2 Methods

4.2.2 Ethical approval and participants

The study was approved by Brunel University London Research Ethics Committee (Appendix 1), and conformed to the most recent standards set by the Declaration of Helsinki (World Medical Association, 2013). Sixteen healthy, non-smoking adults (5 women) between the ages of 18 and 40 y from university student population and surrounding areas volunteered to participate. Biological sex was self-reported as per the standardised health questionnaire (Appendix 2). All participants reported no medical history of cardiovascular, respiratory or neuromuscular disease using a standardised health questionnaire (Appendix 2). Exclusion criteria were BMI ≥30 kg/m^2 and pulmonary function and maximal respiratory mouth pressures outside age-specific limits of normal (Evans & Whitelaw, 2009; Quanjer et al., 2012; Stocks & Quanjer, 1995). Moreover, it was ensured that participants' right hemi-diaphragm could be imaged with appropriate clarity using ultrasound. Participants provided written informed consent (Appendix 2), and were asked to abstain from vigorous exercise for ≥24 h, caffeine and alcohol for ≥12 h, and food for ≥3 h prior to each visit.

4.2.3 Experimental overview

Each participant visited the laboratory on two occasions, separated by no less than 48 h and no more than 14 d. The overall study outline was similar for *Part 1* and *Part 2*: The first visit was for screening and familiarisation, during which participants performed pulmonary function tests and were thoroughly familiarised with the experimental set-up. The second visit was the experimental trial, consisting of anterolateral phrenic nerve stimulation and maximal inspiratory efforts (sniffs) protocols. The protocols were performed in a predetermined, non-randomised order (nerve stimulation followed by sniffs), and, for the assessment of within-day reliability, the protocols were repeated after a standardised period of 20 min. Intrathoracic pressures (P_{di}, oesophageal pressure [P_{oe}] and gastric pressure [P_{ga}]) and diaphragm electromyogram (EMG_{di}) were obtained during all manoeuvres in both parts. For *Part 1* specifically, ultrasound-derived measures of crural diaphragm kinetics (excursion, excursion time, excursion velocity and power) were obtained during all manoeuvres. In *Part 2*, ultrasound-derived measures of costal diaphragm thickening (shortening) were obtained during all manoeuvres.

4.2.4 Screening and familiarisation

General anthropometric characteristics were measured before pulmonary volumes, capacities and flows were assessed using whole-body plethysmography and spirometry (MasterScreen PFT system, CareFusion, Hoechberg, Germany) in line with current guidelines (Graham et al., 2019; Miller et al., 2005; Wanger et al., 2005). Pulmonary function was expressed as absolute values and as percentage of predicted values based on current reference equations (Quanjer et al., 2012; Stocks & Quanjer, 1995). For screening purposes, pulmonary function values were compared to limits of normal (Quanjer et al., 2012; Stocks & Quanjer, 1995). Maximum inspiratory and expiratory mouth pressures (MIP and MEP) were measured as the highest plateau pressure (1 s) generated by maximal efforts from residual volume (RV) and total lung capacity (TLC), respectively. The pressure were measured using a hand-held pressure meter with flanged mouthpiece (MicroRPM, Williams Medical Supplies Ltd., Rhymney, Wales) (Evans & Whitelaw, 2009; Green et al., 2002). The maximum value of three efforts that varied ≤10% was recorded and expressed as the absolute value and as the percentage of predicted calculated from Evans & Whitelaw (2009).

Using a commercially-available ultrasound machine (Vivid 7 Pro, GE Medical, Horten, Norway), thickness of right costal diaphragm was measured in triplicate at FRC and TLC between the inner edges of the pleural and peritoneal membranes (Carrillo-Esper et al., 2016). The relative thickening of the diaphragm from FRC to TLC, in the form of thickening fraction, was calculated with the equation: (thickness at TLC – thickness at FRC)/thickness at FRC (Ferrari et al., 2018). Crural diaphragm maximal excursion (mobility) was measured using AM-mode ultrasound as the excursion from RV to TLC (Ferrari et al., 2018). Specific familiarisation for the experimental trial included familiarisation with phrenic nerve stimulation and practice of maximal sniffs. Familiarisation for *Part 1* also included practice of maximal Müller-expulsive manoeuvres against a semi-occluded mouthpiece for post-activation potentiation.

4.2.5 Part 1

Ten participants (5 women) volunteered for this part of the study. Self-reported, biological sex was taken into account when including participants in other to ensure adequate representation of both sexes (Heidari et al., 2016).

Supramaximal phrenic nerve stimulation and maximal sniffs

Stimulation of phrenic nerves was performed as described in detail in section 3.9 in General Methods. Unilateral magnetic stimulation of the right phrenic nerve was performed using two

commercially-available magnetic stimulators (Magstim 200, Magstim Company Ltd., Whitland, Wales) connected to a paired-pulse stimulator (BiStim, Magstim Company Ltd.) and an insulated figure-eight coil (D70 Alpha B.I, Magstim Company Ltd.) (Mills et al., 1995). The paired-pulse stimulator enabled the use of paired or repetitive stimuli with various inter-stimulus interval to the common coil. The optimal stimulation area was located on the anterior border of the right sternocleidomastoid, and the skin was marked for subsequent stimulations. To check for supramaximality of stimulation, each participant underwent an incremental stimulation protocol at 50 to 100% of the stimulator's maximum power, as described in section 3.9. Supramaximal stimulation was defined when mean $\Delta P_{di,tw}$ at submaximal and maximal stimulation intensities were equal to or less than the coefficient of variation (CV) for all twitches within an individual participant (Geary et al., 2019; Man et al., 2004).

The stimulation protocol comprised five single, non-potentiated twitches (1 Hz) and three sets of paired twitches at 10 Hz (inter-stimulus interval 100 ms), 50 Hz (20 ms) and 100 Hz (10 ms). In addition, participants performed five maximal sniffs and five single, potentiated twitches (1 Hz potentiated). To achieve post-activation potentiation, participants performed Müller-expulsive efforts (2-3 s) against a semi-occluded mouthpiece (0.75 mm ID) while wearing a nose-clip, with the potentiated twitch obtained ≤5 s after each maximal effort. Maximal sniffs were performed under the instruction to "do a short, sharp sniff as hard as possible" (Miller, Moxham, and Green 1985, p. 92). All twitch contractions and sniff efforts were separated by ≥30 s to avoid the influence of twitch potentiation (Kufel et al., 2002; Mador, Magalang, et al., 2000).

Assessment of intrathoracic pressures

The P_{oe} and P_{ga} were measured using two balloon-tipped catheters (86 cm, Cooper Surgical, Berlin, Germany) as described in 3.6.5 in General Methods. Briefly, the catheters were passed pernasally, and swallowed into the stomach via peristalsis. Once in the stomach, the balloons were filled with 1 mL (P_{oe}) and 2 mL (P_{ga}) of ambient air using a 10 mL glass syringe (Cross et al., 2015). The oesophageal catheter was then withdrawn from the stomach until negative deflections were seen in P_{oe} in response to a sniff (~35-45 cm distal from the nostril). The correct position of the oesophageal catheter was confirmed with the "dynamic occlusion test" (Baydur et al., 1982) before both catheters were taped in position at the nose. The volume of air in each catheter was checked at regular intervals to ensure that no leaks had occurred.

Each catheter was connected to a very-low range differential pressure transducer (DP45-3, Validyne Engineering, Northridge, USA) that was calibrated immediately before use. Analogue pressure signals were amplified (CD280, Validyne Engineering), digitised (Micro1401-2, CED, Cambridge, UK) and recorded online at 200 Hz (Spike2, v9.00, CED). Transdiaphragmatic pressure (P_{di}) was calculated by online subtraction of P_{oe} from P_{ga}.

Diaphragm ultrasonography

Ultrasound scans were performed with the participant seated in the semi-recumbent position. In this part of the study, *subcostal* ultrasonography was used to measure right hemi-diaphragm craniocaudal excursion, excursion time, excursion velocity and power (kinetics) in response to stimulation-evoked twitch contractions and maximal sniffs. This approach is described in detail in section 3.10.7, General Methods.

Briefly, a low-frequency phased-array ultrasound transducer (1.5-4.0 MHz, M3S, GE Medical) was placed subcostally on the participant's right mid-clavicular line. The transducer was steered in a cranial direction to image the posterior dome of the right hemi-diaphragm. Penetration depth was adjusted so that the hyperechoic diaphragm position at RV was always within the field of view (~150-250 mm). One focal point was set at the diaphragm position at relaxation volume in order to enhance lateral resolution at the diaphragm. To achieve an adequate sampling rate for capturing the rapid twitch and sniff response, the image width was narrowed to capture only the apex of the hemi-diaphragm, resulting in a sampling rate of 200-220 frames per second (FPS).

Ultrasound cine-loops were recorded using B-mode ultrasound and analysed using three different analysis techniques: *1*) conventional M-mode ultrasound; *2*) AM-mode ultrasound; and *3*) speckle-tracking algorithms. With M-mode ultrasound, diaphragm craniocaudal excursion was measured as the vertical distance between the onset of twitch/sniff excursion and peak excursion. Excursion time was measured as the horizontal distance (seconds) between the two points (Figure 4.2.1). The same measurements were performed using AM-mode, but the dynamic B-mode cursor was oriented along the true axis of diaphragm excursion (Orde et al., 2016b). Successfully analysed cine-loops with M-mode and AM-mode were characterised by a clear hyperechoic line, a distinct baseline (diaphragm at relaxation volume) and a distinct peak excursion upon contraction.

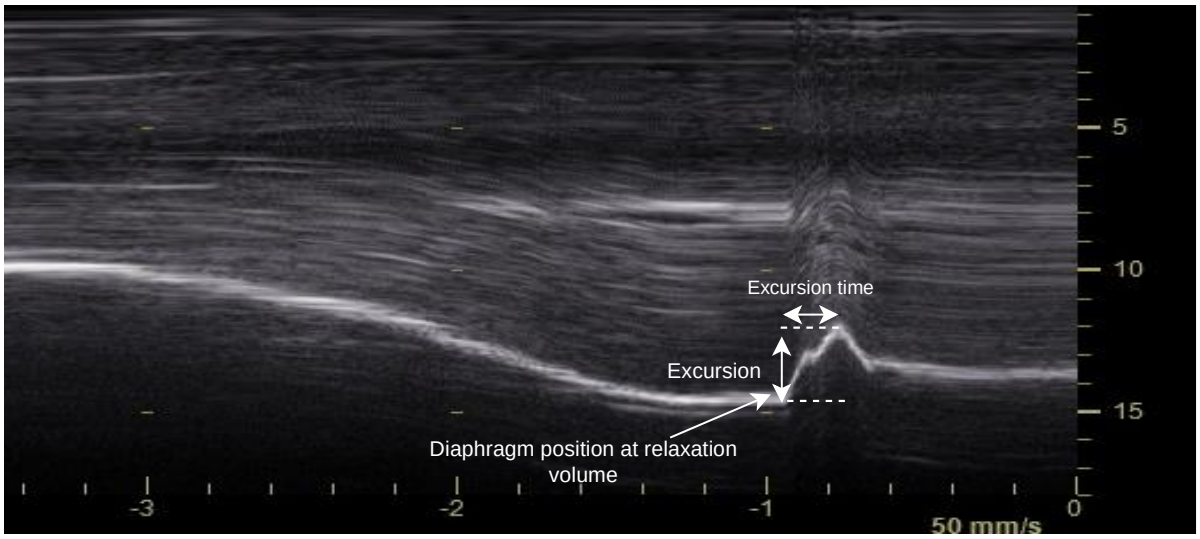

Figure 4.2.1 M-mode and AM-mode ultrasound of crural diaphragm (bright hyperechoic line). Craniocaudal excursion and excursion time were measured as indicated by arrows. This example shows paired (10 Hz) twitch excursion of 3.0 cm in female participant.

Speckle-tracking analysis of diaphragm excursion was performed on the B-mode ultrasound using a specific software (EchoPac, v6.1, GE Medical). A region of interest (ROI) was drawn on the hyperechoic diaphragm structure using the apical long-axis Q-analysis tool. The ROI consisted of 5-7 points and was set to the narrowest width and shortest length allowed by the software. Moreover, the ROI was automatically partitioned into three sub-regions (Figure 4.2.2) that were analysed separately and averaged (Goutman et al., 2017). With speckle-tracking, diaphragm excursion was measured in the longitudinal (vertical) and transverse (horizontal) directions, which were, as per Pythagoras theorem, used in the calculation of diagonal diaphragm excursion (i.e., hypotenuse of a right-angled triangle) (Goutman et al., 2017). For all analysis techniques (M-mode, AM-mode and speckle-tracking), diaphragm excursion velocity (cm/s) was then calculated as the quotient of diaphragm excursion divided by excursion time. Diaphragm power ($cmH_2O/cm/s$) was calculated as the dot product of excursion velocity and $\Delta P_{di,tw}$ or $\Delta P_{di,sn}$.

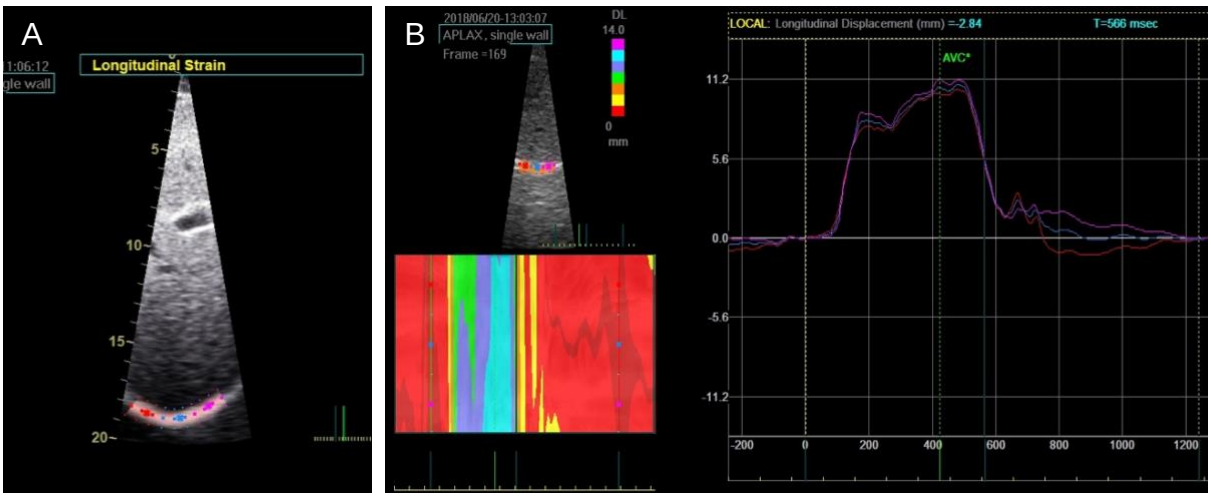

Figure 4.2.2 *A*) Speckle-tracking analysis of diaphragm excursion in response to a sniff. The region of interest (ROI) was drawn on the B-mode ultrasound and automatically divided into three sub-regions, distinguished by colours red, blue and pink. *B)* Diaphragm excursion expressed as a time-capture, with the ordinate representing excursion (mm) and the abscissa as time (ms).

4.2.6 Part 2

Six male participants volunteered for this part of the study. Only participants of (self-reported) male sex were included in this study due to the limited resources and time available to include female participants and to control for menstrual cycle phase in multi-visit studies (see section 3.3 for additional details). One male participant from *Part 1* also participated in this part of the study.

Supramaximal phrenic nerve stimulation and sniffs

Stimulation of phrenic nerves was performed as described in detail in section 3.9 in General Methods. Bilateral phrenic nerve stimulation was performed using the commercially available magnetic stimulators as described above (Magstim 200, Magstim Company Ltd.) connected to a paired-pulse stimulator (BiStim, Magstim Company Ltd.) and two figure-eight coils (D70 Alpha B.I, Magstim Company Ltd.). The paired-pulse stimulator enabled the triggering of both magnetic stimulators simultaneously with one single (1 Hz) twitch to two coils. The optimal stimulation areas were located on the anterior borders of the sternocleidomastoids, and the skin marked for subsequent stimulations (Mills et al., 1996). To check for supramaximal stimulation, each participant underwent an incremental stimulation protocol as described in *Part 1*.

The stimulation protocol comprised five single, non-potentiated twitches (1 Hz) and five maximal sniffs. All perturbations were separated by ≥30 s to avoid twitch potentiation (Wragg et al., 1994). As in *Part 1*, maximal sniffs were performed under the instruction to 'do a short, sharp sniff as hard as possible' (Miller, Moxham, and Green 1985, p.92).

Assessment of intrathoracic pressures and EMG_{di}

The P_{oe}, P_{ga} and EMG_{di} were measured using a gastro-oesophageal catheter (Gaeltec Devices Ltd., Isle of Skye, Scotland), as described in section 3.6.5 in General Methods. Briefly, the catheter was passed pernasally and swallowed into the stomach via peristalsis. The position of the catheter was adjusted such that a maximal sniff elicited negative and positive deflections in P_{oe} and P_{ga}, respectively. The correct position was confirmed with the "dynamic occlusion test" (Baydur et al., 1982), before the catheter was taped in position at the nose. Upon acquisition, the analogue signals for intrathoracic pressures and EMG_{di} were passed through a signal amplifier (1902, CED, Cambridge, UK) and digitised at sampling frequencies of 200 Hz (pressures) and 4 kHz (EMG_{di}) using an analogue-to-digital converter (1401mk-II, CED). Transdiaphragmatic pressure (P_{di}) was calculated online by subtraction of P_{oe} from P_{ga}.

Diaphragm ultrasonography

Measurement of costal diaphragm thickness and thickening is described in detail in section 3.10.6 in General Methods. Briefly, a high-frequency, linear ultrasound transducer (4.0-11.0 MHz, 10L, GE Medical) was positioned at the participant's right anterior or mid-axillary line at the 8-10th intercostal space to image the costal diaphragm at the zone of apposition. The specific position was determined by which pair of ribs produced the clearest image and was least affected by lung obscuration.

Ultrasound cine-loops were recorded and analysed with B-mode ultrasound (EchoPac v6.1, GE Medical). Costal diaphragm thickness was measured in triplicate as the distance between the inner borders of the pleural and peritoneal membranes at relaxation volume (immediately prior to twitch or sniff) and at peak thickness (Carrillo-Esper et al., 2016). Successfully analysed cine-loops were characterised by a clear diaphragm structure (incl. surrounding membranes) and the two adjacent ribs kept within the field of view before, during and after each perturbation. Relative thickening of costal diaphragm was calculated as *1*) thickening ratio = peak thickness / thickness at relaxation volume; and *2)* thickening fraction = (peak thickness – thickness at relaxation volume) / thickness at relaxation volume (Ferrari et al., 2018).

4.2.7 Data processing

Stimulation-evoked twitch pressure responses were measured as absolute pressure swings from point of stimulation to peak pressure response (i.e., $\Delta P_{di,tw}$, $\Delta P_{oe,tw}$ and $\Delta P_{ga,tw}$). The same approach was used for sniff pressure responses (i.e., $\Delta P_{di,sn}$, $\Delta P_{oe,sn}$ and $\Delta P_{ga,sn}$). End-expiratory oesophageal and gastric pressures (EEP_{oe} and EEP_{ga}) were measured at the point of stimulation to ensure that perturbations were performed at similar operating lung volume (Hubmayr et al., 1989) and with similar abdominal compliance (Koulouris, Mulvey, et al., 1989) during both trials. The mean rate of pressure development was calculated by dividing the absolute pressure swing (e.g., $\Delta P_{di,tw}$ and $\Delta P_{di,sn}$) by the time from stimulation to peak pressure response.

For *Part 2*, M-waves that were free of cardiac artefact, with constant shape and with stable baseline were identified (Luo et al., 2008). Next, peak-to-peak amplitude of each M-wave was measured. In addition, phrenic nerve conduction time (latency) was measured from the point of stimulation to the onset of the evoked potential (Aldrich et al., 2005). In *Part 1* and *Part 2*, the two highest twitch/sniff pressure responses, along with the associated ultrasound-derived measures, were averaged (mean) for statistical analysis.

4.2.8 Statistics

Statistical analysis was performed using SPSS (v26.0, IBM Corp., Armonk, NY, USA) and GraphPad Prism (v9.0, GraphPad Software LLC, San Diego, USA). Normal distribution of data was assessed with the Shapiro-Wilk test (incl. analysis of variance; ANOVA), unless otherwise indicated.

Feasibility

Specifically for *Part 1*, feasibility of ultrasound analysis was expressed as the percentage (min-max range) of successfully analysed cine-loops with a given analysis technique (M-mode, AM-mode and speckle-tracking) for each perturbation. To compare the percentage of successfully analysed cine-loops (feasibility) between analysis techniques, a two-way (technique-stimulation frequency) factorial ANOVA was performed. Bonferroni corrections were applied to reduce the probability for making a type I statistical error (i.e., incorrectly rejecting null hypothesis with multiple comparisons). Sphericity was checked using Mauchly's test, and, if violated, Greenhouse-Geisser correction was applied (O'Donoghue, 2012). Effect sizes were reported as partial eta squared (η_p^2) and interpreted as small (η_p^2 ≤0.01), medium (0.01–0.13) or large (≥0.14) (Lakens, 2013). In *Part 2,* feasibility was presented as percentage of successfully analysed cine-loops only.

Concurrent validity

In *Part 1*, differences in ultrasound-derived measures of diaphragm kinetics (excursion, excursion time, excursion velocity and power) between stimulation frequency (1, 10, 50 and 100 Hz) and ultrasound analysis techniques (M-mode, AM-mode and speckle-tracking) were assessed using a two-way (technique-stimulation frequency) factorial ANOVA. Again, Bonferroni corrections were applied for multiple comparisons. In addition, ultrasound-derived measures (excursion and excursion velocity) were validated against diaphragm pressure output ($\Delta P_{di,tw}$ and mean rate of pressure development) using linear regression and Pearson's coefficient of determination (r^2). Pearson's correlation coefficients were interpreted as weak (r^2 ≤0.45), moderate (0.45 – 0.70) or strong (≥0.70) (O'Donoghue, 2012). The effects of post-activation potentiation on intrathoracic pressure responses ($\Delta P_{di,tw}$, $\Delta P_{oe,tw}$, $\Delta P_{ga,tw}$) and diaphragm kinetics were assessed with paired samples *t*-tests between non-potentiated and potentiated twitch responses.

In *Part 2*, ultrasound-derived measures of diaphragm thickness and thickening were validated against $\Delta P_{di,tw}$ and $\Delta P_{di,sn}$ using multiple linear regression adjusted for duplicate measurements (Bland & Altman, 1995a). This approach was taken due to the relatively small sample size (*n* = 6), and enabled the correlation to be calculated based on measurements from trial 1 and trial 2 combined (6 participants × 2 repeated trials = 12 measurements in total) with correction for the paired measurements.

Within-day (between-trial) reliability

In *Part 1* and *Part 2*, within-day reliability of intrathoracic pressure responses ($\Delta P_{di,tw}$, $\Delta P_{oe,tw}$, $\Delta P_{ga,tw}$, $\Delta P_{di,sn}$, $\Delta P_{oe,sn}$ and $\Delta P_{ga,sn}$), compound muscle action potentials (*Part 2* only) and ultrasound-derived measures of diaphragm kinetics, thickness and thickening were assessed as coefficient of variation (CV) using the root mean square method for duplicate measurements (Hyslop & White, 2009):

$$CV\ (\%) = 100\ \times \sqrt{\frac{\Sigma(d/m)^2}{2n}}$$

where *d* is the difference between the two duplicate measurements (trial 1 and trial 2); *m* is the mean of the two duplicate measurements and *n* is the number of data pairs. Standard error of the CV was calculated as per Bland (2006):

$$Standard\ error = {sd_{CV}}\Big/{\sqrt{n}}$$

where *sd* is the standard deviation of the CV and *n* is the sample size. The 95% confidence intervals (CI) were calculated as the mean CV ± 1.96 standard error (Bland, 2006). Intra-class correlation coefficients (ICC) with 95% CI were calculated using a mean-rating (*k* = 2), absolute agreement, two-way mixed effects model. ICCs were defined as poor (ICC ≤0.5), moderate (0.50 – 0.75), good (0.75 – 0.90) or excellent (≥0.90) (Koo & Li, 2016).

4.3 Results

4.3.9 Part 1

Participants

Participant characteristics are shown in Table 4.3.1. Expectedly, male participants were taller and heavier and measured larger chest dimensions compared to women. For maximum respiratory pressures, MEP was greater in men than in women ($p = 0.01$). Diaphragm thickness and thickening fraction were within the range typically reported for healthy adults.

Table 4.3.1 Participant characteristics.

	Total (*n* = 10)	**Men (*n* = 5)**	**Women (*n* = 5)**
Anthropometrics			
Age, y	21.3 ± 2.2	22.0 ± 2.4	21.0 ± 2.4
Stature, cm	167 ± 11	175 ± 8	160 ± 9*
Body mass, kg	66.3 ± 11.7	77.5 ± 4.3	57.4 ± 6.3*
BMI, kg/m	23.5 ± 2.6	25.2 ± 3.1	22.3 ± 0.6
Chest circumference, cm	82.9 ± 9.8	91.8 ± 5.3	75.8 ± 5.2*
Chest depth, cm	19.6 ± 2.3	21.2 ± 2.6	18.3 ± 1.0*
Chest width, cm	27.5 ± 2.7	29.5 ± 0.6	25.6 ± 2.6*
Pulmonary function			
TLC, L (% pred)	5.97 ± 1.27 (100 ± 9)	7.11 ± 0.17 (102 ± 17)	5.02 ± 0.96* (96 ± 3)
RV, L (% pred)	1.56 ± 0.36 (118 ± 27)	1.60 ± 0.36 (115 ± 33)	1.41 ± 0.40* (120 ± 25)
FRC_{pleth}, L (% pred)	3.16 ± 0.85 (104 ± 18)	3.72 ± 0.88 (118 ± 24)	2.51 ± 0.54* (91 ± 13)
FVC, L (% pred)	4.71 ± 1.09 (108 ± 6)	5.69 ± 0.23 (107 ± 7)	3.92 ± 0.80* (106 ± 9)
FEV_1, L (% pred)	3.98 ± 0.84 (104 ± 8)	4.69 ± 0.25 (104 ± 8)	3.40 ± 0.68* (104 ± 10)
FEV_1/FVC (% pred)	0.84 ± 0.03 (97 ± 3)	0.82 ± 0.02 (96 ± 3)	0.86 ± 0.02 (98 ± 3)
MVV_{12}, L/min (% pred)	147 ± 23 (94 ± 13)	163 ± 10 (89 ± 10)	134 ± 23* (100 ± 13)
Maximum respiratory pressures			
MIP, cmH_2O (% pred)	–120 ± 25 (111 ± 21)	–132 ± 24 (115 ± 2)	–111 ± 25 (109 ± 20)
MEP, cmH_2O (% pred)	156 ± 38 (121 ± 19)	187 ± 34 (114 ± 23)	134 ± 23* (129 ± 10)
Diaphragm characteristics			
Mobility, cm[a]	6.46 ± 1.05	8.37 ± 1.16	6.11 ± 0.63*
Thickness at FRC, mm	1.3 ± 0.2	1.4 ± 0.1	1.2 ± 0.1
Thickness at TLC, mm	3.9 ± 0.9	4.4 ± 0.4	3.5 ± 0.4
Thickening fraction, %	287 ± 90	337 ± 35	245 ± 42

Data are mean ± *SD* for ten participants. % pred, percentage of predicted value; BMI, body mass index; TLC, total lung capacity; RV, residual volume; FRC_{pleth}, plethysmography-derived functional residual capacity; FVC, forced vital capacity; FEV_1, forced expiratory volume in 1 s; MVV_{12}. maximal voluntary ventilation in 12 s; MIP, maximum inspiratory mouth pressure; MEP, maximum expiratory mouth pressure. Predicted values for MVV_{12} were calculated as $FEV_1 \times 40$ (Miller et al., 2005). Predicted values for maximum mouth pressures were derived from the equations of Evans & Whitelaw (2009). [a]measured with AM-mode ultrasound; *$p \leq 0.05$ vs. men.

Feasibility

A total of 342 and 102 ultrasound cine-loops were recorded in response to stimulation-evoked twitches and sniffs, respectively. Of those cine-loops, 312 and 71, respectively, were considered technically acceptable, meaning that subsequent analysis could be performed. The proportions of successfully analysed cine-loops with M-mode, AM-mode and speckle-tracking are shown in Table 4.3.2.

Table 4.3.2 Percentage (%) successfully analysed ultrasound cine-loops using M-mode, AM-mode and speckle-tracking in response to twitch contractions and maximal sniffs.

	1 Hz (NPOT)	1 Hz (POT)	10 Hz	50 Hz	100 Hz	Sniffs	Median
Motion-mode ultrasonography							
M-mode	92 (80-100)	93 (70-100)	100 (0)	96 (83-100)	96 (86-100)	94 (80-100)	95 (0-100)
AM-mode	94 (80-100)	98 (90-100)	88 (0)	98 (83-100)	98 (86-100)	96 (80-100)	95 (0-100)
Speckle-tracking							
2/3 ROI[a]	75 (60-90)	71 (60-89)	94 (89-100)	92 (83-100)	83 (0)	47 (0-100)	75 (0-100)
3/3 ROI[b]	65 (40-90)	63 (46-89)	63 (55-72)	83 (0)	67 (50-83)	47 (25-71)	64 (0-90)

Data are median (upper-lower range) for 10 participants. NPOT, non-potentiated; POT, potentiated; M-mode, conventional motion-mode ultrasound; AM-mode, angle-independent motion-mode ultrasound. [a] Two out of three ROI sub-regions successfully analysed (incl. middle region); [b]three out of three ROI sub-regions successfully analysed.

For speckle-tracking, only (median) 64% of the cine-loops had all three ROI sub-regions successfully analysed, whereas 75% had two out of the three sub-regions successfully analysed. Moreover, less than half (47%) of the cine-loops obtained during maximal sniffs could be successfully analysed using speckle-tracking. The main reasons for unsuccessful speckle-tracking analysis were: too rapid and/or large movement for software to track the hyperechoic hemi-diaphragm (46%), lateral excursion (42%); or unsuccessful/aborted tracking reported by the software (12%). Due to the time-consuming process of performing speckle-tracking analysis, and the poor feasibility, it was concluded that speckle-tracking was not feasible in the present study. Accordingly, the analysis technique was excluded from further analysis.

For M-mode and AM-mode, 95% of cine-loops could be successfully analysed. In addition, there was no difference between the proportions analysed for the two techniques, regardless of stimulation frequency ($p = 0.637$), level of post-activation potentiation ($p = 0.425$) or response to sniffs ($p = 0.234$). With M-mode and AM-mode, failed cine-loop analysis was primarily

attributable to an unclear hyperechoic diaphragm structure at the initiation of the stimulation or sniff, at peak excursion, or both.

Supramaximal phrenic nerve stimulation

Pressure responses ($\Delta P_{di,tw}$) to incremental stimulation power are shown in Figure 4.3.1. Although $\Delta P_{di,tw}$ was statistically different between 50 and 60% of stimulation power ($p = 0.02$), participants exhibited a plateau in $\Delta P_{di,tw}$ (as per the CV method described previously) at 85 ($n = 5$), 90 ($n = 3$), 95 ($n = 1$) and 100% ($n = 1$) of maximal stimulation power.

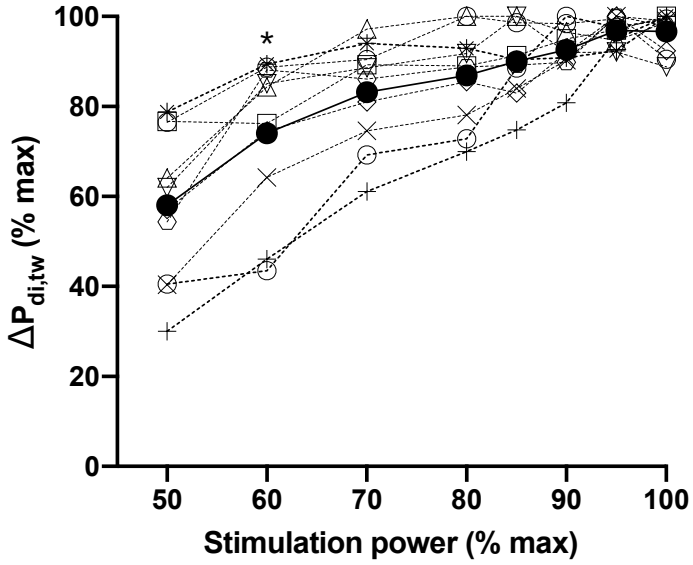

Figure 4.3.1 Individual participant (⋯; $n = 10$ and group mean (—) $\Delta P_{di,tw}$ in response to increasing stimulation power. Data are for 10 participants. *$p \leq 0.05$ vs. previous stimulation power.

Effect of stimulation frequency on intrathoracic pressures and diaphragm kinetics

Expectedly, $\Delta P_{di,tw}$ increased as a function of stimulation frequency in both trials (Figure 4.3.2) Specifically, there was a main effect of stimulation frequency in both trials ($p < 0.001$; $\eta_p^2 = 0.742$), and there was no difference in $\Delta P_{di,tw}$ between the two trials ($p = 0.947$; $\eta_p^2 = 0.001$).

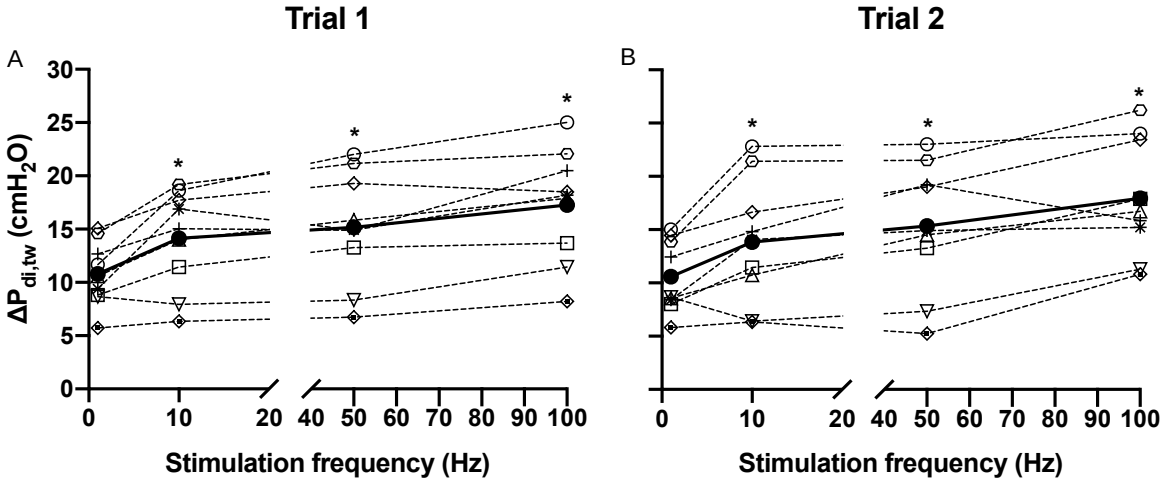

Figure 4.3.2 Individual (---) and group mean (—) $\Delta P_{di,tw}$ in response to increasing stimulation frequency in trial 1 (*A*) and trial 2 (*B*). *$p \leq 0.05$ vs. 1 Hz.

As shown in Figure 4.3.3, diaphragm excursion tended to increase with stimulation frequency. In this figure, four representative equally-scaled AM-mode cine-loops show how excursion increased in a female participant in response to the increasing stimulation frequencies.

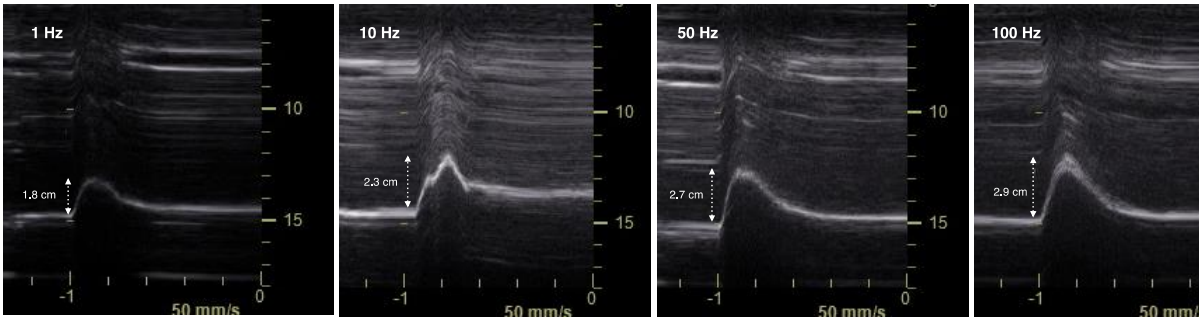

Figure 4.3.3 Representative AM-mode images of crural diaphragm excursion in response to increasing stimulation frequency. The *x*-axes (time) and *y*-axes (excursion) are scaled similarly in each panel for visual comparison. Excursion was measured to 1.8, 2.3, 2.7 and 2.9 cm in response to 1-100 Hz, and were obtained from a female participant.

Also group mean responses showed that diaphragm excursion increased with stimulation frequency (p = 0.024; η_p^2 = 0.884), and did not differ between the two trials (p = 0.960; η_p^2 = 0.001; Figure 4.3.4). Similarly, diaphragm excursion velocity increased as a function of stimulation frequency (p < 0.001; η_p^2 = 0.688), and did not differ between the two trials (p = 0.536; η_p^2 = 0.805). It is worth noting that excursion velocity was lower at 10 Hz compared to 1 Hz and 50 Hz due to the prolonged inter-stimulus interval (100 ms) at this stimulation frequency. Therefore, excursion velocity at 1 Hz did not differ from 10 Hz (p = 0.867) but increased from 10 Hz to 50 Hz (p = 0.001) and to 100 Hz (p = 0.006). Predictably, therefore, diaphragm power also increased as a function of stimulation frequency (p < 0.001; η_p^2 = 0.712), and did not differ between the two trials (p = 0.672; η_p^2 = 0.032; Figure 4.3.5).

Comparing diaphragm kinetics measured with M-mode and AM-mode, it was evident that AM-mode measured greater excursion than M-mode (p = 0.011; η_p^2 = 0.689), with *post hoc* tests showing that this was true in trial 1 at 50 Hz, and in trial 2 at 10 and 100 Hz (Figure 4.3.4). The two techniques did, however, measure similar excursion velocity (p = 0.06; η_p^2 = 0.904) and power (p = 0.138; η_p^2 =0.328; Figure 4.3.5).

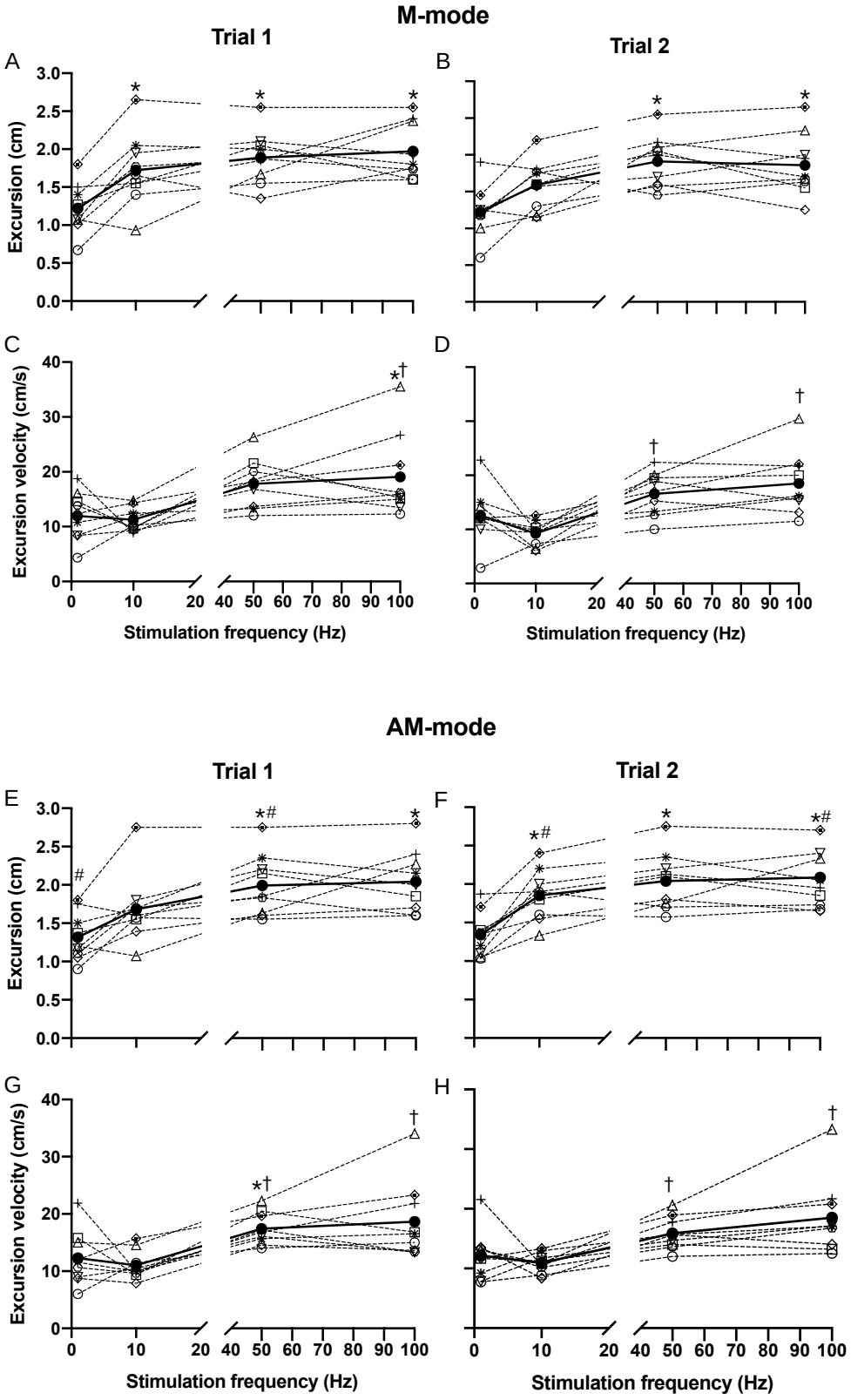

Figure 4.3.4 Individual (---) and group mean (—) ultrasound-derived diaphragm excursion and excursion velocity in response to increasing stimulation frequency in trial 1 and trial 2. Diaphragm excursion was measured with M-mode (*A-D*) and AM-mode (*E-H*). Data are for 10 participants. *$p \leq$ 0.05 vs. 1 Hz; †$p \leq 0.05$ vs. 10 Hz; #$p \leq 0.05$ vs. M-mode ultrasound at same stimulation frequency.

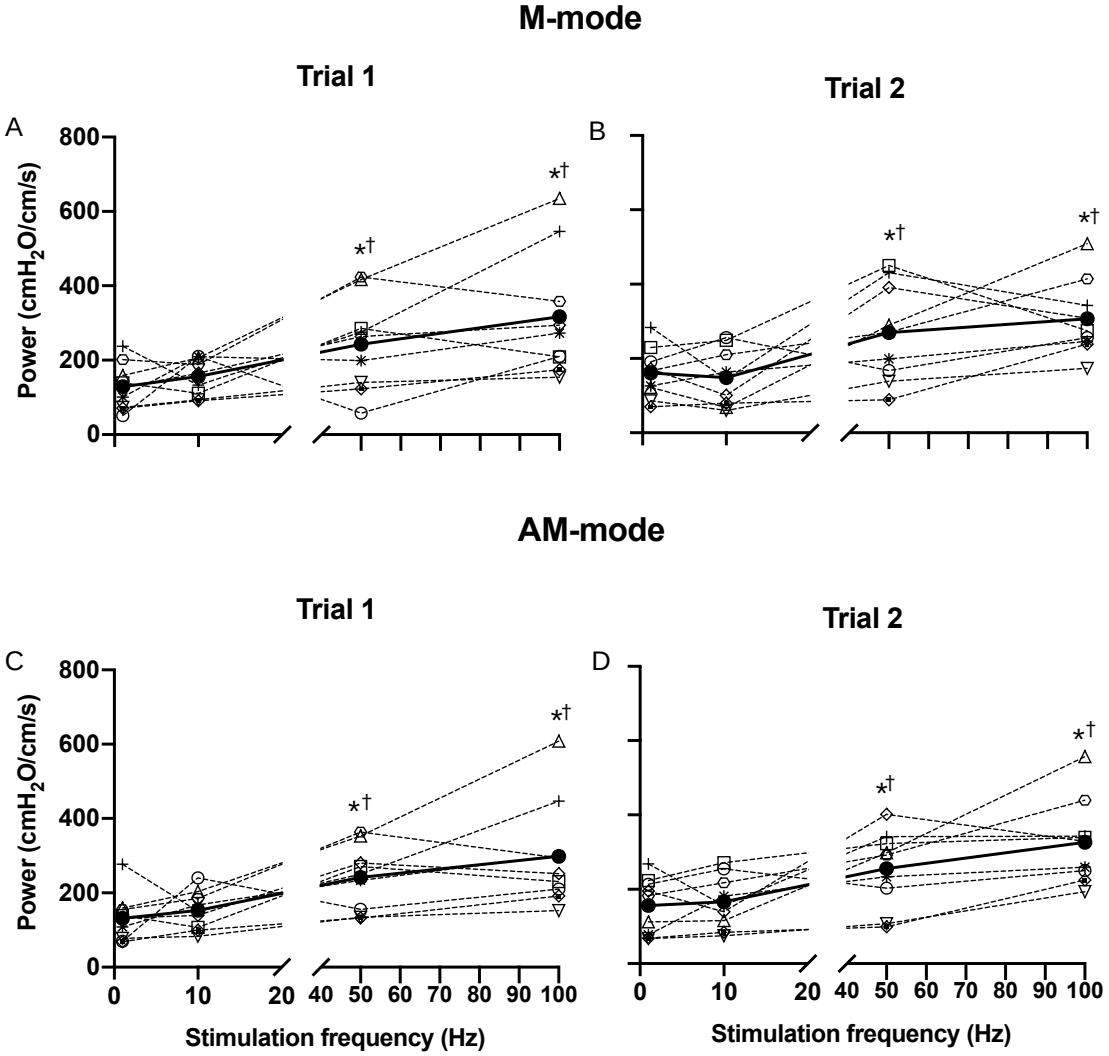

Figure 4.3.5 Individual (---) and group mean (—) ultrasound-derived diaphragm power in response increasing stimulation frequency in trial 1 and trial 2. Diaphragm excursion was measured with M-mode (*A*-*B*) and AM-mode (*C*-*D*). Data are for 10 participants. *$p \leq 0.05$ vs. 1 Hz; †$p \leq 0.05$ vs. 10 Hz.

Within-day reliability

Within-day comparisons of intrathoracic pressure responses to various stimulation frequencies are shown in Table 4.3.3. Similarly, diaphragm kinetics in response to various stimulation frequencies are shown in Table 4.3.4-6. It was evident that ultrasound-derived diaphragm excursion generally exhibited moderate-to-good levels of within-day reliability in the form of ICCs (≥0.638) and CV (≤10%), regardless of stimulation frequency and analysis technique used. With AM-mode, the CV was notably lower compared to M-mode across stimulation frequencies, although ICCs appeared to be similar between the two techniques. Also, diaphragm excursion velocity exhibited moderate-to-excellent levels of within-day reliability in the form of ICCs (≥0.830) and CV (≤11%), with the exception of excursion velocity measured at 50 Hz, which was markedly lower than what was obtained at other stimulation frequencies (M-mode: ICC 0.319, CI 95%: –0.514 – 0.838, $p = 0.228$; Table 4.3.5). Within-day reliability of diaphragm power was, however, more variable across the range of stimulation frequencies; ranging from ICC (95% CI) of 0.173 (–0.571 – 0.734) at 10 Hz assessed with M-mode to ICC of 0.872 (0.556 – 0.969) at 1 Hz assessed with M-mode (Table 4.3.6).

Table 4.3.3 Within-day comparisons of *pressure responses* to twitch contractions with increasing stimulation frequency.

			Coefficient of variation		**Intra-class correlation coefficient**		
	Trial 1 (cmH_2O)	**Trial 2** (cmH_2O)	CV (%)	95% CI (%)	ICC	95% CI	*p*-value
1 Hz							
$\Delta P_{di,tw}$	10.6 ± 3.2	9.6 ± 3.8	5.8 ± 5.2	0.3 – 12.8	0.788	–0.034 – 0.953	0.027
$\Delta P_{oe,tw}$	–6.3 ± 2.9	–4.4 ± 3.3*	13.6 ± 12.6	3.2 – 22.0	0.836	0.313 – 0.960	<0.001
$\Delta P_{ga,tw}$	4.7 ± 2.5	5.4 ± 4.5	24.0 ± 22.4	8.6 – 39.5	0.296	–0.210 – 0.828	0.087
10 Hz							
$\Delta P_{di,tw}$	12.7 ± 4.9	12.5 ± 5.2	6.1 ± 5.1	2.5 – 9.6	0.954	0.794 – 0.990	<0.001
$\Delta P_{oe,tw}$	–8.5 ± 3.9	–6.4 ± 4.2	20.2 ± 19.5	6.6 – 33.7	0.774	0.038 – 0.959	0.030
$\Delta P_{ga,tw}$	5.8 ± 2.8	7.1 ± 4.0	15.6 ± 14.9	5.3 – 25.9	0.387	–0.441 – 0.859	0.179
50 Hz							
$\Delta P_{di,tw}$	14.2 ± 5.3	16.7 ± 7.9	8.5 ± 5.4	4.7 – 12.2	0.859	0.305 – 0.975	0.011
$\Delta P_{oe,tw}$	–9.6 ± 4.2	–8.8 ± 4.9	12.8 ± 12.0	3.1 – 20.9	0.915	0.615 – 0.985	<0.001
$\Delta P_{ga,tw}$	7.3 ± 2.2	9.0 ± 4.9	9.8 ± 8.2	4.1 – 15.5	0.313	–0.275 – 0.814	0.178
100 Hz							
$\Delta P_{di,tw}$	16.1 ± 4.9	18.1 ± 6.1	11.3 ± 8.4	3.0 – 14.7	0.536	–0.163 – 0.884	0.069
$\Delta P_{oe,tw}$	–10.8 ± 3.6	–9.4 ± 4.1	12.6 ± 9.4	7.6 – 20.7	0.850	0.341 – 0.969	0.008
$\Delta P_{ga,tw}$	8.4 ± 3.4	11.0 ± 5.3	16.7 ± 11.4	3.1 – 19.0	0.400	–0.578 – 0.908	0.117

Data are mean ± *SD* for 10 participants. CV, coefficient of variation for duplicate measurements; 95% CI, 95% confidence interval; ICC, intra-class correlation coefficient; $\Delta P_{di,tw}$, twitch transdiaphragmatic pressure; $\Delta P_{oe,tw}$, twitch oesophageal pressure; $\Delta P_{ga,tw}$, twitch gastric pressure. *$p \leq 0.05$ vs. trial 1.

Table 4.3.4 Within-day comparisons of *diaphragm excursion* in response to twitch contractions with increasing stimulation frequency.

			Coefficient of variation		**Intra-class correlation coefficient**		
	Trial 1 (cm)	**Trial 2** (cm)	CV (%)	95% CI (%)	ICC	95% CI	*p*-value
1 Hz							
M-mode	1.32 ± 0.31	1.35 (0.34)	6.8 ± 3.9	4.2 – 9.5	0.782	0.273 – 0.947	0.005
AM-mode	1.40 ± 0.34	1.41 (0.36)	6.4 ± 3.9	3.7 – 9.2	0.799	0.329 - 0.951	0.004
10 Hz							
M-mode	1.79 ± 0.52	1.63 ± 0.37	9.2 ± 5.8	5.1 – 13.2	0.903	0.496 – 0.983	0.004
AM-mode	1.71 ± 0.52	1.90 ± 0.36	8.2 ± 3.3	5.9 – 10.5	0.901	0.480 – 0.980	0.005
50 Hz							
M-mode	1.90 ± 0.41	1.93 ± 0.42	8.4 ± 4.5	5.3 – 11.6	0.638	–0.21 – 0.929	0.057
AM-mode	1.98 ± 0.43	2.06 ± 0.40	3.3 ± 2.9	1.3 – 5.4	0.926	0.673 – 0.987	<0.001
100 Hz							
M-mode	2.01 ± 0.34	1.88 ± 0.42	4.8 ± 5.7	0.9 – 8.8	0.823	0.367 – 0.962	0.002
AM-mode	2.09 ± 0.37	2.08 ± 0.34	3.8 ± 3.8	1.2 – 6.5	0.820	0.316 – 0.962	0.005

Data are mean ± *SD* for 10 participants. CV, coefficient of variation of duplicate measurements; 95% CI, 95% confidence intervals; ICC, intra-class correlation coefficient; M-mode, conventional motion-mode ultrasound; AM-mode, angle-independent motion-mode ultrasound.

Table 4.3.5 Within-day comparisons of *diaphragm excursion velocity* in response to twitch contractions with increasing stimulation frequency.

			Coefficient of variation		**Intra-class correlation coefficient**		
	Trial 1 (cm/s)	**Trial 2** (cm/s)	CV (%)	95% CI (%)	ICC	95% CI	*p*-value
1 Hz							
M-mode	13.88 ± 3.87	14.24 ± 5.01	10.7 ± 6.2	6.4 – 15.0	0.845	0.470 – 0.963	0.001
AM-mode	13.70 ± 5.07	13.49 ± 4.99	9.5 ± 6.2	5.2 – 13.8	0.830	0.401 – 0.959	0.002
10 Hz							
M-mode	19.91 ± 7.62	18.18 ± 6.28	7.3 ± 5.2	3.6 – 11.0	0.893	0.563 – 0.978	<0.001
AM-mode	19.10 ± 7.12	19.25 ± 6.38	5.8 ± 5.3	2.0 – 9.5	0.935	0.711 – 0.987	<0.001
50 Hz							
M-mode	18.92 ± 4.21	17.69 ± 3.50	10.0 ± 7.1	5.1 – 15.0	0.319	–0.514 – 0.838	0.228
AM-mode	17.76 ± 2.76	16.88 ± 2.69	4.7 ± 3.5	2.2 – 7.1	0.458	–0.194 – 0.871	0.095
100 Hz							
M-mode	19.91 ± 7.13	18.17 ± 5.87	7.3 ± 5.2	3.7 – 11.0	0.893	0.563 – 0.978	<0.001
AM-mode	19.09 ± 6.6	19.25 ± 5.97	5.7 ± 5.3	2.1 – 9.5	0.935	0.711 – 0.987	<0.001

Data are mean ± *SD* for 10 participants. CV, coefficient of variation of duplicate measurements; 95% CI, 95% confidence intervals; ICC, intra-class correlation coefficient; M-mode, conventional motion-mode ultrasound; AM-mode, angle-independent motion-mode ultrasound.

Table 4.3.6 Within-day comparisons of *diaphragm power* in response to twitch contractions with increasing stimulation frequency.

	Trial 1	**Trial 2**	**Coefficient of variation**		**Intra-class correlation coefficient**		
	(cmH_2O/cm/s)	(cmH_2O/cm/s)	CV (%)	95% CI (%)	ICC	95% CI	*p*-value
1 Hz							
M-mode	139 ± 64	157 ± 71	8.8 ± 7.5	3.3 – 13.7	0.872	0.556 – 0.969	<0.001
AM-mode	139 ± 61	150 ± 69	14.6 ± 11.9	6.4 – 22.9	0.738	0.242 – 0.933	0.007
10 Hz							
M-mode	154 ± 48	138 ± 66	20.3 ± 16.9	8.6 – 32.0	0.173	–0.571 – 0.734	0.325
AM-mode	150 ± 44	161 ± 64	11.5 ± 15.5	0.7 – 22.2	0.321	–0.455 – 0.789	0.198
50 Hz							
M-mode	274 ± 129	268 ± 135	16.3 ± 8.0	10.7 – 21.8	0.513	–0.394 – 0.898	0.114
AM-mode	252 ± 102	257 ± 125	12.9 ± 3.4	10.5 – 15.3	0.764	0.099 – 0.956	0.018
100 Hz							
M-mode	331 ± 164	313 ± 101	10.4 ± 6.7	5.8 – 15.1	0.787	0.250 – 0.953	0.008
AM-mode	309 ± 140	336 ± 111	12.1 ± 5.5	8.3 – 16.0	0.803	0.494 – 0.978	0.005

Data are mean ± *SD* for 10 participants. CV, coefficient of variation of duplicate measurements; 95% CI, 95% confidence intervals; ICC, intra-class correlation coefficient; M-mode, motion-mode ultrasound; AM-mode, angle-independent motion-mode ultrasound.

Concurrent validity and the relationship with respiratory pressures

Figure 4.3.6A shows the strong relationship between $\Delta P_{di,tw}$ and ultrasound-derived measures of diaphragm excursion, which was similar between M-mode and AM-mode ($p = 0.256$). There were also strong relationships between the mean rate of pressure development and ultrasound-derived measure of diaphragm excursion velocity (Figure 4.3.6B), which also did not differ between M-mode and AM-mode ($p = 0.207$).

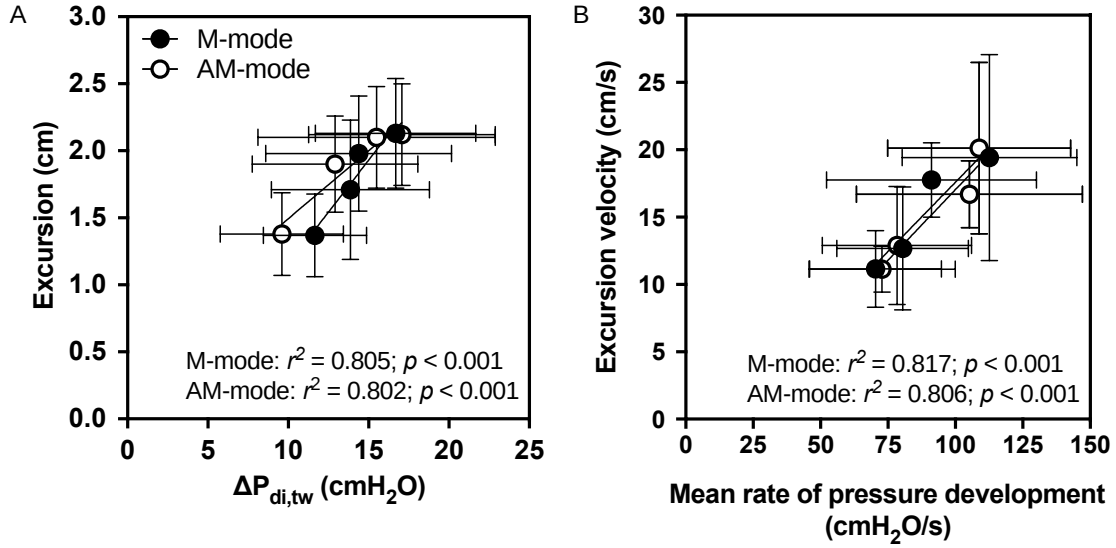

Figure 4.3.6 Relationship between *A*) $\Delta P_{di,tw}$ and diaphragm excursion; *B)* mean rate of pressure development and excursion velocity, measured with M-mode (●) and AM-mode (○). The data represent the responses to 1, 10, 50 and 100 Hz stimulation. Coefficient of determination (r^2) with *p*-values are shown for each relationship. Data are mean ± *SD* of duplicate measures for 10 participants.

Post-activation potentiation

Figure 4.3.7 shows the effect of post-activation potentiation on $\Delta P_{di,tw}$. Following prior activation, $\Delta P_{di,tw}$ increased from 10.8 ± 3.0 to 13.2 ± 4.6 cmH_2O in trial 1 (p = 0.009; 22 ± 2%), and from 12.4 ± 5.0 to 15.8 ± 5.1 cmH_2O in trial 2 (p = 0.023; 27 ± 4%). The effect of post-activation potentiation on $\Delta P_{di,tw}$ was not different between trial 1 and trial 2 (p = 0.192; η_p^2 = 0.248).

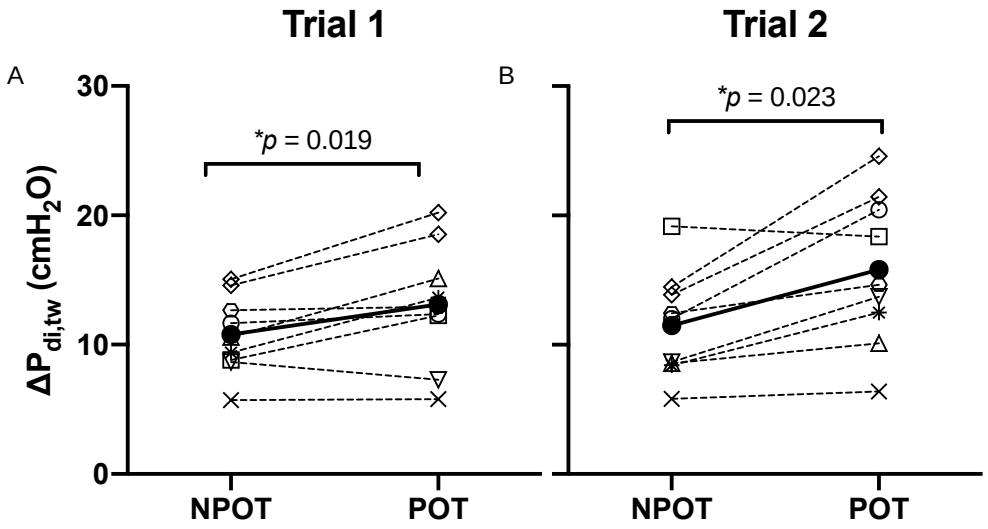

Figure 4.3.7 Individual (---) and group mean (—) non-potentiated (NPOT) and potentiated (POT) $\Delta P_{di,tw}$ in trial 1 and trial 2 for 10 participants. *$p \leq 0.05$.

Figure 4.3.8 shows diaphragm kinetic response to post-activation potentiation. There was a main effect of post-activation potentiation on diaphragm excursion (p = 0.049; η_p^2 = 0.375), with *post hoc* tests showing that excursion increased in trial 1 (p = 0.027) but not in trial 2 (p = 0.186). As with non-potentiated twitches (above), AM-mode measured greater potentiated excursion compared to M-mode in both trial 1 (p = 0.012) and trial 2 (p = 0.004). As shown in Figure 4.3.8, however, there was no effect of post-activation potentiation on diaphragm excursion velocity (p = 0.541; η_p^2 = 0.049). Similarly, potentiated excursion velocity did not differ between the two trials (p = 0.711; η_p^2 = 0.018) and was not different between M-mode and AM-mode (p = 0.562; η_p^2 = 0.044). Combined, these results suggest that the diaphragm muscle may move more, but not necessarily faster, when potentiated.

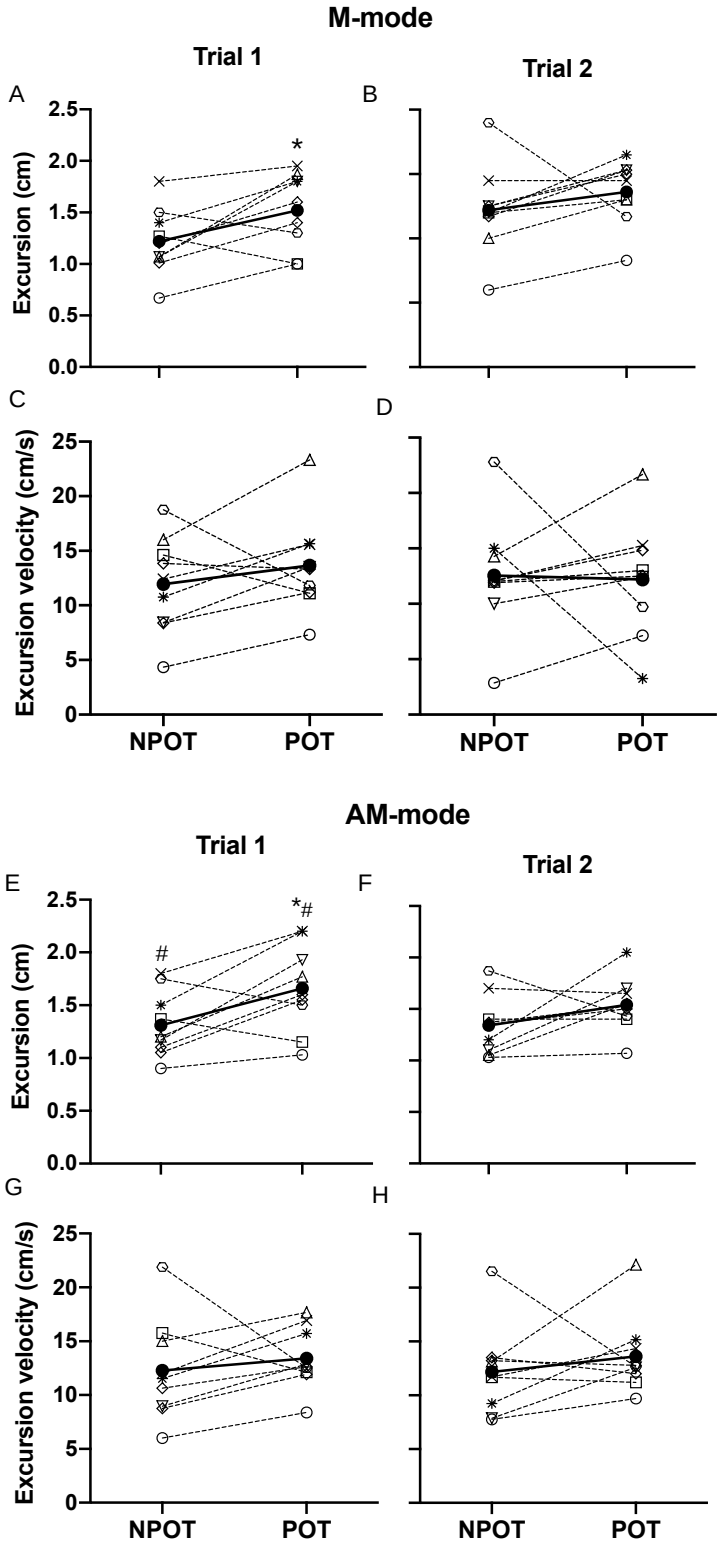

Figure 4.3.8 Individual (---) and group mean (—) responses in ultrasound-derived excursion and excursion velocity to 1 Hz non-potentiated (NPOT) and potentiated (POT), measured with M-mode and AM-mode. *$p \leq 0.05$ vs. NPOT; $^{\#}p \leq 0.05$ vs. M-mode. Data are for 10 participants.

Table 4.3.7 Within-day comparison of intrathoracic pressures and diaphragm kinetic responses to 1 Hz (potentiated) twitch contraction.

			Coefficient of variation		**Intra-class correlation coefficient**		
	Trial 1	**Trial 2**	CV (%)	95% CI (%)	ICC	95% CI	*p*-value
Pressure responses (cmH_2O)							
$\Delta P_{di,tw}$	13.2 ± 4.6	15.8 ± 5.1	15.3 ± 9.6	8.7 – 22.0	0.812	0.249 – 0.957	0.013
$\Delta P_{oe,tw}$	–8.7 ± 2.4	–9.4 ± 3.8	10.5 ± 8.6	4.5 – 16.5	0.845	0.444 – 0.966	0.001
$\Delta P_{ga,tw}$	4.5 ± 2.6	6.4 ± 4	25.4 ± 13.7	15.9 – 34.8	0.722	–0.199 – 0.949	0.045
Excursion (cm)							
M-mode	1.67 ± 0.25	1.45 ± 0.16	8.0 ± 6.0	3.8 – 12.1	0.574	–0.006 – 0.880	0.026
AM-mode	1.82 ± 0.30	1.63 ± 0.21	5.3 ± 4.5	2.1 – 8.3	0.775	0.312 – 0.943	0.003
Excursion velocity (cm/s)							
M-mode	12.71 ± 2.73	12.81 ± 5.62	19.7 ± 25.6	1.9 – 37.4	0.600	–0.015 – 0.891	0.033
AM-mode	12.41 ± 2.8	12.62 ± 3.57	3.9 ± 4.1	1.0 – 6.6	0.842	0.441 – 0.962	0.002
Power (cmH_2O/cm/s)							
M-mode	163.8 ± 64.8	185.1 ± 103.5	20.1 ± 22.9	4.2 – 35.9	0.326	–0.315 – 0.787	0.169
AM-mode	187.0 ± 70.1	204.6 ± 68.0	10.3 ± 8.7	4.2 – 16.2	0.668	0.103 – 0.912	0.009

Data are mean ± *SD* for 10 participants. CV, coefficient of variation of duplicate measurements; 95% CI, 95% confidence interval; ICC, intra-class correlation coefficient; $\Delta P_{di,tw}$, twitch transdiaphragmatic pressure; $\Delta P_{oe,tw}$, twitch oesophageal pressure; $\Delta P_{ga,tw}$, twitch gastric pressure; M-mode, conventional motion-mode ultrasound; AM-mode, angle-independent motion-mode ultrasound.

Maximal sniffs

Maximal sniff pressures, as well as ultrasound-derived measures of diaphragm sniff kinetics are shown in Table 4.3.8. The $\Delta P_{di,sn}$ did not differ between the two trials (p = 0.454), and neither did $\Delta P_{oe,sn}$ (p = 0.259) or $\Delta P_{ga,sn}$ (p = 0.461). Despite the volitional nature of the manoeuvre, maximal sniff pressures exhibited good-to-excellent within-day reliability in the form of ICC (≥0.830) and CV (≤17%). With M-mode, diaphragm sniff excursion was 1.74 ± 0.62 cm and 1.81 ± 0.80 cm in trial 1 and trial 2, respectively, and did not differ between the two trials (p = 0.625). With AM-mode, excursion was 1.84 ± 0.62 cm and 1.99 ± 0.54 cm in trial 1 and trial 2, respectively, and did not differ between the two trials (p = 0.659). Although AM-mode tended to measure greater diaphragm excursion compared to M-mode, this was not statistically significant (p = 0.251). Compared to stimulation-evoked twitch contractions, diaphragm sniff excursion was comparable to that measured in response to the 1 Hz potentiated twitch and the 10 Hz paired twitch (see Table 4.3.7). Diaphragm sniff excursion velocity did not differ between the two trials (p = 0.230), and again, AM-mode tended to measure slower excursion velocity compared to M-mode, but this was not statistically significant (p = 0.089). Predictably, sniff excursion velocity was substantially slower than the excursion velocity measured during twitch contractions (22% slower compared to 1 Hz; –37% slower compared to 100 Hz).

Table 4.3.8 Within-day comparison of intrathoracic pressures and diaphragm kinetics in response to maximal sniffs.

			Coefficient of variation		Intra-class correlation coefficient		
	Trial 1	**Trial 2**	CV (%)	95% CI (%)	ICC	95% CI	*p*-value
Intrathoracic pressures (cmH_2O)							
$\Delta P_{di,sn}$	79.9 ± 40.7	83.5 ± 33.4	9.8 ± 8.6	2.3 – 15.2	0.830	0.389 – 0.965	0.003
$\Delta P_{oe,sn}$	–54.8 ± 23.7	–51.5 ± 20.1	6.6 ± 5.6	2.8 – 10.3	0.834	0.411 – 0.960	0.002
$\Delta P_{ga,sn}$	31.1 ± 28.8	31.1 ± 24.2	16.9 ± 9.6	10.6 – 23.1	0.906	0.633 – 0.978	<0.001
Excursion (cm)							
M-mode	1.74 ± 0.62	1.81 ± 0.80	8.5 ± 5.1	5.1 – 11.8	0.833	0.407 – 0.960	0.001
AM-mode	1.84 ± 0.62	1.99 ± 0.54	7.4 ± 5.6	3.7 – 11.1	0.813	0.408 – 0.954	0.002
Excursion velocity (cm/s)							
M-mode	11.68 ± 5.82	10.74 ± 5.78	13.4 ± 17.6	1.8 – 24.9	0.896	0.557 – 0.976	0.003
AM-mode	10.87 ± 6.36	11.27 ± 4.60	11.3 ± 10.0	4.1 – 18.4	0.887	0.485 – 0.975	0.004
Power (cmH_2O/cm/s)							
M-mode	974 ± 724	964 ± 695	11.4 ± 9.2	5.3 – 17.4	0.954	0.808 – 0.989	<0.001
AM-mode	927 ± 800	910 ± 653	13.2 ± 8.6	7.5 – 18.8	0.912	0.792 – 0.990	<0.001

Data are mean ± *SD* for 10 participants. CV, coefficient of variation of duplicate measurements; 95% CI, 95% confidence intervals; ICC, intra-class correlation coefficient; $\Delta P_{di,sn}$, sniff transdiaphragmatic pressure; $\Delta P_{oe,sn}$, sniff oesophageal pressure; $\Delta P_{ga,sn}$, sniff gastric pressure; M-mode, motion-mode ultrasound; AM-mode, angle-independent motion-mode ultrasound.

4.3.10 Part 2

Participant characteristics are shown in Table 4.3.9. One male participant from *Part 1* also participated in this part of the study. In line with inclusion criteria, participants exhibited clear diaphragm thickening during quiet breathing, and measured diaphragm thickness within the range previously reported in healthy adults.

Table 4.3.9 Participant characteristics.

	Mean ± *SD*
Anthropometry	
Age, y	24.0 ± 7.3
Stature, cm	183.0 ± 5.6
Body mass, kg	81.2 ± 6.8
BMI, kg/m^2	24.4 ± 2.5
Chest depth, cm	21.8 ± 3.1
Chest width, cm	30.5 ± 1.0
Chest circumference, cm	95.3 ± 3.4
Pulmonary function	
TLC, L (% predicted)	7.85 ± 0.81 (104 ± 8)
RV, L (% predicted)	1.99 ± 0.19 (118 ± 13)
FRC_{pleth}, L (% predicted)	3.89 ± 0.77 (113 ± 20)
FVC, L (% predicted)	6.27 ± 0.61 (107 ± 11)
FEV_1, L (% predicted)	5.06 ± 0.52 (104± 8)
FEV_1/FVC (% predicted)	0.80 ± 0.07 (95 ± 7)
MVV_{12} (% predicted)	202 ± 21 (100 ±13)
Maximal respiratory pressures	
MIP, cmH_2O (% predicted)	–129 ± 19 (118 ± 22)
MEP, cmH_2O (% predicted)	179 ± 51 (118 ± 40)
Diaphragm structure and function	
Diaphragm thickness at FRC, mm	1.50 ± 0.51
Diaphragm thickness at TLC, mm	4.22 ± 0.63
Thickening fraction, %	181 ± 21
Maximal diaphragm mobility, cm	6.9 ± 1.4

Data are mean ± *SD* for six participants. BMI, body mass index; TLC, total lung capacity; RV, residual volume; FRC_{pleth}, functional residual capacity via plethysmography; FVC, forced vital capacity; FEV_1, forced expiratory volume in 1 s; MVV_{12}, maximal voluntary ventilation in 12 s; MIP, maximum inspiratory mouth pressure; MEP, maximum expiratory mouth pressure. Predicted values for pulmonary function were derived from Quanjer et al. (2012) for spirometry and Stocks & Quanjer (1995) for whole-body plethysmography. Predicted values for MVV_{12} were calculated as $FEV_1 \times 40$ (Miller et al., 2005). Predicted values for maximum mouth pressures were derived from the equations of Evans & Whitelaw (2009).

Feasibility

A total of 62 and 68 ultrasound-cine-loops were acquired in response to stimulation-evoked twitch contractions and maximal sniffs, respectively. Of those cine-loops, all cine-loops acquired during twitch contractions and 66 (96%) cine-loops acquired during sniffs were considered technically acceptable, meaning that they could be used for subsequent analysis. The small number of technically unacceptable cine-loops for sniffs were recorded in one participant who exhibited a particularly large muscle distortion during the manoeuvre, whereby the diaphragm moved laterally out of the field of view.

Supramaximal phrenic nerve stimulation

Pressure responses ($\Delta P_{di,tw}$) to incremental stimulation power are shown in Figure 4.3.9. Although $\Delta P_{di,tw}$ was statistically different from 50 to 60% ($p = 0.043$), and from 60 to 70% ($p = 0.048$) of maximal stimulation power, participants exhibited a plateau in $\Delta P_{di,tw}$ (per the CV method described previously) at 90% ($n = 2$), at 95% ($n = 2$) or at 100% ($n = 2$) of maximal stimulation power.

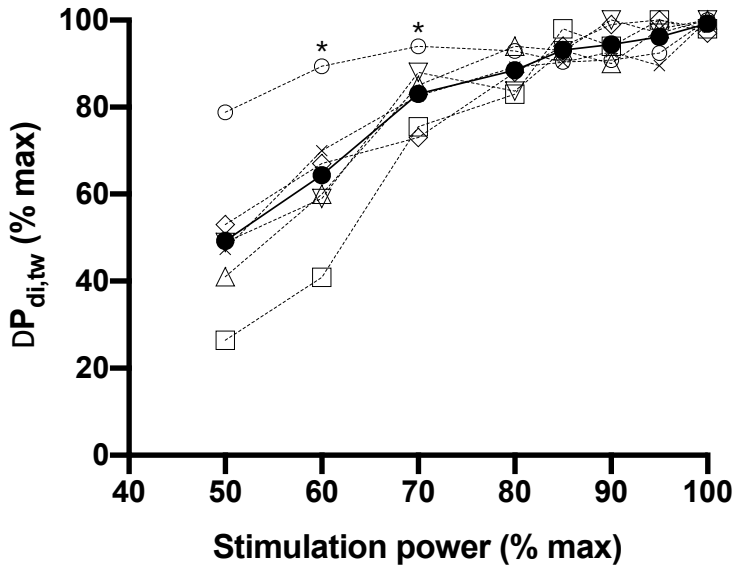

Figure 4.3.9 Individual participant (⋯; $n = 6$) and group mean (—) $\Delta P_{di,tw}$ in response to increasing stimulation power. *$p \leq 0.05$ vs. previous stimulation power.

Intrathoracic twitch pressures and ultrasound-derived diaphragm thickness and thickening are shown in Table 4.3.10. The $\Delta P_{di,tw}$ did not differ between the two trials (p = 0.915), and neither did $\Delta P_{oe,tw}$ (p = 0.685) nor $\Delta P_{ga,tw}$ (p = 0.513). Overall, intrathoracic pressures exhibited excellent within-day reliability (ICC ≥0.977 and CV ≤4.8%). Phrenic nerve conduction time was 8.15 ± 1.99 ms and 8.47 ± 1.95 ms for trial 1 and trial 2 (p = 0.364), respectively, and exhibited moderate within-day reliability (ICC [95%CI] 0.681 [0.431 – 0.982] and CV 2.9 ± 2.3% [0.4 – 0.46%]). M-wave amplitude was 1.33 ± 0.42 mV and 1.22 ± 0.36 mV for trial 1 and trial 2 (p = 0.234), respectively, and exhibited good within-day reliability (ICC 0.881 [0.739 – 0.958] and CV 2.1 ± 1.9% [0.7 – 4.1%]).

Costal diaphragm thickness at relaxation volume (measured immediately before stimulation) was 1.2 ± 0.3 mm in trial 1, and increased by 65 ± 31% during the stimulation-evoked twitch contraction (p = 0.001). In trial 2, diaphragm thickness at relaxation volume was 1.2 ± 0.2 mm, and increased by 64 ± 15% during the twitch contraction (p < 0.001). As shown in Table 4.3.10, there were no differences between two trials for diaphragm thickness at relaxation volume (p = 0.576) or during the twitch contraction (p = 0.862). Furthermore, all ultrasound-derived measures of costal diaphragm thickness and thickening exhibited good-to-excellent within-day reliability (ICC ≥0.803 and CV ≤11%).

Table 4.3.10 Within-day comparison of intrathoracic pressures and diaphragm thickening in response to twitch contractions.

			Coefficient of variation		**Intra-class correlation coefficient**		
	Trial 1	**Trial 2**	CV (%)	95% CI (%)	ICC	95% CI	*p*-value
Intrathoracic pressures (cmH_2O)							
$\Delta P_{di,tw}$	25.7 ± 9.1	25.8 ± 10.0	3.2 ± 2.7	0.8 – 5.6	0.975	0.834 – 0.996	<0.001
$\Delta P_{oe,tw}$	–13.6 ± 5.9	–13.4 ± 6.6	4.8 ± 5.0	0.4 – 9.3	0.988	0.927 – 0.998	<0.001
$\Delta P_{ga,tw}$	13.7 ± 7.5	14.2 ± 6.9	3.6 ± 3.3	0.7 – 6.6	0.977	0.927 – 0.998	<0.001
Diaphragm thickness and thickening							
Thickness at relaxation volume, mm	1.20 ± 0.30	1.23 ± 0.20	4.5 ± 2.9	1.8 – 7.0	0.942	0.595 – 0.992	0.005
Thickness at contraction, mm	1.99 ± 0.40	2.02 ± 0.30	3.6 ± 5.3	1.0 – 8.3	0.926	0.416 – 0.990	0.009
Thickening ratio	1.63 ± 0.28	1.61 ± 0.12	3.8 ± 2.7	6.3 – 14.0	0.803	0.080 – 0.970	0.020
Thickening fraction, %	63 ± 29%	62 ± 13	11.1 ± 8.2	4.1 – 17.7	0.862	0.263 – 0.980	0.009

Data are mean ± *SD* for six participants. CV, coefficient of variation of duplicate measurements; 95% CI, 95% confidence intervals; ICC, intra-class correlation coefficient; $\Delta P_{di,tw}$, twitch transdiaphragmatic pressure; $\Delta P_{oe,tw}$, twitch oesophageal pressure; $\Delta P_{ga,tw}$, twitch gastric pressure.

Concurrent validity and the relationship with respiratory pressures

The relationships between $\Delta P_{di,tw}$ and the ultrasound-derived measures of costal diaphragm thickness and thickening are shown in Figure 4.3.10. As shown, it was only diaphragm thickening fraction that was correlated with $\Delta P_{di,tw}$, and, rather unexpectedly, the two variables were negatively correlated. Although there was a tendency for absolute thickness at the peak of contraction to be negatively correlated with $\Delta P_{di,tw}$ (Figure 4.3.10B), this did not reach statistical significance.

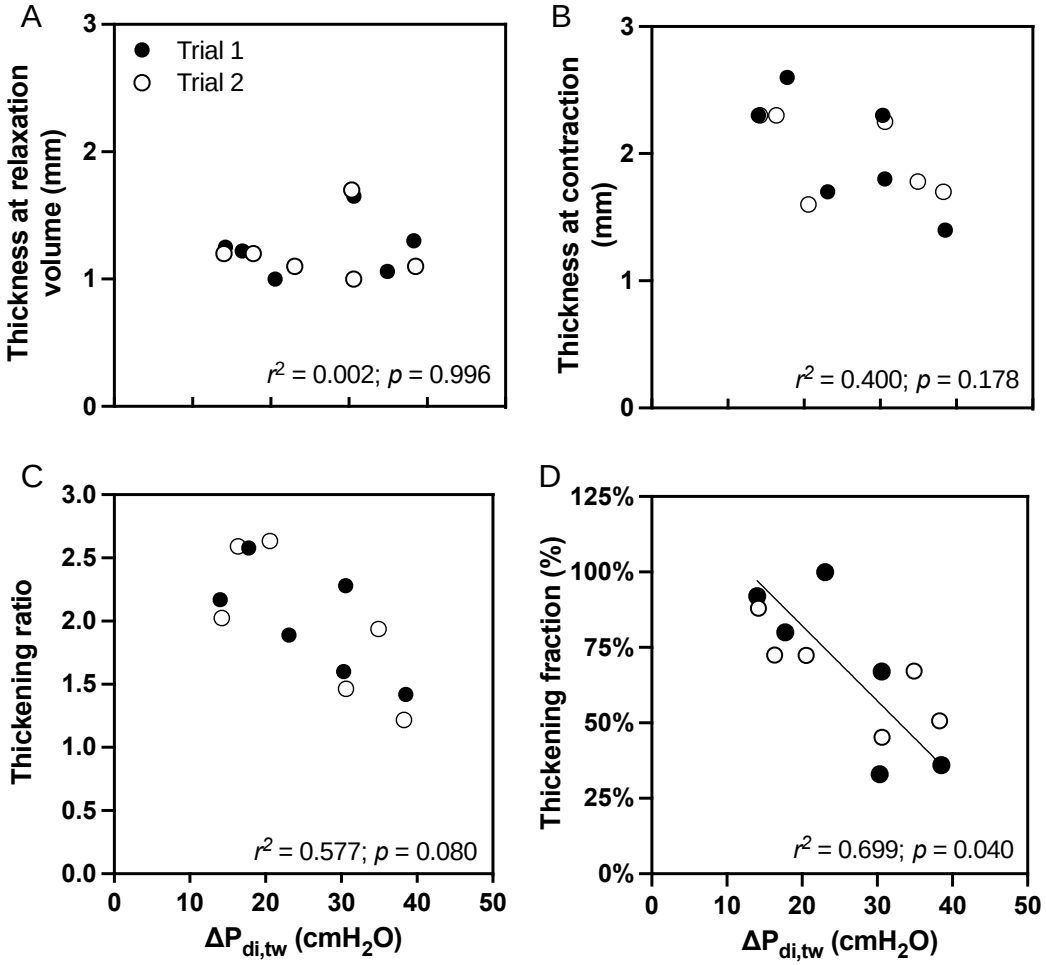

Figure 4.3.10 Relationships between $\Delta P_{di,tw}$ and *A*) diaphragm thickness at relaxation volume; *B*) diaphragm thickness at the peak of twitch contraction; *C*) diaphragm thickening ratio; *D*) and diaphragm thickening fraction. Data are shown for individual subjects in trial 1 (●) and trial 2 (○) for six participants. r^2 and *p*-values are shown in each panel, calculated for within-subject, repeated observations (Bland & Altman, 2006).

Maximal sniffs

Intrathoracic sniff pressures and ultrasound-derived measures of costal diaphragm thickness and thickening are shown in Table 4.3.11. As shown, the $\Delta P_{di,sn}$ did not differ between the two trials ($p = 0.201$), and neither did $P_{oe,sn}$ ($p = 0.095$) and $P_{ga,sn}$ ($p = 0.065$). Moreover, within-day comparisons of maximal sniff pressures exhibited excellent within-day reliability in the form of ICC (≥0.941), with CV for $\Delta P_{di,sn}$ of 4.2 ± 2.7%. Costal diaphragm thickness at relaxation volume was 1.21 ± 0.2 mm in trial 1, and increased by 72 ± 34% during the maximal sniff manoeuvre ($p = 0.002$). In trial 2, thickness at relaxation volume was 1.25 ± 0.5 mm, and increased by 69 ± 20% during the maximal sniff manoeuvre ($p = 0.006$). There were no differences between the two trials in the thickness measured at relaxation volume ($p = 0.296$) or during the sniff contraction ($p = 0.880$). As with intrathoracic sniff pressures, ultrasound-derived measures of costal diaphragm thickness and thickening exhibited good- to-excellent within-day reliability (ICC ≥0.748; CV ≤10%; see Table 4.3.11).

Table 4.3.11 Within-day comparison of intrathoracic pressures and diaphragm thickening in response to maximal sniffs.

	Trial 1 (cmH_2O)	**Trial 2** (cmH_2O)	**Coefficient of variation**		**Intra-class correlation coefficient**		
			CV (%)	95% CI (%)	ICC	95% CI	*p*-value
Intrathoracic pressures							
$\Delta P_{di,sn}$	123 ± 34	118 ± 41	4.2 ± 2.7	1.7 – 6.6	0.983	0.888 – 0.998	<0.001
$\Delta P_{oe,sn}$	–67.2 ± 28.1	–73.5 ± 27.9	6.9 ± 3.6	3.7 – 10.1	0.946	0.592 – 0.993	<0.001
$\Delta P_{ga,sn}$	58.0 ± 42.1	47.3 ± 42.8	16.2 ± 15.4	2.6 – 29.7	0.941	0.483 – 0.992	<0.001
Diaphragm thickness and thickening							
Thickness at relaxation volume, mm	1.21 ± 0.20	1.25 ± 0.20	3.1 ± 2.9	0.5 – 5.7	0.911	0.547 – 0.987	0.003
Thickness at contraction, mm	2.39 ± 0.50	2.40 ± 0.50	3.9 ± 4.5	0.1 – 7.8	0.889	0.380 – 0.984	0.005
Thickening ratio	1.95 ± 0.47	1.96 ± 0.64	7.3 ± 5.9	2.0 – 12.5	0.748	-0.111 – 0.961	0.036
Thickening fraction, %	72 ± 34	68 ± 20	10 ± 7	4 – 16	0.847	0.275 – 0.977	0.010

Data are mean ± *SD* for six participants. CV, coefficient of variation of duplicate measurements; 95% CI, 95% confidence intervals; ICC, intra-class correlation coefficient; $\Delta P_{di,sn}$, sniff transdiaphragmatic pressure; $\Delta P_{oe,sn}$, sniff oesophageal pressure; $\Delta P_{ga,tw}$, sniff gastric pressure.

Concurrent validity and the relationship with respiratory pressures

The relationships between $\Delta P_{di,sn}$ and ultrasound-derived measures of costal diaphragm thickness and thickening are shown in Figure 4.3.11. None of the ultrasound-derived measures of sniff diaphragm thickness or thickening were significantly correlated with $\Delta P_{di,sn.}$ In contrast to diaphragm twitch thickening (above), the relationships tended to be positive between thickness and thickening and $\Delta P_{di,sn}$.

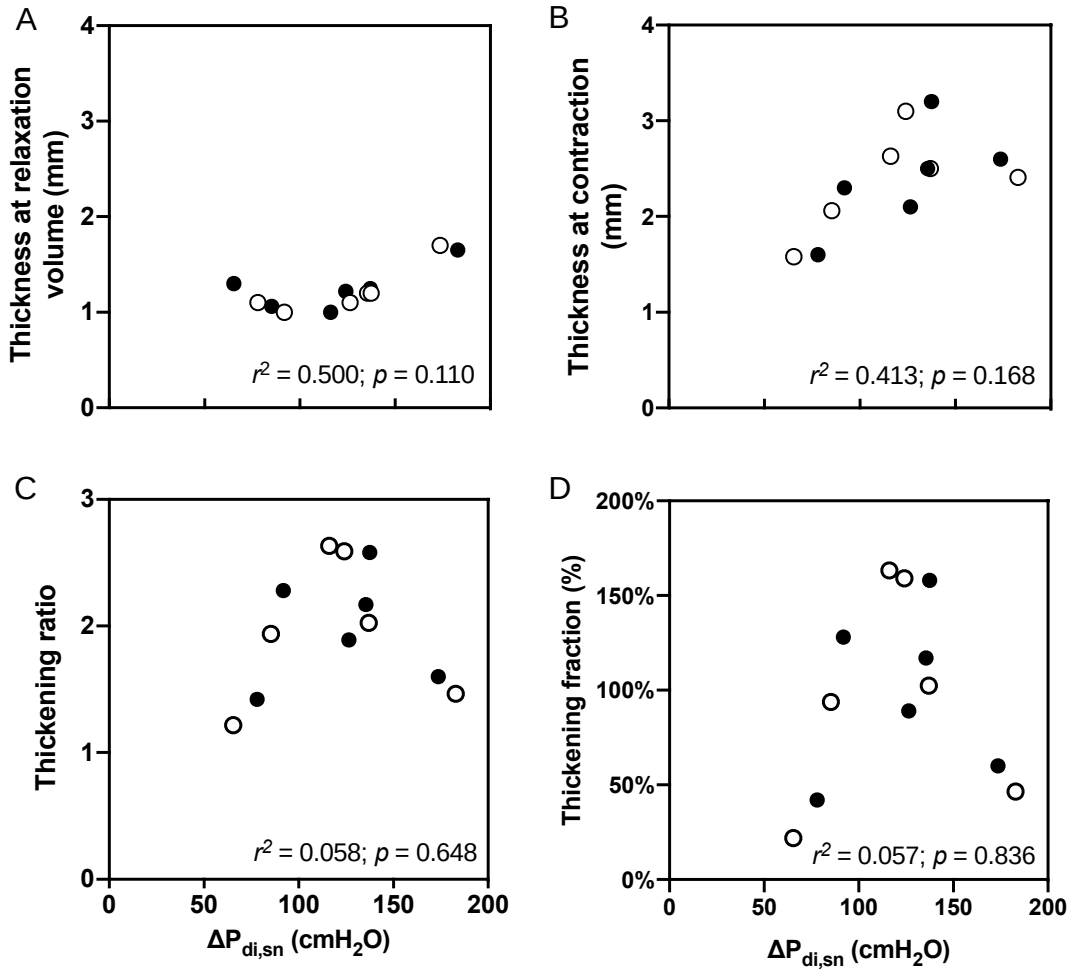

Figure 4.3.11 Relationships between $\Delta P_{di,sn}$ and *A*) diaphragm thickness at relaxation volume; *B*) diaphragm thickness at the peak of sniff contraction; *C*) diaphragm thickening ratio, and *D*) diaphragm thickening fraction. Data are shown for individual subjects in trial 1 (●) and trial 2 (○) for six participants. r^2 and *p*-values are shown in each panel, calculated with within-subject, repeated observations (Bland & Altman, 2006).

4.4 Discussion

The aims of this study were to explore the use of ultrasound for the assessment of diaphragm kinetics and thickening during non-volitional and volitional perturbations. Specifically, the study assessed the feasibility, concurrent validity and within-day, intra-observer reliability of ultrasound-derived measures of crural diaphragm kinetics (excursion, excursion velocity and power) and costal diaphragm thickening (shortening) in response to stimulation-evoked twitch contractions and maximal sniffs.

In *Part 1*, it was feasible to measure crural diaphragm kinetics during single and paired twitch contractions and maximal sniffs, using both M-mode and AM-mode ultrasound. However, speckle-tracking exhibited poor feasibility and was, therefore, excluded from further analysis. Diaphragm excursion and excursion velocity were strongly correlated with diaphragm force ($\Delta P_{di,tw}$ and rate of pressure development), confirming the close relationship between diaphragm kinetics and force. Moreover, the ultrasound-derived diaphragm kinetics generally exhibited good- to-excellent within-day (between-trial) reliability. Combined, these findings suggest that diaphragm kinetics can be readily and reliably assessed using ultrasonography in response to the applied perturbations.

In *Part 2*, it was also feasible to measure costal diaphragm thickness and thickening during single twitch contractions and maximal sniffs, based on the observation that all the acquired cine-loops were successfully analysed during twitch contractions, and nearly all (97%) were successfully analysed during maximal sniffs. Costal diaphragm thickness and thickening were only weakly correlated with $\Delta P_{di,tw}$, but exhibited excellent within-day reliability. This suggests that ultrasound-derived measures of costal diaphragm thickening are reliable but not necessarily related to the absolute force (pressure) generated by the diaphragm in response to the applied perturbations.

4.4.11 Part 1

Feasibility

To determine the feasibility of ultrasound for the assessment of crural diaphragm kinetics, three analysis techniques were used: conventional M-mode, angle-independent AM-mode and speckle-tracking algorithms. Of the three analysis techniques, M-mode and AM-mode ultrasound are the most frequently used for assessing diaphragm kinetics (Boussuges et al., 2009; Testa et al., 2011), although the European Respiratory Society has recently encouraged sonographers to further explore the use of speckle-tracking algorithms on the diaphragm muscle

(Ferrari et al., 2018, p. 133). Nonetheless, due to the low proportions of successfully analysed cine-loops with speckle-tracking in this study (64-75%), the technique was excluded from further analysis. Moreover, speckle-tracking is substantially more time-consuming compared to M-mode and AM-mode: the process of identifying a twitch or sniff contraction within a single cine-loop; cropping the cine-loop only to image the contraction, and then to perform the analysis (incl. subsequent adjustments of ROI) takes ~5-12 min. In comparison, the analysis of a single twitch contraction using M-mode and AM-mode (combined) takes ~1-2 min. Thus, the time-consuming process markedly reduced the feasibility of speckle-tracking algorithms. Moreover, the speckle-tracking software produced outputs that were highly inconsistent, raising a concern regarding the validity of the measurements.

The inconsistency in speckle-tracking algorithms may be attributed to the subcostal ultrasound approach itself. Despite the common misconception that the subcostal ultrasound approach images the hemi-diaphragm dome as skeletal muscle tissue (Ye et al., 2013), the hyperechoic dome-shaped structure – usually attributed to the hemi-diaphragm – is, in fact, the interface of pleural viscera and lower border of the air-filled lung (Ferrari et al., 2018). Thus, the echographic characteristics of this soft tissue interface are significantly different from myocardial tissue for which speckle-tracking analysis was originally intended and validated (Teske et al., 2007). These factors considered, and with almost 400 cine-loops to analyse, it was concluded that diaphragm kinetics could not be feasibly measured with speckle-tracking algorithms in this study.

In contrast to speckle-tracking, M-mode and AM-mode were feasible for the assessment of diaphragm kinetics in response to twitch and sniff contractions. This was based on the observation that almost all (95%) cine-loops could be successfully analysed using the two analysis techniques, regardless of stimulation frequency, presence of post-activation potentiation and the volitional nature of maximal sniffs (Table 4.3.2). One might have expected that unilateral stimulation would have caused the diaphragm to distort laterally out of the narrow field of view, particularly at the higher stimulation frequencies (Bellemare & Poirier, 2005; De Troyer & Boriek, 2011). Although a lateral twitch-induced distortion was in fact visible in the B-mode ultrasound, this was not pronounced enough to negatively affect feasibility. It is worth noting that AM-mode, which has a dynamic scan line (cursor) that can be oriented along the true axis of diaphragm movement, was particularly useful in imaging the diaphragm during high-frequency stimulation and sniffs because the dynamic cursor could be oriented so that the muscle could be imaged throughout the entire contraction.

Concurrent validity

The concurrent (construct) validity of ultrasound-derived measures of diaphragm kinetics was assessed by correlating diaphragm excursion and excursion velocity with diaphragm force (pressure) output. The relationship between diaphragm force and diaphragm kinetics were assumed under the theoretical basis that increasing stimulation frequency of the phrenic nerve would increase $\Delta P_{di,tw,}$ as per the classical force-frequency relationship (Farkas & Rochester, 1988; Moxham et al., 1981), and that diaphragm excursion would increase similarly due to the increased neural activation of the muscle. In this study, diaphragm excursion and excursion velocity were strongly correlated with $\Delta P_{di,tw}$ and rate of pressure development, confirming the close relationship ($r^2 \geq 0.805$) between diaphragm kinetics and force output during stimulation-evoked contractions.

These correlations suggest that four-fifths of the variance in diaphragm excursion and excursion velocity are accounted for by $\Delta P_{di,tw}$. This being said, this relationship leaves one-fifth of the variance in diaphragm excursion and excursion velocity unaccounted for. The variance unaccounted for by this relationship may be explained by one of the following explanations: *i*) anterolateral stimulation of phrenic nerves does not exclusively activate the diaphragm, but also accessory inspiratory muscles, such as the sternocleidomastoids and upper rib cage muscles (Mills et al., 1995, 1996). With unilateral stimulation, there is also evidence of contralateral phrenic nerve coactivation (Mills et al., 1995). Accordingly, the $\Delta P_{di,tw}$ from unilateral stimulation is likely the mechanical output of several muscles that may not be directly associated with right hemi-diaphragm kinetic behaviour. Second, diaphragm twitch contractions have commonly been referred to as quasi-isometric contractions with negligible fibre shortening (Babcock et al., 1996; Grassino & Macklem, 1984). If diaphragm twitch contractions are in fact quasi-isometric, this suggests that $\Delta P_{di,tw}$ could – at least partially – be generated without shortening and craniocaudal descent. Third, unilateral stimulation of phrenic nerves causes the muscle to descend craniocaudally *and* distort laterally (De Troyer & Boriek, 2011). There may, therefore, be movement of the crural diaphragm that cannot be captured by two-dimensional ultrasound imaging, ultimately leaving some of the kinetic movement of the diaphragm unaccounted for.

In order to evaluate the concurrent validity of ultrasound-derived measures of diaphragm kinetics, we also determined the effect of post-activation potentiation on diaphragm excursion and excursion velocity. This was done on the theoretical basis that post-activation potentiation would be expected to increase diaphragm force output ($\Delta P_{di,tw}$) (Wragg et al., 1994). Also,

previous studies in limb locomotor muscles (rat gastrocnemius) have shown that post-activation potentiation increases active-fibre shortening and shortening velocity in response to evoked twitch contractions (MacIntosh & Bryan, 2002). Because human respiratory muscles are also affected by post-activation potentiation, and exhibit similar force-velocity characteristics as limb-locomotor muscles (Ameredes et al., 2006; Coirault et al., 1995, 1997), it was expected that diaphragm excursion and excursion velocity would increase with potentiation. However, despite a significant increase in $\Delta P_{di,tw}$ with post-activation potentiation (+22-27%), it was only in trial 1 that excursion was found to be higher with potentiation while excursion velocity remained unchanged (Figure 4.3.8).

It is not entirely clear why potentiation only affected diaphragm excursion in one trial when the potentiation effect on $\Delta P_{di,tw}$ was relatively similar between the two trials. This finding may, perhaps, speak to reliability as well as validity. Afterall, potentiation was consistently induced in both trials (as evidenced by the similar increase in $\Delta P_{di,tw}$), although potentiation could not be identified repeatedly (reliably) with ultrasound. Moreover, the effect of potentiation in this study was relatively small compared to the 46-64% increase in $\Delta P_{di,tw}$ reported by others (Laghi et al., 1995; Mador, Magalang, et al., 2000). One may wonder, therefore, if a greater potentiation effect is necessary for potentiation to be consistently imaged with ultrasound.

Within-day reliability

Regardless of stimulation frequency or level of potentiation, the ultrasound-derived measures of diaphragm kinetics assessed with M-mode and AM-mode exhibited good- to excellent within-day, between-trial reliability in the form of ICC and CV. Interestingly, it appeared that reliability was generally higher for 1 Hz (non-potentiated) and 100 Hz than 10 Hz and 50 Hz, particularly for diaphragm power (Table 4.3.6). It is not entirely clear why certain stimulation frequencies produced more reliable measures of diaphragm kinetics. Perhaps, as shown in Figure 4.3.3, the prolonged inter-stimulus interval at 10 Hz (100 ms) caused the diaphragm to move differently compared to a single twitch (1 Hz) or paired twitches with shorter inter-stimulus durations (e.g., 10 ms at 100 Hz), ultimately causing the diaphragm to move differently between the various frequencies and trials.

Within-day reliability of diaphragm excursion by conventional M-mode ultrasound has been well-documented for spontaneous tidal breathing (Boussuges et al., 2009; Houston et al., 1994; Testa et al., 2011). For instance, Testa et al. (2011) reported CV of 6.0% and 7.1% during quiet breathing for experienced and inexperienced operators, respectively, confirming the notion that little training is required to obtain reliable measures of diaphragm kinetics using ultrasound.

These measures of reliability are similar to the initial studies by Houston et al.(1994), which reported a CV of 7.5%, also for quiet tidal breathing. Only one former study has evaluated the reliability of ultrasound-derived diaphragm excursion using AM-mode relative to conventional M-mode (Orde et al., 2016a). Although the study only assessed reliability of diaphragm excursion during quiet breathing and inspiratory capacity (IC) manoeuvres (not evoked twitches or maximal sniffs), the authors showed that diaphragm excursion measured with AM-mode exhibited higher within-day reliability (ICC [95% CI] 0.92 [0.70 – 0.98]) compared to M-mode (0.88 [0.47 – 0.97]). Thus, the authors concluded that AM-mode ultrasound is superior to conventional M-mode ultrasound due to the dynamic cursor in AM-mode, likely making the analysis technique subject to less orientation and translation errors compared to conventional M-mode.

4.4.12 Part 2

Feasibility

In order to determine the feasibility of ultrasound for assessing costal diaphragm thickness and thickening, ultrasound cine-loops were recorded from the intercostal approach during 1 Hz twitch contractions (bilateral) and maximal sniffs. Costal diaphragm thickness and thickening were readily measured in all (100%) of cine-loops during evoked contractions and in the majority (97%) of cine-loops during maximal sniffs. These results are in line with previous studies, which have reported that all (100%) cine-loops containing quiet tidal breathing can be readily measured in healthy adults (Harper et al., 2013). Slightly lower levels of feasibility (range 85-100%) have been reported in critically ill patients (Goligher, Laghi, et al., 2015; Umbrello et al., 2015; Vivier et al., 2012). We extended these previous findings by showing that costal diaphragm thickness and thickening can be assessed during rapid perturbations, such as evoked twitch contractions and maximal sniffs. A noteworthy observation was that the small number of unsuccessfully analysed cine-loops for maximal sniffs were acquired from one participant, caused by extensive rib distortion and costal diaphragm movement during the maximal manoeuvre. Due to the volitional nature of maximal sniffs, some participants may recruit accessory inspiratory muscles (e.g., scalenes, intercostals, sternocleidomastoids) in such a way that causes the diaphragm to distort more than usual (Katagiri et al., 2003; Nava et al., 1993), thereby making it difficult to image the contracting diaphragm at the zone of apposition.

Concurrent validity

The concurrent (construct) validity of ultrasound-derived measures of diaphragm thickness and thickening was assessed by correlating the measures with diaphragm force (pressure) output

($P_{di,tw}$). The relationship between $\Delta P_{di,tw}$ and diaphragm thickness was assumed under the theoretical basis that the peak force of skeletal muscle is directly dependent on fibre diameter and muscle cross-sectional area, because larger fibres and muscles with greater cross-sectional area contain greater amounts of contractile protein (Fitts et al., 1991). The relationship between muscle cross-sectional and peak force has also been proposed for the diaphragm muscle *in vivo*, in which diaphragm structural attributes (e.g., thickness and cross-sectional area) appear to be strongly related to both MIP and $P_{di,max}$ in healthy adults (McCool, Benditt, et al., 1997; McCool, Conomos, et al., 1997).

Rather unexpectedly, only thickening fraction was correlated with $\Delta P_{di,tw}$, and this relationship was negative (r^2 = 0.699; p = 0.04; Figure 4.3.10). In practical terms, this meant that the participants whose diaphragms generated highest twitch pressure ($\Delta P_{di,tw}$) also thickened the least during the contraction. This finding was rather surprising, opposing the intuitive idea that the more a muscle shortens (thickens), the more force it will generate. Seeing as the relationship between crural diaphragm excursion and $\Delta P_{di,tw}$ was very strong (Figure 4.3.6), one may suggest that there is limited activation of costal diaphragm during anterolateral phrenic nerve stimulation. In fact, the phrenic nerve motor point (i.e., the point at which the nerve branch enters the muscle belly and where the highest excitability of the muscle occurs) is only 5 cm from the central tendon and 9-14 cm from the costal insertions on the lower ribs (McKenzie & Gandevia, 1985). Thus, the magnitude of the evoked CMAP of the costal diaphragm is only one-third of the CMAP for the crural diaphragm, suggesting that the stimuli dissipate with conduction distance (McKenzie and Gandevia 1985). Assuming that evoked diaphragm activation is concentrated to the area proximal to the phrenic nerve motor point, this could explain why the excursion of the *crural* diaphragm dome was strongly correlated with $\Delta P_{di,tw}$ while thickening of the *costal* diaphragm was not.

Within-day reliability

Ultrasound-derived measures of costal diaphragm thickness and thickening in response to 1 Hz bilateral phrenic nerve stimulation and maximal sniffs exhibited good-to-excellent within-day, between-trial reliability (ICC 0.803 to 0.988 for evoked contractions; ICC 0.748 to 0.911 for sniffs). Similarly, CV for the ultrasound-derived measures were generally low, ranging from 3.1% (thickness at relaxation volume) to 11% (thickening fraction during evoked contractions). Previous studies have assessed within-day reliability for diaphragm thickness and thickening in healthy adults at various lung volumes. For instance, Baldwin et al. (2011) reported ICC of 0.990 (95% CI 0.918 – 0.998) for diaphragm thickness at EELV, which is similar to that also

reported by others (Harper et al., 2013). The present study expanded these previous findings, showing that within-day reliability is preserved even during rapid twitch and sniff contractions.

In a recent study, Poulard et al. (2020) investigated the relationship between $\Delta P_{di,tw}$ in response to cervical stimulation of phrenic nerves and diaphragm thickening fraction in healthy adults. The authors reported that the stimulation-evoked $\Delta P_{di,tw}$ (11.6 ± 15.6 cmH_2O) resulted in a costal diaphragm thickening of 19 ± 16%, which is substantially lower than the 63 ± 20% thickening fraction measured in the present study. The reason for this discrepancy is not entirely clear. The authors did, however, use ultrafast ultrasound, which – despite the higher sampling rate compared to conventional ultrasound – produces an ultrasound image of poorer quality. Thus, accurate measures of diaphragm thickness may have been more difficult to make with the novel ultrasound technique. The poor image quality by ultrafast ultrasound may also be the reason why the authors reported within-day reliability as low as ICC 0.560 (95% CI 0.430 – 0.660) for thickening fraction during twitches; rendering it markedly lower than the reliability shown in the present study (ICC 0.860 [95%CI 0.263 – 0.980]).

4.4.13 Ultrasound assessment during maximal sniffs

Whilst anterolateral magnetic stimulation of the phrenic nerves is relatively specific to the diaphragm muscle, with only minor activation of additional muscles (Mills et al., 1995; Mills et al., 1996), the external intercostals, parasternal intercostals, scalenes, sternocleidomastoids and rectus abdominis may all be recruited during maximal sniffs (Katagiri et al., 2003; Nava et al., 1993). Based on these considerations, we expected greater within-subject variability and poorer within-day reliability when assessing mechanical and contractile responses to maximal sniffs compared to evoked contractions. It must therefore be remarked that participants generated lower sniff pressures ($\Delta P_{di,sn}$; 81.2 ± 35 cmH_2O in *Part 1*; 120 ± 37 cmH_2O in *Part 2*) and diaphragm sniff excursion (~1.85 cm) than previously reported. For instance, Miller et al. (1985) reported $\Delta P_{di,sn}$ of 135 ± 28 cmH_2O for healthy, young adults (122 ± 25 cmH_2O for women; 148 ± 24 cmH_2O for men) and calculated lower limits of normal of 82 cmH_2O and 112 cmH_2O for women and men, respectively. Moreover, Boussuges et al. (2009) reported diaphragm sniff excursions of 3.1 ± 0.6 cm and 2.7 ± 0.5 cm for healthy men and women, respectively, which is similar to that reported by others (Fayssoil et al., 2019). Seeing as participants in the present study were healthy and recreationally active, it is unlikely that the lower $\Delta P_{di,sn}$ and diaphragm sniff excursion were caused by respiratory muscle weakness and/or impaired diaphragm mobility (Mier-Jedrzejowicz et al., 1988). Moreover, all participants were

well-acquainted with the manoeuvre prior to the experimental visit, making unfamiliarity an unlikely cause of the low values.

A more likely explanation for the sub-optimal values may, therefore, be the semi-recumbent posture in which all perturbations were performed. In this posture, the diaphragm moves to a more effective portion of its length-tension relationship versus in the upright posture, whereas the accessory inspiratory muscles move to less effective portions of their length-tension relationships (De Troyer & Boriek, 2011). Given that accessory inspiratory muscles play a significant role in force generation during maximal volitional efforts (Nava et al., 1993), this might explain why the sniff pressures were lower in the semi-recumbent versus the upright posture. Moreover, there is evidence that accessory muscle contribution (e.g., from sternocleidomastoids and scalenes) during sniffs declines from upright to supine posture (Katagiri et al., 2003), thereby reducing the overall mechanical output of the inspiratory muscles. Thus, the lower $\Delta P_{di,sn}$ in the present study (particularly in *Part 1*) may have been attributable to the unconventional posture (semi-recumbent) from which sniff pressures were generated.

It is also worth noting that normative values for diaphragm sniff excursion have been reported from the supine posture (Ayoub et al., 1997; Boussuges et al., 2009; Ferrari et al., 2018; Gerscovich et al., 2001; Testa et al., 2011). Compared to the supine posture, the semi-recumbent posture would exhibit lower abdominal compliance with an increased resistance to diaphragm descent (Estenne et al., 1985). In turn, the diaphragm would be expected to move less (reduced craniocaudal descent) upon contraction in the upright posture due to the elevated resistance from abdominal content (De Troyer & Boriek, 2011). Again, the lower diaphragm sniff excursion in *Part 1* of this study may, therefore, have been attributable to the unconventional posture from which the sniffs were performed.

4.4.14 Methodological considerations

The present study is subject to limitations. Due to the narrow field of view necessary to achieve a sampling rate of ≥200 FPS required to capture diaphragm excursion during evoked contractions (*Part 1*), it was not feasible to use conventional anatomical landmarks (i.e., intrahepatic vein and inferior vena cava) to ensure the ultrasound transducer was held firmly in place. Anatomical landmarks are of paramount importance in order to monitor the target tissue in relation to fixed reference points. To compensate for the lack of anatomical landmarks, the hyperechoic apex of the hemi-diaphragm was positioned in the middle of the B-mode image at relaxation volume and this position was marked with a focal point. This ensured a consistent

insonation angle and penetration depth in both trials as well as optimal lateral resolution at the level of the hyperechoic diaphragm (Forsha et al., 2015; Ng & Swanevelder, 2011). Moreover, the skin was thoroughly marked prior to the experiment. Thus, we are confident that our assessment of diaphragm kinetics was not adversely affected by passive movement of the ultrasound transducer during the perturbations in this study.

Although the narrow B-mode image chosen for *Part 1* was considered a necessity to achieve adequate sampling rate to capture the stimulation-evoked twitch contraction, such a high sampling rate violates the optimal frame rate suggested for speckle-tracking analysis (70-110 FPS)(Teske et al., 2007). Thus, the high sampling rate may have caused the software's poor tracking of diaphragm kinetics. With M-mode and AM-mode, however, the high frame rate did not appear to affect negatively the analysis, but instead allowed for a more accurate assessment of diaphragm kinetics due to the high resolution afforded.

4.4.15 Conclusions

Ultrasonography for the assessment of crural diaphragm kinetics and costal diaphragm thickening is feasible and highly reliable within-day in response to evoked twitch contractions and maximal sniffs. Further, ultrasound-derived diaphragm kinetics appear to be strongly related to diaphragm force, and may provide novel information regarding the muscle's ability to shorten and descend during these rapid perturbations. Because costal diaphragm thickening was not related to diaphragm twitch force, it may be suggested that costal diaphragm is not a significant contributor to diaphragm force generation during these rapid perturbations. Accordingly, the results of this study will be used to inform the subsequent studies of this thesis: more specifically, subcostal ultrasonography (AM-mode) will be used to evaluate the effect of external loading on diaphragm twitch kinetics in Chapter 7. Intercostal ultrasonography will be used to evaluate the effect of external loading on diaphragm thickening in response to evoked twitches and maximal sniffs in Chapter 8.

Chapter 5

Feasibility, Validity and Reliability of Ultrasonography for the Assessment of Diaphragm Kinetics and Thickening During Hypercapnic Hyperpnoea in Healthy Men

5.1 Introduction

During inspiration, the diaphragm muscle shortens and descends, thereby generating negative intrathoracic pressure, an increase in lung volume, and inspiratory airflow. As with other striated skeletal muscles, diaphragm function is characterised by the ability to shorten, generate force, produce power and perform work (Green et al., 2002). However, a major limitation of current techniques, such as magnetic or electric stimulation of phrenic nerves, is that they do not provide information regarding the muscle's ability to shorten and generate power under physiologic conditions, such as during voluntary increases in ventilation (hyperpnoea). Rather, as the principal muscle of inspiration (Grimby et al., 1976), the diaphragm's role is to contract rapidly during quiet breathing and hyperpnoea in order to maintain normal alveolar ventilation while simultaneously overcoming resistance to chest wall expansion, lung inflation and inspiratory airflow (De Troyer & Boriek, 2011). Conversely, an inability of the diaphragm to contract under load – as seen with fatigue – may limit exercise tolerance and increase the perception of dyspnoea (Romer & Polkey, 2008). During hyperpnoea, an inability of the fatigued diaphragm to contract may be manifested as a decrement in diaphragm force (Yan, Lichros, et al., 1993), altered breathing pattern (Gallagher et al., 1985; Yan, Sliwinski, et al., 1993), and reduced CO_2 sensitivity (Mador & Tobin, 1992). However, it remains to be addressed empirically to what extent shortening and contractile (excursion) velocity may also be impaired in the fatigued human diaphragm under dynamic, physiologic conditions.

Indeed, former research into human diaphragm contractile properties during hyperpnoea has primarily focused on understanding the fatigue-induced decline in force (pressure) as well as the ventilatory implications of an impaired diaphragm muscle, such as ventilatory response, CO_2 sensitivity, and breathing pattern. As such, little is known about the muscle's ability to shorten and descend during hyperpnoea, and how these contractile properties may be affected by fatigue. Thus, novel approaches and further investigations are needed to better understand the dynamic contractile properties of the fresh and fatigued human diaphragm during hyperpnoea.

From the ICU, ultrasonography of the diaphragm is a well-established tool to quantify crural diaphragm kinetics and costal diaphragm thickness and thickening during quiet breathing (Ferrari et al., 2018). In patients undergoing mechanical ventilation, the tool is principally used to monitor disuse atrophy (Goligher, Fan, et al., 2015), and to identify patient-ventilator asynchrony (Vivier et al., 2020) so as to predict liberation from mechanical ventilation and to

avoid potential reintubation. There is also evidence that ultrasound-derived measures of diaphragm thickening during spontaneous breathing is moderately- to strongly associated with transdiaphragmatic pressure-time index [PTI_{di}]; that is, and established measure of diaphragm work (Umbrello et al., 2015; Vivier et al., 2012). Despite the well-established use of diaphragm ultrasonography in the clinical setting, the tool is yet to be used to assess human diaphragm function during reflexively-driven hyperpnoea. If found to be feasible, ultrasonography may offer new insight into the contractile properties of the human diaphragm during physiologic, dynamic conditions.

In Chapter 4, we explored the use of subcostal and intercostal ultrasonography to quantify crural diaphragm kinetics and costal diaphragm thickening in response to stimulation-evoked twitch contractions and maximal sniffs. Moreover, it was shown that diaphragm power can be estimated as the dot product of excursion velocity multiplied by the $\Delta P_{di,tw}$. Herein, these ultrasonography approaches are extended to assess the dynamic contractile properties of the human diaphragm during hyperpnoea.

5.1.1 Aims and hypotheses

In *Part 1* of this study, the aim was to determine the feasibility, validity and within-day, intra-observer reliability of ultrasound-derived measures of crural diaphragm kinetics (i.e., excursion, excursion time, excursion velocity and power) by *subcostal* ultrasonography during hypercapnic hyperpnoea. It was hypothesised that the assessment of diaphragm kinetics would be feasible, but adversely affected by progressively increasing tidal volume (i.e., rib cage expansion); that ultrasound-derived diaphragm kinetics would be strongly correlated with conventional measures of diaphragm contractile properties and ventilatory indices, and that the measures would exhibit acceptable within-day reliability.

In *Part 2*, the aim was to determine the feasibility, concurrent validity and within-day, intra-observer reliability of ultrasound-derived measures of costal diaphragm thickening (shortening) by *intercostal* ultrasonography during hypercapnic hyperpnoea. It was hypothesised that the assessment of costal diaphragm thickening would be feasible but adversely affected by progressively increasing tidal volume; that ultrasound-derived costal diaphragm thickening would be strongly correlated with conventional measures of diaphragm contractile properties and ventilatory indices, and that the measures would exhibit acceptable within-day reliability.

5.2 Methods

5.2.2 Ethical approval and participants

The study was approved by the Brunel University London Research Ethics Committee (Appendix 1), and conformed to the most recent standards set by the Declaration of Helsinki (World Medical Association, 2013). Eleven healthy, non-smoking men between the ages of 18 and 40 y from university student population and surrounding areas volunteered to participate. Only participants of (self-reported) male sex were included in this study due to the limited resources and time available to include female participants and to control for menstrual cycle phase in multi-visit studies (see section 3.3 for additional details). All participants reported no medical history of cardiovascular, respiratory, or neuromuscular disease using a standardised health questionnaire (Appendix 2). Exclusion criteria were BMI ≥30 kg/m^2 and pulmonary function and maximal respiratory mouth pressures outside age-specific limits of normal (Evans & Whitelaw, 2009; Quanjer et al., 2012; Stocks & Quanjer, 1995). Moreover, it was ensured that participants' right hemi-diaphragm could be imaged with appropriate clarity using ultrasound, and that all participants exhibited shortening of right costal diaphragm during quiet breathing (Harper et al., 2013). Participants provided written informed consent prior to the study (Appendix 2) and abstained from vigorous exercise for ≥24 h, caffeine and alcohol for ≥12 h, and food for ≥3 h prior to each visit.

5.2.3 Experimental overview

Each participant visited the laboratory on two occasions separated by no less than 48 h and no more than 14 d. The study outline was similar for *Part 1* and *Part 2*: The first visit was for screening and familiarisation, during which participants performed pulmonary function tests and were thoroughly familiarised with the experimental set-up. The second visit was the experimental trial, consisting of two repeated hypercapnic hyperpnoea tests (CO_2-rebreathe) separated by a standardised period of 20 min. Intrathoracic pressures (P_{di}, P_{oe}, and P_{ga}) and ventilatory- and gas-exchange indices were measured continuously before (rest), during, and after (recovery) each hyperpnoea test. For *Part 1* specifically, ultrasound-derived measures of crural diaphragm kinetics were acquired at regular intervals. Similarly, in *Part 2*, ultrasound-derived measures of costal diaphragm thickening were acquired at regular intervals. Three participants participated in both parts of this study.

5.2.4 Screening and familiarisation

Screening was performed as described in Chapter 4 (section 4.2.4). Specific familiarisation for the experimental trial included verbal instructions from the investigator on how to perform the CO_2-rebreathe test, followed by a demonstration as to how to end the test prematurely in the case of discomfort. Here, all participants also completed a practice CO_2-rebreathe test.

5.2.5 PART 1

Eight participants volunteered for *Part 1* of this study.

Hypercapnic hyperpnoea (CO_2-rebreathe)

Hypercapnic hyperpnoea was performed using the CO_2-rebreathe method described in section 3.11 in General Methods, and similar to that described by Read et al. (1966; 1967). However, the original gas composition of 7% CO_2 and 93% O_2 used by Read et al. (1966) was substituted with a certified gas composition of 5% CO_2 and 95% O_2 in a disposable, plastic rebreathe bag (7-8 L). This bag volume was approximately 1 L larger than vital capacity, making the bag as small as possible without encroaching on tidal volume (Read & Leigh, 1967). The rebreathe bag was connected to a three-way valve (2560, T-shape valve, Hans Rudolph Inc., Shawanee, KA, US) and a flanged mouthpiece. All rebreathe tests were performed in the semi-recumbent position, and the laboratory was kept silent before, during and after the rebreathe test to avoid the potential influence of external stimuli on the ventilatory response and breathing pattern (Homma & Masaoka, 2008; Spengler & Shea, 2001).

Prior to initiating the CO_2-rebreathe test, participants rested in the semi-recumbent position for ~10 min during which they breathed room air without a mouthpiece or nose-clip to ensure a steady state of relaxed wakefulness (Spengler & Shea, 2001). Next, participants breathed through the rebreathe valve for 3 min (still from room air) while resting measurements were made over the final 30 s. Rebreathing was then initiated by the participants exhaling to RV, at which point the three-way valve was closed, and participants equilibrated with the now-closed rebreathing circuit by taking three deep, rapid breaths from the circuit (MacKay et al., 2016). Equilibration was followed by the instruction to relax and breathe as needed. When $P_{ET}CO_2$ reached 7.33 kPa (55 mmHg), the rebreathe circuit was re-opened to ambient air with the participant continuing to breathe as needed for 3 min (recovery). After a standardised period of 20 min, the above procedures were repeated for the assessment of within-day reliability.

Assessment of intrathoracic pressures

The P_{oe} and P_{ga} were measured using a gastro-oesophageal catheter (Gaeltec Devices Ltd., Isle of Skye, Scotland), as described in section 3.6.5 in General Methods. Briefly, the catheter was passed pernasally and swallowed into the stomach via peristalsis. The position of the catheter was adjusted such that a maximal sniff elicited negative and positive deflections in P_{oe} and P_{ga}, respectively. The correct position was confirmed with the "dynamic occlusion test" (Baydur et al., 1982), before the catheter was taped in position at the nose. The analogue signals for intrathoracic pressures were passed through a signal amplifier (1902, CED, Cambridge, UK) and digitised at sampling frequencies of 200 Hz using an analogue-to-digital converter (1401mk-II, CED). Transdiaphragmatic pressure (P_{di}) was calculated online by subtraction of P_{oe} from P_{ga}.

Assessment of ventilatory and gas-exchange indices

Pulmonary airflow and gas-exchange were measured breath-by-breath using a metabolic cart with online gas analysis system (Oxycon Pro, Jaeger, Viasys Healthcare, Hoechberg, Germany), comprising a calibrated turbine flow-meter and O_2 and CO_2 gas analysers. Digital signals from the metabolic cart were input into the data acquisition system using an external device (DAQ-30A16, Eagle Technology, Cape Town, South Africa) and recorded online as waveforms. Inspired and expired tidal volumes were calculated offline by numerical integration of flow using a bespoke script (Horseman, 2020a).

Diaphragm ultrasonography

The assessment of crural diaphragm kinetics is outlined in detail in General Methods (section 3.10.7). Briefly, all ultrasound scans were performed using a commercially-available system (Vivid 7 Pro, GE Medical, Horten, Norway) with the participant in a semi-recumbent position. EMG electrodes were attached on the right and left mid-clavicular lines so that tidal volume and breathing pattern could be traced directly by the ultrasound system. For this part of the study specifically (*Part 1*), a low-frequency, curvilinear ultrasound transducer (2.4-5.0 MHz, 3.5C, GE Medical) was positioned subcostally on the right mid-clavicular line. Here, the right hemi-diaphragm dome was imaged at the interface of the visceral pleura and air-filled lung. Beam penetration depth was adjusted so that the hyperechoic diaphragm position at RV was always within the field of view (~200-250 mm). In addition, one focal point was set at the diaphragm position at relaxation volume for optimised lateral resolution.

Ultrasound cine-loops were acquired as B-mode ultrasound, and analysed offline using specialty analysis software (EchoPac, v6.1, GE Medical, Horten, Norway). Diaphragm kinetics were measured using: *i*) conventional M-mode ultrasound; and *ii*) angle-independent AM-mode ultrasound, which are described in detail in section 3.10.7, in General Methods. Briefly, with conventional M-mode, diaphragm excursion and excursion time were measured with a digital calliper tool as the absolute excursion amplitude and the time from onset of excursion (EELV) to peak excursion (EILV), as indicated by arrows in Figure 5.2.1. Excursion velocity (cm/s) was calculated as the quotient of diaphragm excursion divided by excursion time. Diaphragm power was estimated as the dot product of excursion velocity and the active component of $\overline{P}_{di}$ ($\overline{P}_{di,a}$; see calculation below). The same measurements were performed using AM-mode, but the dynamic B-mode cursor was visually oriented along the true axis of diaphragm excursion (Orde et al., 2016b). Successfully analysed cine-loops were characterised by clear hyperechoic lines that distinctively marked the diaphragm position at EELV and EILV, as shown in Figure 5.2.1.

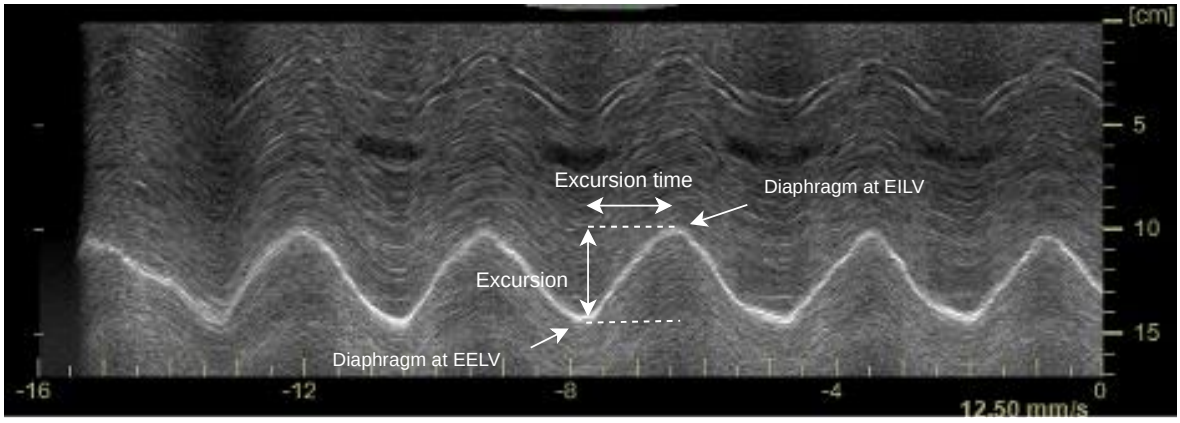

Figure 5.2.1 M-mode ultrasound of crural diaphragm excursion during hypercapnic hyperpnoea. Diaphragm excursion and excursion time were measured as shown by white arrows. *X*-axis represents time (s) and *y*-axis represents distance (cm) from transducer. This cine-loop was recorded in a male participant at $\dot{V}_I$ 19.6 L/min and V_{TI} 1.7 L, with diaphragm excursion measuring 4.8 ± 0.2 cm and excursion velocity of 2.6 ± 0.3 cm/s.

5.2.6 PART 2

Six male participants volunteered for this part of the study. Because three of the participants had previously volunteered for *Part 1*, they were familiar with the experimental set-up. CO_2-rebreathe was performed as described in *Part 1*. Similarly, intrathoracic pressures and ventilatory and gas-exchange indices were acquired on a breath-by-breath basis as described in *Part 1*. For *Part 2* specifically, costal diaphragm thickness and thickening (shortening) were assessed using an intercostal approach, as described below.

Diaphragm ultrasonography

The assessment of costal diaphragm thickness and thickening are outlined in detail in General Methods (section 3.10.6). Briefly, all ultrasound scans were performed using a commercially available system (Vivid 7 Pro, GE Medical) with the participant in a semi-recumbent position. A high-frequency, linear ultrasound transducer (4.0-11.0 MHz, 10L, GE Medical) was positioned at the participant's right anterior or mid-axillary line at the 8-10th intercostal space to image the costal diaphragm at the zone of apposition. The specific transducer position was determined by which pair of ribs produced the clearest image and was least affected by lung obscuration.

Ultrasound cine-loops were recorded and analysed as B-mode ultrasound using the same software package described above (EchoPac v6.1, GE Medical). Costal diaphragm thickness was measured in triplicate as the distance between the inner borders of the pleural and peritoneal membranes at end-expiratory lung volume (EELV) and at end-inspiratory lung volume (EILV) (Figure 5.2.2). Relative thickening of the costal diaphragm was calculated as: *1*) thickening ratio = thickness at EILV / thickness at EELV; and *2*) thickening fraction = (thickness at EILV – thickness at EELV) / thickness at EELV (Ferrari et al., 2018).

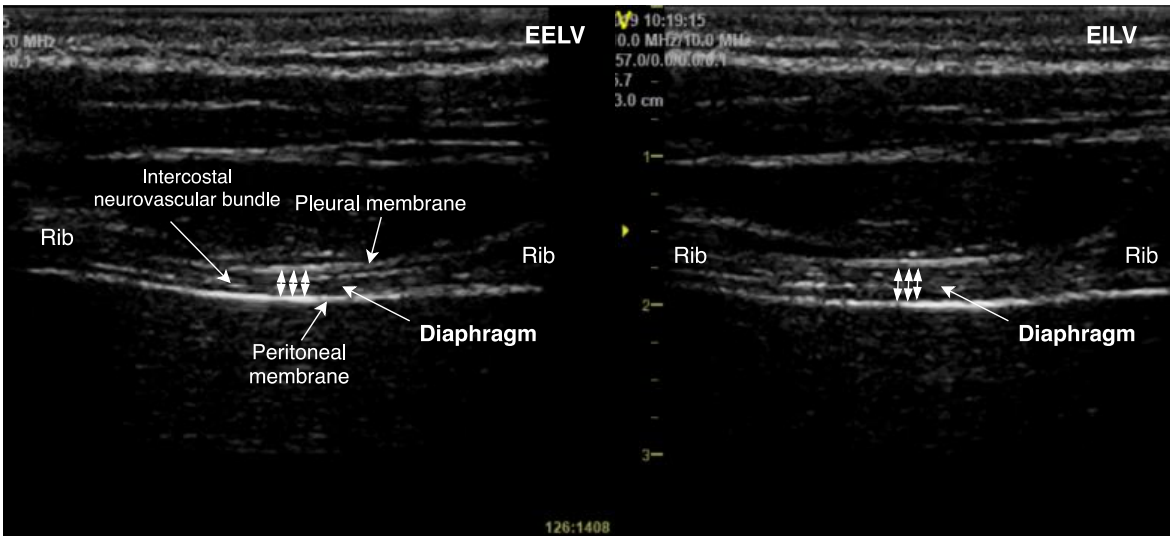

Figure 5.2.2 Diaphragm thickening during spontaneous breathing. Diaphragm thickness was measured in triplicate at EELV and EILV, as indicated by arrows. The cine-loop was recorded in a male participant during quiet breathing at rest. Diaphragm thickness was 1.7 mm and 2.4 mm at EELV and EILV, respectively.

5.2.7 Data analysis and processing

Ventilatory indices ($\dot{V}_I$, V_{TI}, f_R, T_I, T_I/T_{TOT}) and intrathoracic pressures (P_{di}, P_{ga}, P_{oe}) were recorded as waveforms on a breath-by-breath basis for offline analysis. The start and finish of each breath was marked at the point of zero flow and anomalous breaths (e.g., swallows, coughs or sighs, and breaths not crossing zero flow) were manually excluded. Ventilatory indices were expressed for inspiration only.

Tidal pressures were calculated as the active components of mean inspiratory pressure (i.e., $\overline{P}_{di,a}$, $\overline{P}_{ga,a}$ and $\overline{P}_{oe,a}$), using the equation from Barnard & Levine (1986) with $\overline{P}_{di,a}$ as an example:

$$\bar{P}_{di,a} = \Sigma_0^n P_{di}/n,$$

where baseline P_{di} (0) was the P_{di} immediately preceding the inspiratory upswing, and n was equal to the number of data points during inspiration. Accordingly, $\overline{P}_{di,a}$ was the mean pressure generated during tidal inspiration based on tidal pressure swings, without the passive component of inspiratory pressure. See General Methods, section 3.6.5 for details.

The ultrasound and data acquisition systems were not synchronised, so particular attention was paid to the timing of ultrasound acquisition during CO_2-rebreathe in order that the respiratory cycles within each ultrasound cine-loop could be correctly identified and matched with breath-by-breath ventilatory and pressure data. Specifically, ultrasound cine-loops were recorded over

15 s every 30 s during hyperpnoea and the three subsequent minutes of recovery (1 × 30 s at rest). All breaths recorded within a 15 s cine-loop (1 × 30 s for rest) were identified in the data acquisition system, then averaged over 15 s (30 s for rest). Since all participants reached a test duration of at least 1.75 min, data up to and including this timepoint (iso-time) were used for further analysis. The final 15 s of hyperpnoea, independent of test duration, was recorded and defined as the peak response.

5.2.8 Statistics

Statistical analysis was performed using SPSS (v26.0, IBM Corp., Armonk, NY, USA) and GraphPad Prism (v9.0, GraphPad Software LLC, San Diego, USA). Normal distribution of data was assessed with the Shapiro-Wilk test. All variables met the assumptions required for parametric statistics (incl. analysis of variance; ANOVA), unless otherwise indicated.

Feasibility

Specifically for *Part 1*, feasibility of ultrasound analysis was expressed as the percentage (min-max range) of successfully analysed cine-loops with a given analysis technique (i.e., M-mode and AM-mode). For instance, a cine-loop with three out of five breaths successfully analysed was considered 60% successful. Because the distribution of the percentage of successfully analysed cine-loops were not normally distributed, the difference between M-mode and AM-mode feasibility was assessed by Wilcoxon signed-rank test. Effect sizes were reported as rank-biserial correlation (r_{pb}), and interpreted as small (≤0.23), moderate (0.24 – 0.36) and large (≥0.37) (O'Donoghue, 2012). In *Part 2,* feasibility was presented as percentage of successfully analysed cine-loops only.

Concurrent validity

Concurrent validity of ultrasound-derived measures was assessed in two ways. First, to determine the relationship between ultrasound-derived measures and conventional measures of diaphragm contractile properties, coefficient of determination (r^2) for repeated observations was calculated in line with the description of Bland & Altman (1995b). Specifically, all participants were represented by *one* pair of duplicate measurements (trial 1 and trial 2, equally-weighted means), and the calculation mirrored a regular linear regression but with the initial *p*-value ignored. Instead, the *p*-value was derived from a statistical table of critical values, adjusting for duplicate measurements in the regression with degrees of freedom of $n - 2$. Coefficients of determination were interpreted as weak (r^2 <0.45), moderate (0.45 – 0.70) or strong (>0.70) (O'Donoghue, 2012).

Second, to determine the effect of time on ventilatory responses ($\dot{V}_I$, V_{TI}, f_R, T_I, T_I/T_{TOT}), intrathoracic pressures ($\overline{P}_{di,a}$, $\overline{P}_{oe,a}$, $\overline{P}_{ga,a}$) and ultrasound-derived measures during CO_2-rebreathe, a one-way (time) repeated-measures ANOVA was performed. Sphericity was assessed using Mauchly's test ($p \geq 0.05$ assumed sphericity). For *Part 1*, it was necessary to elucidate the effect of ultrasound analysis technique (M-mode and AM-mode) over the time-course of CO_2-rebreathe; thus, a two-way (time-analysis technique) repeated-measures ANOVA was performed. Bonferroni corrections were applied to account for multiple comparisons. Effect sizes were reported as partial eta squared (η_p^2) and interpreted as poor (≤ 0.01), medium (0.01-0.14) or large (>0.14) (Lakens, 2013).

Within-day (between-trial) reliability

In *Part 1* and *Part 2*, the rate of change (slopes) of ventilatory indices ($\dot{V}_I$, V_{TI}, f_R, T_I, T_I/T_{TOT}) and intrathoracic pressures ($\overline{P}_{di,a}$, $\overline{P}_{ga,a}$ and $\overline{P}_{oe,a}$) with respect to $P_{ET}CO_2$ were calculated on a breath-by-breath basis for each participant using linear regression. The slopes from the repeated trials were then converted to *t*-scores using the equation:

$$t = \frac{b_1 - b_2}{\sqrt{S^2 b_1 + S^2 b_2}}$$

where b_1 and b_2 were the two slopes (trial 1 and trial 2), and *S* was the standard error of the two slopes (Zar, 2014). To determine the difference in slope responses between the two repeated trials, group mean and individual slopes were compared using two-tailed, paired samples *t*-test.

Within-day variability of slope and peak responses to CO_2-rebreathe was expressed as coefficient of variation (CV), calculated using the root mean square method for duplicate measurements (Bland, 2006):

$$CV\ (\%) = 100 \times \sqrt{\frac{\Sigma (d/m)^2}{2n}}$$

where *d* was the difference between the duplicate measurements (trial 1 and trial 2), *m* was the mean of the duplicate measurements and *n* was the number of data pairs (*n* = 8 in *PART 1*; *n* = 6 in *Part 2*). In line with Bland (2006), standard error of the CV was calculated as:

$$Standard\ error = {SD_{CV}}/{\sqrt{n}}$$

where *SD* was the standard deviation of the CV and *n* was the sample size. The 95% confidence intervals (CI) were calculated as mean CV ± 1.96 standard error (Bland, 2006). Intra-class correlation coefficient (ICC) with 95% CI was calculated using a mean-rating ($k = 2$), absolute agreement, 2-way mixed effects model. ICCs were defined as poor (<0.500), moderate (0.500 – 0.750), good (0.750 – 0.900) or excellent (>0.900) (Koo & Li, 2016). All statistical tests were performed on absolute values, and alpha level was set *a priori* at $p \leq 0.05$. Data are mean ± *SD*, unless otherwise indicated.

5.3 Results

5.3.9 PART 1

Participant characteristics are shown in Table 5.3.1. In line with inclusion criteria, all participants exhibited pulmonary volumes, capacities, flows and pressures within normal limits. Measures of diaphragm structure and function were within the ranges typically reported for healthy, young men.

Table 5.3.1 Participant characteristics.

	Mean ± *SD*
Anthropometry	
Age, y	23 ± 7
Stature, cm	181 ± 5
Body mass, kg	77 ± 10
BMI, kg/m^2	23.7 ± 3.0
Chest depth, cm	20.0 ± 1.1
Chest width, cm	30.3 ± 1.7
Chest circumference, cm	94.4 ± 2.6
Pulmonary function	
TLC, L (% predicted)	7.46 ± 0.87 (107 ± 10)
RV, L (% predicted)	1.86 ± 0.23 (112 ± 14)
FRC_{pleth}, L (% predicted)	3.97 ± 0.72 (116 ± 18)
FVC, L (% predicted)	5.74 ± 0.47 (100 ± 6)
FEV_1, L (% predicted)	4.75 ± 0.41 (101 ± 7)
FEV_1/FVC (% predicted)	0.82 ± 0.05 (100 ± 4)
MVV_{12}, L/min (% predicted)	188 ± 28 (102 ± 14)
Maximal respiratory pressures	
MIP, cmH_2O (% predicted)	–125 ± 16 (113 ± 15)
MEP, cmH_2O (% predicted)	173 ± 19 (112 ± 11)
Diaphragm structure and function	
Diaphragm thickness at FRC, mm	1.6 ± 0.5
Diaphragm thickness at TLC, mm	4.1 ± 0.7
Thickening fraction, %	156 ± 40
Maximal diaphragm mobility, cm	6.8 ± 1.5

Data are mean ± *SD* for eight participants. BMI, body mass index; TLC, total lung capacity; RV, residual volume; FRC_{pleth}, functional residual capacity via plethysmography; FVC, forced vital capacity; FEV_1, forced expiratory volume in 1 s; MVV_{12}, maximal voluntary ventilation in 12 s; MIP, maximum inspiratory mouth pressure; MEP, maximum expiratory mouth pressure. Predicted values for pulmonary function were derived from Quanjer et al. (2012) for spirometry, and Stocks & Quanjer (1995) for plethysmography. Predicted values for MVV_{12} were calculated as $FEV_1 \times 40$ (Miller et al., 2005). Predicted values for MIP and MEP were from Evans & Whitelaw (2009).

Ventilatory and intrathoracic pressure responses to CO_2

All participants completed the two repeated trials without untoward events. Resting $P_{ET}CO_2$ was not different between trial 1 and 2 (39.2 ± 3.7 vs. 38.0 ± 5.1 mmHg, $p = 0.106$). All CO_2-rebreathe tests were terminated at the standardised cut-off of 55 mmHg (55.6 ± 0.2 mmHg), with mean duration of 2.48 ± 0.70 min (range 1.78 – 3.83 min) in trial 1, and 2.99 ± 1.37 min (range 1.75 – 5.80 min) in trial 2 ($p = 0.097$).

Expectedly, CO_2-rebreathe elicited an increase in $\dot{V}_I$ relative to $P_{ET}CO_2$, with group mean slope responses and linear equations shown in Figure 5.3.1A. Neither the ventilatory slopes nor intercepts differed between the two trials ($p = 0.978$ and $p = 0.397$, respectively). The increase in $\dot{V}_I$ was driven by a combined increase in V_{TI} and f_R in all participants (see group mean breathing pattern responses in Table 5.3.2, incl. within-day comparisons). It is worth noting that, despite similar group mean slope responses in the two trials, evaluation of individual slope responses showed that one participant ($n = 1$) adopted a breathing pattern with lower f_R and larger V_{TI} in trial 2 than in trial 1 ($p < 0.001$), while still achieving the same level of ventilation. As shown in Figure 5.3.1B and Table 5.3.2, intrathoracic pressures also increased relative to $P_{ET}CO_2$.

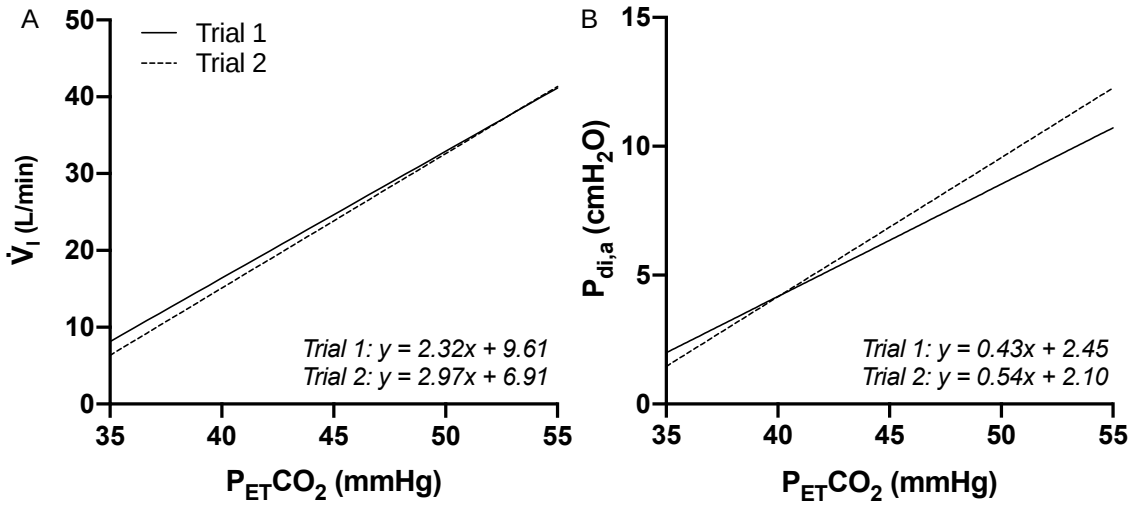

Figure 5.3.1 Breath-by-breath slope responses for *A*) inspiratory minute ventilation ($\dot{V}_I$), and *B*) mean inspiratory transdiaphragmatic pressure ($\overline{P}_{di,a}$) in trial 1 (—) and trial 2 (---). Data are group mean for eight participants.

Group mean ventilatory and intrathoracic pressure responses at the peak of hyperpnoea are shown in Table 5.3.3. Peak $\dot{V}_I$ represented 15-18% of MVV_{12}, and did not differ between the two trials (p = 0.147). Peak V_{TI}, on the other hand, was different between the two trials (p = 0.034). Generally, ventilatory and intrathoracic pressure responses exhibited good- to excellent within-day, between-trial reliability in the form of ICCs and CV (Table 5.3.2 and Table 5.3.3). As an example, all intrathoracic pressure slopes exhibited good ICC (≥0.795) and CV (≤5.7%). However, some of the peak responses in breathing pattern were variable, particularly T_I and inspiratory duty cycle (T_I/T_{TOT}), exhibiting poor ICC (0.049 – 0.125) and CV (≥12%).

Table 5.3.2 Within-day comparison of ventilatory, breathing pattern and intrathoracic pressure *slope* responses to CO_2.

			Coefficient of variation		Intra-class correlation coefficients		
	Trial 1	**Trial 2**	CV (%)	95% CI (%)	ICC	95% CI	*p*-value
Ventilatory responses							
$\dot{V}_I$ vs. $P_{ET}CO_2$, L/min/mmHg	1.65 ± 0.73	1.79 ± 1.47	5.9 ± 5.5	3.1 – 8.9	0.844	0.151 – 0.969	0.017
V_{TI} vs. $P_{ET}CO_2$, mL/mmHg	73.2 ± 53.2	72.4 ± 63.4	12.5 ± 12.3	6.1 – 19.1	0.870	0.313 – 0.974	0.010
f_R vs. $P_{ET}CO_2$, breaths/mmHg	0.11 ± 0.29	0.18 ± 0.42	20.3 ± 22.5	8.5 – 32.1	0.837	0.218 – 0.967	0.016
T_I vs. $P_{ET}CO_2$, s/mmHg	0.20 ± 0.72	0.17 ± 1.49	15.5 ± 14.6	2.1 – 30.2	0.829	0.085 – 0.966	0.021
Intrathoracic pressures							
$\overline{P}_{di,a}$ vs. $P_{ET}CO_2$, cmH_2O/mmHg	0.53 ± 0.43	0.39 ± 0.30	5.4 ± 7.0	0.5 – 10.2	0.810	0.183 – 0.961	0.017
$\overline{P}_{oe,a}$ vs. $P_{ET}CO_2$, cmH_2O/mmHg	–0.43 ± 0.18	–0.32 ± 0.25	4.6 ± 5.4	0.8 – 8.4	0.928	0.648 – 0.986	0.002
$\overline{P}_{ga,a}$ vs. $P_{ET}CO_2$, cmH_2O/mmHg	0.19 ± 0.15	0.18 ± 0.13	5.7 ± 8.5	0.1 – 11.6	0.795	0.111 – 0.958	0.015

Data are mean ± *SD* for eight participants. CV, coefficient of variation for duplicate measurements; CI, confidence interval; ICC, intra-class correlation coefficient; $\dot{V}_I$, inspiratory minute ventilation; $P_{ET}CO_2$; end-tidal partial pressure of CO_2; V_{TI}, inspiratory tidal volume; f_R, respiratory frequency; $\overline{P}_{di,a}$, active component of mean inspiratory transdiaphragmatic pressure; $\overline{P}_{oe,a}$, active component of mean inspiratory oesophageal pressure; $\overline{P}_{ga,a}$, active component of mean inspiratory gastric pressure.

Table 5.3.3 Within-day comparison of ventilatory, breathing pattern and intrathoracic pressure *peak* responses to CO_2.

			Coefficient of variation		Intra-class correlation coefficients		
	Trial 1	**Trial 2**	CV (%)	95% CI (%)	ICC	95% CI	*p*-value
Ventilatory responses							
$\dot{V}_I$, L/min	33.2 ± 11.0	28.3 ± 8.7	27.1 ± 16.2	15.0 – 38.9	0.727	–0.102 – 0.942	0.039
V_{TI}, L	2.38 ± 0.71	2.21 ± 0.57*	19.1 ± 9.4	13.3 – 25.2	0.796	0.001 – 0.959	0.008
f_R, breaths/min	14.1± 3.4	15.0 ± 2.0	19.7 ± 19.6	6.0 – 33.3	0.572	–0.527 – 0.111	0.111
T_I, s	1.86 ± 0.45	2.20 ± 1.05	23.2 ± 27.1	4.4 – 42.0	0.125	–0.613 – 0.734	0.378
T_I/T_{TOT}	0.46 ± 0.03	0.47 ± 0.08	12.8 ± 15.1	2.3 – 23.3	0.049	–0.866 – 0.671	0.544
Intrathoracic pressures							
$\overline{P}_{di,a}$ cmH_2O	13.9 ± 5.0	13.8 ± 4.7	25.7 ± 14.1	15.6 – 35.5	0.821	0.008 – 0.965	0.025
$\overline{P}_{oe,a,}$ cmH_2O	–6.8 ± 1.8	–6.8 ± 2.5	34.8 ± 23.4	18.6 – 51.5	0.119	–0.652 – 0.773	0.318
$\overline{P}_{ga,a}$, cmH_2O	6.7 ± 4.4	6.9 ± 5.1	15.6 ± 12.7	6.8 – 24.3	0.988	0.943 – 9.998	<0.001

Data are mean ± *SD* for eight participants. CV, coefficient of variation for duplicate measurements; CI, confidence interval; ICC, intra-class correlation coefficient; $\dot{V}_I$, inspiratory minute ventilation; $P_{ET}CO_2$; end-tidal partial pressure of CO_2; V_{TI}, inspiratory tidal volume; f_R, respiratory frequency; $\overline{P}_{di,a}$, active component of mean inspiratory transdiaphragmatic pressure; $\overline{P}_{oe,a}$, active component of mean inspiratory oesophageal pressure; $\overline{P}_{ga,a}$, active component of mean inspiratory gastric pressure. * $p \leq 0.05$ vs. trial 1.

Diaphragm ultrasonography

A total of 206 ultrasound-derived cine-loops were acquired during the two rebreathe trials combined (incl. cine-loops obtained at rest and during recovery). Of these cine-loops, 96% and 98% were successfully analysed using M-mode and AM-mode, respectively. To examine the influence of increasing tidal volume on ultrasound feasibility, the percentage of successfully analysed cine-loops were plotted as a function of V_{TI}, as shown in Figure 5.3.2. Except for one cine-loop, in which one breath could not be analysed using M-mode, all cine-loops in trial 1 were successfully analysed using the two analysis techniques. In trial 2, the percentages were slightly lower for both techniques (range 83 – 100%).

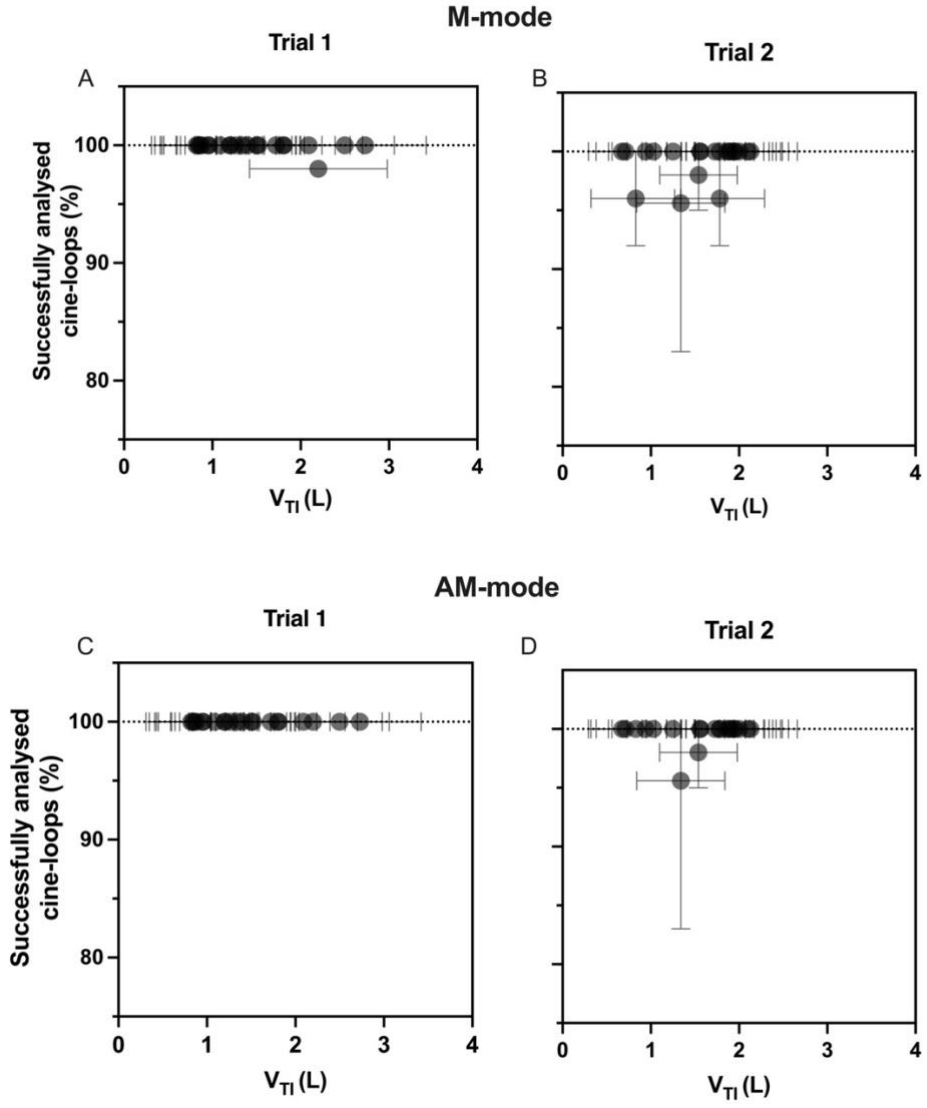

Figure 5.3.2 Percentage of successfully analysed cine-loops plotted against V_{TI} for M-mode (*A-B*) and AM-mode (*C-D*) in trial 1 and trial 2 during hypercapnic hyperpnoea. Data are median (min-max range) for eight participants at all timepoints.

The primary reason for the unsuccessfully analysed cine-loops was large and/or lateral diaphragm excursion, thereby causing the hyperechoic diaphragm apex to move out of the field of view. Yet, as shown in Figure 5.3.2, neither M-mode nor AM-mode were negatively affected by the increasing V_{TI}. Moreover, there were no differences in the percentage of successfully analysed cine-loops between M-mode and AM-mode in trial 1 (p = 0.312, r_{pb} = 0.154) or in trial 2 (p = 0.162, r_{pb} = 0.218). However, from visual inspection of the cine-loops it was evident that the static M-mode cursor underestimated actual diaphragm excursion, as the diaphragm rarely moved vertically along the strict vertical axis of M-mode. Rather, the diaphragm moved diagonally, particularly at moderate-to-high ventilatory loads (see example in Figure 5.3.3). So, despite high levels of feasibility, M-mode did not measure the excursion of the contractile hemi-diaphragm apex per sé, but rather the excursion of the non-contractile central tendon of the crural diaphragm.

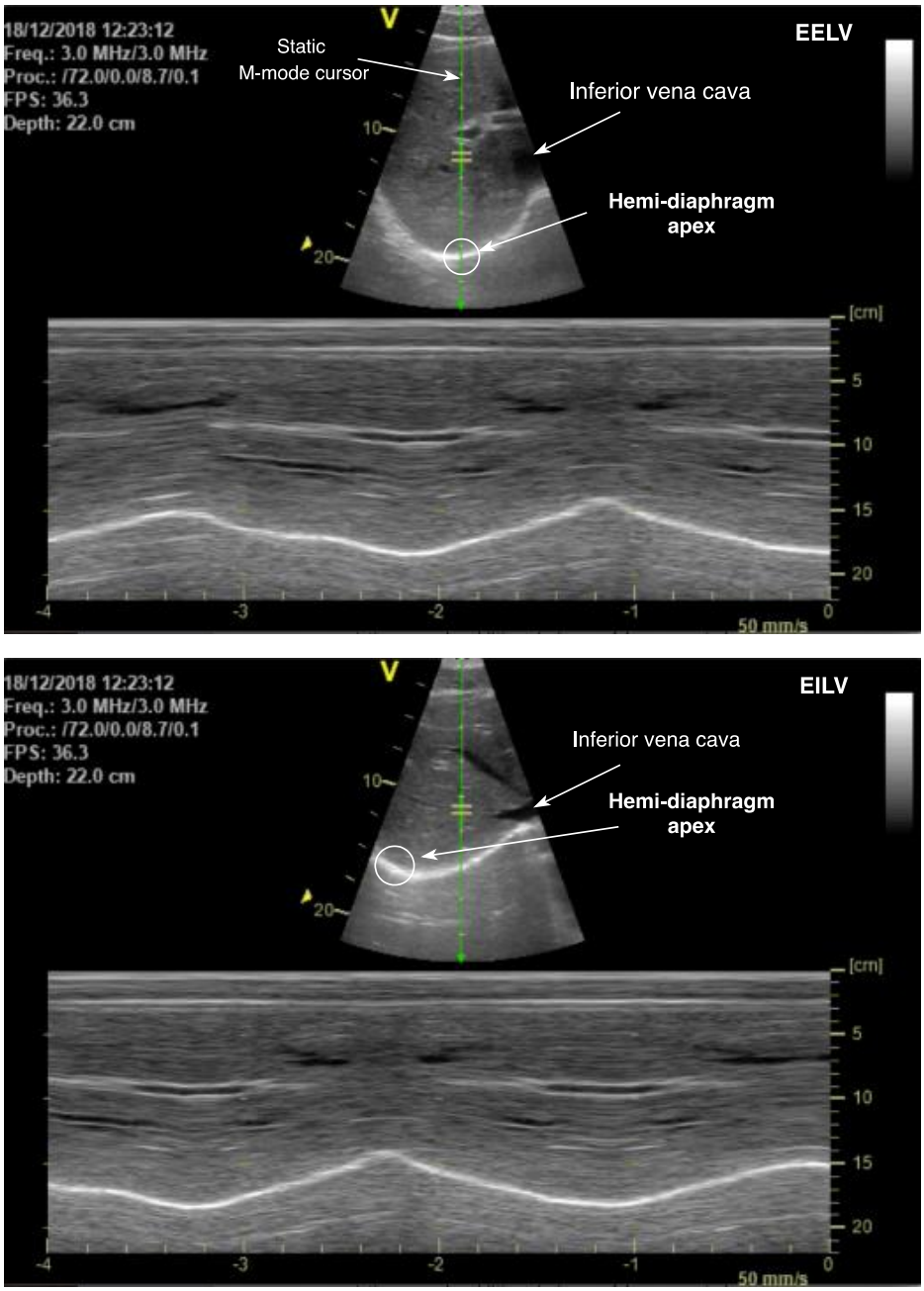

Figure 5.3.3 B-mode and M-mode ultrasound at EELV and EILV during hyperpnoea. The hemi-diaphragm apex (indicated with white circle) moved diagonally away from the static cursor (green arrow), thus capturing excursion of the non-contractile central tendon rather than the contractile apex of hemi-diaphragm dome.

Concurrent validity: the effect of time on diaphragm kinetics

Expectedly, diaphragm excursion increased as a function of time during CO_2-rebreathe: from 3.0 ± 1.6 cm (M-mode) and 3.14 ± 1.6 cm (AM-mode) at rest to 5.8 ± 1.7 cm (M-mode) and 4.6 ± 1.8 cm (AM-mode) at peak rebreathe ($p < 0.001$; $\eta_p^2 = 0.485$; Figure 5.3.4A). At the peak of rebreathe, diaphragm excursion ranged from 60% to 83% of maximal diaphragm mobility. During the subsequent three minutes of recovery, diaphragm excursion returned to resting levels, with 4.7 ± 1.7 cm (M-mode) and 4.5 ± 1.2 cm (AM-mode) during the final 15 s of recovery (vs. rest: $p = 0.652$ and $p = 0.990$ for M-mode and AM-mode, respectively).

Diaphragm excursion measured with M-mode and AM-mode differed only at peak, at which point M-mode measured larger excursion compared to AM-mode ($p = 0.002$). For excursion time, there was no main effect of time ($p = 0.073$; $\eta_p^2 = 0.221$) or of analysis technique ($p = 0.753$; $\eta_p^2 = 0.015$). On excursion velocity, however, there was a main effects of time ($p < 0.001$; $\eta_p^2 = 0.499$) and analysis technique ($p = 0.004$; $\eta_p^2 = 0.713$), with *post hoc* tests showing that M-mode measured more rapid excursion velocity at the peak of rebreathe and into recovery (Figure 5.3.4C).

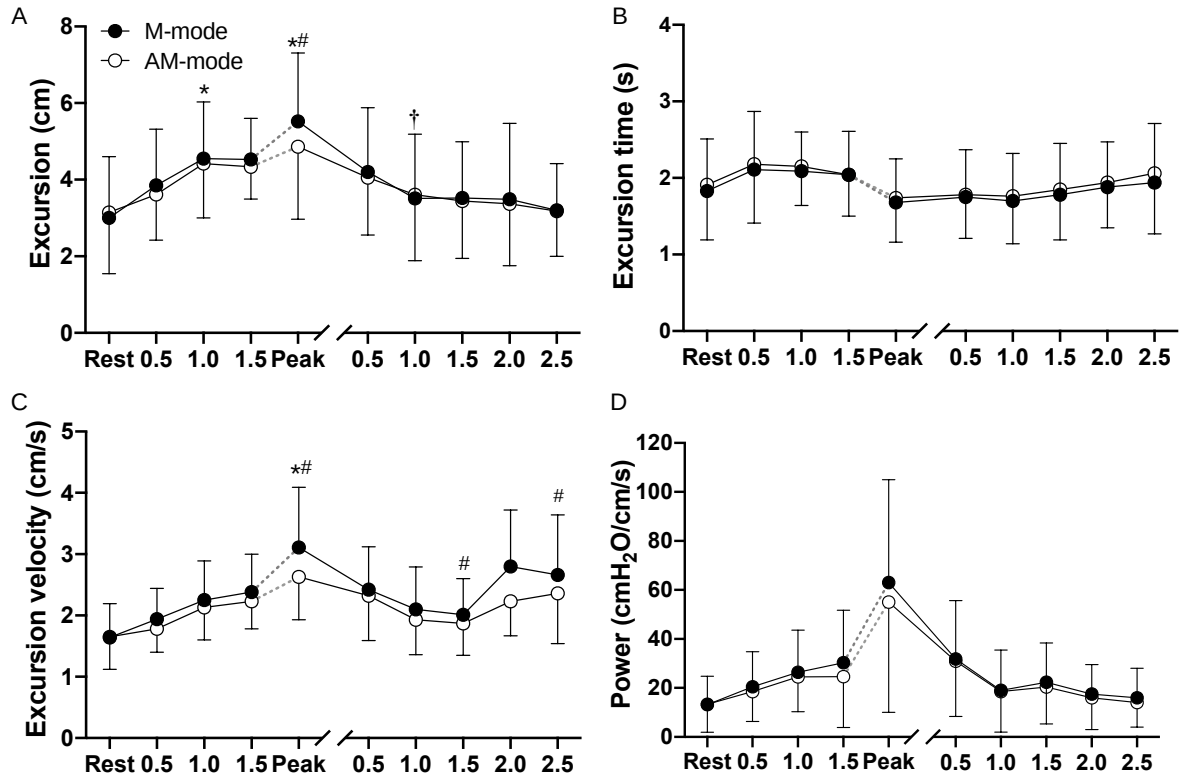

Figure 5.3.4 Ultrasound-derived kinetics as a function of time during hyperpnoea. Broken *x*-axis is the transition from CO_2-rebreathe to recovery. Data are mean ± *SD* for eight participants. **p* ≤ 0.05 vs. rest; †*p* ≤ 0.05 vs. peak; #*p* ≤ 0.05 vs. AM-mode at same timepoint.

Figure 5.3.5 shows ultrasound-derived diaphragm kinetics as a function of ventilatory indices (V_{TI}, T_I and V_{TI}/T_I). As there were no significant differences between responses in trial 1 vs. trial 2, the lines of best fit were calculated to represent the mean relationships adjusted for duplicate measures.

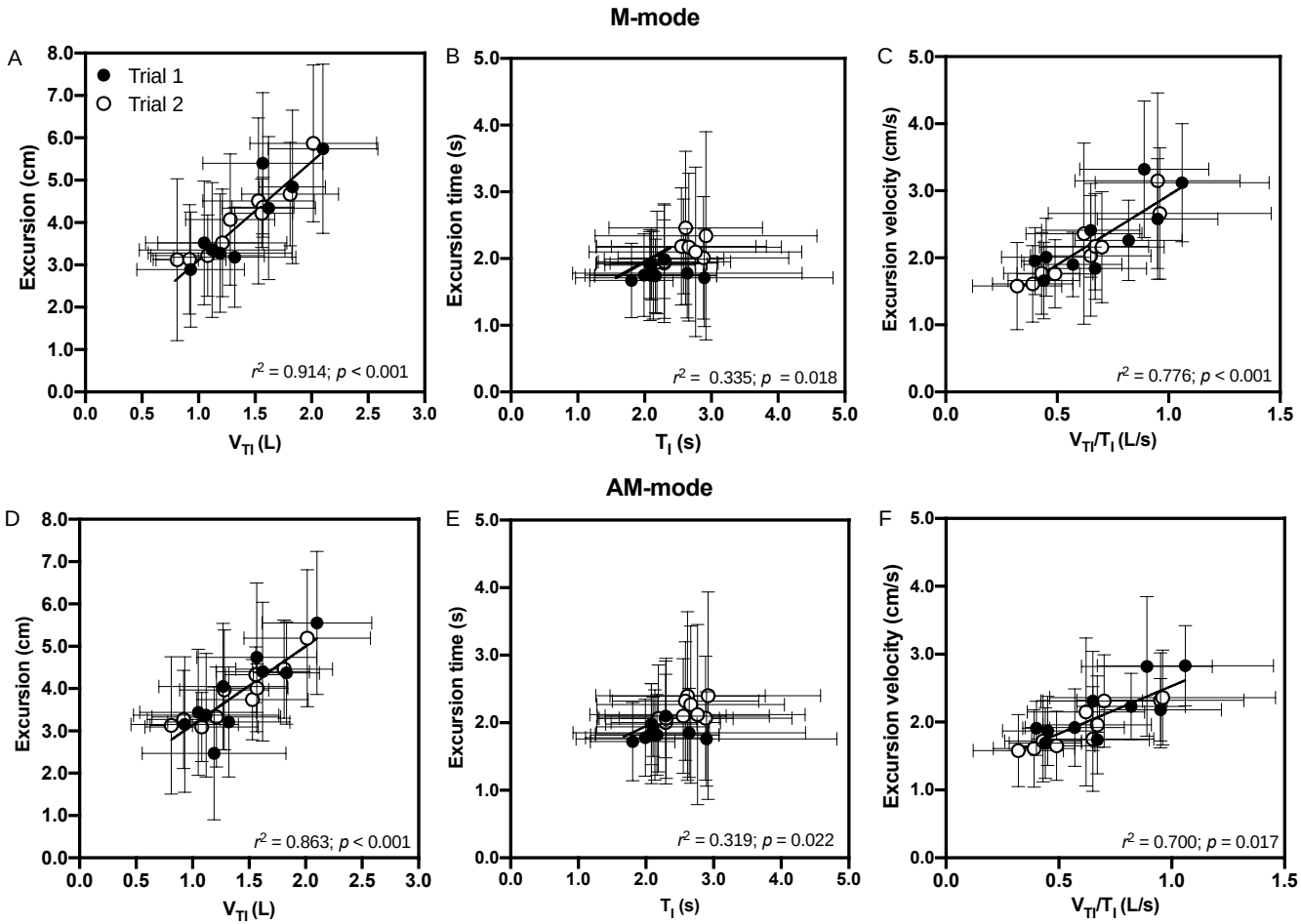

Figure 5.3.5 Ultrasound-derived diaphragm kinetics as a function of V_{TI}, T_I and V_{TI}/T_I. Diaphragm kinetics were measured with M-mode (*A-C*) and AM-mode (*D-F*). Data are mean ± *SD* for eight participants at all time-points during trial 1 (●) and trial 2 (○), including rest and three subsequent minutes of recovery. r^2 and *p*-values, corrected for duplicate measurements are shown in each panel.

Within-day reliability

Because ultrasound images were acquired at 15 s intervals (not breath-by-breath), slope responses to $P_{ET}CO_2$ could not be calculated for the ultrasound-derived measures of diaphragm kinetics. Instead, within-day comparisons were performed on peak kinetic responses to CO_2. Figure 5.3.6 shows the individual peak responses to CO_2, plotted as trial 1 vs. trial 2. Within-day comparisons of peak diaphragm kinetics showed that diaphragm excursion, excursion velocity and power all exhibited good- to excellent within-day reliability in the form of ICC (≥0.713). The CV was more variable ranging from 1.1% (excursion measured with AM-mode) to 28% (power measured with M-mode; Table 5.3.4). There were, however, no apparent differences between within-day reliability of M-mode and AM-mode.

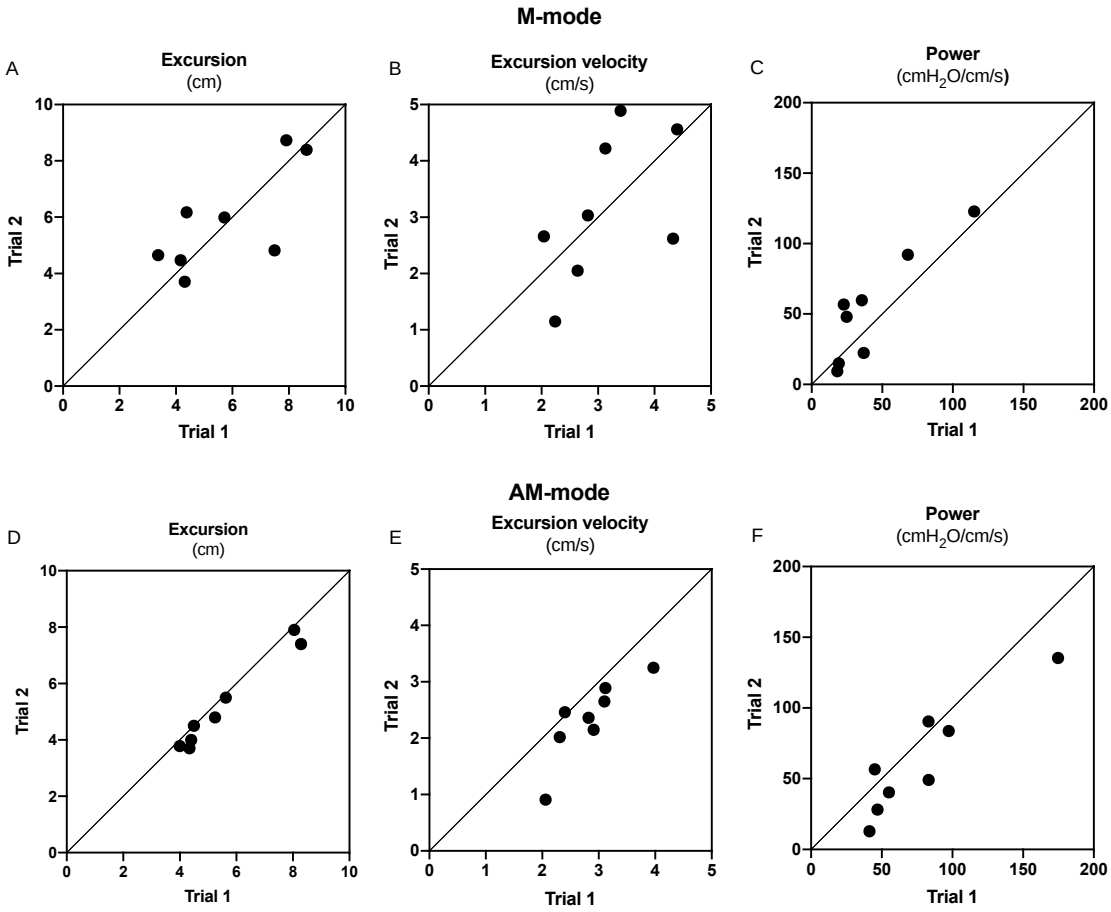

Figure 5.3.6 Individual peak responses to CO_2 in ultrasound-derived diaphragm kinetics, plotted as trial 1 vs. trial 2 for eight participants. Diaphragm kinetics were measured with M-mode (*A*-*C*) and AM-mode (*D*-*F*). Diagonal lines are lines of identity ($y = x$).

Table 5.3.4 Within-day comparison of diaphragm kinetics *peak* responses to CO_2.

			Coefficient of variation		Intra-class correlation coefficient		
	Trial 1	**Trial 2**	CV (%)	95% CI (%)	ICC	95% CI	*p*-value
M-mode							
Excursion, cm	5.7 ± 2.0	5.9 ± 1.8	5.6 ± 7.1	3.1 – 8.1	0.870	0.313 – 0.974	0.010
Excursion time, s	1.99 ± 0.58	2.00 ± 0.92	15.6 ± 22.5	7.7 – 23.6	0.067	–0.885 – 0.663	0.559
Excursion velocity, cm/s	3.12 ± 0.88	3.14 ± 1.30	12.6 ± 13.9	7.7 – 17.5	0.713	–0.715 – 0.944	0.075
Power, $cmH_2O/cm/s$	42 ± 33	53 ± 39	28 ± 24	19 – 36	0.820	0.616 – 0.984	0.001
AM-mode							
Excursion, cm	5.5 ± 1.7	5.2 ± 1.6	1.1 ± 1.0	0.4 – 2.1	0.981	0.658 – 0.997	< 0.001
Excursion time, s	2.10 ± 0.62	2.06 ± 0.91	14.9 ± 21.8	7.2 – 22.6	0.066	–0.883 – 0.663	0.558
Excursion velocity, cm/s	2.8 ± 0.6	2.4 ± 0.8*	10.1 ± 20.3	0.3 – 17.3	0.831	–0.142 – 0.970	0.002
Power, $cmH_2O/cm/s$	55.6 ± 54.9	46.5 ± 36.8	23 ± 34	12 – 35	0.722	–0.178 – 0.942	0.050

Data are mean ± *SD* for eight participants. CV, coefficient of variation for duplicate measurements; CI, confidence interval; ICC, intra-class correlation coefficient; M-mode, motion-mode ultrasound; AM-mode, angle-independent motion-mode ultrasound *$p \leq 0.05$ vs. trial 1.

5.3.10 PART 2

Participant characteristics are shown in Table 5.3.5. As per the inclusion criteria, all participants exhibited pulmonary volumes, capacities, flows and pressures within normal limits. Furthermore, measures of diaphragm structure and function were within the ranges typically reported for healthy, young men, and all participants exhibited costal diaphragm thickening during quiet breathing.

Table 5.3.5 Participant characteristics.

	Mean ± *SD*
Anthropometry	
Age, y	24.0 ± 7.3
Stature, cm	183.0 ± 5.6
Body mass, kg	81.2 ± 6.8
BMI, kg/m^2	24.4 ± 2.5
Chest depth, cm	21.8 ± 3.1
Chest width, cm	31.7 ± 1.8
Chest circumference, cm	95.3 ± 3.4
Pulmonary function	
TLC, L (% predicted)	7.85 ± 0.81 (104 ± 8)
RV, L (% predicted)	1.99 ± 0.19 (118 ± 13)
FRC_{pleth}, L (% predicted)	3.89 ± 0.77 (113 ± 20)
FVC, L (% predicted)	6.27 ± 0.61 (107 ± 11)
FEV_1, L (% predicted)	5.06 ± 0.52 (104 ± 8)
FEV_1/FVC (% predicted)	0.80 ± 0.07 (95 ± 7)
MVV_{12} (% predicted)	202 ± 21 (100 ±13)
Maximal respiratory pressures	
MIP, cmH_2O (% predicted)	–129 ± 19 (118 ± 22)
MEP, cmH_2O (% predicted)	179 ± 51 (118 ± 40)
Diaphragm structure and function	
Diaphragm thickness at FRC, mm	1.50 ± 0.51
Diaphragm thickness at TLC, mm	4.22 ± 0.63
Thickening fraction, %	181 ± 21
Maximal diaphragm mobility, cm	6.9 ± 1.4

Data are mean ± *SD* for six participants. BMI, body mass index; TLC, total lung capacity; RV, residual volume; FRC_{pleth}, functional residual capacity via plethysmography; FVC, forced vital capacity; FEV_1, forced expiratory volume in 1 s; MVV_{12}, maximal voluntary ventilation in 12 s; MIP, maximum inspiratory mouth pressure; MEP, maximum expiratory mouth pressure. Predicted values for pulmonary function were derived from Quanjer et al. (2012) for spirometry, and Stocks & Quanjer (1995) for plethysmography. Predicted values for MVV_{12} were calculated as $FEV_1 \times 40$ (Miller et al., 2005). Predicted values for maximum mouth pressures were derived from the equations of Evans & Whitelaw (2009).

Ventilatory and intrathoracic pressure responses to CO_2

All participants completed the two repeated trials without untoward events. Resting $P_{ET}CO_2$ measured 40.4 ± 3.2 mmHg in trial 1 and 39.6 ± 3.3 mmHg in trial 2, and was not different between the two trials ($p = 0.256$). All CO_2-rebreathe tests were terminated at the standardised cut-off point of 55 mmHg (55.1 ± 0.3 mmHg), with rebreathe durations of 2.30 ± 0.40 min (range 1.83 – 2.68 min) in trial 1, and 1.93 ± 0.28 min (range 1.83 – 2.35 min) in trial 2, which was not different between the two trials ($p = 0.116$).

CO_2-rebreathe elicited an increase in $\dot{V}_I$ in all participants (see Figure 5.3.7 for group mean ventilatory slopes). In most participants, the increase in $\dot{V}_I$ was driven by the combined increase in V_{TI} and f_R, although one participant adopted a different breathing pattern (V_{TI} and f_R slope responses) between the two trials ($p = 0.002$). As shown in Figure 5.3.7B and Table 5.3.6, intrathoracic pressures also increased as a function of $P_{ET}CO_2$. However, the intrathoracic pressure responses were notably more variable and with lower within-day reliability compared to the ventilatory and breathing pattern slopes.

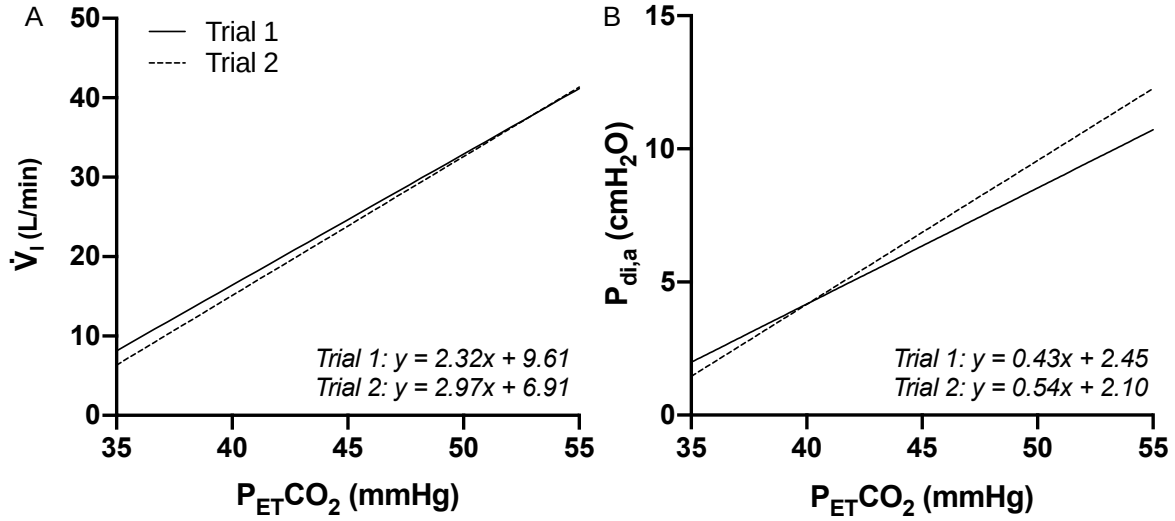

Figure 5.3.7 Slope responses for *A*) inspiratory minute ventilation ($\dot{V}_I$), and *B*) mean inspiratory transdiaphragmatic pressure ($\overline{P}_{di,a}$) in trial 1 (—) and trial 2 (---). Data are group mean for six participants.

Group mean ventilatory and intrathoracic pressure responses at the peak of rebreathe are shown in Table 5.3.7. At the peak of rebreathe, $\dot{V}_I$ was ~17% of $MVV_{12,}$ and did not differ between the two trials (p = 0.567). Generally, ventilatory slopes and peak responses exhibited moderate- to excellent within-day reliability in the form of ICC (≥0.507 T_I/T_{TOT} at peak of rebreathe), although CV was notably more variable, ranging from 1% (f_R at peak of rebreathe) to 26% (f_R vs. $P_{ET}CO_2$; Table 5.3.6 and Table 5.3.7). The within-day reliability of intrathoracic pressure responses were also highly variable and of poor level.

Table 5.3.6 Within-day comparison of ventilatory, breathing pattern and intrathoracic pressure *slope* responses to CO_2.

			Coefficient of variation		**Intra-class correlation coefficients**		
	Trial 1	**Trial 2**	CV (%)	95% CI (%)	ICC	95% CI	*p*-value
Ventilatory responses							
$\dot{V}_I$ vs. $P_{ET}CO_2$, L/min/mmHg	2.32 ± 1.69	2.97 ± 1.64	17 ± 28	6.0 – 29.4	0.862	0.214 – 0.980	0.017
V_{TI} vs. $P_{ET}CO_2$, mL/mmHg	132 ± 120	166 ± 88	25 ± 13	4.6 – 54.7	0.733	–0.895 – 0.963	0.095
f_R vs. $P_{ET}CO_2$, breaths/mmHg	0.43 ± 0.63	0.60 ± 0.30	26 ± 21	8.1 – 47.1	0.659	–0.403 – 0.909	0.138
T_I vs. $P_{ET}CO_2$, s/mmHg	–0.13 ± 0.15	–0.18 ± 0.24	17 ± 21	10.5 – 26.7	0.901	0.415 – 0.986	0.011
Intrathoracic pressures							
$\overline{P}_{di,a}$ vs. $P_{ET}CO_2$, cmH_2O/mmHg	0.43 ± 0.45	0.54 ± 0.31	6.4 ± 5.9	2.2 – 10.2	–0.444	–0.867 – 0.584	0.785
$\overline{P}_{oe,a}$ vs. $P_{ET}CO_2$, cmH_2O/mmHg	–0.27 ± 0.49	–0.55 ± 0.32*	20.0 ± 18.3	7.1 – 31.7	–0.343	–0.916 – 0.575	0.777
$\overline{P}_{ga,a}$ vs. $P_{ET}CO_2$, cmH_2O/mmHg	0.15 ± 0.12	0.20 ± 0.13	11.8 ± 19.6	1.0 – 25.4	–0.441	–0.916 – 0.578	0.789

Data are mean ± *SD* for six participants. CV, coefficient of variation for duplicate measurements; CI, confidence interval; ICC, intra-class correlation coefficient; $\dot{V}_I$, inspiratory minute ventilation; $P_{ET}CO_2$; end-tidal partial pressure of CO_2; V_{TI}, inspiratory tidal volume; f_R, respiratory frequency; $\overline{P}_{di,a}$, active component of mean inspiratory transdiaphragmatic pressure; $\overline{P}_{oe,a}$, active component of mean inspiratory oesophageal pressure; $\overline{P}_{ga,a}$, active component of mean inspiratory gastric pressure.*$p \leq 0.05$ vs. trial 1.

Table 5.3.7 Within-day comparison of ventilatory, breathing pattern and intrathoracic pressure *peak* responses to CO_2.

			Coefficient of variation		Intra-class correlation coefficients		
	Trial 1	**Trial 2**	CV (%)	95% CI (%)	ICC	95% CI	*p*-value
Ventilatory responses							
$\dot{V}_I$, L/min	35.1 ± 17.8	35.8 ± 13.5	17.2 ± 15.1	6.7 – 27.7	0.964	0.740 – 0.995	0.002
V_{TI}, L	2.26 ± 1.01	2.29 ± 0.64	14.0 ± 8.7	7.9 – 20.0	0.955	0.670 – 0.994	0.003
f_R, breaths/min	16.2 ± 4.8	16.3 ± 4.5	1.02 ± 0.54	0.01 – 2.12	0.990	0.935 – 0.999	< 0.001
T_I, s	1.92 ± 0.64	1.86 ± 0.61	11.6 ± 11.5	3.5 – 19.6	0.915	0.371 – 0.988	0.012
T_I/T_{TOT}	0.47 ± 0.03	0.47 ± 0.06	6.8 ± 7.8	1.4 – 12.3	0.571	–0.482 – 0.929	0.112
Intrathoracic pressures							
$\overline{P}_{di,a}$ cmH_2O	7.7 ± 4.3	10.4 ± 3.2	33 ± 43	18 – 48	0.261	–0.413 – 0.883	0.260
$\overline{P}_{oe,a,}$ cmH_2O	–4.51 ± 4.06	–7.37 ± 3.07*	58 ± 54	39 – 77	0.171	–0.920 – 0.836	0.375
$\overline{P}_{ga,a}$, cmH_2O	3.74 ± 1.70	3.96 ± 1.51	22 ± 25	13 – 31	0.677	–0.369 – 0.950	0.060

Data are mean ± *SD* for six participants. CV, coefficient of variation for duplicate measurements; CI, confidence intervals; ICC, intra-class correlation coefficient; $\dot{V}_I$, inspiratory minute ventilation; $P_{ET}CO_2$; end-tidal partial pressure of CO_2; V_{TI}, inspiratory tidal volume; f_R, respiratory frequency; $\overline{P}_{di,a}$, active component of mean inspiratory transdiaphragmatic pressure; $\overline{P}_{oe,a}$, active component of mean inspiratory oesophageal pressure; $\overline{P}_{ga,a}$, active component of mean inspiratory gastric pressure.*$p \leq 0.05$ vs. trial 1.

Diaphragm ultrasonography

A total of 116 ultrasound cine-loops were obtained during the two rebreathe trials (incl. cine-loops obtained at rest and during subsequent recovery). From these cine-loops, 115 (99%) could be successfully analysed. When the percentages of successfully analysed cine-loops were plotted against V_{TI}, it was evident that ultrasound feasibility was not adversely affected by tidal volumes within the measured range (0.320 – 2.55 L; Figure 5.3.8). The only cine-loop that could not be analysed was obtained at V_{TI} 1.5 L, and contained two breaths that could not be analysed due to lateral movement of the diaphragm and ribs out of the field of view.

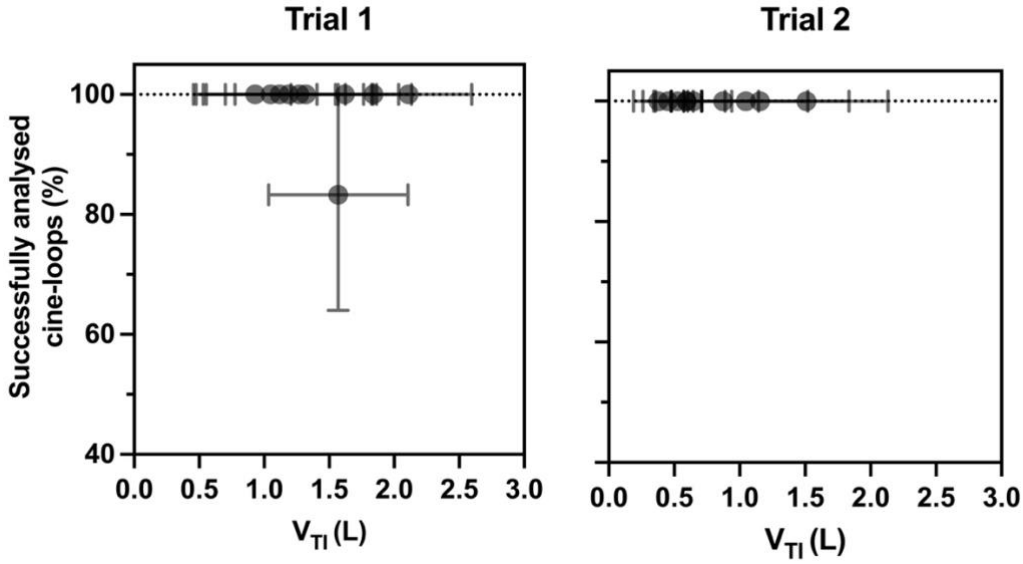

Figure 5.3.8 Percentage of successfully analysed cine-loops plotted against V_{TI} in trial 1 and trial 2. Data are mean ± *SD* for six participants at all time-points.

Concurrent validity: the effect of time on diaphragm thickening

Costal diaphragm thickness and thickening during rebreathe trials are shown in Figure 5.3.9. Diaphragm thickness at EELV did not change during rebreathe (p = 0.463; η_p^2 = 0.250) and did not differ between the two trials (p = 0.391; η_p^2 = 0.250; Figure 5.3.9A). By contrast, diaphragm thickness at EILV increased as a function of time (p < 0.001; η_p^2 = 0.795; Figure 5.3.9B), with *post hoc* tests showing that thickness at EILV increased significantly from rest to peak (from 1.88 ± 0.40 mm to 2.78 ± 0.56 mm; p = 0.041), then returned to resting values within the first minute of recovery (1.88 ± 0.50 mm; p = 0.980 from rest). Again, there was no difference between trials (p = 0.053; η_p^2 = 0.650). As expected, therefore, there was a main effect of time on thickening fraction (p < 0.001; η_p^2 = 0.759) and on thickening ratio (p < 0.001; η_p^2 = 0.766),

but no difference between the two trials (thickening fraction: p = 0.616; η_p^2= 0.094; thickening ratio: p = 0.459; η_p^2 = 0.108).

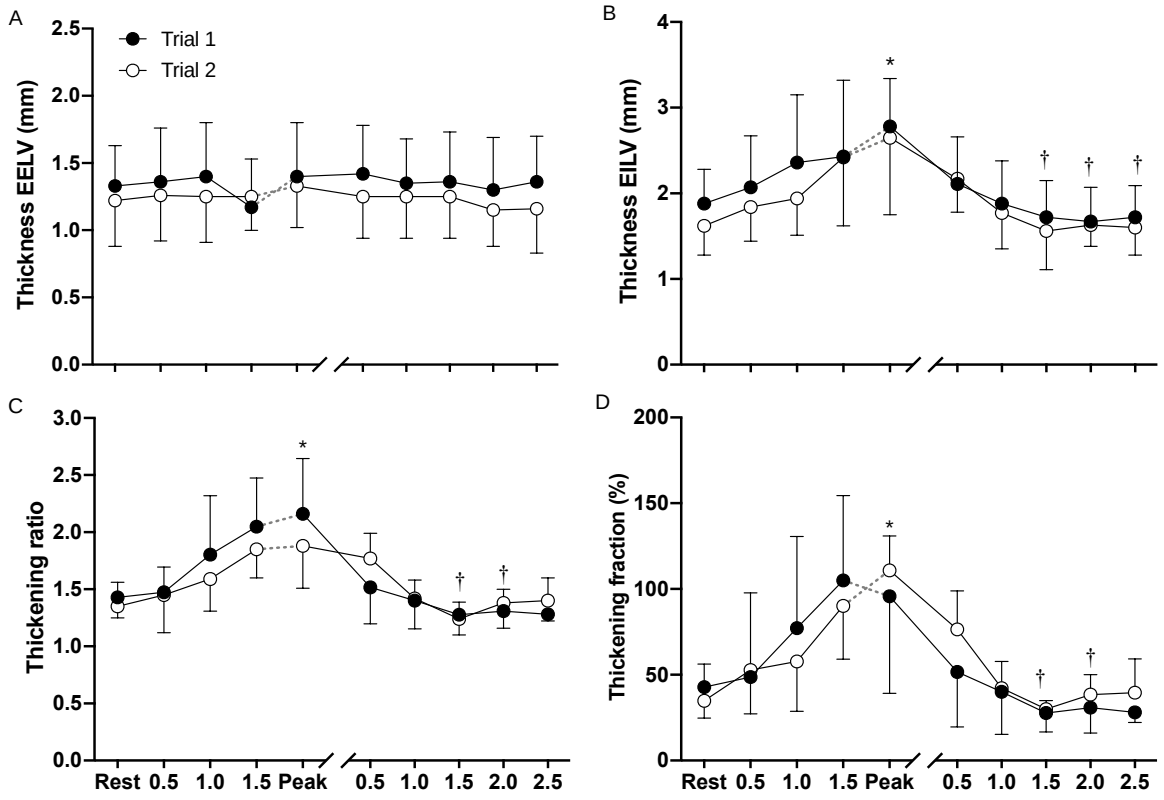

Figure 5.3.9 Ultrasound-derived thickness and relative thickening of diaphragm as a function of time during hyperpnoea during trial 1 (●) and trial 2 (○). Broken *x*-axis represents transition from hyperpnoea to recovery. Data are mean ± *SD* for six participants. *$p \leq 0.05$ vs. rest for M-mode and AM-mode; †$p \leq 0.05$ vs. peak for M-mode and AM-mode.

Figure 5.3.10 shows the ultrasound-derived measures of diaphragm thickness at EILV and relative thickening plotted against V_{TI} and $\overline{P}_{di,a.}$ Because of the low sample size in this part of the study, and because there were no significant differences between the responses in trial 1 and trial 2, the lines of best fit were calculated to represent the mean relationships for duplicate measures. As shown, costal diaphragm thickness at EILV was moderately and strongly correlated with V_{TI} and $\overline{P}_{di,a}$, respectively. Of particular interest, perhaps, were the strong relationships between $\overline{P}_{di,a}$ and thickness at EILV and thickening fraction (Figure 5.3.10B and D, respectively).

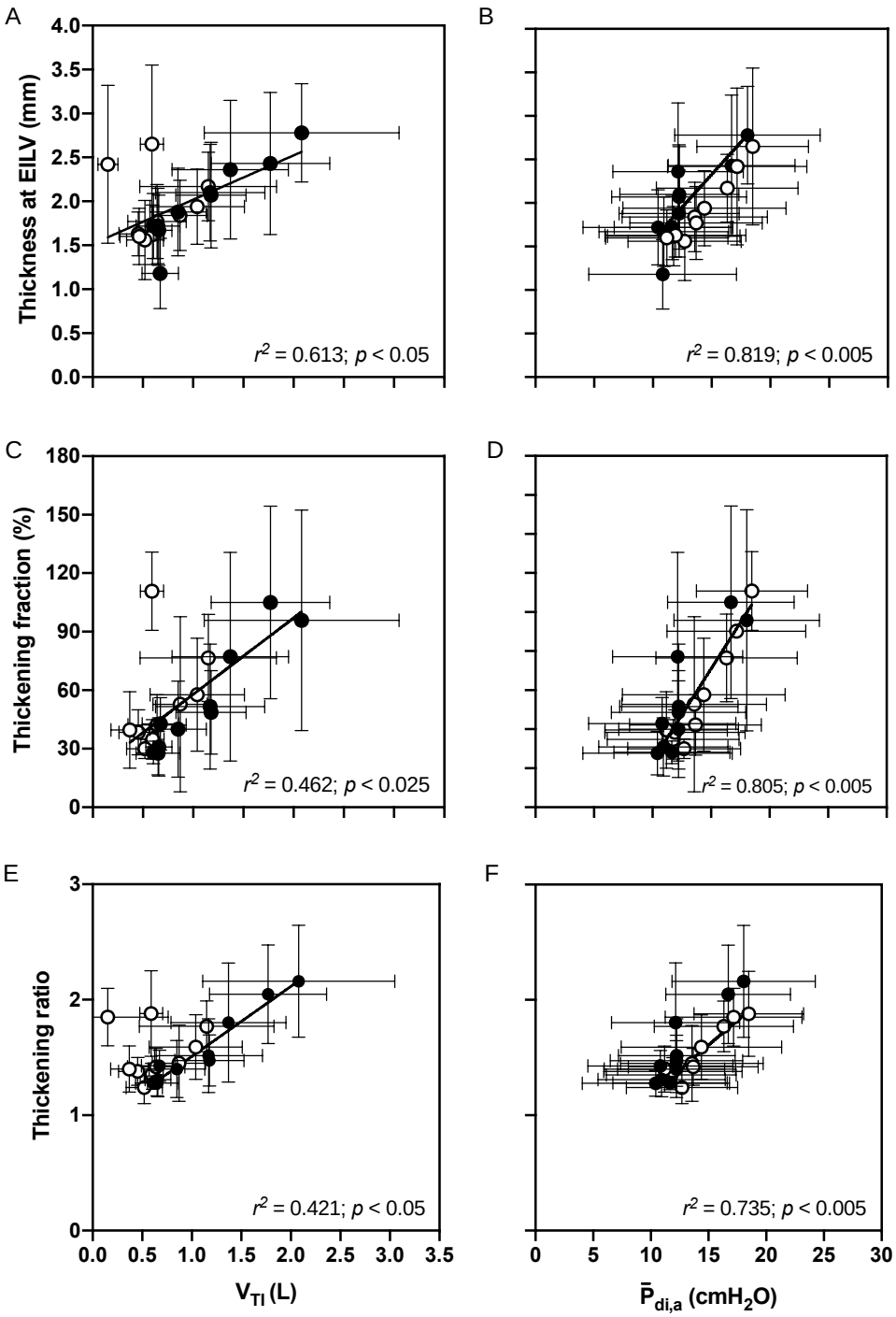

Figure 5.3.10 Diaphragm thickness at EILV (*A-B*), thickening fraction (*C-D*) and thickening ratio (*E-F*) as a function of V_{TI} and $\bar{P}_{di,a}$. Data are the mean ± *SD* for all timepoints during trial 1 (●) and trial 2 (○), including rest and three subsequent minutes of recovery for six participants. r^2 and *p*-values were corrected for duplicate measurements (Bland & Altman, 1995).

Within-day reliability

As in *Part 1*, ultrasound-derived measures were acquired at 15 s intervals and averaged and could, therefore, not be plotted as slope responses to CO_2. Thus, within-day comparisons were performed on peak diaphragm thickness at EELV and EILV, as well as thickening fraction and thickening ratio. Figure 5.3.11 shows the individual peak responses to CO_2, plotted as trial 1 vs. trial 2. Moreover, within-day comparisons of peak diaphragm thickness and thickening showed that all ultrasound-derived measures exhibited moderate- to excellent within-day reliability in the form of ICC (≥0.404) and CV (≤14.2%) (Table 5.3.8).

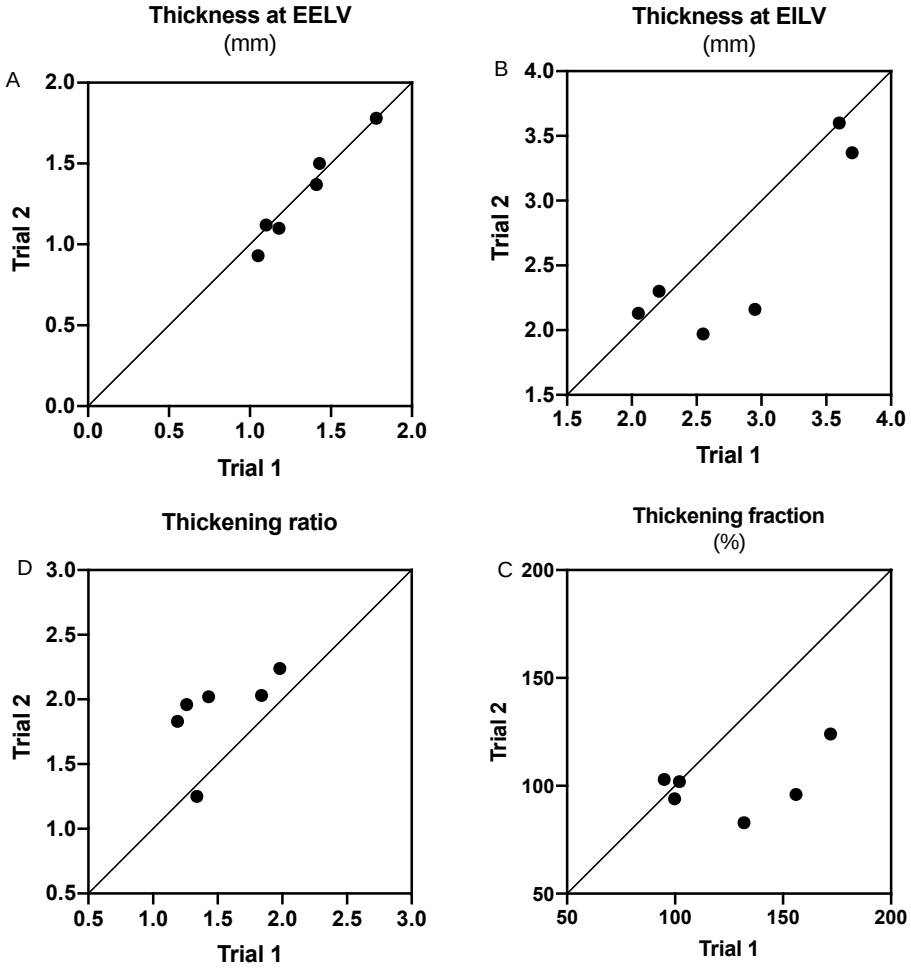

Figure 5.3.11 Individual peak responses to CO_2 in ultrasound-derived thickness and thickening of diaphragm plotted as trial 1 vs. trial 2 for six participants Diagonal lines are lines of identity ($y = x$).

Table 5.3.8 Within-day comparison of diaphragm thickness and thickening *peak* responses to CO_2.

	Trial 1	**Trial 2**	**Coefficient of variation**		**Intraclass correlation coefficient**		
			CV (%)	95% CI (%)	ICC	95% CI	*p*-value
Thickness at EELV, mm	1.37± 0.27	1.33 ± 0.33	2.6 ± 2.1	1.5 – 3.7	0.985	0.892 – 0.998	0.001
Thickness at EILV, mm	2.97 ± 0.69	2.64 ± 0.77	7.0 ± 6.8	3.4 – 10.5	0.898	0.162 – 0.980	0.012
Thickening ratio	2.01 ± 0.14	1.53 ± 0.35	14.2 ± 8.1	10.0 – 18.5	0.404	–.207 – 0.900	0.117
Thickening fraction, %	132 ± 33	102 ± 15	13.3 ± 10.9	7.6 – 19.0	0.511	–0.679 – 0.938	0.092

Data are mean ± *SD* for six participants. CV, coefficient of variation for duplicate measurements; CI, confidence interval; ICC, intra-class correlation coefficient; EELV, end-expiratory lung volume; EILV, end-inspiratory lung volume.

5.4 Discussion

The aim of this study was to explore the use of ultrasonography for the assessment of diaphragm contractile properties during hypercapnic hyperpnoea. Specifically, this was the first study to determine the feasibility, concurrent validity and within-day, intra-observer reliability of ultrasound-derived measures of diaphragm kinetics and thickening during hypercapnic hyperpnoea. In *Part 1*, the assessment of crural diaphragm kinetics was shown to be highly feasible during hyperpnoea, and was not adversely affected by increasing tidal volume. Interestingly, AM-mode ultrasound appeared to capture more closely crural diaphragm kinetics compared to M-mode due to the dynamic AM-mode cursor that can be oriented along the true axis of diaphragm excursion. With the exception of excursion time, which exhibited poor within-day reliability, ultrasound-derived diaphragm kinetics generally exhibited good- to excellent within-day reliability.

In *Part 2*, the assessment of costal diaphragm thickness and thickening (shortening) during hypercapnic hyperpnoea was shown to be highly feasible. At the peak of hyperpnoea, diaphragm thickness at EILV and the relative thickening (fraction and ratio) were all strongly correlated with $\overline{P}_{di,a}$, confirming the close relationship between muscle thickening and force output during dynamic contractions. Overall, ultrasound-derived diaphragm thickness and thickening obtained at the peak of hyperpnoea exhibited moderate- to excellent within-day reliability. Collectively, these findings suggest that subcostal and intercostal ultrasound approaches are feasible to perform, and produce reliable measures of diaphragm kinetics and thickening during hypercapnic hyperpnoea.

5.4.11 Feasibility of diaphragm ultrasound during hyperpnoea

Given the high percentages of successfully analysed cine-loops found in both *Part 1* and *Part 2* of this study, it was concluded that ultrasonography was highly feasible for assessing crural diaphragm kinetics and costal diaphragm thickening during hypercapnic hyperpnoea. It was expected that an increase in tidal volume would adversely affect feasibility owing to passive movement of the transducer on the ribs during inspiration, thereby making it more difficult to acquire clear images. However, our findings did not support this hypothesis.

A number of previous studies have reported similar levels of feasibility for the assessment of diaphragm function using ultrasound. For instance, Testa et al. (2011) reported feasibility of 95% in experienced sonographers (92.5% for inexperienced sonographers) for assessing diaphragm kinetics during quiet breathing and forced expiratory manoeuvres. This is in line

with feasibility levels reported by others for assessing diaphragm kinetics during quiet breathing (Boussuges et al., 2009; Gerscovich et al., 2001). Similarly, Ueki et al. (1995) reported feasibility of 100% for assessing costal diaphragm thickening in healthy men during maximal static inspiratory pressure manoeuvres (MIP efforts), while Goligher et al. (2015) reported feasibility of 95% for diaphragm thickening during quiet breathing in patients undergoing mechanical ventilation. Accordingly, the present study extends these previous reports, showing that ultrasound feasibility is preserved in the face of increasing ventilatory loads.

CO_2-rebreathe offers unique insight into dynamic diaphragm function without the influence of participant motivation and movement artefact. However, there are technical challenges associated with performing ultrasound scans during hyperpnoea. First, both subcostal and intercostal ultrasound approaches require the transducer to be positioned *on* (intercostal approach) or directly *below* (subcostal approach) the ribs. As tidal volume and rib cage distortion increase during hyperpnoea, the ultrasound transducer may move *with* the rib cage, thereby making it more difficult to perform ultrasound scans. Still, when plotting the percentage of successfully analysed cine-loops as a function of V_{TI}, it was evident that feasibility was not adversely affected by the increased ventilatory drive induced by CO_2 (see Figure 5.3.2 and Figure 5.3.8). Still, it must be noted that great emphasis was placed on marking the skin thoroughly before each experimental trial, and using anatomical landmarks (i.e., inferior vena cava and intrahepatic vein) throughout data acquisition. This way, it was ensured that the ultrasound transducer did not move passively on the skin (due to rib cage distortion) and that the target tissue (diaphragm) was imaged in relation to fixed reference points.

Second, the subcostal ultrasound approach (*Part 1*) may be limited by the diaphragm's depth within the thorax. That is, with the subcostal approach, the posterior hemi-diaphragm dome is imaged at a depth of 15-25 cm depending on chest dimensions of the individual. As such, in individuals with chest depths of >22-23 cm, visualisation of the diaphragm at EELV was occasionally difficult because the hyperechoic diaphragm moved deeper than what could be imaged with the low-frequency transducer. A similar challenge was reported by Ueki et al. (1995), who found that the intercostal ultrasound approach was particularly difficult in obese individuals because the increased volume of thoracic subcutaneous adipose tissue increased the distance between ultrasound transducer and target tissue. Although none of our participants were obese (BMI <30 kg/m^2), the acquisition of technically acceptable cine-loops and subsequent analysis was at times challenging, even in men of meso-endomorphic somatotype.

Lastly, it is worth discussing the potential underestimation of diaphragm excursion measured by conventional M-mode compared to AM-mode in *Part 1*. Although both analysis techniques demonstrated acceptable feasibility, it was apparent upon visual inspection of each cine-loop that the excursion measured with M-mode did not represent the contractile hemi-diaphragm apex, but rather the non-contractile central tendon (Figure 5.3.3). As shown, the hemi-diaphragm apex does not move along a strictly craniocaudal (vertical) axis, but rather diagonally, particularly when tidal volumes are large. Thus, the static and vertical M-mode cursor may not capture the true excursion of the contractile diaphragm. It may be concluded, therefore, that AM-mode with dynamic cursor is the most feasible analysis technique for use during hyperpnoea.

5.4.12 Concurrent validity of diaphragm ultrasonography

In *Part 1*, the concurrent validity of ultrasound-derived diaphragm kinetics was assessed by plotting correlations of diaphragm excursion, excursion time and excursion velocity with ventilatory indices (i.e., V_{TI}, T_I and V_{TI}/T_I). The relationships between diaphragm kinetics and ventilatory indices were assumed under the theoretical basis that diaphragm descent is strongly related to the displacement of volume during inspiration (Singh et al., 2003), and that there is a moderate- to strong relationship between the rate of diaphragm fibre shortening (by sonomicrometry) and inspiratory flow (Easton et al., 1993; Fitting et al., 1985). Thus, when V_{TI} and V_{TI}/T_I increases as a function of $P_{ET}CO_2$, so should diaphragm excursion and excursion velocity. The present data support this relationship (Figure 5.3.5).

Nonetheless, the relationships between ultrasound-derived diaphragm kinetics and ventilatory indices suggest that there is still variance in the relationships unaccounted for. This was particularly evident for the relationship between T_I and excursion time (r^2 = 0.319; p = 0.022 with AM-mode; Figure 5.3.5E). The variance unaccounted for may be attributed to the fact that ventilatory indices are measured at the mouth, and result from finely coordinated recruitment and shortening of both the diaphragm and accessory inspiratory muscles. The timing and rate of inspiration at the mouth may, therefore, not align accurately with the timing and rate of diaphragm shortening and descent as measured at the muscle. In fact, intra-breath analysis of (canine) costal and crural diaphragm shortening by sonomicrometry has shown that inspiratory airflow occurs before significant shortening of either costal and crural diaphragm under hypercapnic conditions (Easton et al., 1995). Additionally, the dissonance between inspiratory airflow and diaphragm shortening appears to be exacerbated under hypercapnic and hypoxic conditions compared to under eucapnic and normoxic conditions (Easton et al., 1993).

Accordingly, the variance unaccounted for by our results may be attributed to a naturally occurring shift in timing of airflow and diaphragm shortening during the specific hypercapnic stimuli used in this study.

In *Part 2*, the concurrent validity of ultrasound-derived diaphragm thickness and thickening was assessed by plotting correlations between ultrasound-derived measures and V_{TI} under the theoretical basis that diaphragm thickness measured at autopsy appears to be strongly related to static lung volumes (Cohn et al., 1997; Ueki et al., 1995; Wait et al., 1989), and should therefore be closely related to tidal volume during spontaneous breathing. Moreover, the relationship between ultrasound-derived measures and diaphragm force (pressure) was assessed under the theoretical basis that costal diaphragm thickening – being an estimate of costal fibre shortening (Wait et al., 1989) – should be closely related to the active force output of the shortening muscle, as per the sliding filament theory (Huxley, 1957). Overall, the ultrasound-derived measures were moderately- to strongly correlated with ventilatory indices and $\overline{P}_{di,a}$, confirming the notion that diaphragm structural attributes and kinetics are closely related to force output and ventilatory indices. This being said, the novelty of these ultrasound measurements is that it provides a *direct* insight into diaphragm function at the level of the muscle; specifically, the direct measures of dynamic properties of the muscle. As discussed in detail in the following chapters, ultrasound may, therefore, provide useful information when trying to better understand the influence of fatigue on dynamic diaphragm contractile properties.

Concurrent validity of ultrasound-derived measures of resting diaphragm function have been addressed in multiple previous studies. For instance, Houston et al. (1995) compared diaphragm descent obtained by fluoroscopy to that obtained with subcostal ultrasonography, and concluded that ultrasound was easier to perform (and non-ionising) while measuring similar diaphragm movement as fluoroscopy. Similarly, Noh et al. (2014) assessed the relationship between ultrasound-derived excursion with the excursion measured with x-ray imaging, and found that the measures were strongly correlated during inspiration and expiration ($r \geq 0.78$). Moreover, concurrent validity of ultrasound-derived costal diaphragm thickness has been validated against autopsy measurements of diaphragm thickness, reporting strong correlations ($r^2 = 0.89$) (Cohn et al., 1997). Accordingly, we extended these previous findings by showing that ultrasound-derived diaphragm kinetics and thickening are related to ventilatory indices and intrathoracic pressures, also for dynamic contraction during hyperpnoea.

5.4.13 Within-day, intra-observer reliability

Within-day reliability of ventilatory indices and intrathoracic pressures

To ensure optimal conditions of reliable ultrasound acquisition during hyperpnoea, we also assessed the within-day reliability of ventilatory and intrathoracic pressure responses hypercapnic hyperpnoea. Although most ventilatory and pressure responses in this study generally exhibited good- to excellent levels of reliability, regardless if measured as slope or peak response, it was evident that slope responses generally exhibited greater levels of within-day reliability compared to peak responses (*Part 1*: Table 5.3.2 and Table 5.3.3; *Part 2:* Table 5.3.6 and Table 5.3.7). The discrepancy between slope and peak responses may be explained by slope responses being calculated on a breath-by-breath basis over the course of each rebreathe test, whereas peak responses were based on 15 s averages (i.e., 3-6 breaths).

Nonetheless, as pointed out by others (Spengler & Shea, 2001), CO_2-rebreathe tests are inherently associated with great variability from both explained and unexplained sources. For instance, Jensen et al. (2010) reported a CV of 38% for the within-day variability of ventilatory slope assessed over quadruplicate measurements using Duffin's modified rebreathe method. Using the Read rebreathe method, Sahn et al. (1977) reported a CV of 18% (range 8-26%) for the ventilatory slope. In fact, even after adjusting for circadian rhythm under stable environmental and behavioural conditions, Spengler & Shea (2001) found that one-third of the variability in CO_2-sensitity to the Read method could not be accounted for in awake humans. Accordingly, the authors concluded that there is an inherent variability component associated with the test. In order to reduce the influence of external factors (such as arousal level and environmental conditions) on the ventilatory response to rebreathe, we went to great efforts to standardise our laboratory conditions. For instance, the laboratory was kept silent before, during and after each rebreathe trial; the lightning and ambient temperature were kept stable; and a thorough familiarisation test was instituted prior to the experimental visit to reduce the potential influence of arousal (Spengler & Shea, 2001). Moreover, participants were asked to abstain from caffeine ≥12 h prior to testing, so as to eliminate the potential influence of caffeine on CO_2 sensitivity (D'Urzo et al., 1990; see General Methods, section 3.3).

Within-day reliability of ultrasound-derived diaphragm kinetics and thickening

Unlike ventilatory indices and intrathoracic pressures, ultrasound was not assessed on a breath-by-breath basis, and within-day reliability was therefore assessed for the final 15 s cine-loop (peak) during CO_2-rebreathe. Because within-day reliability of diaphragm ultrasound has

already been thoroughly assessed in previous studies during quiet breathing (Baldwin et al., 2011; Boussuges et al., 2009; Gerscovich et al., 2001; Harper et al., 2013), this study expanded on these previous reports by assessing the within-day reliability of ultrasound-derived diaphragm kinetics and thickening during hyperpnoea.

In *Part 1*, both M-mode and AM-mode measured diaphragm excursion at the peak of hyperpnoea with good- to excellent within-day reliability (ICC ≥0.870; CV ≤5.6%; Table 5.3.4). This was true also for excursion velocity and power, particularly measured with AM-mode, exhibiting good within-day reliability. In fact, this level of reliability is similar to that reported for diaphragm twitch and sniff excursion in Chapter 4 and during quiet breathing (Scarlata et al., 2018). In *Part 2*, costal diaphragm thickness at EELV and EILV were measured with excellent reliability, as evidenced by the high ICC (≥0.898) and low CV (≤7%). As with diaphragm kinetics, this level of reliability is similar to that reported for costal diaphragm thickness before and during twitch and sniff contractions in Chapter 4 (ICC ≥0.926; CV ≤4.5%), and at EILV (Harper et al., 2013) and EELV (Baldwin et al., 2011), ranging from 0.940 (95%CI 0.79–0.980) to 0.990 (0.918 – 0.998). Accordingly, this study extends previous work using ultrasound to assess diaphragm function during quiet breathing. The findings suggest that diaphragm ultrasound be used reliably within-day to measure diaphragm kinetics and thickening during hyperpnoea, and without notable adverse effects of increasing ventilatory load and tidal volume.

5.4.14 Methodological considerations

In this study, only kinetics and thickening of the right hemi-diaphragm were measured. There is, however, a significant difference between left and right hemi-diaphragm excursion, with a right-to-left ratio of 1.0-1.2 reported for quiet, spontaneous breathing (Houston et al., 1992). With deep breathing, the ratio has been found to increase to 1.1-1.4 (Boussuges et al., 2009). When calculating excursion velocity and diaphragm power, it was therefore assumed that both hemi-diaphragms moved uniformly, and that the measures derived from right hemi-diaphragm were representative for both hemi-diaphragms. As a result, our measures of diaphragm kinetics may have been slightly overestimated for the muscle as a whole.

5.4.15 Conclusions

Subcostal ultrasonography for the assessment of diaphragm kinetics and thickening is feasible, and the ultrasound-derived measures can be reliably quantified in healthy adults during hypercapnic hyperpnoea. Based on the findings of this study, ultrasonography of the costal and

crural diaphragm may offer new insight into the contractile properties of the *in vivo* human diaphragm under applied, dynamic conditions. Moreover, these findings will help to inform the subsequent chapters in this thesis. For instance, in Chapter 6, subcostal ultrasonography (AM-mode) will be used to quantify and compare diaphragm kinetics during two modes of reflexively-driven hyperpnoea in order to elucidate the mechanisms that underpin postural-ventilatory modulation of the diaphragm muscle. In Chapter 7 and 8, subcostal and intercostal ultrasonography will be used to assess the influence of pressure- and flow loading on crural diaphragm kinetics and costal diaphragm thickening to elucidate the mechanisms underpinning task-dependency of diaphragm fatigue.

Chapter 6

Application of Subcostal Ultrasonography for the Assessment of Diaphragm Kinetics During Exercise- and CO_2-Induced Hyperpnoea in Healthy Adults

6.1 Introduction

The diaphragm is the principal muscle of inspiration in healthy humans (Grimby et al., 1976). In addition, the diaphragm muscle plays a significant role in postural support and trunk stability during limb movement (Hodges et al., 1997; Hodges & Gandevia, 2000b). Upon contraction, the diaphragm descends and flattens, thereby expanding the lower ribcage and generating the negative pressure gradient that drives inspiratory airflow (De Troyer & Boriek, 2011). Diaphragm descent also increases intraabdominal pressure, which stabilises the spine during limb movement (Hodges et al., 1997) and lifting (Hemborg et al., 1985). In other words, the diaphragm must maintain a 'balancing act' when both postural support and high rates of ventilation are required, such as during whole-body exercise.

There is evidence, however, showing that during exercise, the postural role of the diaphragm becomes of secondary importance as central respiratory drive increases. Indeed, Hodges et al. (2001) found that diaphragm contribution to postural support was reduced, or even absent, when arm movement was superimposed on hypercapnic hyperpnoea. Consequently, the authors concluded that there might be pre-synaptic inhibition of postural inputs to the phrenic motoneurons when tasks that challenge posture are superimposed on hyperpnoea. A pre-synaptic inhibition of postural inputs during hyperpnoea would ensure that the postural role of the diaphragm is diminished while prioritising the muscle's ventilatory role to meet the ventilatory demand (Gandevia et al., 2002; Hodges et al., 2001). If the ventilatory role of the diaphragm is always prioritised during hyperpnoea, even with concurrent limb movement, this implies that the kinetic behaviour of the diaphragm muscle (i.e., excursion, excursion velocity, force and power) must also be similar in response to hyperpnoea induced with and without limb movement.

In order to elucidate the mechanisms that underpin postural-ventilatory modulation of the human diaphragm, subcostal ultrasonography can be used to quantify the crural diaphragm excursion and rate of excursion during spontaneous breathing (Testa et al., 2011). Although diaphragm ultrasonography has primarily been used in the ICU for the assessment of diaphragm function in patients undergoing mechanical ventilation (Ferrari et al., 2018; Laursen et al., 2021), results from Chapter 5 demonstrated that ultrasonography may offer new insight into dynamic contractile properties, particularly if used in combination with conventional measures or intrathoracic pressures and ventilatory indices. Furthermore, the results of this chapter demonstrated that angle-independent AM-mode ultrasound is a feasible and reliable method to

assess diaphragm kinetics across a wide range of tidal volumes, and may be used to estimate diaphragm power.

6.1.1 Aims and hypotheses

The aims of this study were: *i*) to evaluate the feasibility of ultrasonography for the assessment of diaphragm kinetics (excursion, excursion velocity and power) during two modes of reflexively-driven hyperpnoea (CO_2-rebreathe and exercise); and *ii*) to compare diaphragm kinetics across the two modes of hyperpnoea in order to elucidate the mechanisms that underpin postural-ventilatory modulation of the diaphragm.

It was hypothesised that diaphragm ultrasonography would be feasible for use during both modes of hyperpnoea, but that the motion artefacts associated with leg and hip movements during exercise would adversely affect ultrasound feasibility during exercise-induced hyperpnoea. Due to the proposed inhibition of postural drive to the diaphragm during hyperpnoea, it was further hypothesised that diaphragm kinetic behaviour would be similar during exercise-induced hyperpnoea and non-exercise-induced hyperpnoea (CO_2-rebreathe).

6.2 Methods

6.2.2 Ethical approval and participants

The study was approved by the Brunel University London Research Ethics Committee (Appendix 1) and conformed to the most recent standards set by the Declaration of Helsinki (World Medical Association, 2013). Ten healthy, non-smoking adults (5 women) between the ages of 18 and 30 y from university student population volunteered to participate. Self-reported, biological sex was taken into account when including participants in order to ensure adequate representation of both sexes (Heidari et al., 2016). Further, all participants reported to have no medical history of cardiovascular, respiratory or neuromuscular disease using a standardised health questionnaire (Appendix 2). Exclusion criteria were BMI ≥30 kg/m^2 and pulmonary function and maximal respiratory mouth pressures outside age-specific limits of normal (Evans & Whitelaw, 2009; Quanjer et al., 2012; Stocks & Quanjer, 1995). Participants provided written informed consent (Appendix 2), and were asked to abstain from vigorous exercise for ≥24 h, from caffeine and alcohol for ≥12 h, and from food for ≥3 h prior to each visit.

6.2.3 Experimental overview

Each participant visited the laboratory on two occasions, separated by no less than 48 h and no more than 14 d. The first visit was for screening and familiarisation, during which participants performed pulmonary function tests and was thoroughly familiarised with the experimental set-up. The second visit was the experimental trial, consisting of reflexively-driven hyperpnoea induced by: *i*) a hyperoxic, hypercapnic rebreathe test (Read rebreathe method); and *ii*) a maximal incremental exercise test on a semi-recumbent cycle ergometer. The hyperpnoea tests were performed in a pre-determined, non-randomised order (CO_2-rebreathe followed by exercise) to limit the potential influence of exercise-induced diaphragm fatigue on CO_2 sensitivity and physiological responses to CO_2-rebreathe (Mador & Tobin, 1992). Intrathoracic pressures, cardiorespiratory indices and ultrasound-derived measures of diaphragm kinetics (excursion, excursion time, excursion velocity and power) were assessed at regular intervals before (rest), during, and after (recovery) both hyperpnoea tests.

6.2.4 Screening and familiarisation

The screening was performed as described in Chapter 4 (section 4.2.4). Specific familiarisation for the experimental trial included thorough familiarisation with the CO_2-rebreathe method and semi-recumbent cycling exercise. Specifically, for CO_2-rebreathe, familiarisation included verbal instructions followed by a practice rebreathe test. For the semi-recumbent cycling exercise, participants performed a practice test during which they maintained a pedal cadence of 55-60 rpm at 50 W for 10 min.

6.2.5 Experimental visit

Hypercapnic hyperpnoea (CO_2-rebreathe)

The CO_2-rebreathe test was similar to the modified Read rebreathe method (1966; Read & Leigh, 1967) described in Chapter 5. Briefly, the participant rested in the semi-recumbent position for ~10 min, breathing ambient air without a mouthpiece to ensure a steady state of relaxed wakefulness (Figure 6.2.1) (Spengler & Shea, 2001). Next, the participant breathed ambient air through a mouthpiece-valve assembly for 3 min while resting measurements were made over the final 30 s. The participant then exhaled to RV, at which point the rebreathe valve was closed and the participant equilibrated with the now-closed rebreathe circuit by taking three deep, rapid breaths. This was followed by the instruction to ‘close your eyes, relax and breathe as needed’. When $P_{ET}CO_2$ reached 7.33 kPa (55 mmHg), the rebreathe circuit was opened to ambient air with the participant continuing to breathe as needed for 3 min (recovery). The

laboratory was kept silent before, during and after the rebreathe trial to avoid the potential influence of external stimuli on ventilatory responses (Homma & Masaoka, 2008; Spengler & Shea, 2001).

Exercise-induced hyperpnoea

Exercise was performed on an electromagnetically braked, semi-recumbent cycle ergometer (Angio Imaging, Lode, Groningen, Netherlands), as described in detail in section 3.12. Briefly, prior to initiating the test, the participant rested in a semi-recumbent position for ~10 min, breathing ambient air *without* a mouthpiece and with feet fastened to pedals. Next, the participant breathed ambient air through a mouthpiece-valve assembly for 3 min, during which resting measurements were recorded over the final 30 s. The exercise test was initiated by cycling at 10 W with a cadence of 55-60 rpm for 3 min (warm-up), after which the work rate increased as a ramp by 15-30 W/min (Figure 6.2.1). The ramp rate was calculated on a participant-to-participant basis by calculating the predicted peak oxygen uptake (L/min) and assuming a work efficiency ($\Delta\dot{V}O_2/\Delta WR$) of 10.0 mL/min/W over a test duration of 8 min (Wasserman et al., 2012; Wasserman & Whipp, 1975). Although the above work efficiency was originally derived from healthy, recreationally-active men during upright cycling exercise (Wasserman & Whipp, 1975), there were – to our knowledge – no existing predictive equations (incl. established work efficiency) for semi-recumbent cycling at the time of data collection. The above duration was chosen on the basis that it was near the expected duration for CO_2-rebreathe (~2-3 min), yet still at the lower end of the range expected to elicit peak physiological responses (Buchfuhrer et al., 1983). Exercise was terminated when the participant could no longer sustain pedal cadence ≥50 rpm for >5 s despite verbal encouragement. Following exercise termination, participants continued to breathe on the mouthpiece for an additional 3 min for the collection of recovery data.

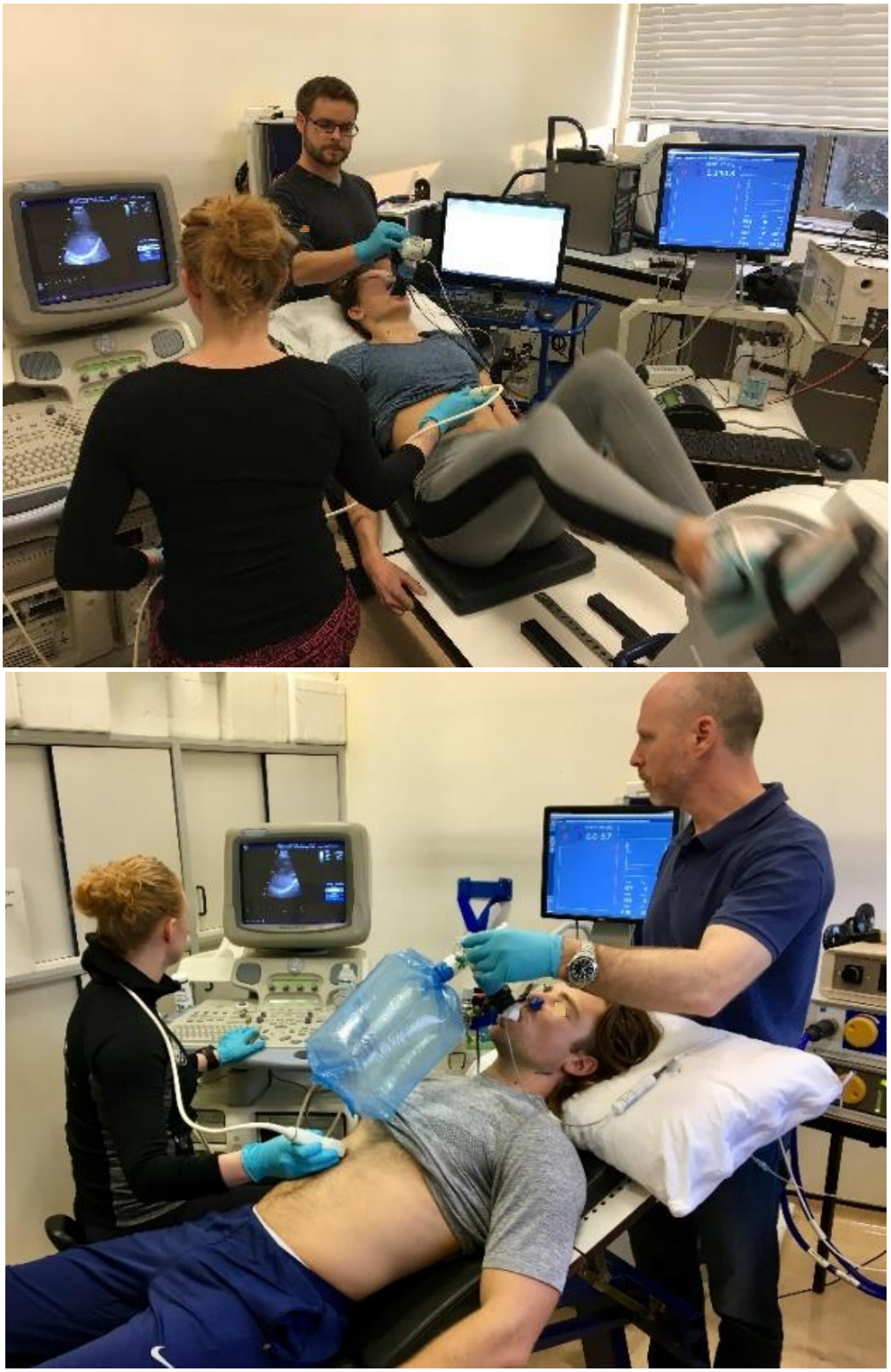

Figure 6.2.1 Laboratory set-up for exercise (top) and CO_2-rebreathe (bottom).

Assessment of intrathoracic pressures

The P_{oe} and P_{ga} were measured using two balloon-tipped catheters (86 cm, Cooper Surgical, Berlin, Germany) as described in 3.6.5 in General Methods. Briefly, the catheters were passed pernasally, and swallowed into the stomach via peristalsis. Once in the stomach, the balloons were filled with 1 mL (P_{oe}) and 2 mL (P_{ga}) of ambient air using a 10 mL glass syringe (Cross et al., 2015). The oesophageal catheter was then withdrawn from the stomach until negative deflections were seen in P_{oe} in response to a sniff (~35-45 cm distal from the nostril). The correct position of the oesophageal catheter was confirmed with the "dynamic occlusion test" (Baydur et al., 1982) before both catheters were taped in position at the nose. The volume of air in each catheter was checked at regular intervals to ensure that no leaks had occurred.

Each catheter was connected to a very-low range differential pressure transducer (DP45-3, Validyne Engineering, Northridge, USA) that was calibrated immediately before use. Analogue pressure signals were amplified (CD280, Validyne Engineering), digitised (Micro1401-2, CED, Cambridge, UK) and recorded online at 200 Hz (Spike2, v9.00, CED). Transdiaphragmatic pressure (P_{di}) was calculated by online subtraction of P_{oe} from P_{ga}.

Assessment of ventilatory and gas-exchange indices

Pulmonary airflow and gas-exchange were measured breath-by-breath using a metabolic cart with online gas analysis system (Oxycon Pro, Jaeger, Viasys Healthcare, Hoechberg, Germany), comprising a calibrated turbine flow-meter and O_2 and CO_2 gas analysers. Digital signals from the metabolic cart were input into the data acquisition system using an external device (DAQ-30A16, Eagle Technology, Cape Town, South Africa) and recorded online as waveforms. Inspired and expired tidal volumes were calculated offline by numerical integration of flow using a bespoke script (Horseman, 2020a).

Diaphragm ultrasonography

The assessment of crural diaphragm kinetics is outlined in detail in General Methods (section 3.10). Briefly, a low-frequency, curvilinear ultrasound transducer (2.4-5.0 MHz, 3.5C, GE Medical, Horten, Norway) was positioned subcostally on the right mid-clavicular line. Here, the right hemi-diaphragm dome was imaged at the interface of the visceral pleura and air-filled lung. Beam penetration depth was adjusted so that the hyperechoic diaphragm position at RV was always within the field of view (~200-250 mm). In addition, one focal point was set at the diaphragm position at relaxation volume for optimised lateral resolution.

Ultrasound cine-loops were acquired as B-mode ultrasound, and analysed offline as angle-independent AM-mode ultrasound using dedicated software (EchoPac v6.1, GE Medical). The dynamic cursor was visually oriented along the true axis of diaphragm movement (Orde et al., 2016b). Diaphragm excursion and excursion time were measured with a digital calliper tool as the absolute excursion amplitude and the time from onset of excursion (EELV) to peak excursion (EILV). Diaphragm excursion velocity (cm/s) was calculated as the quotient of diaphragm excursion divided by excursion time. Diaphragm power was estimated as the dot product of excursion velocity and the active component of $\overline{P}_{di}$ ($\overline{P}_{di,a}$; see calculation below). Successfully analysed cine-loops were characterised by clear hyperechoic lines that distinctively marked the start and the end of a respiratory cycle.

Data processing and time-matching

Ventilatory indices ($\dot{V}_I$, V_{TI}, f_R, T_I, T_I/T_{TOT}) and intrathoracic pressures (P_{di}, P_{ga}, P_{oe}) were recorded as waveforms on a breath-by-breath basis for offline analysis. The start and finish of each breath was marked at the point of zero flow and anomalous breaths (e.g., swallows, coughs or sighs, and breaths not crossing zero flow) were manually excluded. Ventilatory indices were expressed for inspiration only. Tidal pressures were calculated as the mean inspiratory pressure (i.e., $\overline{P}_{di}$, $\overline{P}_{ga}$ and $\overline{P}_{oe}$). As an example, $\overline{P}_{di}$ was calculated using the equation from Barnard and Levine (1986):

$$\bar{P}_{di} = \Sigma_0^n (P_{di}/n),$$

where baseline P_{di} (0) was the absolute P_{di} at the onset of inspiration and n was equal to the number of data points during inspiration (from the onset of inspiration to end-inspiration). Because this value included both the passive ($\overline{P}_{di,p}$) and active ($\overline{P}_{di,a}$) components of inspiratory pressure, the two components were further distinguished by subtracting the lowest pressure during any given respiratory cycle from the instantaneous $\overline{P}_{di}$. Accordingly, $\overline{P}_{di,a}$ was the mean pressure generated during tidal inspiration based on tidal pressure swings, whereas $\overline{P}_{di,p}$ was the pressure generated passively (e.g., isometric contractions, such as 'bracing' and trunk stabilisation with elevated intraabdominal pressure). End-expiratory oesophageal pressure (EEP_{oe}) was measured at end-expiratory lung volume.

The ultrasound and data acquisition systems were not synchronised, so particular attention was paid to the timing of ultrasound acquisition during hyperpnoea in order that the respiratory cycles within each ultrasound cine-loop could be correctly identified and matched with breath-

by-breath ventilatory and pressure data. Specifically, ultrasound cine-loops were recorded over 15 s every 30 s during hyperpnoea and the three subsequent minutes of recovery (1 × 30 s for rest). Accordingly, all breaths recorded within a 15 s cine-loop (1 × 30 s for rest) were identified in the data acquisition system, then averaged over 15 s (30 s for rest). Since all participants reached a test duration of at least 1.75 min, data up to and including this timepoint (iso-time) were used for further analysis. The final 15 s of hyperpnoea, independent of test duration, was recorded and defined as the peak response.

Rating scales and qualitative descriptors

Immediately after hyperpnoea, participants rated their perceived breathing discomfort; defined as 'the sensation of laboured or difficult breathing' on Borg's category ratio 10 scale (CR10) (Borg, 1998; Cory et al., 2015). The scale was anchored at 0 ('no breathing discomfort') and 10 ('the most severe breathing discomfort ever experienced or imagined'). Participants were also asked to select one or more phrases from a list of 15 qualitative descriptions that best described their breathing sensation during the final 15 s of hyperpnoea (Simon et al., 1990).

After exercise, participants were asked to specify their main reason(s) for exercise termination: 'breathing discomfort', 'leg discomfort', 'a combination of both' or 'other reason(s)'. In addition, participants rated their overall perceived exertion (RPE) on the Borg CR10 scale, anchored from 0 ('no exertion at all') to 10 ('maximal exertion') (Borg, 1998). Leg discomfort was rated using Borg's CR10 scale, anchored at 0 ('no leg discomfort') and 10 ('the most severe leg discomfort ever experienced or imagined').

6.2.6 Statistics

Statistical analyses were performed using dedicated software (SPSS v26.0, IBM Corp., Armonk, NY, US). Normal distribution of data was assessed with the Shapiro-Wilk test. All variables met the assumptions required for parametric statistics (incl. analysis of variance; ANOVA), unless otherwise indicated. Descriptive characteristics for men and women were compared using independent-samples *t*-tests.

Feasibility

Feasibility of ultrasound was expressed as the percentage (min-max range) of successfully analysed cine-loops. For example, a cine-loop with all respiratory cycles successfully analysed, the cine-loop was 100% successfully analysed. However, a cine-loop with only two out of four respiratory cycles successfully analysed, the cine-loop was 50% successfully analysed. Because

the percentages were not normally distributed, non-parametric tests were performed. So, to compare feasibility between the two hyperpnoea conditions (exercise vs. CO_2-rebreathe), a two-tailed Wilcoxon signed-rank test was performed. Spearman's rank correlation coefficient (ρ) was calculated to assess the relationship between the percentage of successfully analysed cine-loops and V_{TI}.

CO_2-rebreathe versus exercise

Ratings of perceived breathing discomfort during exercise and CO_2-rebreathe were compared using paired-samples *t*-test. To determine the differences between CO_2-rebreathe and exercise, ventilatory indices ($\dot{V}_I$, V_{TI}, f_R, T_I, T_I/T_{TOT}), intrathoracic pressures ($\overline{P}_{di}$, $\overline{P}_{ga}$, $\overline{P}_{oe}$, EEP_{oe}, $\overline{P}_{di,a}$, $\overline{P}_{ga,a}$, $\overline{P}_{oe,a}$, $\overline{P}_{di,p}$, $\overline{P}_{ga,p}$, $\overline{P}_{oe,p}$) and diaphragm kinetics (excursion, excursion time, excursion velocity and power) were compared using a two-way (time × hyperpnoea condition) repeated-measures ANOVA with Bonferroni corrections. Sphericity was assessed in all variables using Mauchly's test ($p \geq 0.05$ assumed sphericity). Effect sizes were reported as partial eta squared (η_p^2), and interpreted as poor (≤0.01), medium (0.01-0.14) or large (>0.14) (Lakens, 2013). All statistical tests were performed with absolute values, and alpha level set *a priori* at $p \leq 0.05$. Data are shown as mean ± *SD*, unless otherwise indicated.

6.3 Results

6.3.7 Participant characteristics

Participant characteristics are shown in Table 6.3.1. Expectedly, men were significantly taller and heavier than women, and exhibited greater chest dimensions. Moreover, men measured significantly larger static and dynamic lung volumes and MEP compared to women. Nonetheless, all participants exhibited pulmonary function and maximal pressures within normal limits. Whilst diaphragm thickness was similar for both sexes, diaphragm mobility was significantly lower in women.

Table 6.3.1 Participant characteristics.

	Total (*n* = 10)	**Men (*n* = 5)**	**Women (*n* = 5)**
Anthropometrics			
Age, y	21.3 ± 2.2	22.0 ± 2.4	21.0 ± 2.4
Stature, cm	167 ± 11	175 ± 8	160 ± 9*
Body mass, kg	66.3 ± 11.7	77.5 ± 4.3	57.4 ± 6.3*
BMI, kg/m	23.5 ± 2.6	25.2 ± 3.1	22.3 ± 0.6
Chest circumference, cm	82.9 ± 9.8	91.8 ± 5.3	75.8 ± 5.2*
Chest depth, cm	19.6 ± 2.3	21.2 ± 2.6	18.3 ± 1.0*
Chest width, cm	27.5 ± 2.7	29.5 ± 0.6	25.6 ± 2.6*
Pulmonary function			
TLC, L (% pred)	5.97 ± 1.27 (100 ± 9)	7.11 ± 0.17 (102 ± 17)	5.02 ± 0.96* (96 ± 3)
RV, L (% pred)	1.56 ± 0.36 (118 ± 27)	1.60 ± 0.36 (115 ± 33)	1.41 ± 0.40* (120 ± 25)
FRC_{pleth}, L (% pred)	3.16 ± 0.85 (104 ± 18)	3.72 ± 0.88 (118 ± 24)	2.51 ± 0.54* (91 ± 13)
FVC, L (% pred)	4.71 ± 1.09 (108 ± 6)	5.69 ± 0.23 (107 ± 7)	3.92 ± 0.80* (106 ± 9)
FEV_1, L (% pred)	3.98 ± 0.84 (104 ± 8)	4.69 ± 0.25 (104 ± 8)	3.40 ± 0.68* (104 ± 10)
FEV_1/FVC (%pred)	0.84 ± 0.03 (97 ± 3)	0.82 ± 0.02 (96 ± 3)	0.86 ± 0.02 (98 ± 3)
MVV_{12}, L/min (% pred)	147 ± 23 (94 ± 13)	163 ± 10 (89 ± 10)	134 ± 23* (100 ± 13)
Maximum respiratory pressures			
MIP, cmH_2O (% pred)	–120 ± 25 (111 ± 21)	–132 ± 24 (115 ± 2)	–111 ± 25 (109 ± 20)
MEP, cmH_2O (% pred)	156 ± 38 (121 ± 19)	187 ± 34 (114 ± 23)	134 ± 23* (129 ± 10)
Diaphragm characteristics			
Mobility, cm[a]	6.46 ± 1.05	8.37 ± 1.16	6.11 ± 0.63*
Thickness at FRC, mm	1.3 ± 0.2	1.4 ± 0.1	1.2 ± 0.1
Thickness at TLC, mm	3.9 ± 0.9	4.4 ± 0.4	3.5 ± 0.4
Thickening fraction, %	287 ± 90	337 ± 35	245 ± 42

Data are mean ± *SD* for 10 participants. % pred, percentage of predicted value; BMI, body mass index; TLC, total lung capacity; RV, residual volume; FRC_{pleth}, plethysmography-derived functional residual capacity; FVC, forced vital capacity; FEV_1, forced expiratory volume in 1 s; MVV_{12}. maximal voluntary ventilation in 12 s; MIP, maximum inspiratory mouth pressure; MEP, maximum expiratory mouth pressure. Predicted values for MVV_{12} were calculated as $FEV_1 \times 40$ (Miller et al., 2005). Predicted values for maximum mouth pressures were derived from the equations of Evans & Whitelaw (2009). [a] measured with AM-mode ultrasound; *$p \leq 0.05$ vs. men.

6.3.8 Responses to hyperpnoea

Durations for CO_2-rebreathe and exercise were 3.3 ± 1.1 and 8.4 ± 1.6 min, respectively (p < 0.001). All participants terminated CO_2-rebreathe at the standardised cut-off of 55mmHg (55 ± 0.4 mmHg) without untoward events. Upon test cessation, ratings of breathing discomfort during CO_2-rebreathe and exercise were 4.0 ± 2.0 and 5.5 ± 2.8 (p = 0.016), respectively. Overall RPE at end-exercise was 7.3 ± 1.8, with 70% of participants indicating leg discomfort as the primary reason for exercise termination. The remaining 30% of participants rated a combination of breathing *and* leg discomfort. Ratings of leg discomfort were 7.8 ± 1.9.

Ventilatory and pressure responses

During exercise, participants achieved peak $\dot{V}O_2$ of 2.58 ± 0.18 L/min (38.1 ± 2.7 mL/kg/min). This value was equal to 111 ± 4% of estimated peak $\dot{V}O_2$ for healthy adults. Additional responses at peak exercise were: work rate 172 ± 50 W; $\dot{V}_I$ 66 ± 19 L/min (48 ± 12% of MVV_{12}); RER 1.03 ± 0.06; and $P_{ET}CO_2$ 5.54 ± 0.30 kPa (41.6 ± 2.3 mmHg).

Ventilatory and intrathoracic pressure responses to CO_2-rebreathe and exercise are shown in Table 6.3.2. Expectedly, there was a main effect of time on ventilatory responses during both hyperpnoea conditions: $\dot{V}_I$ (p < 0.001; η_p^2 = 0.860), V_{TI} (p < 0.001; η_p^2 = 0.779), f_R (p < 0.001; η_p^2 = 0.561) and V_{TI}/T_I (p < 0.001; η_p^2 = 0.857). Similarly, there was a main effect of hyperpnoea condition on all ventilatory indices: $\dot{V}_I$ (p = 0.001; η_p^2 = 0.787), V_{TI} (p = 0.040; η_p^2 = 0.401), f_R (p < 0.001; η_p^2 = 0.794) and V_{TI}/T_I (p = 0.003; η_p^2 = 0.744). *Post hoc* analyses showed that the two hyperpnoea conditions elicited similar ventilatory responses from rest to peak, except for V_{TI} which was higher during CO_2-rebreathe compared to exercise at 1.0 and 1.5 min (Figure 6.3.1). Throughout recovery, ventilatory responses were greater during exercise compared to CO_2-rebreathe due to the higher ventilatory demand elicited by peak exercise.

Table 6.3.2 Ventilatory and breathing pattern responses to hyperpnoea.

	Rest	Hyperpnoea				Recovery				
		0.50 – 0.75 min	1.00 – 1.25 min	1.50 – 1.75 min	Peak	0.50 – 0.75 min	1.00 – 1.25 min	1.50 – 1.75 min	2.00 – 2.25 min	2.50 – 2.75 min
CO_2-rebreathe										
$\dot{V}_I$, L/min	9.1 ± 3.9	17.3 ± 5.1	23.9 ± 8.2	27.0 ± 13.5	36.7 ± 12.2*	19.9 ± 7.5*	15.8 ± 5.6*	13.7 ± 6.4*	12.6 ± 5.4*	11.8 ± 8.5*
V_{TI}, L	0.59 ± 0.41	1.00 ± 0.56	1.38 ± 0.85*	1.62 ± 0.90*	1.83 ± 0.85*	1.08 ± 0.36*	0.91 ± 0.47*	0.81 ± 0.51*	0.75 ± 0.47*	0.69 ± 0.54*
f_R, br/min	15.5 ± 4.3	17.5 ± 7.8	17.3 ± 5.6*	17.8 ± 4.7	20.1 ± 4.9*	18.4 ± 4.4*	17.4 ± 5.3*	16.9 ± 5.8*	16.8 ± 6.7*	17.1 ± 7.4*
V_{TI}/T_I, L/s	0.29 ± 0.13	0.50 ± 0.17	0.68 ± 0.28	0.85 ± 0.43	1.15 ± 0.43*	0.73 ± 0.15*	0.53 ± 0.21*	0.45 ± 0.21*	0.40 ± 0.19*	0.40 ± 0.28*
T_I/T_{TOT}	0.46 ± 0.06	0.44 ± 0.04	0.45 ± 0.05	0.47 ± 0.04	0.48 ±0.05	0.47 ± 0.03	0.44 ± 0.06	0.47 ± 0.09	0.48 ± 0.07	0.46 ± 0.07
Exercise										
$\dot{V}_I$, L/min	10.0 ± 4.1	16.5 ± 5.7	20.0 ± 5.5	22.0 ± 4.5	66.8 ± 18.9	54.6 ± 23.2	46.5 ± 17.3	37.3 ± 13.5	28.3 ± 9.6	25.6 ± 7.7
V_{TI}, L	0.60 ± 0.26	0.87 ± 0.44	0.95 ± 0.78	1.10 ± 0.69	2.51 ± 0.92	2.26 ± 0.92	1.92 ± 0.93	1.57 ± 0.71	1.30 ± 0.66	1.18 ± 0.49
f_R, br/min	16.7 ± 3.7	18.6 ± 4.1	20.5 ± 3.5	20.0 ± 3.5	29.5 ± 6.4	24.2 ± 4.2	24.2 ± 7.5	23.8 ± 7.8	21.8 ± 6.9	21.7 ± 6.1
V_{TI}/T_i, L/s	0.39 ± 0.16	0.60 ± 0.22	0.61 ± 0.24	0.71 ± 0.15	2.53 ± 0.74	1.78 ± 0.95	0.71 ± 0.62	1.39 ± 0.43	1.02 ± 0.39	0.95 ± 0.25
T_I/T_{TOT}	0.41 ± 0.01	0.42 ± 0.03	0.41 ± 0.01	0.40 ± 0.03	0.47 ± 0.02	0.45 ± 0.02	0.44 ± 0.03	0.43 ± 0.04	0.42 ± 0.05	0.41 ± 0.03

Data are mean ± *SD* for 10 participants. $\dot{V}_I$, inspiratory minute ventilation; V_{TI}, inspiratory tidal volume; f_R, respiratory frequency; V_{TI}/T_I, mean inspiratory flow; T_I/T_{TOT}, inspiratory duty cycle. Peak is the final 15 s before test cessation, regardless of timepoint. *$p \leq 0.05$ vs. exercise at same timepoint.

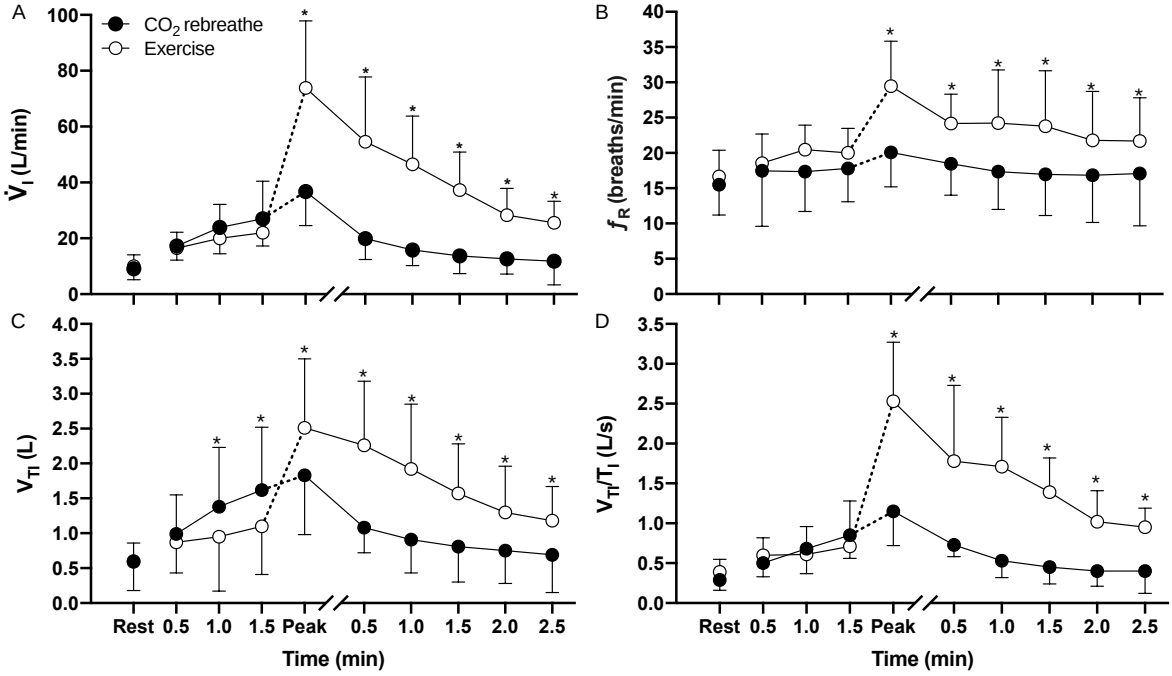

Figure 6.3.1 Ventilatory responses to CO_2-rebreathe (●) and exercise (○). Broken *x*-axis indicates the transition from hyperpnoea to recovery. *Peak* is the final 15 s before test cessation, regardless of timepoint. Data are mean ± *SD* for 10 participants. *$p \leq 0.05$ at same timepoint.

There was also an effect of time on $\overline{P}_{di}$, $\overline{P}_{oe}$ and $\overline{P}_{ga}$ (all $p < 0.001$; Table 6.3.3). The EEP_{oe} remained unchanged from rest throughout both conditions ($p = 0.157$; $\eta_p^2 = 0.567$). For $\overline{P}_{di}$, resting values were similar for both conditions ($p = 0.372$), but from 0.5 min through to the first minute of recovery, exercise elicited greater $\overline{P}_{di}$ responses compared to CO_2-rebreathe (Figure 6.3.2A). Upon evaluating the active and passive components of inspiratory pressure, however, it was evident that the difference in $\overline{P}_{di}$ between conditions was attributed only to the passive component (e.g., 'bracing' and stabilisation of the trunk for postural support through isometric diaphragm contraction), because $\overline{P}_{di,p}$ was greater during exercise compared to CO_2-rebreathe at rest ($p = 0.034$) and through to the first minute of recovery (all $p < 0.05$; Figure 6.3.3). By contrast, the active pressure components ($\overline{P}_{di,a}$, $\overline{P}_{oe,a}$ and $\overline{P}_{ga,a}$; i.e., tidal pressure swings) were similar between the two conditions from rest through to peak (Table 6.3.3). For $\overline{P}_{ga}$ specifically, there was a main effect of condition ($p = 0.026$; $\eta_p^2 = 0.532$) and an interaction effect of time and condition ($p = 0.015$; $\eta_p^2 = 0.303$). *Post hoc* tests showed that resting values differed between the two conditions and, upon exercise initiation, a steep increase was elicited during the initial minutes of hyperpnoea before returning to resting baseline values at peak and throughout recovery (Figure 6.3.2B).

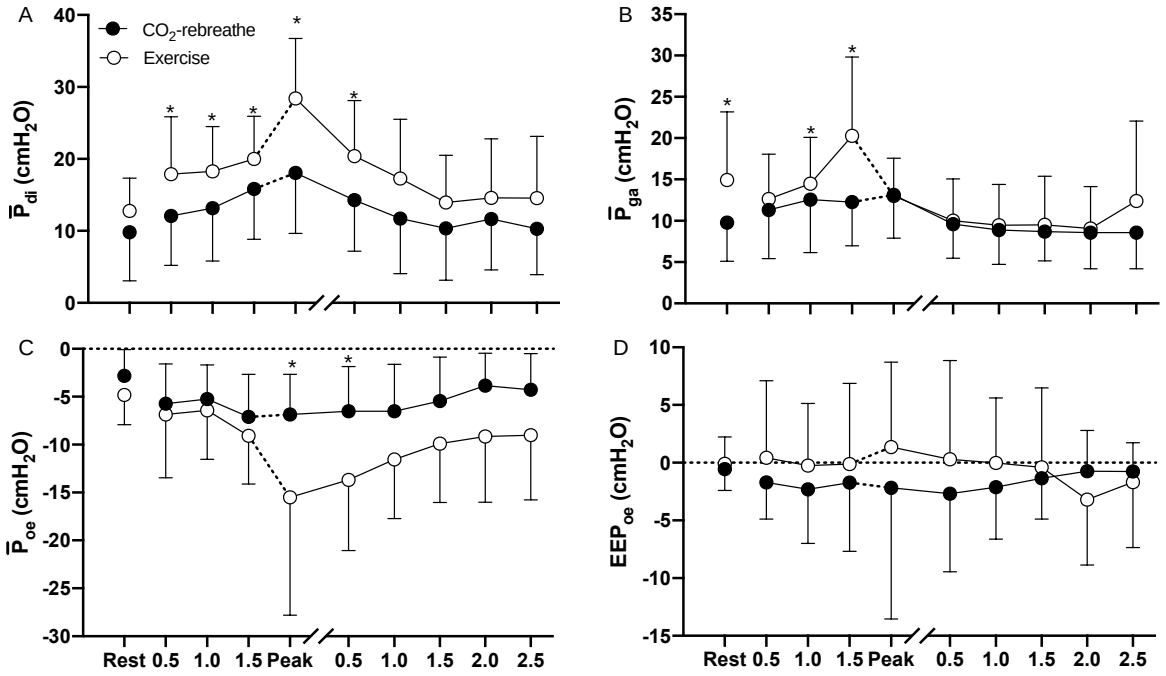

Figure 6.3.2 Intrathoracic pressure responses to CO_2-rebreathe (●) and exercise (○). Broken *x*-axis is the transition between hyperpnoea and recovery. Data are mean ± *SD* for 10 participants. *$p \leq 0.05$ at same timepoint.

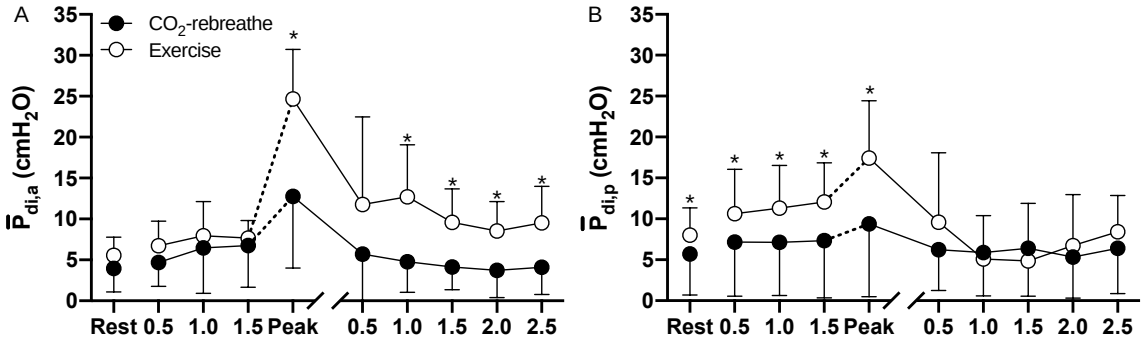

Figure 6.3.3 Active (*A*, $\bar{P}_{di,a}$) and passive (*B*, $\bar{P}_{di,p}$) mean inspiratory transdiaphragmatic pressure in response to CO_2-rebreathe (●) and exercise (○). Broken *x*-axis is the transition between hyperpnoea and recovery. Data are mean ± *SD* for 10 participants. *$p \leq 0.05$ at same timepoint.

Table 6.3.3 Intrathoracic pressure responses to hyperpnoea.

	Rest	Hyperpnoea				Recovery				
		0.50 – 0.75 min	1.00 – 1.25 min	1.50 – 1.75 min	Peak	0.50 – 0.75 min	1.00 – 1.25 min	1.50 – 1.75 min	2.00 – 2.25 min	2.50 – 2.75 min
CO_2-rebreathe										
$\overline{P}_{di}$, cmH_2O	11.1 ± 4.5	15.3 ± 7.2*	10.9 ± 17.5	17.6 ± 8.9*	18.9 ± 9.3*	13.8 ± 5.8*	12.7 ± 6.5	11.2 ± 6.3	11.7 ± 5.9	11.6 ± 4.9
$\overline{P}_{ga}$, cmH_2O	9.8 ± 4.7*	11.3 ± 5.9	12.5 ± 6.4*	12.2 ± 5.3*	13.1 ± 5.2	9.6 ± 4.1	8.9 ± 4.1	8.7 ± 3.6	8.6 ± 4.4	8.6 ± 3.8
$\overline{P}_{oe}$, cmH_2O	–2.8 ± 2.7	–5.7 ± 4.1	–5.2 ± 3.6	–7.1 ± 4.4	–6.8 ± 4.2*	–6.5 ± 4.7*	–6.5 ± 4.9	–5.5 ± 4.6	–3.8 ± 3.4	–4.3 ± 3.8
EEP_{oe}, cmH_2O	0.4 ± 2.2	–2.8 ± 3.3	–3.6 ± 4.7	–3.7 ± 6.5	–7.3 ± 10.4	–4.9 ± 6.2	–3.9 ± 4.0	–2.3 ± 3.9	–1.9 ± 3.8	–1.2 ± 3.0
$\overline{P}_{di,a}$, cmH_2O	3.9 ± 2.9	4.7 ± 2.9	6.5 ± 5.5	6.8 ± 5.1	12.8 ± 8.8*	5.7 ± 5.8	4.8 ± 3.7*	4.1 ± 2.3*	3.7 ± 3.3*	4.1 ± 3.3*
$\overline{P}_{ga,a}$, cmH_2O	2.4 ± 2.0	2.7 ± 1.7	3.0 ± 2.6	3.2 ± 1.5	11.9 ± 4.7*	2.8 ± 1.7	1.9 ± 2.2	2.4 ± 1.6	2.0 ± 1.6	2.0 ± 1.6*
$\overline{P}_{oe,a}$, cmH_2O	–1.6 ± 2.0	–2.2 ± 2.4	–4.1 ± 4.8	–5.0 ± 5.4	–8.9 ± 7.3*	–2.5 ± 6.3	–3.5 ± 3.9*	–1.8 ± 2.5	–2.0 ± 3.2	–2.2 ± 3.5*
Exercise										
$\overline{P}_{di}$, cmH_2O	13.1 ± 4.7	20.8 ± 10.3	16.0 ± 7.4	20.0 ± 7.7	32.6 ± 14.9	22.1 ± 12.2	18.2 ± 11.7	15.4 ± 12.7	17.1 ± 10.8	14.8 ± 10.2
$\overline{P}_{ga}$, cmH_2O	14.9 ± 8.2	12.6 ± 5.4	14.5 ± 5.6	20.3 ± 9.5	12.9 ± 4.6	10.0 ± 5.1	9.5 ± 5.0	9.5 ± 5.9	9.0 ± 5.1	12.3 ± 9.7
$\overline{P}_{oe}$, cmH_2O	–4.8 ± 3.1	–6.9 ± 6.6	–6.4 ± 5.1	–9.1 ± 5.0	–15.5 ± 12.3	–13.7 ± 7.4	–11.6 ± 6.2	–9.9 ± 6.2	–9.1 ± 6.9	–9.0 ± 6.8
EEP_{oe}, cmH_2O	–0.3 ± 2.8	–1.8 ± 6.1	–2.5 ± 4.4	–3.2 ± 5.1	–1.1 ± 7.8	–4.0 ± 8.1	–3.4 ± 4.8	–4.3 ± 5.4	–4.8 ± 6.0	–4.5 ± 5.1
$\overline{P}_{di,a}$, cmH_2O	5.6 ± 2.2	6.7 ± 3.0	7.9 ± 4.2	7.6 ± 2.2	24.7 ± 6.1	11.8 ± 11.1	12.7 ± 6.3	9.6 ± 4.1	8.5 ± 3.6	9.5 ± 4.5
$\overline{P}_{ga,a}$, cmH_2O	2.5 ± 1.4	2.5 ± 1.2	2.6 ± 1.5	2.5 ± 1.6	15.2 ± 6.0	3.2 ± 2.2	2.3 ± 1.4	4.5 ± 3.4	3.6 ± 2.1	3.6 ± 2.4
$\overline{P}_{oe,a}$, cmH_2O	–3.1 ± 1.4	–4.2 ± 3.3	–5.4 ± 3.5	–5.2 ± 1.3	–21.2 ± 8.9	–8.6 ± 12.0	–10.4 ± 5.7	–5.1 ± 5.4	–4.9 ± 2.4	–9.1 ± 7.1

Data are mean ± *SD* for 10 participants.$\overline{P}_{di}$, mean inspiratory transdiaphragmatic pressure; $\overline{P}_{ga}$, mean inspiratory gastric pressure; $\overline{P}_{oe}$, mean inspiratory oesophageal pressure; EEP_{oe}, end-expiratory oesophageal pressure; $\overline{P}_{di,a}$, active component of mean inspiratory transdiaphragmatic pressure; $\overline{P}_{ga,a}$, active component of mean inspiratory gastric pressure; $\overline{P}_{oe,a}$, active component of mean inspiratory oesophageal pressure. Peak is the final 15 s before test cessation, regardless of timepoint. *$p \leq 0.05$ vs. exercise at same timepoint.

Diaphragm kinetic responses to hyperpnoea

A total of 140 and 228 ultrasound cine-loops were obtained during CO_2-rebreathe and exercise, respectively. Of these cine-loops, 138 (99%) and 211 (93%) were technically acceptable (i.e., with acceptable image quality and without excessive movement artefacts). Of the technically acceptable cine-loops, the median (min-max range) successfully analysed cine-loops was 100% (96 – 100%) and 90% (70 – 100%) for CO_2-rebreathe and exercise, respectively (p = 0.004). Despite slightly lower feasibility during exercise, the percentage of successfully analysed cine-loops did not fall below 70%, meaning that there were always ≥2 successfully analysed breaths for each participant at each timepoint during both conditions.

To evaluate the influence of tidal volume (associated with rib cage expansion) on ultrasound feasibility, the percentage of successfully analysed cine-loops was plotted against V_{TI} (Figure 6.3.4). During CO_2-rebreathe, V_{TI} ranged from 0.29 at rest to 3.21 L at peak. As evidenced by the positive relationship between the percentage of analysed cine-loops and V_{TI}, feasibility was not adversely affected by increasing V_{TI} within the given range (ρ = 0.281; p = 0.006; Figure 6.3.4A). During exercise, V_{TI} ranged from 0.53 at rest to 4.54 L at peak. Although the percentage of successfully analysed cine-loops was more variable during exercise compared to CO_2-rebreathe, increasing V_{TI} did not appear to adversely affect feasibility of ultrasound acquisition during exercise within the given range (ρ = 0.150; p = 0.029).

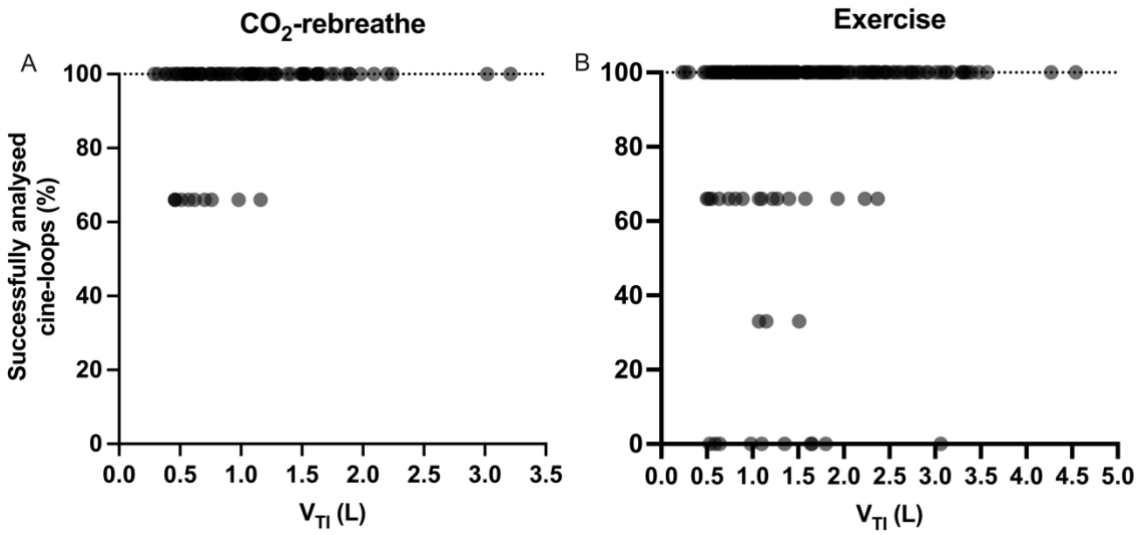

Figure 6.3.4 Percentage of successfully analysed cine-loops plotted against V_{TI} during CO_2-rebreathe and exercise. A total of 138 and 211 cine-loops were included for CO_2-rebreathe and exercise, respectively.

There was a main effect of time on the ultrasound-derived measures of diaphragm excursion, excursion time, excursion velocity and power during hyperpnoea (all $p < 0.001$). Moreover, there was a main effect of hyperpnoea condition on diaphragm excursion ($p = 0.009$; $\eta_p^2 = 0.692$), excursion time ($p = 0.022$; $\eta_p^2 = 0.663$), excursion velocity ($p < 0.001$; $\eta_p^2 = 0.965$) and for diaphragm power ($p = 0.003$; $\eta_p^2 = 0.632$). At rest, diaphragm excursion measured 1.90 ± 0.40 cm and 1.81 ± 0.61 cm prior to CO_2-rebreathe and exercise, respectively, and did not differ between conditions ($p = 0.781$). From rest to peak CO_2-rebreathe, excursion increased to 4.17 ± 0.81 cm, which was equivalent to 56 ± 12% of maximal diaphragm mobility (see Table 6.3.1). At peak exercise, diaphragm excursion was 5.91 ± 1.09 cm, which was equivalent to 78 ± 15% of maximal diaphragm mobility. From the onset of hyperpnoea to iso-time (1.5-1.75 min), CO_2-rebreathe elicited significantly greater diaphragm excursion relative to exercise (Figure 6.3.5A), meaning that the diaphragm moved less during exercise compared to CO_2-rebreathe at sub-peak ventilatory loads. Resting diaphragm power was 5.9 ± 4.8 $cmH_2O/cm/s$ and 6.6 ± 3.1 $cmH_2O/cm/s$ prior to CO_2-rebreathe and exercise, respectively, and did not differ between conditions ($p = 0.799$). From rest to peak CO_2-rebreathe, diaphragm power increased more than fourfold (429 ± 87%; $p = 0.047$; Figure 6.3.5D). From rest of peak exercise, the relative increase in diaphragm power was almost fifteen-fold (1416 ± 326%; $p = 0.002$).

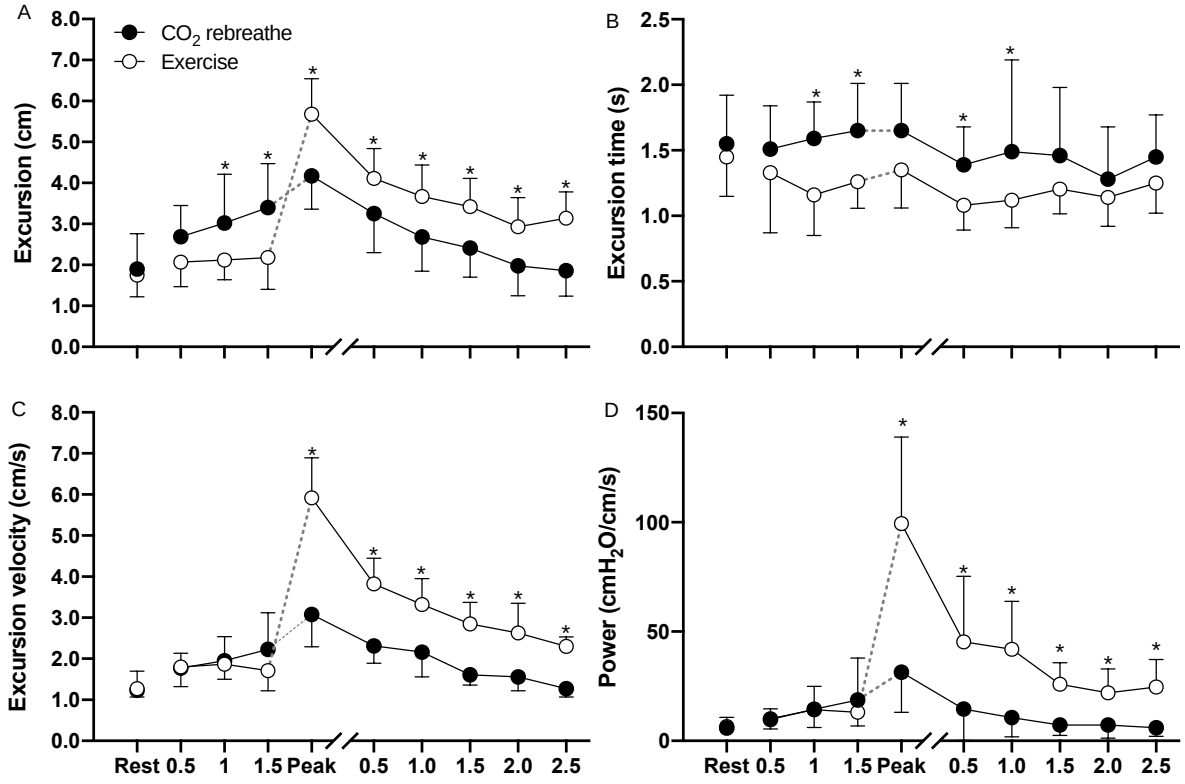

Figure 6.3.5 Ultrasound-derived kinetics in response to CO_2-rebreathe (●) and exercise (○). Broken x-axis is the transition between hyperpnoea and recovery. Data are mean ± *SD* for 10 participants. *$p \leq 0.05$ at same timepoint.

Table 6.3.4 Diaphragm kinetic responses to hyperpnoea.

	Rest	Hyperpnoea				Recovery				
		0.50 – 0.75 min	1.00 – 1.25 min	1.50 – 1.75 min	Peak	0.50 – 0.75 min	1.00 – 1.25 min	1.50 – 1.75 min	2.00 – 2.25 min	2.50 – 2.75 min
CO_2-rebreathe										
Excursion, cm	1.90 ± 0.90	2.69 ± 0.77*	3.03 ± 1.19*	3.41 ± 1.07*	4.17 ± 0.81*	3.25 ± 0.96*	2.68 ± 0.84*	2.42 ± 0.71*	1.99 ± 0.74*	1.86 ± 0.63*
Excursion time, s	1.55 ± 0.42	1.51 ± 0.33	1.55 ± 0.36*	1.60 ± 0.28*	1.65 ± 0.36	1.40 ± 0.29*	1.27 ± 0.23	1.53 ± 0.53	1.28 ± 0.40	1.45 ± 0.32*
Excursion velocity, cm/s	1.24 ± 0.35	1.78 ± 0.37	1.95 ± 0.63	2.23 ± 0.95	3.08 ± 0.79*	2.31 ± 0.34*	2.03 ± 0.40	1.60 ± 0.26	1.56 ± 0.35	1.27 ± 0.22
Power, cmH_2O/cm/s	5.9 ± 4.8	9.8 ± 4.3	14.5 ± 10.5	18.7 ± 16.1	31.4 ± 18.3*	14.6 ± 14.5*	10.7 ± 8.8*	7.3 ± 4.8*	7.2 ± 5.9*	6.0 ± 3.9*
Exercise										
Excursion, cm	1.81 ± 0.61	2.21 ± 0.79	2.37 ± 0.89	2.47 ± 1.16	5.91 ± 1.09	4.31 ± 0.93	3.79 ± 0.81	3.53 ± 0.73	3.04 ± 0.76	3.17 ± 0.61
Excursion time, s	1.47 ± 0.40	1.34 ± 0.41	1.34 ± 0.70	1.47 ± 0.67	1.44 ± 0.40	1.12 ± 0.22	1.15 ± 0.22	1.29 ± 0.33	1.20 ± 0.27	1.26 ± 0.22
Excursion velocity, cm/s	1.23 ± 0.19	1.66 ± 0.27	1.88 ± 0.38	1.70 ± 0.33	5.88 ± 0.92	3.85 ± 0.68	3.33 ± 0.72	2.79 ± 0.57	2.61 ± 0.68	2.48 ± 0.60
Power, cmH_2O/cm/s	6.6 ± 3.1	10.1 ± 4.5	14.3 ± 8.2	14.0 ± 6.3	99.5 ± 39.5	45.3 ± 41.9	41.9 ± 21.9	25.9 ± 9.8	21.9 ± 10.9	24.7 ± 12.5

Data are mean ± *SD* for 10 participants. Peak is the final 15 s before test cessation, regardless of timepoint. *$p \leq 0.05$ vs. exercise at same timepoint.

6.4 Discussion

The aims of this study were to evaluate the feasibility of subcostal ultrasonography for the assessment of diaphragm kinetics during reflexively-driven hyperpnoea (CO_2-rebreathe and exercise), and to compare diaphragm kinetics across the two conditions of hyperpnoea in order to elucidate the mechanisms that underpin postural-ventilatory modulation of the diaphragm. The main findings were that *i*) subcostal diaphragm ultrasonography was feasible during reflexively-driven hyperpnoea, regardless of hyperpnoea condition, tidal volume and motion artefacts elicited by limb movement; and *ii)* at similar levels of ventilation, the diaphragm generated higher pressure during exercise-induced compared to non-exercise-induced hyperpnoea, despite moving significantly less. This latter finding suggests that the diaphragm is constrained during exercise due to the quasi-isometric contractions required for the modulation of postural and ventilatory tasks.

6.4.9 Feasibility of subcostal diaphragm ultrasonography

In line with the original hypothesis, the results showed that diaphragm excursion and excursion time can be quantified using AM-mode ultrasound during non-exercise-induced and exercise-induced hyperpnoea. This being said, the established method for assessing diaphragm excursion is by conventional M-mode ultrasound, during which the B-mode cursor is vertically positioned and static. In Chapter 5, it was argued that M-mode does not capture accurately the full excursion of the hemi-diaphragm apex because rarely is the ultrasonographic diaphragm movement craniocaudal (vertical) but rather diagonal. AM-mode may, therefore, be the superior imaging modality, allowing the operator to orient the dynamic scan line along the true axis of the diaphragm excursion. Consequently, AM-mode reduces orientation and translation errors and may, therefore offer a more accurate measure of diaphragm kinetics relative to conventional M-mode (Orde et al., 2016b).

It is worth noting, however, that the dynamic AM-mode cursor must still be manually adjusted along the axis of diaphragm excursion; that is, an adjustment based on visual (and subjective) evaluation by the operator. One may therefore be left with measurement bias and poor inter- and intra-rater reliability if guidelines are not established and followed for accurate cursor positioning. As there are currently no established guidelines for cursor orientation for AM-mode assessment of diaphragm excursion, the recommendation of Orde et al. (2016b) was followed in this study, with the cursor "rotated and placed on the exact axis of diaphragm displacement" (p. 2616), which was similar to the procedure followed in Chapter 5. This

procedure also included playing the cine-loops multiple times for optimal cursor positioning so that hemi-diaphragm excursion at the apex of the dome could be imaged throughout each breath.

Influence of V_{TI} on feasibility of diaphragm ultrasound

Because the ultrasound transducer was positioned subcostally and held firmly against the lower ribs, it was expected that the acquisition and subsequent analysis of cine-loops would be less feasible at higher ranges of V_{TI} compared to acquisition at rest. Although we addressed a similar question in Chapter 6, the present study took into consideration the larger V_{TI} elicited by exercise-induced hyperpnoea (range 0.53 – 4.54 L *vs*. 0.29 – 3.21 L during CO_2-rebreathe), as well as the hip and leg movement elicited by semi-recumbent cycling. In contrast to the original hypothesis, however, the percentage of successfully analysed cine-loops was only negligibly affected by limb movement, and was similarly not adversely affected by increasing V_{TI} (Figure 6.3.4). If anything, feasibility was instead poorer at the lower ranges of V_{TI} and persistently high at larger tidal volumes, regardless of hyperpnoea condition.

As rib cage distortion is negligible at rest, and is considered to be minimal up to 70% of maximal workload (Aliverti et al., 1997), it is reasonable to assume that the poorer feasibility at lower tidal volumes was not caused by motion artefact or rib cage distortion. Instead, breathing at rest (and to some extent towards the end of recovery) is under conscious, volitional control, with the implication that volitional respiratory adjustments may interfere with central respiratory drive to breathe (Butler, 2007). Indeed, visual inspection of each cine-loop and breath-by-breath data at rest and during recovery showed that diaphragm kinetic behaviour changed within some ultrasound-derived cine-loops. These changes in kinetic behaviour were primarily caused by breath-holds, sighs and gasps as participants transitioned from rest to hyperpnoea and from hyperpnoea to rest (recovery). Although the majority of anomalous breaths were manually excluded from the analysis, they may still have negatively affected the ultrasound resolution and image quality of the subsequent breaths within the cine-loop.

6.4.10 Diaphragm kinetics during hyperpnoea

The second aim of this study was to compare diaphragm kinetics during two modes of reflexively-driven hyperpnoea (exercise-induced and non-exercise-induced), with the objective to elucidate the mechanisms that underpin postural-ventilatory modulation of the diaphragm. For similar levels of ventilation, the diaphragm generated higher force ($\overline{P}_{di}$), but moved significantly less, during exercise compared to CO_2-rebreathe (Figure 6.3.1 and Figure 6.3.5).

When partitioning the active and passive components of inspiratory pressures, it became evident that the difference in $\overline{P}_{di}$ between conditions was due only to the passive component ($\overline{P}_{di,p}$) being elevated during exercise, as the active component ($\overline{P}_{di,a}$) was similar between the two conditions. Whereas the active pressure component is primarily determined by the tidal pressure swing, the passive pressure component is determined by the amount of 'bracing' needed for postural support and trunk stabilisation; that is, the isometric (tonic) activity of the diaphragm and other thoracic muscles (e.g., transverse abdominis) that passively elevate intraabdominal pressure (i.e., $\overline{P}_{ga}$) (Hodges & Gandevia, 2000b). Accordingly, the diaphragm appears to adopt a quasi-isometric contractile pattern when modulation of ventilatory and postural tasks is necessary. This is in line with the early work of Hodges & Gandevia (2000b, 2000a), suggesting that the neural input to the diaphragm at the phrenic motoneurons during concurrent limb movement is the summation of ventilatory *and* postural inputs. Summation of ventilatory and postural inputs would cause the diaphragm to be 'tonically' active (for postural support), with phasic modulation for diaphragm contraction, descent and inspiration (Hodges & Gandevia, 2000b, 2000a).

The findings of Hodges & Gandevia (2000a, 2000b) were later expanded by the same group when postural tasks were imposed during hyperpnoea (Hodges et al., 2001). Under this condition, the group demonstrated that postural input at the phrenic motoneurons was reduced – or 'occluded' – when ventilatory demand increased. Nonetheless, the present results suggest that the opposite may also be true. That is, that diaphragm kinetic behaviour during hyperpnoea is reduced (constrained) when postural demand increases, as the quasi-isometric contractile pattern constrains the range over which the diaphragm can move upon contraction. In turn, this manifests in the breathing pattern whereby V_{TI} is reduced and f_R increased to sustain ventilatory demand when postural tasks are imposed on hyperpnoea, as well as the elevation of $\overline{P}_{ga}$ and $P_{di,p}$ necessary for postural support and trunk stabilisation (Figure 6.3.2 and Figure 6.3.3).

6.4.11 Diaphragm power during hyperpnoea

To help better understand diaphragm contractile and kinetic responses to hyperpnoea, *in vivo*, diaphragm power was calculated as the dot product of $\overline{P}_{di,a}$ and diaphragm excursion velocity. However, this calculation involves several assumptions. First, it assumes that the left and right hemi-diaphragms contract synergistically and descend with similar magnitude during quiet breathing, and that this uniformity continues in the face of increasing ventilatory load. Studies of canine diaphragm suggest that the two hemi-diaphragms contract synergistically at rest and when contractile intensity ($\Delta P_{di,tw}$) increases (De Troyer et al., 2003; De Troyer & Boriek,

2011), although there is no evidence that this is the case also during hyperpnoea. It is, however, well-established that the magnitude of diaphragm excursion is dissimilar between the two hemi-diaphragm domes due to the anatomical position of the myocardium, constraining diaphragm excursion on the left side (Ferrari et al., 2018). Moreover, due to the small acoustic window of the spleen on the left side, making subcostal ultrasonography more difficult (Boussuges et al., 2009), only the kinetic behaviour of the right hemi-diaphragm could be measured in the present study.

The second assumption is that the crural region of the diaphragm has the principal role in pressure- and inspiratory flow generation during hyperpnoea. Generally, it is believed that the crural and costal segments have distinct roles: whereas the costal segment acts with an appositional force on the lower rib cage for inspiratory expansion (De Troyer et al., 1982; De Troyer & Boriek, 2011; Farkas & Rochester, 1988), the crural segment is thought to have a more important role in gastro-oesophageal functions such as retching and vomiting and a significant role as a barrier during gastro-oesophageal reflux (Menezes & Herbella, 2017; Miller, 1990). Moreover, analyses of intra-breath profiles during hypercapnia have shown that EMG activity of crural diaphragm precedes that of the costal diaphragm during inspiration under hypoxic and hypercapnic conditions (Easton et al., 1993, 1995), and that the costal diaphragm is fully shortened earlier in the inspiration compared to the crural diaphragm (Easton et al., 1993, 1995). However, when comparing the mean shortening of both costal and crural segments during the course of an entire hypercapnic rebreathe trial, Fitting et al. (1985) concluded that there was no significant difference in fibre shortening, shortening velocity or EMG activity between the two diaphragm segments. Thus, we are confident that the ultrasound assessment of crural diaphragm kinetics, and subsequent estimation of power, is a good representation of crural diaphragm function during reflexively-driven hyperpnoea.

6.4.12 Conclusions

Diaphragm kinetics – in the form of excursion, excursion velocity and power – can be readily quantified during exercise-induced and non-exercise-induced hyperpnoea. In addition to facilitating a high percentage of successfully analysed cine-loops, AM-mode ultrasound has a dynamic cursor that can be accurately positioned to follow the apex of the hemi-diaphragm dome in the face of non-vertical movement. This feature may be of particular importance for ultrasound acquisition during hyperpnoea in order to overcome movement artefacts and large tidal volumes. For similar levels of ventilation, the diaphragm generated higher pressure but moved significantly less during exercise-induced hyperpnoea compared to non-exercise-

induced hyperpnoea. This finding suggests that diaphragm kinetic responses may be constrained during exercise-induced hyperpnoea due to the quasi-isometric contractile pattern required for postural-ventilatory modulation, whereby the diaphragm must be tonically active for postural support with phasic contractions to meet ventilatory demand.

Chapter 7

Application of Subcostal Ultrasonography for the Assessment of Pressure-Flow Specificity of Diaphragm Fatigue in Healthy Men

7.1 Introduction

Skeletal muscle fatigue is defined as the loss of force, shortening velocity and/or power of a muscle resulting from muscle activity under load (Respiratory Muscle Fatigue Workshop Group, 1990). In contrast to muscle weakness, for which the contractile properties of a rested muscle are impaired, fatigue is the acute reduction in the ability to perform a motor task that is reversible by rest. The underlying mechanisms of fatigue are diverse, ranging from central to peripheral mechanisms (Sundberg & Fitts, 2019). The exact mechanism(s) that cause fatigue, however, are dictated by the specific details of the task performed. These details include the type of contraction (isometric, eccentric or concentric), external load, shortening velocity and duration of the contractions. This specificity of fatigue is also referred to as *fatigue task-dependency*.

More specifically, studies of isolated muscle preparations show that fatigue by *high force-low velocity* contractions primarily impair the maximum force in the force-velocity spectrum (Enoka, 1995). The loss of maximum force typically occurs via a reduction in the number of active cross-bridges secondary to intra-cellular accumulation of inorganic phosphate and altered Ca^{2+} release and reuptake from sarcoplasmic reticulum (Allen et al., 2008; Jones, 2010; Westerblad et al., 1998). Conversely, fatigue by *low force-high velocity* contractions primarily impairs maximum shortening velocity by impairing ATPase activity and increasing cross-bridge attachment times secondary to the accumulation of intra-cellular ADP and H^+ (Cooke et al., 1988). Fatigue task-dependency of mammalian diaphragm has been repeatedly demonstrated *in vitro* (e.g., Ameredes et al., 2006; Coirault et al., 1995, 1997), although little is known about fatigue task-dependency of human diaphragm *in vivo*.

Fatigue of the human diaphragm has traditionally been identified as a decline in the quasi-isometric, stimulation-evoked $P_{di,tw}$ (Johnson et al., 1993). Moreover, attempts have been made to quantify the effect of diaphragm fatigue on ventilatory responses, CO_2 sensitivity and breathing pattern during hypercapnic hyperpnoea (Gallagher et al., 1985; Yan, Lichros, et al., 1993), during which the muscle contracts dynamically under the reflexively-driven stimulation of central chemoreceptors. Nevertheless, fatigue-induced changes in dynamic diaphragm contractile properties have been insufficiently explored, most likely due to the anatomic location of the muscle, the complexity of its function and the need for technological advancements. The overarching aim of this study, therefore, was to evaluate the usefulness of

diaphragm ultrasonography for the assessment of dynamic contractile properties (i.e., kinetics) to better understand the effect external loading and fatigue on these contractile properties.

There is only one former study in which ultrasonography has been used to evaluate the effect of external loading and fatigue on diaphragm contractile properties. In a pioneering study, Kocis et al. (1997) quantified dynamic contractile properties of piglet diaphragm in the form of excursion velocity by using conventional M-mode ultrasound during hypercapnic hyperpnoea. After induction of diaphragm fatigue by electrical stimulation, the authors showed that the loss of force (P_{di}; ~25%) was accompanied by an even greater loss of diaphragm excursion velocity (~39%). These findings emphasised the importance of understanding also the contractile velocity of the human diaphragm beyond force (pressure) as well as the occurrence of fatigue task-dependency of the human diaphragm. Afterall, even small-to-moderate decrements in force and/or shortening velocity would have a substantial effect on diaphragm power (power = force × velocity), and may even influence negatively breathing pattern and perception of dyspnoea during exercise (Romer & Polkey, 2008).

In Chapter 4, it was established that diaphragm excursion velocity can be quantified in healthy humans using AM-mode ultrasound in response to stimulation-evoked twitch contractions with good-to-excellent within-day reliability. Similarly, in Chapter 5, it was established that diaphragm excursion velocity can also be quantified during the dynamic contractions elicited by hypercapnic hyperpnoea with good-to-excellent reliability. Due to these recent methodological and technological advances, both sides of the force-velocity spectrum can now be readily quantified for the human diaphragm *in vivo*. These advances now allow for greater understanding of the task-dependency of diaphragm muscle fatigue.

7.1.1 Aim and hypotheses

The aim of this study was to assess the effects of two external loading tasks (pressure- and flow-loading) on diaphragm kinetics and force in order to elucidate the mechanisms that underpin task-dependency of human diaphragm fatigue. In line with our current understanding of fatigue task-dependency, it was hypothesised that a *low force-high velocity* task would primarily impair diaphragm contractile (excursion) velocity with negligible effect on diaphragm force. Conversely, a *high force-low velocity* task would primarily impair diaphragm force, with negligible effect on diaphragm contractile (excursion) velocity.

7.2 Methods

7.2.2 Ethical approval and participants

This study was approved by the Brunel University Research Ethics Committee (Appendix 1), and conformed to the most recent standards set by the Declaration of Helsinki (World Medical Association, 2013). Eight healthy, non-smoking men between the ages of 18 and 40 y from university student population and surrounding area volunteered to participate. Only participants of (self-reported) male sex were included in this study due to the limited resources and time available to include female participants and to control for menstrual cycle phase in multi-visit studies (see Section 3.3 for additional details). All participants reported to have no medical history of cardiovascular, respiratory or neuromuscular disease using a standardised health questionnaire (Appendix 2). Exclusion criteria were BMI ≥30 kg/m^2 and pulmonary function and maximal respiratory mouth pressures outside age-specific limits of normal (Evans & Whitelaw, 2009; Quanjer et al., 2012; Stocks & Quanjer, 1995). Written informed consent was provided prior to the study (Appendix 2), and participants were asked to abstain from vigorous exercise for ≥24 h, caffeine and alcohol for ≥12 h, and food for ≥3 h prior to each visit.

7.2.3 Experimental overview

Participants visited the laboratory on three occasions, each separated by no less than 48 h and no more than 14 d. The first visit was for screening and familiarisation, during which participants performed pulmonary function tests and were thoroughly familiarised with the experimental set-up. The subsequent two visits were experimental trials, and involved *i*) a low force-high velocity task in the form of voluntary isocapnic hyperpnoea (VIH), or *ii*) a high force-low velocity task in the form of inspiratory resistive loading (IRL). The two trials were performed in randomised order and at the same time of day. Diaphragm contractile properties were assessed before (PRE) and at 10 and 30 min after the loading tasks ($POST_{10}$ and $POST_{30}$, respectively) via transdiaphragmatic pressure (P_{di}), diaphragm electromyogram (EMG_{di}) and ultrasound-derived kinetic responses to phrenic nerve stimulation, maximal sniffs and hypercapnic hyperpnoea.

7.2.4 Screening and familiarisation

Screening was performed as described in Chapter 4 (section 4.2.4). Specific familiarisation for experimental trials included a thorough familiarisation with bilateral phrenic nerve stimulation and the CO_2-rebreathe test. For CO_2-rebreathe specifically, familiarisation included verbal instructions followed by a practice rebreathe test. Moreover, participants received verbal

instructions from the investigator on how to perform the external loading tasks, followed by shortened practice trials of each task, comprising 1 min of VIH and 5 min of IRL (see details below).

7.2.5 Pressure- and flow-loading

Voluntary isocapnic hyperpnoea (VIH)

Participants were seated in the upright position and breathed through a flanged mouthpiece connected to a three-way valve (112050-2100, Hans Rudolph Inc., KS, USA) while wearing a nose-clip (Figure 7.2.1A). Proximal to the participant, the valve was connected to a flow-turbine and, distal to the participant, an open-ended rebreathe tube (3 × 60 cm; ~425 mL). The dimensions of the rebreathe tube were selected to minimise hypocapnia by having the participant rebreathe partially exhaled breath. To maintain isocapnia, humidified hypercapnic gas (5% CO_2 and 95% O_2) was fed into the distal end of the tube whenever $P_{ET}CO_2$ dropped below resting values.

The protocol was performed for 2 min under the instruction to 'breathe as much as you can from the onset of the test and continue without pacing'. The participants received verbal encouragement throughout the test, including feedback every 30 s about time remaining. In addition, the participants could see their minute ventilation on a computer screen and were encouraged to keep the value as high as possible throughout the test.

Inspiratory resistive loading (IRL)

Participants were seated in the upright position while breathing through a modified two-way non-rebreathing valve (50-0975, Harvard Apparatus, Cambridge, UK; Figure 7.2.1). The valve offered resistance on inspiration and negligible resistance on expiration (<0.1 kPa at 15 L/s from the flow turbine). Inspiratory resistance was created by occluding the inspiratory valve with a rubber stopper with individualised orifice sizes (ID 2.5-4.0 mm). The correct orifice size for each participant was identified during familiarisation visit, and was determined when maximal inspiration could be performed as a square-wave with a duty cycle of 0.60 for five consecutive minutes.

The protocol consisted of 3 × 5 min intervals of loaded breathing, with each interval separated by 5 min of unloaded breathing. The rest periods prevented CO_2 retention and the consequent increase in breathing discomfort (Gorman et al., 1999; McKenzie et al., 1997). Participants were instructed to perform maximal inspiratory efforts with a T_I/T_{TOT} of 0.60 and f_R of 12

breaths/min with assistance from dual-tone auditory cues. Diaphragm activation was targeted by participants placing one hand on their abdomen with the emphasis on moving only the abdomen (not rib cage) during inspiratory efforts (Ramsook et al., 2016). In addition, P_{di} waveforms were visualised on a computer screen so that $P_{di,max}$ could be targeted and inspirations could be performed as square-waves. The $P_{ET}CO_2$ at the mouth (Oxycon Pro, Jaeger, Viasys Healthcare, Hoechberg, Germany) and SpO_2 via earlobe pulse oximetry (2500A,

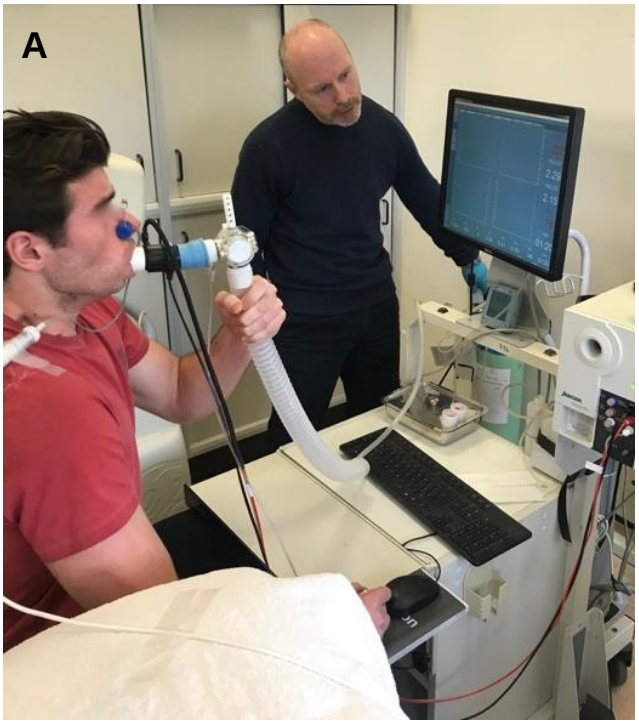

Figure 7.2.1 *A*) Voluntary isocapnic hyperpnoea (VIH), and *B*) inspiratory resistive loading (IRL).

Nonin Medical Ltd., Plymouth, US) were monitored closely throughout the trial.

7.2.6 Supramaximal phrenic nerve stimulation and sniffs

Stimulation of phrenic nerves was performed as described in detail in section 3.9 in General Methods. Bilateral phrenic nerve stimulation was performed using two commercially available magnetic stimulators (Magstim 200, Magstim Company Ltd., Whitland, Wales) connected to a paired-pulse stimulator (BiStim, Magstim Company Ltd.), and two figure-eight coils (D70 Alpha B.I, Magstim Company Ltd.) (Mills et al., 1996). The optimal stimulation areas were located on the anterior borders of the sternocleidomastoids, and the skin was marked for subsequent stimulations. To check for supramaximality of stimulation, each participant underwent an incremental stimulation protocol at 50 to 100% of the stimulator's maximum power, as described in section 3.9 and Chapter 4. Supramaximal stimulation was defined when mean $\Delta P_{di,tw}$ at submaximal and maximal stimulation intensities were equal to or less than the coefficient of variation (CV) for all twitches within an individual participant (Geary et al., 2019; Man et al., 2004).

Five successfully evoked, supramaximal twitches were performed at relaxation volume with participants wearing a nose-clip. Simulations were performed at 100% of maximum stimulator power before and after (10 and 30 min) each loading condition. Participants also performed five maximal inspiratory efforts (sniffs) from relaxation volume under the instructions to 'do a short, sharp sniff as hard as possible' (Miller et al., 1985, p. 92). Each twitch and sniff was separated by ≥30 s to avoid post-activation potentiation (Mador, Magalang, et al., 2000; Wragg et al., 1994).

7.2.7 Hypercapnic hyperpnoea (CO_2-rebreathe)

Hyperpnoea was induced by the CO_2-rebreathe method described in General Methods (section 3.11) and Chapter 5. Briefly, the method was similar to that described by Read et al. (1966; 1967), but with the original gas composition of 7% CO_2 and 93% O_2 substituted by a certified gas composition of 5% CO_2 and 95% O_2 and with the use of a disposable, plastic rebreathe bag (8 L) adjusted to ~1 L greater than vital capacity. Intrathoracic pressures and ventilatory and gas-exchange indices were recorded on a breath-by-breath basis at rest, during hyperpnoea and during three subsequent minutes of recovery. In addition, diaphragm ultrasonography was performed at regular intervals during all three phases (rest, hyperpnoea and recovery; see below).The laboratory was kept silent before (rest), during and after (recovery) each rebreathe trial to avoid the potential influence of external stimuli on ventilatory responses (Homma & Masaoka, 2008; Spengler & Shea, 2001).

7.2.8 Assessment of ventilatory and gas-exchange indices

Pulmonary airflow and gas-exchange were measured breath-by-breath using a metabolic cart with online gas analysis system (Oxycon Pro, Jaeger, Viasys Healthcare, Hoechberg, Germany), comprising a calibrated turbine flow-meter and O_2 and CO_2 gas analysers. Digital signals from the metabolic cart were input into the data acquisition system using an external device (DAQ-30A16, Eagle Technology, Cape Town, South Africa) and recorded online as waveforms. Inspired and expired tidal volumes were calculated offline by numerical integration of flow using a bespoke script (Horseman, 2020a).

7.2.9 Assessment of intrathoracic pressures and EMG_{di}

The P_{oe}, P_{ga} and EMG_{di} were measured using a gastro-oesophageal catheter (Gaeltec Devices Ltd., Isle of Skye, Scotland), as described in section 3.6.5 in General Methods. Briefly, the catheter was passed pernasally and swallowed into the stomach via peristalsis. The position of the catheter was adjusted such that a maximal sniff elicited negative and positive deflections in P_{oe} and P_{ga}, respectively. The correct position was confirmed with the "dynamic occlusion test" (Baydur et al., 1982), before the catheter was taped in position at the nose. Upon acquisition, the analogue signals for intrathoracic pressures and EMG_{di} were passed through a signal amplifier (1902, CED, Cambridge, UK) and digitised at sampling frequencies of 200 Hz (pressures) and 4 kHz (EMG_{di}) using an analogue-to-digital converter (1401mk-II, CED). Transdiaphragmatic pressure (P_{di}) was calculated online by subtraction of P_{oe} from P_{ga}.

7.2.10 Diaphragm ultrasonography for crural diaphragm kinetics

Ultrasonography of crural diaphragm kinetics was performed as described in Chapter 4 and 5 (*Part 1*). Briefly, all ultrasound scans were performed using a commercially available system (Vivid 7 Pro, GE Medical, Horten, Norway) with the participant in a semi-recumbent position. For evoked twitches, a low-frequency phased-array ultrasound transducer (1.5-4.0, M3S, GE Medical) was positioned subcostally on the right mid-clavicular line, steering in a cranial direction to image the posterior portion of the right hemi-diaphragm dome. Beam penetration depth was adjusted so that the hyperechoic diaphragm position at RV was always within the field of view (~200-250 mm). In addition, one focal point was set at the diaphragm position at relaxation volume for optimised lateral resolution. To achieve adequate sampling frequency for capturing the rapid twitch response (200-220 FPS), the B-mode image width was set to capture only the hemi-diaphragm apex.

For hypercapnic hyperpnoea, a low-frequency, curvilinear ultrasound transducer (2.4-5.0 MHz, 3.5C, GE Medical) was used and positioned as described above. Sampling frequency was set to 40 FPS, with a wide field of view ranging from the costophrenic angle laterally to the inferior vena cava medially. Again, penetration depth was adjusted so that the hyperechoic diaphragm structure at RV was always within the field of view.

Assessment of diaphragm excursion, excursion velocity and power

Ultrasound cine-loops were acquired as B-mode ultrasound, and analysed offline with AM-mode ultrasound using specialty software (EchoPac, v6.1, GE Medical). The dynamic AM-mode cursor was visually oriented along the true axis of the diaphragm movement (Orde et al., 2016b). Using a digital calliper tool, excursion was measured as the swing amplitude of diaphragm descent during evoked contraction or inspiration during hyperpnoea. Excursion time was measured as the time from onset of excursion to peak excursion. Excursion velocity (cm/s) was calculated as the quotient of diaphragm excursion divided by excursion time. Diaphragm power was estimated as the dot product of excursion velocity and $\overline{P}_{di,a}$.

7.2.11 Data processing and time-matching

Evoked twitch responses were measured as absolute pressure swing from the point of stimulation ($\Delta P_{di,tw}$, $\Delta P_{oe,tw}$ and $\Delta P_{ga,tw}$). End-expiratory oesophageal and gastric pressures (EEP_{oe} and EEP_{ga}) were measured at the point of stimulation to ensure that stimulation was performed at similar operating lung volume (muscle fibre length) (Hubmayr et al., 1989) and with similar abdominal compliance (Koulouris, Mulvey, et al., 1989) before and after each loading condition. M-waves that were free of cardiac artefact and with a constant shape with stable baseline before and after stimulation were identified. The peak-to-peak amplitude of the compound muscle action potential (M-wave) was assessed as a measure of neuromuscular propagation. Phrenic nerve conduction time (latency) was measured from the time of stimulation to the onset of the evoked potential (Aldrich et al., 2005; Luo et al., 1999).

During hyperpnoea, ventilatory indices ($\dot{V}_I$, V_{TI}, f_R, T_I, T_I/T_{TOT}) and intrathoracic pressures (P_{di}, P_{ga} and P_{oe}) were recorded breath-by-breath and analysed offline (Spike2, CED). Each breath was marked at the point of zero flow, and anomalous breaths (e.g., swallows, coughs or sighs, and breaths not crossing zero flow) were manually excluded from the analysis. Ventilatory indices were expressed for inspiration only.

Tidal pressures were calculated as the active components of mean inspiratory pressure ($\overline{P}_{di,a}$, $\overline{P}_{ga,a}$ and $\overline{P}_{oe,a}$), using the equation from Barnard & Levine (1986) with $\overline{P}_{di,a}$ as an example:

$$\bar{P}_{di,a} = \Sigma_0^n P_{di}/n,$$

where baseline P_{di} (*0*) was the P_{di} immediately preceding the inspiratory upswing, and *n* was equal to the number of data points during inspiration. Accordingly, $\overline{P}_{di,a}$ was the mean pressure generated during tidal inspiration based on tidal pressure swings, without the passive component of inspiratory pressure. See General Methods, section 3.6.5 for details.

To characterise the force output of the diaphragm during loading tasks, diaphragm pressure-time product was calculated on a breath-by-breath basis as the integral of pressure down to zero during inspiration ($\int P_{di}$). For the cumulative force output generated during loading tasks, $\int P_{di}$ was first multiplied by respiratory frequency (f_R), and then multiplied by the duration of each fatigue task (i.e., 1 × 2 min for VIH and 3 × 5 min for IRL; $\Sigma\int P_{di} \times f_R$). Diaphragm pressure-time index (PTI_{di}) was calculated as ($\overline{P}_{di}/P_{di,max}$) × ($T_I/T_{TOT}$) (Bellemare & Grassino, 1982). Note that $\overline{P}_{di}$ (not $\overline{P}_{di,a}$) was used in the calculation of PTI_{di} as to include both passive and active components of inspiratory pressure.

The ultrasound and data acquisition systems were not synchronised, so particular attention was paid to the timing of ultrasound acquisition during hyperpnoea in order that the respiratory cycles within each ultrasound cine-loop could be correctly identified and matched with breath-by-breath ventilatory and pressure data. Specifically, ultrasound cine-loops were recorded over 15 s every 30 s during hyperpnoea and the three subsequent minutes of recovery (1 × 30 s for rest). All breaths recorded within the 15 s cine-loop (1 × 30 s for rest) were identified in the data acquisition system (i.e., intrathoracic pressures and ventilatory indices), then averaged over 15 s (30 s for rest). The final 15 s of hyperpnoea, independent of test duration, was recorded and defined as the *peak* response.

7.2.12 Statistics

Statistical analysis was performed using SPSS (v26.0, IBM Corp., Armonk, NY, USA) and GraphPad Prism (v9.0, GraphPad Software LLC, San Diego, USA). Normal distribution of data was assessed with the Shapiro-Wilk test. All variables met the assumptions required for parametric statistics (incl. analysis of variance; ANOVA).

To compare ventilatory indices ($\dot{V}_I$, f_R, V_{TI}, T_I, T_I/T_{TOT}) and the inspiratory muscle force output ($\int P_{di}$, PTI_{di}, $\Sigma\int P_{di} \times f_R$ and $\overline{P}_{di}/P_{di,max}$) during loading tasks (VIH and IRL), a two-tailed, paired samples *t*-tests was performed. The effects of loading tasks on evoked twitch responses, sniff pressures and peak responses to hyperpnoea (incl. ultrasound-derived diaphragm kinetics) were assessed using two-way, repeated-measures ANOVA, with time (PRE, $POST_{10}$ and $POST_{30}$) and loading condition (VIH and IRL) as within-subject factors. Bonferroni corrections were applied to correct for multiple comparisons. Sphericity was checked using Mauchly's test, and, if violated, Greenhouse-Geisser correction was applied (O'Donoghue, 2012). Effect sizes were reported as partial eta squared (η_p^2) and interpreted as small (η_p^2 0.01–0.05), medium (0.06–0.13) or large (≥0.14) (Lakens, 2013).

During hyperpnoea, rates of change (slopes) in ventilatory indices ($\dot{V}_I$, f_R, V_{TI}, T_I and T_I/T_{TOT}) and intrathoracic pressures ($\overline{P}_{di,a}$, $\overline{P}_{ga,a}$ and $\overline{P}_{oe,a}$) with respect to $P_{ET}CO_2$ were calculated for each participant using simple linear regression. The slopes were converted into *t*-scores using the equation:

$$t = \frac{b_1 - b_2}{\sqrt{S^2 b_1 + S^2 b_2}}$$

where b_1 and b_2 are the two slopes being compared, and *S* is the standard error of the slopes (Zar, 2014). Group mean slope responses, and individual slope responses, were then compared using two-tailed, paired samples *t*-test.

Diaphragm fatigue was considered present if there was a ≥10% reduction in $\Delta P_{di,tw}$ relative to PRE-loading (Mador, Kufel, et al., 2000). This definition coincided with a change in $\Delta P_{di,tw}$ that was approximately two-fold greater than the normal variability observed in the same group of participants for bilateral phrenic nerve stimulation (CV = 5.8%; see Chapter 4, Table 4.3.3). Loading-induced changes in ventilation, breathing pattern and intrathoracic pressures during hyperpnoea were considered present when the rates of rise with respect to $P_{ET}CO_2$ (slopes) were statistically different relative to PRE baseline (Mador & Tobin, 1992; Yan, Sliwinski, et al., 1993). All statistical tests were performed using absolute values. Statistical significance was set at $p \leq 0.05$ and data are presented as mean ± *SD*.

7.3 Results

7.3.13 Participant characteristics and loading tasks

Participant characteristics are shown in Table 7.3.1. In line with inclusion criteria, participants exhibited pulmonary flows, volumes and capacities within normal limits. This was the case also for maximal respiratory mouth pressures. Diaphragm structure and function were within the ranges reported elsewhere for healthy men.

Table 7.3.1 Participant characteristics.

	Mean ± *SD*
Anthropometry	
Age, y	23 ± 7
Stature, cm	180 ± 5
Body mass, kg	77 ± 10
BMI, kg/m^2	23.7 ± 3.0
Chest depth, cm	20.0 ± 1.1
Chest width, cm	30.3 ± 1.7
Chest circumference, cm	94.4 ± 2.6
Pulmonary function	
TLC, L (% predicted)	7.46 ± 0.87 (107 ± 10)
RV, L (% predicted)	1.86 ± 0.23 (112 ± 14)
FRC_{pleth}, L (% predicted)	3.97 ± 0.72 (116 ± 18)
FVC, L (% predicted)	5.74 ± 0.47 (100 ± 5)
FEV_1, L (% predicted)	4.75 ± 0.41 (101 ± 7)
FEV_1/FVC (% predicted)	0.82 ± 0.05 (100 ± 4)
MVV_{12}, L/min (% predicted)	188 ± 28 (102 ± 14)
Maximal respiratory pressures	
MIP, cmH_2O (% predicted)	–125 ± 16 (113 ± 15)
MEP, cmH_2O (% predicted)	173 ± 19 (112 ± 11)
Diaphragm structure and function	
Diaphragm thickness at FRC, mm	1.6 ± 0.5
Diaphragm thickness at TLC, mm	4.1 ± 0.7
Thickening fraction, %	156 ± 40
Maximal diaphragm mobility, cm	6.78 ± 1.50

Data are mean ± *SD* for eight participants. BMI, body mass index; TLC, total lung capacity; RV, residual volume; FRC_{pleth}, functional residual capacity via plethysmography; FVC, forced vital capacity; FEV_1, forced expiratory volume in 1 s; MVV_{12}, maximal voluntary ventilation in 12 s; MIP, maximum inspiratory mouth pressure; MEP, maximum expiratory mouth pressure. Predicted values for pulmonary function were derived from Quanjer et al. (2012) for spirometry and Stocks & Quanjer (1995) for plethysmography. Predicted values for MVV_{12} were calculated as $FEV_1 \times 40$ (Miller et al., 2005). Predicted values for maximum mouth pressures were from Evans & Whitelaw (2009).

Quantitative characteristics of the two loading tasks are shown in Table 7.3.2. As there were no significant differences between the three intervals of IRL, data are shown as mean ± *SD* for all intervals combined. By design, the two fatigue conditions exhibited different ventilatory and pressure characteristics, targeting the two extremes of the force-velocity spectrum. During VIH, minute ventilation was highest during the initial 20 s (~220 L/min; 117% of MVV_{12}), and then stabilised at ~160 L/min (85% of MVV_{12}) for the remaining duration. In Table 7.3.2, particularly noteworthy are the higher V_{TI}/T_I and lower $\int P_{di}$ during VIH compared to IRL (both $p < 0.001$).

Table 7.3.2 Ventilatory indices and diaphragm force output during voluntary isocapnic hyperpnoea (VIH) and inspiratory resistive loading (IRL).

	VIH	**IRL**
$\dot{V}_I$, L/min	165 ± 18	22 ± 6*
V_{TI}, L	1.97 ± 0.37	1.98 ± 0.55
f_R, breaths/min	86.6 ± 19.0	11.9 ± 0.8*
V_{TI}/T_I, L/s	5.95 ± 0.63	0.75 ± 0.20*
T_I/T_{TOT}	0.47 ± 0.01	0.56 ± 0.06*
$\overline{P}_{di}/P_{di,max}$, %	33.2 ± 15.9	77.3 ± 5.1*
PTI_{di}	0.16 ± 0.07	0.43 ± 0.06*
$\int P_{di}$, $cmH_2O/s/breath$	20.9 ± 6.9	56.9 ± 13.1*
$\Sigma\int P_{di} \times f_R$, $cmH_2O/s/min$	3566 ± 1093	9467 ± 2416*

Data are mean ± *SD* for eight participants. $\dot{V}_I$, inspiratory minute ventilation; V_{TI}, inspiratory tidal volume; f_R, respiratory frequency; V_{TI}/T_I, mean inspiratory flow; T_I/T_{TOT}, inspiratory duty cycle; $\overline{P}_{di}/P_{di,max}$, mean inspiratory transdiaphragmatic pressure relative to maximum transdiaphragmatic pressure; PTI_{di}, diaphragm pressure-time index ($\overline{P}_{di}/P_{di,max} \times T_I/T_{TOT}$); $\int P_{di}$, time integral of transdiaphragmatic pressure during inspiration; $\Sigma\int P_{di}$, sum of time integral of transdiaphragmatic pressure over the total duration of loading task. *$p \leq 0.05$ vs. VIH.

7.3.14 Supramaximal phrenic nerve stimulation

Pressure responses ($\Delta P_{di,tw}$) to incremental stimulation power are shown in Figure 7.3.1. There were no differences in the absolute values for $\Delta P_{di,tw}$ between the two experimental visits (p = 0.315), and in both visits, $\Delta P_{di,tw}$ increased statistically from 50 to 60% of stimulator power (p = 0.043). However, a plateau in $\Delta P_{di,tw}$ (per the CV method described above) occurred at 80% (n = 1), 85% (n = 1), 90% (n = 3) or 95% (n = 3) during the VIH visit, and at 80% (n = 1), 90% (n = 4) or 95% (n = 3) during IRL visits.

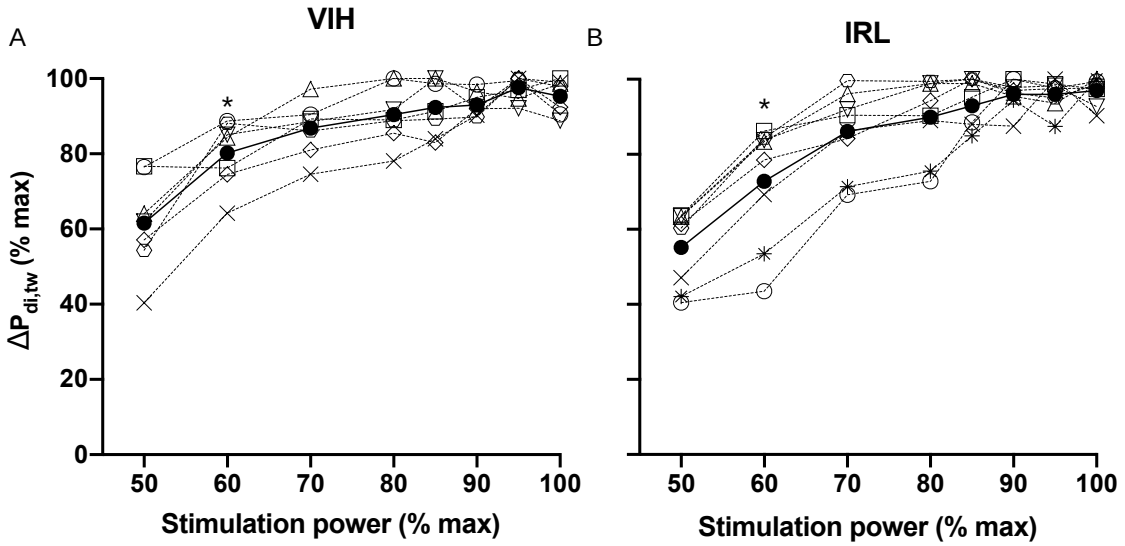

Figure 7.3.1 Individual participant (---) and group mean (—) $\Delta P_{di,tw}$ in response increasing stimulation power. Data are for eight participants. *$p \leq 0.05$ vs. previous stimulation power.

Intrathoracic pressures and EMG_{di}

Twitch pressure responses are shown in Table 7.3.3. At baseline (PRE), $\Delta P_{di,tw}$ was similar across both loading conditions (p = 0.932), which was the case also for $\Delta P_{oe,tw}$ (p = 0.535) and $\Delta P_{ga,tw}$ (p = 0.094). The $EEP_{oe,tw}$ did not differ over time (p = 0.688; η_p^2= 0.038) or between the two loading conditions (p = 0.614; η_p^2= 0.117), suggesting that phrenic nerve stimulation was performed at the same operating lung volume (diaphragm fibre length) before and after loading during both conditions. Similarly, $EEP_{ga,tw}$ remained unchanged after loading (p = 0.375; η_p^2 = 0.277) and between loading conditions (p = 0.627; η_p^2 = 0.036), confirming that abdominal compliance was similar before and after loading during both conditions.

Table 7.3.3 Twitch pressure responses pre and post voluntary isocapnic hyperpnoea (VIH) and inspiratory resistive loading (IRL).

	PRE	$POST_{10}$	$POST_{30}$
VIH			
$\Delta P_{di,tw}$, cmH_2O	30.2 ± 9.9	28.7 ± 8.7	26.5 ± 7.8
$\Delta P_{oe,tw}$, cmH_2O	–16.1 ± 6.1	–15.9 ± 5.9	–13.4 ± 6.6
$\Delta P_{ga,tw}$, cmH_2O	14.2 ± 8.9	12.6 ± 6.1	13.1 ± 7.2
EEP_{oe}, cmH_2O	–7.7 ± 4.6	–7.3 ± 4.	–8.7 ± 4.9
EEP_{ga}, cmH_2O	4.6 ± 7.1	2.4 ± 7.3	3.0 ± 7.2
IRL			
$\Delta P_{di,tw}$, cmH_2O	28.8 ± 10.2	25.3 ± 10.4*	25.9 ± 9.2*
$\Delta P_{oe,tw}$, cmH_2O	–17.1 ± 6.3	–13.2 ± 7.0*	–13.8 ± 6.4*
$\Delta P_{ga,tw}$, cmH_2O	11.7 ± 6.2	12.3 ± 6.8	12.1 ± 6.2
EEP_{oe}, cmH_2O	–5.5 ± 7.0	–7.6 ± 9.2	–5.9 ± 10.4
EEP_{ga}, cmH_2O	4.3 ± 6.3	1.5 ± 4.6	1.0 ± 6.3

Data are mean ± *SD* for eight participants. $\Delta P_{di,tw}$; twitch transdiaphragmatic pressure; $\Delta P_{oe,tw}$; twitch oesophageal pressure; $\Delta P_{ga,tw}$, twitch gastric pressure; EEP_{oe}, end-expiratory oesophageal pressure; EEP_{ga}, end-expiratory gastric pressure. *$p \leq 0.05$ vs. PRE.

For the $\Delta P_{di,tw}$, there was a main effect of time ($p = 0.020$; $\eta_p^2 = 0.728$). However, *post hoc* tests showed that $\Delta P_{di,tw}$ was significantly reduced only after IRL (not VIH): by –13.4% at $POST_{10}$ ($p = 0.013$; range +2.1 to –40.3%) and –13.4% at $POST_{30}$ ($p = 0.05$; range +5.7 to –32.2%). Six out of the eight participants measured ≥10% fall in $\Delta P_{di,tw}$ post IRL, regardless of timepoint. The largest reduction in $\Delta P_{di,tw}$ after IRL was found at $POST_{10}$ in the majority (62.5%) of participants. Following VIH, however, only four participants measured ≥10% reduction in $\Delta P_{di,tw}$, with the mean relative change of –5.5% at $POST_{10}$ ($p = 0.617$; range +5.6 to –18.4%) and –11.7% at $POST_{30}$ ($p = 0.113$; range +2.5 to –26.4%). After VIH, six of eight participants measured their largest drop in $\Delta P_{di,tw}$ at $POST_{30}$.

At pre-VIH and pre-IRL, $\Delta P_{di,sn}$ was 111 ± 47 cmH_2O and 107 ± 38 cmH_2O, respectively, and was similar between the two loading conditions ($p = 0.729$). For $\Delta P_{di,sn}$, there was a main effect of time ($p = 0.005$; $\eta_p^2 = 0.533$) but not of loading condition ($p = 0.800$; $\eta_p^2 = 0.010$), with *post hoc* tests showing that it was only after IRL ($POST_{10}$) that $\Delta P_{di,sn}$ was reduced (94 ± 34 cmH_2O; $p = 0.032$). The reduction in $\Delta P_{di,sn}$ following IRL was primarily attributed to a reduction in $\Delta P_{oe,sn}$, which declined from –70 ± 16 cmH_2O at PRE to –58 ± 13 cmH_2O ($p = 0.016$) and –62 ± 18 cmH_2O ($p = 0.035$) at $POST_{10}$ and $POST_{30}$, respectively. There was no effect for loading condition ($p = 0.958$; $\eta_p^2 = 0.001$) or time ($p = 0.421$; $\eta_p^2 = 0.116$) on $\Delta P_{ga,sn}$.

Unfortunately, it was not feasible to assess M-waves as cardiac artefacts and/or electrical artefacts evoked by the triggering of the magnetic stimulators interfered with the EMG signal in most participants during both conditions. For instance, there were only three participants from whom M-waves could be obtained at all three timepoints during the VIH condition. For IRL, only one participant had ≥2 M-waves available for analysis across all three timepoints. Thus, there were insufficient data for statistical pre-post comparisons. For the participants with acceptable M-waves at PRE (n = 5), latency was 7.49 ± 1.76 ms and peak-to-peak amplitude was 1.37 ± 0.37 mV, with no apparent differences between the two experimental visits.

Diaphragm kinetic responses

Ultrasound-derived measures of diaphragm kinetics in response to twitch contractions are shown in Figure 7.3.2. For diaphragm excursion, there were no main effects of time (p = 0.294; η_p^2 = 0.160) nor of loading condition (p = 0.171; η_p^2 = 0.249). Interestingly, however, there was an interaction effect of loading condition and time on diaphragm excursion time (p = 0.049; η_p^2 = 0.349), with *post hoc* tests showing that the excursion time was prolonged after IRL: from 0.11 ± 0.04 s at PRE to 0.14 ± 0.03 s at $POST_{10}$ (p = 0.017) and 0.13 ± 0.02 s at $POST_{30}$ (p = 0.013). Conversely, diaphragm excursion time remained unchanged after VIH.

For diaphragm excursion velocity, there was a main effect of time (p = 0.024; η_p^2 = 0.414) but not of loading condition (p = 0.277; η_p^2 = 0.166). Moreover, there was an interaction effect of time and loading condition (p = 0.021; η_p^2 = 0.552), with *post hoc* tests showing that the excursion velocity was slower only after IRL (not VIH), dropping from 16.3 ± 5.8 cm/s to 9.9 ± 3.0 cm/s (p = 0.043; range +1.4 to –66%) $POST_{10}$ and to 10.2 ± 4.2 cm/s at $POST_{30}$ (p = 0.034; range +0.9 to –81%) relative to PRE-IRL. Accordingly, the combined loss of diaphragm force ($\Delta P_{di,tw}$) and slowing of excursion velocity resulted in a substantial decline in diaphragm power at both timepoints after IRL: –46% at $POST_{10}$ (p = 0.033; range +4 to –75%) and –44% at $POST_{30}$ (p = 0.031; range –5% to –80%) relative to PRE. Diaphragm power did not change after VIH (Figure 7.3.3A).

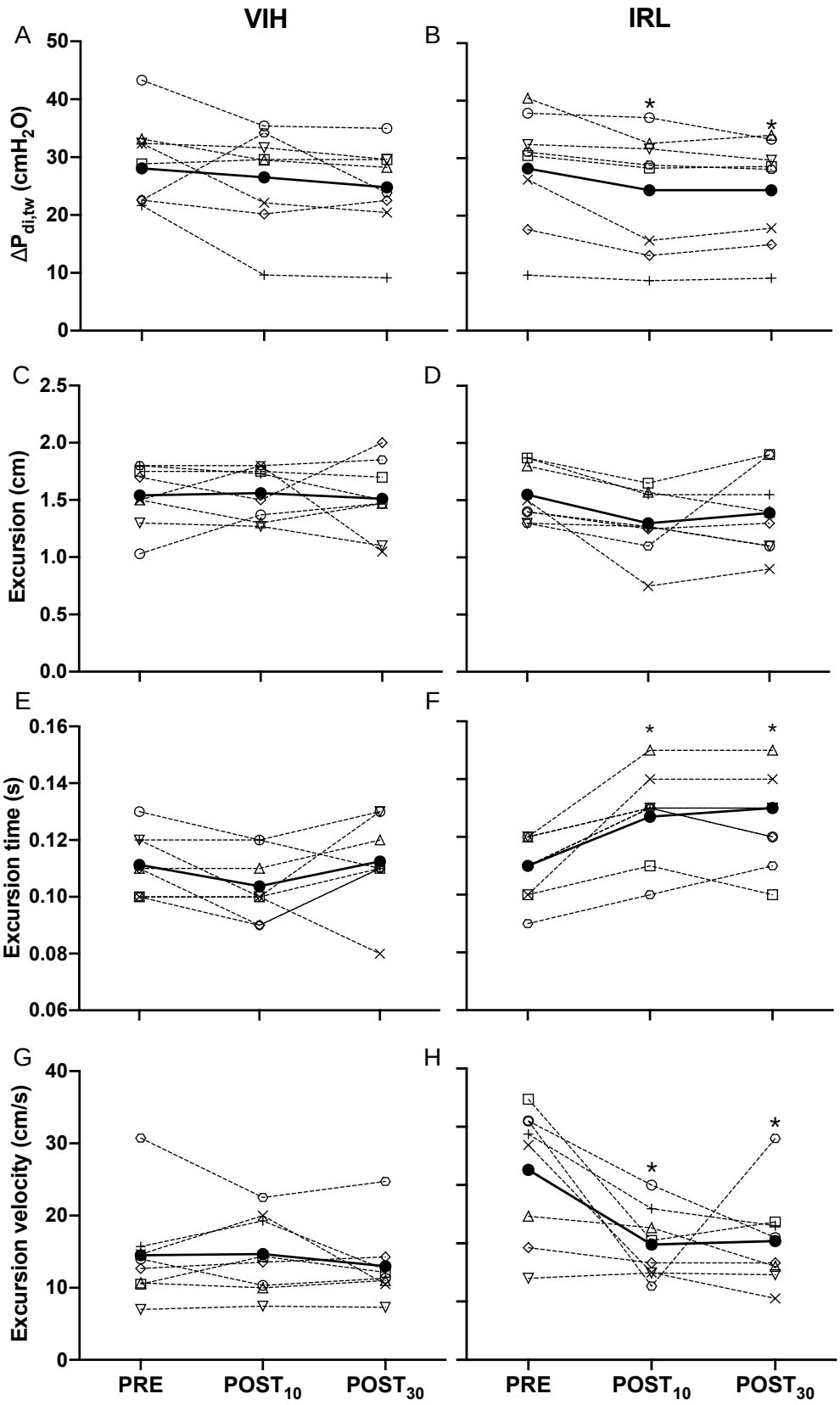

Figure 7.3.2 Individual (---) and group mean (---) $\Delta P_{di,tw}$ (*A-B*); diaphragm excursion (*C-D*); excursion time (*E-F*) and excursion velocity (G-H*)* pre- and post-loading. Data are for eight participants. *$p \leq 0.05$ vs. PRE.

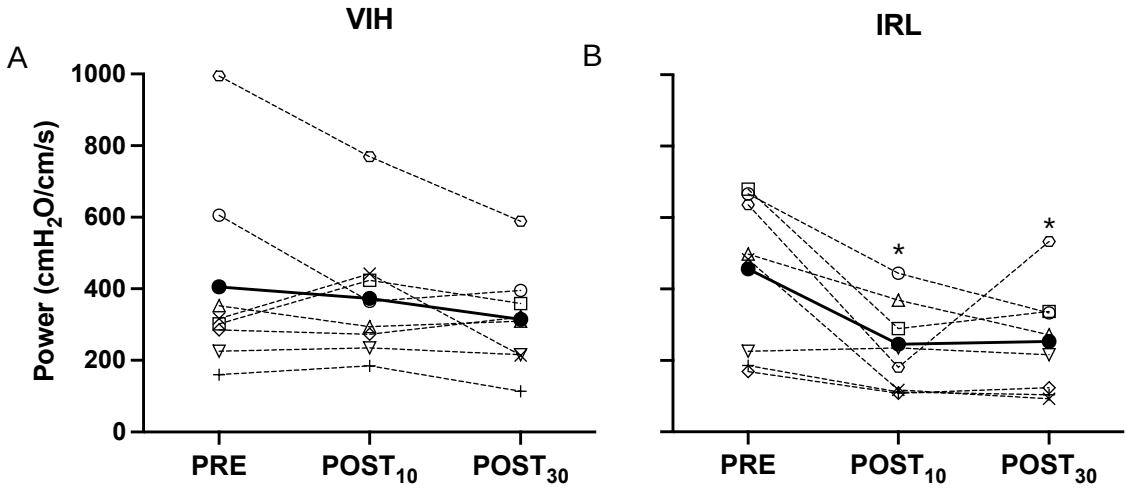

Figure 7.3.3 Individual (---) and group mean (—) diaphragm power pre- and post-loading. Data are for eight participants. *$p \leq 0.05$ vs. PRE.

7.3.15 Hypercapnic hyperpnoea

All participants completed CO_2-rebreathe tests without untoward events. Mean $P_{ET}CO_2$ at rest was 40.4 ± 1.9 mmHg and 40.7 ± 1.7 mmHg for VIH and IRL trials, respectively, and did not differ between loading conditions ($p = 0.745$; $\eta_p^2 = 0.681$) or timepoint ($p = 0.491$; $\eta_p^2 = 0.312$). There was, however, a main effect for loading condition on CO_2-rebreathe duration ($p = 0.027$; $\eta_p^2 = 0.525$), with *post hoc* tests showing that rebreathe lasted longer during VIH compared to IRL at PRE (2.99 ± 1.37 vs. 2.23 ± 0.94 min; $p = 0.038$) and $POST_{30}$ (2.74 ± 0.96 vs. 2.16 ± 0.79 min; $p = 0.023$).

Slope responses to hypercapnic hyperpnoea

Figure 7.3.4 shows the ventilatory slope responses to CO_2 ($\dot{V}_I$ vs. $P_{ET}CO_2$) at the three timepoints in VIH and IRL conditions. As shown, the ventilatory response did not change following VIH. After IRL, however, the ventilatory slope response was ~10% steeper ($p < 0.001$; range –86 to +31%) at $POST_{10}$, and ~8% steeper at $POST_{30}$ ($p < 0.001$; range –46 to +47%) compared to PRE-IRL (Figure 7.3.4B). The steeper ventilatory response at post-IRL was likely due to two participants in whom CO_2 only elicited a small ventilatory response at PRE (slopes ≤ 0.1 L/min/mmHg), and then elicited 'normal' responses post-IRL (slopes ≥1.2 L/min/mmHg). For the remaining six participants, four exhibited reduced ventilatory response at both timepoints post-IRL, and two exhibited no significant change.

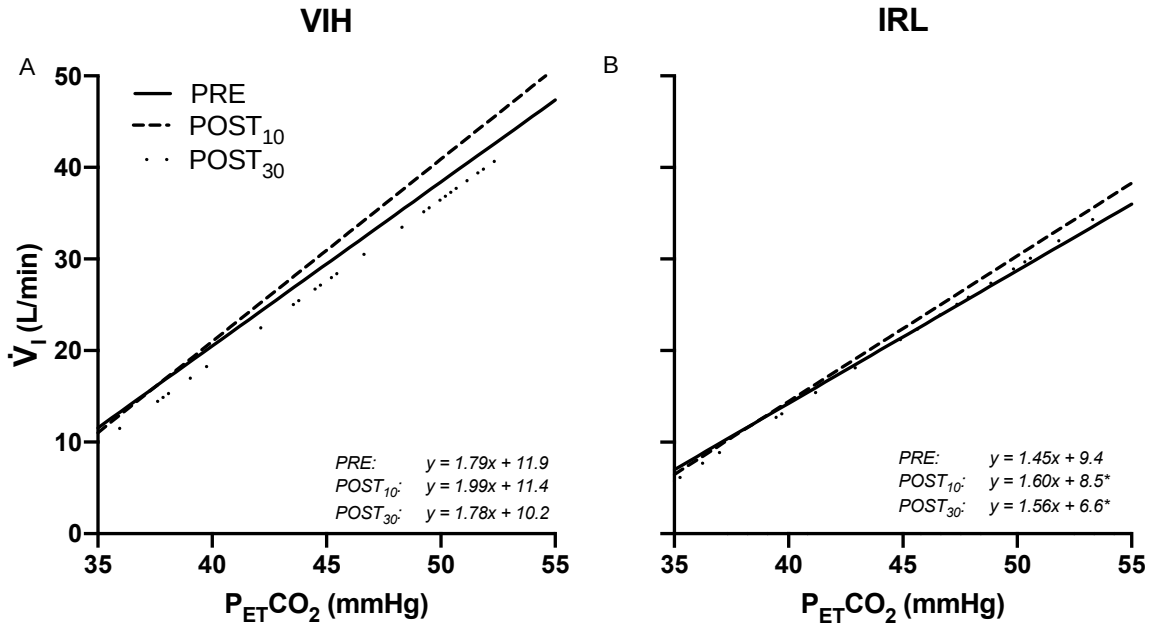

Figure 7.3.4 Slope responses for inspiratory minute ventilation ($\dot{V}_I$) at PRE (—), $POST_{10}$ (---) and $POST_{30}$ (⋯) loading in eight participants. Linear regression equations are shown in lower right corner of each panel. *$p \leq 0.05$ vs. PRE.

Group mean data (slopes) for breathing pattern and intrathoracic pressure responses during hyperpnoea are shown in Table 7.3.4. Although group mean responses did not change after VIH, it was evident that some participants exhibited altered intrathoracic pressure responses when evaluating *individual* slope responses: for instance, four participants exhibited lower $\overline{P}_{di,a}$ and $\overline{P}_{oe,a}$ at both timepoints post-VIH. One of these participants also adopted at breathing pattern with lower V_{TI} ($p = 0.01$) and higher f_R ($p = 0.013$) at both timepoints, suggesting that VIH may have caused a tachypnoeic breathing pattern in this participant. There were no consistent changes in breathing pattern or intrathoracic pressures in the remaining four participants.

Following IRL, group mean breathing pattern during hyperpnoea was significantly altered at both timepoints. This change in breathing pattern was manifested as reduced V_{TI} and increased f_R ($p < 0.001$ both timepoints). Interestingly, however, the changes in breathing pattern were not associated with a change in intrathoracic pressures, as $P_{di,a}$ remained unaltered from pre-IRL ($POST_{10}$ $p = 0.301$; $POST_{30}$ $p = 0.17$). Upon evaluating individual slope responses, it was evident that five out of the eight participants adopted a tachypnoeic breathing pattern post-IRL. These participants also exhibited lower $\overline{P}_{di,a}$ response during hyperpnoea, primarily caused by a

reduced $\overline{P}_{oe}$ response (n = 2) and/or a reduced $\overline{P}_{ga}$ response to CO_2 (n = 3). The remaining three participants did not show any consistent changes in breathing pattern or intrathoracic pressure responses after IRL.

Table 7.3.4 Ventilatory and intrathoracic *slope* responses to hyperpnoea pre and post voluntary isocapnic hyperpnoea (VIH) and inspiratory resistive loading (IRL).

	PRE	**POST$_{10}$**	**POST$_{30}$**
VIH			
$\dot{V}_I$ vs. $P_{ET}CO_2$, L/min/mmHg	1.79 ± 1.47	1.99 ± 1.44	1.78 ± 0.95
V_{TI} vs. $P_{ET}CO_2$, mL/mmHg	85.8 ± 76	95.1 ± 61.2	64.6 ± 47.0
f_R vs. $P_{ET}CO_2$, breaths/mmHg	0.18 ± 0.42	0.23 ± 0.25	0.48 ± 0.25
T_I vs. $P_{ET}CO_2$, s/mmHg	–0.05 ± 0.12	–0.06 ± 0.05	–0.12 ± 0.10
T_I/T_{TOT} vs. $P_{ET}CO_2$	–0.07 ± 0.19	–0.14 ± 0.39	–0.04 ± 0.01
$\overline{P}_{di,a}$ vs. $P_{ET}CO_2$, cmH_2O/mmHg	0.39 ± 0.21	0.39 ± 0.40	0.44 ± 0.43
$\overline{P}_{oe,a}$ vs. $P_{ET}CO_2$, cmH_2O/mmHg	–0.31 ± 0.26	–26 ± 0.28	–0.34 ± 0.37
$\overline{P}_{ga,a}$ vs. $P_{ET}CO_2$, cmH_2O/mmHg	0.17 ± 0.14	0.12 ± 0.13	0.18 ± 0.17
IRL			
$\dot{V}_I$ vs. $P_{ET}CO_2$, L/min/mmHg	1.45 ± 1.07$^{\#}$	1.60 ± 1.59*$^{\#}$	1.56 ± 1.48*$^{\#}$
V_{TI} vs. $P_{ET}CO_2$, mL/mmHg	118 ± 75$^{\#}$	114 ± 140*$^{\#}$	98 ± 84*$^{\#}$
f_R vs. $P_{ET}CO_2$, breaths/mmHg	0.12 ± 0.30	0.28 ± 1.18*	0.18 ± 0.29*$^{\#}$
T_I vs. $P_{ET}CO_2$, s/mmHg	–0.06 ± 0.11	0.01 ± 0.08*	–0.06 ± 0.31*
T_I/T_{TOT} vs. $P_{ET}CO_2$	–0.04 ± 0.09	–0.02 ± 0.07$^{\#}$	–0.07 ± 0.02*
$\overline{P}_{di,a}$ vs. $P_{ET}CO_2$, cmH_2O/mmHg	0.37 ± 0.21	0.45 ± 0.33	0.42 ± 0.50
$\overline{P}_{oe,a}$ vs. $P_{ET}CO_2$, cmH_2O/mmHg	–0.29 ± 0.27	–0.35 ± 0.23	–0.27 ± 0.45
$\overline{P}_{ga,a}$ vs. $P_{ET}CO_2$, cmH_2O/mmHg	0.13 ± 0.78	0.11 ± 0.10	0.12 ± 0.10

Data are mean ± *SD* for eight participants. $\dot{V}_I$, inspiratory minute ventilation; V_{TI}, inspiratory tidal volume; f_R, respiratory frequency; T_I, inspiratory time; T_I/T_{TOT}, inspiratory duty cycle; $\overline{P}_{di,a}$, active component of mean inspiratory transdiaphragmatic pressure; $\overline{P}_{oe,a}$, active component of mean inspiratory oesophageal pressure; $\overline{P}_{ga,a}$, active component of mean inspiratory gastric pressure. *$p \leq 0.05$ vs. PRE; $^{\#}p \leq 0.05$ vs. VIH at same timepoint.

Peak responses to hypercapnic hyperpnoea

Peak ventilatory responses, breathing pattern and intrathoracic pressures are shown in Table 7.3.5. As shown, all peak ventilatory indices remained unchanged pre- vs. post-loading, with no main or interaction effects of neither time nor loading condition. Despite the altered slope responses in breathing pattern after IRL (see Table 7.3.5 above), breathing pattern at the peak of hyperpnoea did not appear to be affected by the loading task. For instance, for peak V_{TI}, there was no main effect of time (p = 0.084; η_p^2 = 0.298) nor of loading condition (p = 0.441; η_p^2 = 0.087). Similarly, for f_R, there were no main effects of time (p = 0.589; η_p^2 = 0.073) or loading condition (p = 0.817; η_p^2 = 0.008), suggesting that peak ventilatory indices were unaffected by the two loading tasks. This was the case also for peak intrathoracic pressures ($\overline{P}_{di,a}$, $\overline{P}_{oe,a}$ and $\overline{P}_{ga,a}$), which all remained unaffected by the two loading tasks.

Table 7.3.5 Ventilatory and intrathoracic pressure *peak* responses to hyperpnoea pre and post voluntary isocapnic hyperpnoea (VIH) and inspiratory resistive loading (IRL

	PRE	**POST$_{10}$**	**POST$_{30}$**
VIH			
$\dot{V}_I$, L/min	27.6 ± 12.6	30.5 ± 8.7	31.5 ± 11.6
V_{TI}, L	2.02 ± 0.63	2.16 ± 0.62	2.34 ± 0.84
f_R, breaths/min	14.2 ± 4.8	15.0 ± 2.0	14.2 ± 3.8
T_I, s	2.14 ± 1.01	1.91 ± 0.29	1.91 ± 0.35
T_I/T_{TOT}	0.45 ± 0.08	0.47 ± 0.04	0.43 ± 0.07
$\overline{P}_{di,a}$, cmH_2O	13.8 ± 4.7	10.6 ± 3.2	11.9 ± 4.5
$\overline{P}_{oe,a}$, cmH_2O	–7.6 ± 2.8	–6.5 ± 2.1	–7.4 ± 3.6
$\overline{P}_{ga,a}$, cmH_2O	6.9 ± 5.1	3.8 ± 1.5	5.7 ± 2.5
IRL			
$\dot{V}_I$, L/min	27.9 ± 13.3	28.0 ± 15.4	29.6 ± 14.1
V_{TI}, L	2.02 ± 0.63	2.06 ± 0.73	2.17 ± 0.64
f_R, breaths/min	14.0 ± 3.8	14.6 ± 5.4	14.0 ± 4.2
T_I, s	2.13 ± 0.65	2.21 ± 1.05	2.28 ± 0.90
T_I/T_{TOT}	0.47 ± 0.06	0.46 ± 0.04	0.48 ± 0.05
$\overline{P}_{di,a}$, cmH_2O	9.4 ± 3.4	10.6 ± 3.4	9.5 ± 3.2
$\overline{P}_{oe,a}$, cmH_2O	–6.7 ± 2.8	–7.1 ± 2.8	–5.8 ± 2.8
$\overline{P}_{ga,a}$, cmH_2O	3.9 ± 2.0	4.0 ± 1.6	4.2 ± 2.0

Data are mean ± *SD* for eight participants. $\dot{V}_I$, inspiratory minute ventilation; V_{TI}, inspiratory tidal volume; f_R, respiratory frequency; T_I, inspiratory time; T_I/T_{TOT}, inspiratory duty cycle; $\overline{P}_{di,a}$, active component of mean inspiratory transdiaphragmatic pressure; $\overline{P}_{oe,a}$, active component of mean inspiratory oesophageal pressure; $\overline{P}_{ga,a}$, active component of mean inspiratory gastric pressure.

Because ultrasound images were acquired at 15 s intervals (not breath-by-breath), slope responses to $P_{ET}CO_2$ could not be calculated for the ultrasound-derived measures of diaphragm kinetics. Instead, we compared kinetic responses at the peak of hyperpnoea between timepoints and across loading conditions. From rest to peak hyperpnoea, diaphragm excursion increased from (mean ± *SD* of all timepoints) 2.82 ± 1.10 cm to 5.35 ± 1.57 cm in VIH trials, and from 2.75 ± 1.03 cm to 5.02 ± 0.95 cm in IRL trials. The increase in excursion from rest to peak hyperpnoea was 82-85%, and was equal to 78-81% of maximal excursion (mobility).

As with peak ventilatory indices and intrathoracic pressure responses (Table 7.3.5 above), peak diaphragm excursion did not differ between loading conditions (p = 0.613; η_p^2 = 0.039) or with time (p = 0.765; η_p^2 = 0.038) (Figure 7.3.5C and D). This was true also for excursion time and excursion velocity, which did not differ across loading tasks or timepoints. Although diaphragm power tended to be lower after both loading tasks (Figure 7.3.6), there were no main effects of time (p = 0.069; η_p^2 = 0.318) or loading condition (p = 0.204; η_p^2 = 0.219). Still, it is worth noting that mean diaphragm power declined from 94 ± 71 $cmH_2O/cm/s$ at PRE to 52 ± 27 $cmH_2O/cm/s$ at $POST_{10}$ (–45%; p = 0.251) after VIH, and from 70 ± 18 $cmH_2O/cm/s$ at PRE to 35 ± 11 $cmH_2O/cm/s$ at $POST_{30}$ (–50%; p = 0.143) after IRL, although this did not reach statistical significance.

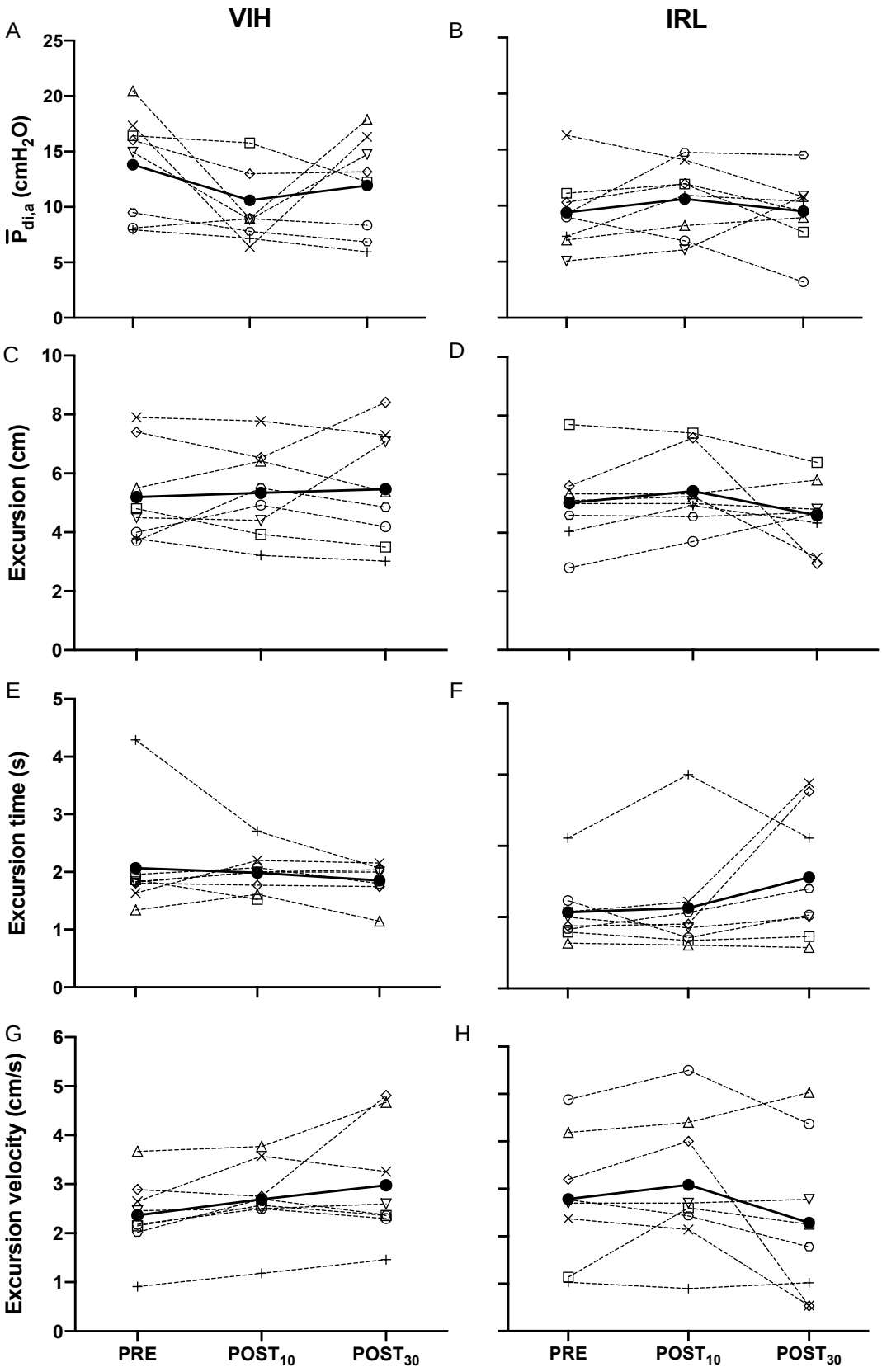

Figure 7.3.5 Individual responses (---) and group mean (—) *peak* responses to hyperpnoea in $\overline{P}_{di,a}$ *(A-B)*; diaphragm excursion (*C-D*); excursion time (*E-F*) and excursion velocity (*G-H*) pre- and post-loading. Data are for eight participants.

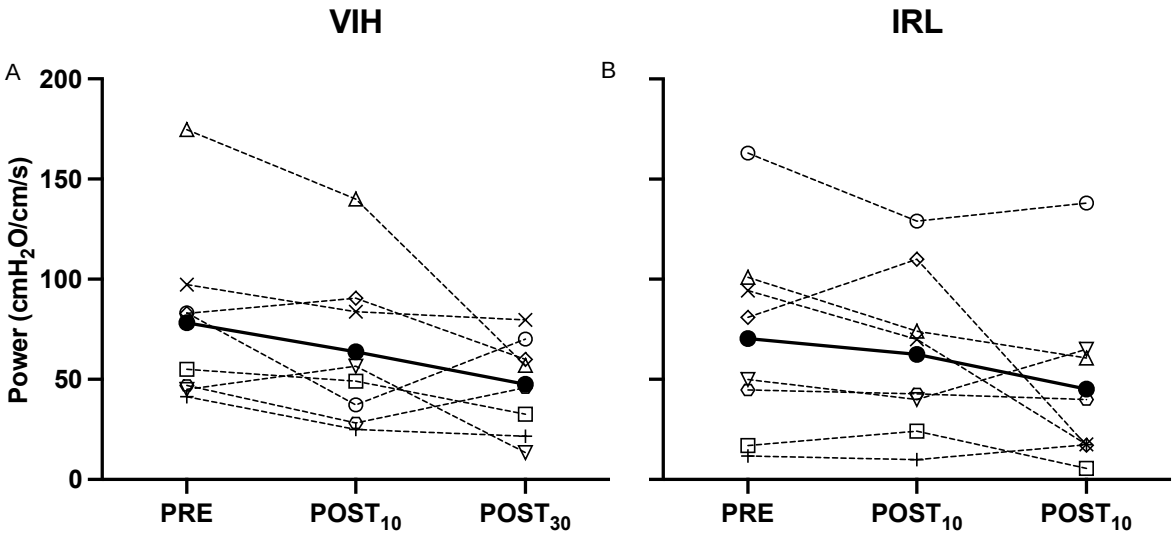

Figure 7.3.6 Individual responses (---) and group mean (—) *peak* responses to hyperpnoea in diaphragm power pre- and post-loading. Data are for eight participants.

7.4 Discussion

7.4.16 Main findings

This is the first study to assess effect of external loading on dynamic contractile properties of human diaphragm *in vivo* using subcostal ultrasonography. The main finding was that external loading of the inspiratory muscles using pressure-loading (IRL), but not flow-loading (VIH), caused a substantial loss of stimulation-evoked diaphragm twitch force and excursion velocity, resulting in a significant loss of evoked power to approximately half of pre-fatigue baseline values. Also following pressure-loading, most participants met the ventilatory demand imposed by CO_2 by adopting a breathing pattern of smaller tidal volumes, higher respiratory frequency and a reduced diaphragm force output at a given level of CO_2 compared to pre-loading. However, diaphragm kinetics appeared to be well-preserved, even at the peak of hyperpnoea. Although task-dependency of diaphragm muscle fatigue could not be clearly demonstrated in this study, the findings show that subcostal ultrasonography of the crural diaphragm can be used to quantify loading-induced changes in response to twitch contractions.

7.4.17 Mechanisms of diaphragm muscle fatigue

The external loading tasks applied in this study was a pressure-loaded task (IRL) and a flow-loaded task (VIH) that targeted opposite ends of the force-velocity spectrum. Both loading tasks have previously been shown to induce substantial fatigue of the diaphragm in the form of reduced $\Delta P_{di,tw}$ (Luo et al., 2001) or increased relaxation rate of maximal sniffs (Mulvey et al., 1991). McCool et al. (1992) also used similar tasks to elicit a loss in $P_{di,max}$ and maximal inspiratory flow in an attempt to demonstrate task-dependency of diaphragm fatigue, although loading tasks here were continued until 'task failure' instead of pre-determined task durations (as applied in the present study).

In line with the study hypothesis, $\Delta P_{di,tw}$ was reduced post-IRL, but not after VIH. The prolonged inspiratory duty cycle during IRL (0.56 ± 0.06) in combination with high load ($\overline{P}_{di}/P_{di,max}$ 77 ± 8%) may limit, or even fully occlude, blood flow to the diaphragm, and thereby greatly reduce O_2 supply to the working muscle (Bellemare et al., 1983; Bellemare & Grassino, 1982). In the absence of O_2, the muscle must instead rely on anaerobic metabolic pathways that result in an accelerated accumulation of anaerobic by-products (e.g., $H^+$and P_i). In turn, intra-muscular pH declines, reducing sarcoplasmic reticulum Ca^{2+} release and reuptake (Allen et al., 2008). Moreover, because H^+ competes with Ca^{2+} in troponin binding, intra-cellular accumulation of H^+ also has an inhibitory effect on actin-myosin interaction, further favouring

a decline in force (Allen et al., 2008; Sundberg & Fitts, 2019). Indeed, this finding is in line with the early work of Bellemare & Grassino (1982), who suggested that a diaphragm contractile pattern above the critical PTI_{di} (0.15-0.18) elicits fatigue via blood flow limitation to the muscle. Thus, a PTI_{di} of 0.43 ± 0.06 (see Table 7.3.2) was likely sufficient load to induce fatigue of the diaphragm.

The reductions in force ($\Delta P_{di,tw}$) were negligible post-VIH. Although this finding is in line with the study hypothesis, the low force-high velocity task (2-min VIH) was not associated with slowing of excursion velocity as originally hypothesised. Even though a similar protocol has been shown to induce substantial diaphragm fatigue – in the form of reduced $\Delta P_{di,tw}$ (Luo et al., 2001; Mulvey et al., 1991) and maximal inspiratory flow during volitional efforts (McCool et al., 1992) – these findings could not be replicated in the present study. Thus, the loading task may have been insufficient to elicit diaphragm fatigue in the present study sample. This notion is supported by the PTI_{di} during VIH (0.16 ± 0.07), which was barely above the critical PTI_{di} of 0.15-0.18 (Bellemare & Grassino, 1982). It is also worth noting that the majority of participants were physically active, with some engaged in competitive sport (e.g., middle-distance running, rowing, volleyball and rugby). Accordingly, the VIH protocol may have offered inadequate load to elicit diaphragm fatigue in the most highly endurance-trained participants (Babcock et al., 1996; Johnson et al., 1993).

7.4.18 Effect of loading on hypercapnic hyperpnoea

Slope responses

A modified Read rebreathe method (1966; 1967) was used to assess the effect of external loading on ventilation, breathing pattern and intrathoracic pressures, as well as on ultrasound-derived diaphragm kinetics (i.e., excursion, excursion velocity and power). Although rebreathe methods are frequently used to assess the effect of respiratory muscle fatigue on physiological and neuromechanical indices, there is an inherent variability associated with the ventilatory response to CO_2 (Spengler & Shea, 2001). This methodological challenge was discussed in detail in Chapter 5, and has also been remarked by others (e.g. Jensen et al., 2010; Sahn et al., 1977). To reduce the variability of ventilatory response to CO_2, it is worth emphasising that steps were taken to standardise our laboratory conditions (e.g., light, temperature and noise), and that a thorough familiarisation test was instituted prior to the experimental visit to reduce the potential influence of arousal level (Spengler & Shea, 2001; section 3.3 in General Methods).

In the present study, the ventilatory slope response ($\dot{V}_I$ vs. $P_{ET}CO_2$) changed from pre- to post-IRL. More specifically, the ventilatory slope was ~8-10% steeper post-IRL, which is in stark contrast to earlier reports on the influence of inspiratory muscle fatigue on CO_2 sensitivity. For instance, the majority of former studies have measured a reduced (Mador & Tobin, 1992; Moxham et al., 1982) or unaltered (Yan, Lichros, et al., 1993; Yan, Sliwinski, et al., 1993) ventilatory response to CO_2 after the induction of respiratory muscle fatigue. However, there is reason to believe that the group mean slope response at pre-IRL was subnormal, as there were two participants who did not have a marked ventilatory response to CO_2 during this initial trial (slope responses ≤0.1 L/min/mmHg), yet demonstrated normal responses during the two remaining trials (slope responses ≥1.20 L/min/mmHg). It is not entirely clear why these two participants did not have a pronounced ventilatory response at pre-IRL. It is known, however, that ventilatory responses to CO_2 are influenced by 'inherent noise', consisting of undefined physiological variability (incl. circadian variability) and random and/or systematic fluctuations in measurement error (Spengler & Shea, 2001). It must be noted that both experimental visits were performed at the same time of day to avoid the influence of circadian variability, and that participants were asked to refrain from caffeine ≥12 h prior to visits to eliminate the influence of caffeine on ventilatory response to hypercapnia (D'Urzo et al., 1990).

In addition, breathing pattern (i.e., V_{TI}, f_R, T_I and T_I/T_{TOT}) was altered from pre- to post-IRL (see Table 7.3.4), and upon evaluating individual slope responses it was evident that the majority of participants adopted a tachypnoeic breathing pattern (i.e., lower V_{TI} and higher f_R) combined with decreased $\overline{P}_{di,a}$ for a given level of CO_2 after IRL. These results align with the findings of Yan et al. (1993), who found that participants adopted a tachypnoeic breathing pattern with decreased P_{di} (tidal swings) after inducing global inspiratory muscle fatigue by IRL until task failure. When inducing fatigue of the diaphragm specifically, however, Yan et al. (1993) reported that the ventilatory response and breathing pattern were both unaltered, suggesting that only global inspiratory muscle fatigue adversely affects ventilation and breathing pattern. A third observation was made by Mador & Tobin (1992), who showed that global inspiratory muscle fatigue reduced ventilatory response to CO_2 but without adversely affecting breathing pattern. Conclusively, the effect of diaphragm fatigue on ventilation and breathing pattern is not fully understood, and should be the subject for future investigations.

Peak responses to CO_2

Traditionally, only slope responses have been considered when assessing the effect of respiratory muscle fatigue on hypercapnic ventilation, breathing pattern and intrathoracic pressure responses (Luo et al., 2001; Mador & Tobin, 1992; Yan, Lichros, et al., 1993; Yan, Sliwinski, et al., 1993). Results from Chapter 5, however, showed that diaphragm kinetics could be reliably measured with AM-mode ultrasound at the peak of hyperpnoea (Table 5.3.4), as technological limitations prevents breath-by-breath acquisition of ultrasound throughout the entire duration of the test. In the present study, however, none of the peak responses to CO_2 were adversely affected by either of the two loading tasks (Table 7.3.5 and Figure 7.3.5). One may wonder, therefore, whether the Read rebreathe test imposes adequate load on the respiratory system to expose potential acute changes in diaphragm kinetics and contractile function. Afterall, $\dot{V}_I$ reached ~15-17% of MVV_{12} with a $\overline{P}_{di}$ of 12-19% of $P_{di,max}$, which suggests that the ventilatory load was small relative to maximum capacity. Considering that significant fatigue-induced changes in breathing pattern appear to be more pronounced during high-intensity (≥75% of maximal work load) whole-body exercise sustained to exhaustion (Mador & Acevedo, 1991), one may not be able to fully observe the effect of diaphragm fatigue during CO_2-rebreathe.

7.4.19 Ultrasonography for the assessment of diaphragm fatigue

Ultrasonography has proven to be a useful tool for assessing skeletal muscle anatomy and architecture, as well as muscle deformation during dynamic contractions (Hodges et al., 2003; Hooren & Teratsias, 2020; Pillen, 2010). With measurements considered both reliable and valid, ultrasonography also provides a non-invasive method of monitoring acute muscular changes with fatigue (Sheng et al., 2020; Witte et al., 2006) and chronic adaptation associated with atrophy and weakness (Goligher, Laghi, et al., 2015; Nakanishi et al., 2019). Diaphragm ultrasonography, specifically, is a well-established tool in the ICU and has replaced fluoroscopy (Houston et al., 1992, 1995) and magnetic resonance imaging (Gierada et al., 1995) for the assessment of diaphragm craniocaudal excursion. Crural diaphragm ultrasonography has been used primarily to identify diaphragm paralysis and weakness (Gerscovich et al., 2001; Gottesman & McCool, 1997), to monitor patient-ventilator interactions (Matamis et al., 2013; Umbrello et al., 2015) and to predict weaning outcome (Dres et al., 2017). Until now, however, the use of ultrasonography to identify diaphragm muscle fatigue has not been addressed adequately.

As stated in the Introduction, Kocis et al. (1997) showed that subcostal ultrasonography could be used to quantify diaphragm contractile velocity – in the form of excursion velocity – during hypercapnic hyperpnoea in piglets. After the induction of diaphragm fatigue by transvenous phrenic nerve pacing (2000 ms trains at 30 Hz and 15-25 mV with duty cycle 0.33), the authors showed that the fatigue-induced loss of diaphragm force (P_{di}; –25%) was associated with an even greater loss of contractile (excursion) velocity (–33%; from 12 ± 3 cm/s to 8 ± 1 cm/s) during dynamic contractions. Nevertheless, these findings could not be replicated in the present study, as neither diaphragm excursion nor excursion velocity during hyperpnoea were significantly affected by loading (Figure 7.3.5). One explanation for this discrepancy may be the different loading tasks used in the two studies: whilst IRL and VIH induce low-frequency fatigue under physiological conditions using volitional muscle contractions (Jones, 1996; Moxham et al., 1981), there is evidence that phrenic nerve pacing (i.e., repetitive stimulation) may impair diaphragm contractility by disturbing the excitation-contraction coupling at the sarcolemma and t-tubular system secondary to ionic disturbances (Kido et al., 1988; Stephenson et al., 1995). In addition, because phrenic nerve pacing is non-volitional, the technique may induce a more severe degree of fatigue, and thereby impair muscle contractility to a greater extent than what can be achieved with volitional contractions.

7.4.20 Methodological considerations

Post-activation potentiation

Post-loading measurements were made at 10 and 30 min after both loading tasks. Although evidence suggests that post-activation potentiation of the diaphragm should be diminished within 10 min (Mador, Magalang, et al., 2000), there may be participants with elevated $\Delta P_{di,tw}$ up to 20 min post-activation; particularly after contractions of high force (≥ 75% of $P_{di,max}$) and long duration (Wragg et al., 1994). Consequently, it cannot be ruled out that post-activation potentiation was still present at $POST_{10}$, particularly after IRL. If this were the case, the effect of loading on $\Delta P_{di,tw}$ may have been underestimated. Similarly, evidence from medial gastrocnemius suggests that muscle fibre shortening and shortening velocity increase with prior activation (MacIntosh & Bryan, 2002). Indeed, as shown in Chapter 4, ultrasound-derived diaphragm excursion tended to increase with potentiation, suggesting that the effect of loading on excursion velocity and power may have been underestimated in the presence of potentiation.

Task-dependency of diaphragm muscle fatigue

The aim of this study was to assess the effect of two external loading tasks (a low force-high velocity task and a high force-low velocity task) to elucidate the mechanisms that underpin task-dependency of diaphragm fatigue. However, despite our efforts to create isolated force- and velocity-based tasks, it is evident that the two tasks cannot be fully isolated *in vivo*. For instance, the muscle contractions required to generate square-wave intrathoracic pressures during IRL are dynamic, involving a high rate of pressure development ('rising edge' of square wave) before entering the sustained, quasi-isometric phase. As a result, the high force-low velocity task may encroach on the velocity side of the force-velocity spectrum, and thereby explain why diaphragm twitch excursion velocity was significantly impaired after IRL. Similarly, the pressure generation during VIH was substantial (33% of $P_{di,max}$), making the diaphragm susceptible to pressure loading even during an 'unloaded' task.

McCool et al. (1992) investigated the task-dependency of inspiratory muscle fatigue using a 'pressure task' (IRL with a target oesophageal pressure-time product of 40-50 cmH_2O) and a 'flow task' (eucapnic hyperpnoea targeting peak inspiratory flow of 5-6 L/s), with both performed until 'task failure'. The authors found that maximal inspiratory muscle force (i.e., $P_{oe,max}$ measured against a closed glottis) was significantly lower after the force task compared to the flow task (–25 ± 7% vs. –8 ± 8%). Conversely, maximal inspiratory flow, measured during a maximal inspiratory effort without added resistance, was significantly lower after the flow task compared to the pressure task (–16 ± 3% vs. –3 ± 4%). The study by McCool et al. (1992) was the first to investigate fatigue task-dependency of inspiratory muscles in humans. Moreover, the study suggested that fatigue task-dependency of inspiratory muscles may be similar to that found in isolated diaphragm fibre preparations *in vitro* (Ameredes et al., 2006; Coirault et al., 1995). Compared to the study by McCool et al. (1992), which used volitional (effort-dependent) manoeuvres, the strength of the present study was that diaphragm function was assessed using non-volitional perturbations (bilateral phrenic nerve stimulation and CO_2-rebreathe). Moreover, McCool et al. (1992) used maximal inspiratory flow as a surrogate measure of inspiratory shortening velocity, whereas the present study imaged diaphragm velocity at the level of the muscle, thereby providing a direct measure of diaphragm contractile velocity.

Diaphragm muscle fatigue versus global inspiratory muscle fatigue

Maximal sniffs were performed to assess the dynamic, volitional activation of the inspiratory muscles before and after the two loading tasks. Following IRL, there was a reduction in $\Delta P_{di,sn}$

(–12%) and $\Delta P_{oe,sn}$ (–17%), but no change in $\Delta P_{ga,sn}$ (+0.25%). Given that we specifically targeted the diaphragm with the loading tasks, a reduction in $\Delta P_{di,sn}$ is not unexpected. However, given that the reduction in $\Delta P_{di,sn}$ was a result of a reduction in $\Delta P_{oe,sn}$ only, it is likely that accessory inspiratory muscles were fatigued after IRL (Laroche et al., 1988). Indeed, inspiratory loading tasks are usually performed with substantial contribution from the external intercostals (Roussos et al., 1979), sternocleidomastoids (Ramsook et al., 2016), as well as chest wall and trunk muscles (e.g., latissimus dorsi, scalenes, pectoralis major and parasternal intercostals) (Cala et al., 1992). It should, therefore, be considered that fatigue of the diaphragm, as well as of the accessory inspiratory muscles, may have been present in the participants following IRL.

7.5 Conclusion

Pressure-loading (IRL), but not flow-loading (VIH), caused a decline in stimulation-evoked diaphragm twitch force and excursion velocity, resulting in a substantial loss of evoked power to approximately half of pre-loading baseline values. Also following pressure-loading, most participants exhibited impaired diaphragm force and adopted a tachypnoeic breathing pattern to meet ventilatory demand. However, diaphragm kinetics appeared to be well-preserved, even at the peak of hyperpnoea. Although task-dependency of diaphragm muscle fatigue could not be clearly demonstrated in this study, ultrasonography still offers novel insight into the dynamic contractile properties of the human diaphragm that may shape our understanding of how the muscle is impacted by external loading.

Chapter 8

Application of *Intercostal* Ultrasonography for the Assessment of Pressure-Flow Specificity of Diaphragm Fatigue in Healthy Men

8.1 Introduction

Skeletal muscle fatigue is characterised by a loss of force and/or slowing of shortening velocity, resulting in a marked decline in skeletal muscle power and increased curvature of the force-velocity relationship (Fitts, 1994; Jones, 2010). While the loss of force is the result of increased levels of myofibrillar hydrogen (H^+) and inorganic phosphate (P_i) associated with intense muscular activity, the slowing of shortening velocity is attributed to transient increases of ADP in the myoplasm (Fitts, 1994, 2008). Moreover, fatigue induced by dynamic contractions of heavy load has been associated with impaired fibre shortening (Mardini & McCarter, 1987); likely caused by dephosphorylation of the regulatory light chain of myosin filament (Hortemo et al., 2013; Munkvik et al., 2009). Evidently, our current understanding of contractile properties of fatigued skeletal muscle is primarily derived from studies *in vitro* and *in situ* using isolated fibre preparations. However, to better understand contractile properties of skeletal muscle *in vivo*, ultrasonography has become a useful tool to assess fatigue-induced changes in locomotor muscle architecture (Pillen, 2010), strain (Sheng et al., 2020), and shear modulus (Morel et al., 2019). Perhaps the most consequential muscular changes detectable with ultrasound are the acute shortening of fascicle length and increase of pennation angle (Brancaccio et al., 2008; Mademli & Arampatzis, 2005), as both phenomena alter the length-tension properties of the intact muscle.

For the respiratory muscles, the use of ultrasonography has primarily been limited to the ICU as a non-invasive tool to monitor diaphragm function. In clinical populations, ultrasound-derived measures of costal diaphragm thickening (an estimate of costal diaphragm shortening) are strongly related to breathing effort during spontaneous breathing (Umbrello et al., 2015). Diaphragm thickening is also related to PTI_{di} during quiet breathing (Vivier et al., 2012); that is, an established estimate of diaphragm contractile function. Moreover, the absolute thickness of costal diaphragm is strongly related to $P_{di,max}$ and MIP in healthy individuals and clinical populations (McCool, Benditt, et al., 1997; McCool, Conomos, et al., 1997; Ueki et al., 1995). Overall, these reports suggest that the structural attributes of the costal diaphragm, and its ability to thicken (shorten), closely reflect the muscle's ability to generate force. Based on these considerations, it is intuitive that acute changes in diaphragm contractile properties, as induced by external loading and fatigue, can be identified and quantified using ultrasonography.

Indeed, ultrasound-derived measures of costal diaphragm thickness and thickening exhibit excellent repeatability and reproducibility during quiet breathing (Baldwin et al., 2011;

Goligher, Laghi, et al., 2015; Harper et al., 2013). As recalled from Chapter 4 and 5, ultrasound-derived diaphragm thickness and thickening also exhibit good-to-excellent within-day reliability in response to evoked twitch contractions, maximal sniffs and hypercapnic hyperpnoea. Yet, it has not been determined if costal diaphragm is susceptible to impairments after external loading, and to what extent these potential impairments may be quantified using ultrasound.

8.1.1 Aims and hypotheses

The aim of this study was to determine the effect of two external loading tasks (pressure- and flow-loading) on ultrasound-derived thickening (shortening) of costal diaphragm. In line with our current understanding of peripheral muscle fatigue, and in light of recent technological advances in the area of diaphragm ultrasonography, it was hypothesised that external loading of the diaphragm, regardless of loading task, would impair ultrasound-derived diaphragm thickening alongside a loss in diaphragm force (pressure).

8.2 Methods

Except from the ultrasonography approach, the methods used in this study were identical to those described in Chapter 7. To avoid unnecessary repetition, this section includes only an abridged description of the methods, and the reader is referred to the previous chapter and General Methods for additional details. It is also worth noting that the intention was to include eight participants in this study. However, data collection was put to a halt during the spring of 2020 due to the outbreak of COVID-19, and the subsequent closure of university laboratories. Accordingly, only six participants completed all experimental visits before university closure.

8.2.2 Ethical approval and participants

This study was approved by Brunel University Research Ethics Committee (Appendix 1), and conformed to the most recent standards set by the Declaration of Helsinki (World Medical Association, 2013). Six healthy, non-smoking men between the ages of 18 and 40 y volunteered to participate. Three participants had previously participated in Chapter 7, and were thus familiar with the study protocol. Only participants of (self-reported) male sex were included in this study due to the limited resources and time available to include female participants and to control for menstrual cycle phase in multi-visit studies (see section 3.3 for additional details). All participants reported to have no medical history of cardiovascular, respiratory or neuromuscular disease using a standardised health questionnaire (Appendix 2). Exclusion criteria were BMI $\geq$30 kg/m^2, and pulmonary function and maximal respiratory mouth pressures

outside limits of normal (Evans & Whitelaw, 2009; Quanjer et al., 2012; Stocks & Quanjer, 1995). It was ensured that participants' right costal diaphragm could be clearly imaged with ultrasound, and that all participants exhibited costal diaphragm thickening during quiet breathing (Harper et al., 2013). Written informed consent was provided prior to the study (Appendix 2), and participants were asked to abstain from vigorous exercise for ≥24 h, caffeine and alcohol for ≥12 h, and food for ≥3 h prior to each visit.

8.2.3 Experimental overview

Participants visited the laboratory on three occasions, each separated by no less than 48 h and no more than 14 d. The first visit was for screening and familiarisation, during which participants performed pulmonary function tests and were thoroughly familiarised with the experimental set-up. The subsequent two visits were experimental trials, and involved a *low force-high velocity* task (voluntary isocapnic hyperpnoea [VIH]), or a *high force-low velocity* task (inspiratory resistive loading [IRL]). The two trials were performed in randomised order and at the same time of day. Diaphragm contractile properties were assessed before (PRE) and at 10 and 40 min after the loading tasks ($POST_{10}$ and $POST_{40}$, respectively), as intrathoracic pressures, EMG_{di}, ventilatory indices, and ultrasound-derived diaphragm thickening in response to phrenic nerve stimulation, maximal sniffs and hypercapnic hyperpnoea.

8.2.4 Screening and familiarisation

Screening and familiarisation were performed as described in Chapter 7 (section 7.2.4). Briefly, familiarisation included a thorough familiarisation with bilateral phrenic nerve stimulation and the CO_2-rebreathe test, including a practice rebreathe test. Participants also received verbal instructions from the investigator on how to perform external loading tasks, followed by shortened practice trials of each task, comprising 1 min of VIH and 5 min of IRL (see details below).

8.2.5 Pressure- and flow-loading

Voluntary isocapnic hyperpnoea (VIH)

Participants breathed through a flanged mouthpiece connected to a three-way valve (112050-2100, Hans Rudolph Inc., KS, USA) while wearing a nose-clip. The valve was connected to a flow-turbine and an open-ended rebreathe tube, and, to maintain isocapnia, humidified hypercapnic gas (5% CO_2 and 95% O_2) was fed into the distal end of the tube whenever $P_{ET}CO_2$ dropped below resting values. The protocol was performed for 2 min under the instruction to 'breathe as much as you can from the onset of the test and continue without pacing'. Participants

could see their minute ventilation on a computer screen and were verbally encouraged to keep the value as high as possible throughout the test.

Inspiratory resistive loading (IRL)

Participants breathed through a modified two-way, non-rebreathing valve (50-0975, Harvard Apparatus, Cambridge, UK), which offered resistance on inspiration and negligible resistance on expiration (<0.1 kPa at 15 L/s). Inspiratory resistance was created by a rubber stopper with individualised orifice sizes (ID 2.5-4.0 mm) that allowed the participant to inhale maximally as a square wave with a duty cycle of 0.60 for five consecutive minutes. The protocol consisted of 3 × 5 min intervals with loaded breathing, each separated by 5 min of rest. Participants performed maximal inspiratory efforts with a T_I/T_{TOT} of 0.60 and f_R of 12 breaths/min with assistance from dual-tone auditory queues. Diaphragm activation was targeted by participants placing one hand on their abdomen with the emphasis on moving only the abdomen (not rib cage) during inspiratory efforts (Ramsook et al., 2016). The $P_{ET}CO_2$ and SpO_2 via earlobe pulse oximetry (2500A, Nonin Medical Ltd., Plymouth, US) were monitored throughout the trial.

8.2.6 Supramaximal phrenic nerve stimulation and sniffs

Bilateral stimulation of the phrenic nerves was performed using two figure-eight coils (The Magstim Company Ltd., Carmarthenshire, UK) positioned on the anterior borders of sternocleidomastoids (Mills et al., 1995). To check for supramaximal stimulation, participants underwent an incremental stimulation protocol consisting of three single twitches at stimulation intensities ranging from 50 to 100% of the stimulators' maximum power (see details in General Methods, section 3.9). Supramaximal stimulation was defined when mean $\Delta P_{di,tw}$ at submaximal and maximal stimulation power were equal to or less than the coefficient of variation (CV) for all twitches within an individual participant (Geary et al., 2019; Man et al., 2004).

Five successfully evoked, supramaximal twitches were performed at relaxation volume with participants wearing a nose-clip. Stimulations were performed at 100% of maximum stimulator before and after (10 and 40 min) each loading condition. Participants also performed five maximal sniffs from relaxation volume under the instructions to perform 'a short, sharp sniff' (Miller et al., 1985, p. 92). Each twitch and sniff was separated by 30 s to avoid post-activation potentiation (Wragg et al., 1994).

8.2.7 Hypercapnic hyperpnoea (CO_2-rebreathe)

Hyperpnoea was induced by the CO_2-rebreathe method as described in section 3.11 and Chapters 5-7, and similar to that described by Read et al. (1966; 1967). The test was terminated when $P_{ET}CO_2$ reached 7.33 kPa (55 mmHg), and laboratory conditions were kept stable and quiet before (rest), during and after (recovery) each test (Homma & Masaoka, 2008; Spengler & Shea, 2001).

8.2.8 Assessment of ventilatory and gas-exchange indices

Pulmonary airflow and gas-exchange were measured breath-by-breath using a metabolic cart with online gas analysis system (Oxycon Pro, Jaeger, Viasys Healthcare, Hoechberg, Germany), comprising a calibrated turbine flow-meter and O_2 and CO_2 gas analysers. Digital signals from the metabolic cart were input into the data acquisition system using an external device (DAQ-30A16, Eagle Technology, Cape Town, South Africa) and recorded online as waveforms. Inspired and expired tidal volumes were calculated offline by numerical integration of flow using a bespoke script (Horseman, 2020a).

8.2.9 Assessment of intrathoracic pressures and EMG_{di}

The P_{oe}, P_{ga} and EMG_{di} were measured using a gastro-oesophageal catheter (Gaeltec Devices Ltd., Isle of Skye, Scotland), as described in section 3.6.5 in General Methods. Briefly, the catheter was passed pernasally and swallowed into the stomach via peristalsis. The position of the catheter was adjusted such that a maximal sniff elicited negative and positive deflections in P_{oe} and P_{ga}, respectively. The correct position was confirmed with the "dynamic occlusion test" (Baydur et al., 1982), before the catheter was taped in position at the nose. Upon acquisition, the analogue signals for intrathoracic pressures and EMG_{di} were passed through a signal amplifier (1902, CED, Cambridge, UK) and digitised at sampling frequencies of 200 Hz (pressures) and 4 kHz (EMG_{di}) using an analogue-to-digital converter (1401mk-II, CED). Transdiaphragmatic pressure (P_{di}) was calculated online by subtraction of P_{oe} from P_{ga}.

8.2.10 Diaphragm ultrasonography for costal diaphragm thickening

Ultrasonography of costal diaphragm thickening was performed as described in Chapter 4 and 5 (*Part 2*). All scans were performed using a commercially-available system (Vivid 7, GE Medical). A high-frequency, linear ultrasound transducer (4.0-11.0 MHz, 10L, GE Medical) was positioned at the right anterior or mid-axillary line at the 8-10th intercostal space.

All cine-loops were recorded as B-mode and analysed offline (EchoPac v6.1, GE Medical). In response to evoked twitches and maximal sniffs, diaphragm thickness was measured as the

distance between the inner borders of the pleural and peritoneal membrane at relaxation volume (immediately prior to twitch), and at peak thickness in response to twitch. During hyperpnoea, diaphragm thickness was measured at EELV and at EILV. Costal diaphragm thickening was calculated as *1*) thickening ratio = peak thickness / thickness at relaxation volume; and *2)* thickening fraction = (peak thickness – thickness at relaxation volume) / thickness at relaxation volume (Ferrari et al., 2018).

8.2.11 Data processing and time-matching

Evoked twitch and sniff pressure responses were measured as the absolute pressure swing from point of stimulation to peak pressure ($\Delta P_{di,tw}$, $\Delta P_{oe,tw}$ and $\Delta P_{ga,tw}$). End-expiratory oesophageal and gastric pressures (EEP_{oe} and EEP_{ga}) were measured at the point of stimulation. The peak-to-peak amplitude of the compound muscle action potential (M-wave) was assessed as a measure of neuromuscular propagation. Phrenic nerve conduction time (latency) was measured from the time of stimulation to the onset of the evoked potential (Aldrich et al., 2005; Luo et al., 1999).

During hyperpnoea, ventilatory indices ($\dot{V}_I$, V_{TI}, f_R, T_I, T_I/T_{TOT}) and intrathoracic pressures (P_{di}, P_{ga} and P_{oe}) were recorded on a breath-by-breath basis at rest, during CO_2-rebreathe and the three subsequent minutes of recovery, and then analysed offline: breath was marked at the point of zero flow, and anomalous breaths were manually excluded from the analysis. Ventilatory indices were expressed for inspiration only.

Tidal pressures were calculated as the active components of mean inspiratory pressure ($\overline{P}_{di,a}$, $\overline{P}_{ga,a}$ and $\overline{P}_{oe,a}$), using the equation from Barnard & Levine (1986) with $\overline{P}_{di,a}$ as an example:

$$\bar{P}_{di,a} = \Sigma_0^n P_{di}/n,$$

where baseline P_{di} (*0*) was the P_{di} immediately preceding the inspiratory upswing, and *n* was equal to the number of data points during inspiration. Accordingly, $\overline{P}_{di,a}$ was the mean pressure generated during tidal inspiration based on tidal pressure swings, without the passive component of inspiratory pressure. See General Methods, section 3.6.5 for details.

To characterise the force output of the diaphragm during loading tasks, the pressure-time product was calculated as the integral of pressure down to zero during inspiration ($\int P_{di}$). For the cumulative force output generated during loading tasks, $\int P_{di}$ was first multiplied by f_R, and then multiplied by the duration of each fatigue task ($\Sigma \int P_{di} \times f_R$). Diaphragm pressure-time index (PTI_{di}) was calculated as ($\overline{P}_{di}/P_{di,max}$) × ($T_I/T_{TOT}$) (Bellemare & Grassino, 1982).

Ultrasound cine-loops were recorded over 15 s every 30 s during hyperpnoea and the three subsequent minutes of recovery (1 × 30 s for rest). All breaths recorded within the 15 s cine-loop (1 × 30 s for rest) were identified in the data acquisition system (i.e., intrathoracic pressures and ventilatory indices), then averaged over 15 s (30 s for rest). The final 15 s of hyperpnoea, independent of test duration, was recorded and defined as the *peak* response.

8.2.12 Statistics

Statistical analysis was performed using GraphPad Prism (v9.0, GraphPad Software LLC, San Diego, USA) and Microsoft Excel (v16.4, Microsoft Corp., Washington, USA). During hyperpnoea, the rate of change (slopes) in ventilatory indices ($\dot{V}_{I,}$ f_R, V_{TI}, T_I and T_I/T_{TOT}) and intrathoracic pressures ($\overline{P}_{di,a}$, $\overline{P}_{ga,a}$ and $\overline{P}_{oe,a}$) with respect to $P_{ET}CO_2$ were calculated for each participant using simple linear regression. The slopes were converted into *t*-scores using the equation:

$$t = \frac{b_1 - b_2}{\sqrt{S^2 b_1 + S^2 b_2}}$$

where b_1 and b_2 are the two slopes being compared, and *S* is the standard error of the slopes (Zar, 2014). Accordingly, individual slopes (not group mean) could be compared between timepoints and conditions using two-tailed, paired samples *t*-test.

Diaphragm fatigue was considered present if there was a ≥10% decline in $\Delta P_{di,tw}$ relative to PRE-loading (Mador, Kufel, et al., 2000). This definition of fatigue coincided with a change in $\Delta P_{di,tw}$ that was two-to three-fold greater than the normal variability observed in the same group of participants for bilateral phrenic nerve stimulation (CV = 3.2%; see Chapter 4, Table 4.3.10). Loading-induced changes in individual slope responses for ventilation, breathing pattern and intrathoracic pressures during hyperpnoea were considered present if the slopes were statistically different from PRE-loading. Meaningful changes in slope or peak responses to hyperpnoea were considered present when there was a change two-fold greater than the normal variability (CV) observed in the same group of participants in Chapter 5 (Table 5.3.7). Statistical significance was set at $p \leq 0.05$ and data are shown as mean ± *SD*.

8.3 Results

8.3.13 Participant characteristics and loading tasks

Participant characteristics are shown in Table 8.3.1. In line with inclusion criteria, participants exhibited pulmonary flows, volumes and capacities within normal limits. This was the case also for maximal respiratory mouth pressures. Diaphragm structure and function was within the ranges reported elsewhere for healthy men.

Table 8.3.1 Participant characteristics.

	Mean ± *SD*
Anthopometry	
Age, y	24.0 ± 7.3
Stature, cm	183.0 ± 5.6
Body mass, kg	81.2 ± 6.8
BMI, kg/m^2	24.4 ± 2.5
Chest depth, cm	21.8 ± 3.1
Chest width, cm	31.2 1.7
Chest circumference, cm	95.3 ± 3.4
Pulmonary function	
TLC, L (% predicted)	7.85 ± 0.81 (104 ± 8)
RV, L (% predicted)	1.99 ± 0.19 (118 ± 13)
FRC_{pleth}, L (% predicted)	3.89 ± 0.77 (113 ± 20)
FVC, L (% predicted)	6.27 ± 0.61 (107 ± 11)
FEV_1, L (% predicted)	5.06 ± 0.52 (104 ± 8)
FEV_1/FVC (% predicted)	0.80 ± 0.07 (95 ± 7)
MVV_{12} (% predicted)	202 ± 21 (100 ±13)
Maximal respiratory pressures	
MIP, cmH_2O (% predicted)	–129 ± 19 (118 ± 22)
MEP, cmH_2O (% predicted)	179 ± 51 (118 ± 40)
Diaphragm structure and function	
Diaphragm thickness at FRC, mm	1.50 ± 0.51
Diaphragm thickness at TLC, mm	4.22 ± 0.63
Thickening fraction, %	181 21
Maximal diaphragm mobility, cm	6.9 ± 1.4

Data are mean ± *SD* for six participants. BMI, body mass index; TLC, total lung capacity; RV, residual volume; FRC_{pleth}, functional residual capacity via plethysmography; FVC, forced vital capacity; FEV_1, forced expiratory volume in 1 s; MVV_{12}, maximal voluntary ventilation in 12 s; MIP, maximum inspiratory mouth pressure; MEP, maximum expiratory mouth pressure. Predicted values for pulmonary function were derived from Quanjer et al. (2012) for spirometry and Stocks & Quanjer (1995) for plethysmography. Predicted values for MVV_{12} were calculated as $FEV_1 \times 40$ (Miller et al., 2005). Predicted values for maximum mouth pressures were from Evans & Whitelaw (2009).

Quantitative characteristics of the two loading tasks are shown in Table 8.3.2. As there were no apparent differences between the three intervals of IRL, data are shown as mean ± *SD* for the three intervals combined. By design, the two conditions exhibited different ventilatory and pressure characteristics, targeting the two extremes of the force-velocity spectrum. During VIH, minute ventilation was high for the initial ~20 s (~210 L/min; 103% of MVV_{12}), before stabilising at ~150 L/min (~74% of MVV_{12}) for the remaining duration.

Table 8.3.2 Ventilatory indices and diaphragm force output during voluntary isocapnic hyperpnoea (VIH) and inspiratory resistive loading (IRL).

	VIH	**IRL**
$\dot{V}_I$, L/min	145 ± 34	27 ± 7
V_{TI}, L	1.82 ± 0.43	3.21 ± 0.65
f_R, breaths/min	67 ± 11	11 ± 0.5
V_{TI}/Ti, L/s	4.81 ± 1.44	0.98 ± 0.34
T_I/T_{TOT}	0.52 ± 0.06	0.60 ± 0.08
$\overline{P}_{di}/P_{di,max}$, %	18.6 ± 10.4	51.1 ± 15.2
PTI_{di}	0.10 ± 0.05	0.30 ± 0.10
$\int P_{di}$, $cmH_2O/s/breath$	15.2 ± 5.4	56.5 ± 21.0
$\Sigma\int P_{di} \times f_R$, $cmH_2O/s/min$	2035 ± 792	9289 ± 4356

Data are mean ± *SD* for six participants. $\dot{V}_I$, inspiratory minute ventilation; V_{TI}, inspiratory tidal volume; f_R, respiratory frequency; V_{TI}/T_I, mean inspiratory flow; T_I/T_{TOT}, inspiratory duty cycle; $\overline{P}_{di}/P_{di,max}$, mean inspiratory transdiaphragmatic pressure relative to maximum transdiaphragmatic pressure; PTI_{di}, diaphragm pressure-time index ($\overline{P}_{di}/P_{di,max} \times T_I/T_{TOT}$); $\int P_{di}$, time integral of transdiaphragmatic pressure during inspiration; $\Sigma\int P_{di}$, sum of time integral of P_{di} over the total duration of loading task.

8.3.14 Supramaximal phrenic nerve stimulation

The $\Delta P_{di,tw}$ in response to incremental stimulation power are shown in Figure 8.3.1. A plateau in $\Delta P_{di,tw}$ (per the CV method described above) occurred at 90% (n = 2), 95% (n = 2) or at 100% (n = 1) prior to VIH, with one participant without an established plateau. Prior to IRL, participants exhibited plateau in $\Delta P_{di,tw}$ at 90% (n = 1), 95% (n = 3) or 100% (n = 2).

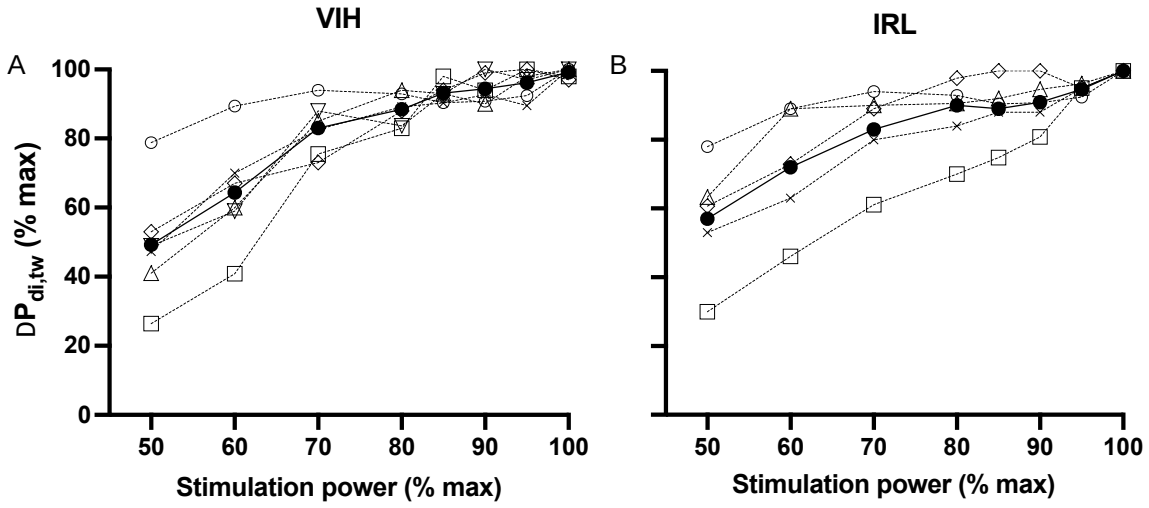

Figure 8.3.1 Individual participant (---) and group mean (—) $\Delta P_{di,tw}$ in response to increasing stimulation power prior to voluntary isocapnic hyperpnoea (VIH) and inspiratory resistive loading (IRL) trials. Data are for six participants.

Intrathoracic pressures and EMG$_{di}$

Twitch and sniff pressure responses are shown in Table 8.3.3. There were no apparent changes in $EEP_{oe,tw}$ across timepoints or loading condition, suggesting that phrenic nerve stimulation was performed at similar lung volume (diaphragm fibre length) across all perturbations. Similarly, $EEP_{ga,tw}$ did not appear to change across timepoints or loading condition, confirming that also abdominal compliance was similar across perturbations.

After VIH, the $\Delta P_{di,tw}$ declined by 9.9% (range 0 to –32%) at $POST_{10}$, and by 9.7% (–1 to –31%) at $POST_{40}$ relative to PRE. The majority of participants (n = 4) experienced their largest drop in $\Delta P_{di,tw}$ at $POST_{10}$. At this timepoint, these participants (n = 4) also exhibited ≥10% decline in $\Delta P_{di,tw}$ relative to pre-VIH. After IRL, the $\Delta P_{di,tw}$ declined by 11.5% (range 0 to –40%) at $POST_{10}$, and by 12.6% (0 to –30%) at $POST_{40}$ relative to PRE. Again, the majority of participants (n = 4) experienced their largest drop in $\Delta P_{di,tw}$ at $POST_{10}$, which also coincided with ≥10% decrement in $\Delta P_{di,tw}$. The remaining participants (n = 2) later experienced ≥10% decline in $\Delta P_{di,tw}$ at $POST_{40}$. Thus, diaphragm fatigue was confirmed in all participants after IRL.

Table 8.3.3 Evoked twitch and maximal sniff responses pre and post voluntary isocapnic hyperpnoea (VIH) and inspiratory resistive loading (IRL).

	PRE	POST$_{10}$	POST$_{40}$
VIH			
$\Delta P_{di,tw}$, cmH_2O	24.0 ± 10.2	21.6 ± 11.4	21.7 ± 11.5
$\Delta P_{oe,tw}$, cmH_2O	–13.5 ± 6.6	–10.9 ± 6.6	–10.9 ± 7.0
$\Delta P_{ga,tw}$, cmH_2O	14.2 ± 7.0	13.4 ± 6.5	13.1 ± 6.1
$EEP_{oe,tw}$, cmH_2O	–7.2 ± 4.5	–7.4 ± 5.2	–7.5 ± 5.2
$EEP_{ga,tw}$, cmH_2O	1.2 ± 8.2	1.1 ± 7.5	1.0 ± 7.5
$\Delta P_{di,sn}$, cmH_2O	118 ± 41	111 ± 49	112 ± 47
$\Delta P_{oe,sn}$, cmH_2O	–73 ± 28	–68 ± 22	–72 ± 21
$\Delta P_{ga,sn}$, cmH_2O	47 ± 42	44 ± 43	42 ± 45
$EEP_{oe,sn}$, cmH_2O	–6.8 ± 5.5	–7.0 ± 4.8	-6.9 ± 5.1
$EEP_{ga,sn}$, cmH_2O	1.3 ± 7.1	1.3 ± 7.0	1.1 ± 7.7
IRL			
$\Delta P_{di,tw}$, cmH_2O	26.4 ± 10.5	23.3 ± 12.2	23.1 ± 11.3
$\Delta P_{oe,tw}$, cmH_2O	–14.5 ± 4.3	–10.94 ± 4.95	–11.63 ± 4.8
$\Delta P_{ga,tw}$, cmH_2O	15.2 ± 7.5	15.4 ± 8.3	14.4 ± 6.7
$EEP_{oe,tw}$, cmH_2O	–5.0 ± 2.8	–4.8 ± 2.8	–5.1 ± 3.3
$EEP_{ga,tw}$, cmH_2O	3.8 ± 8.6	4.1 ± 9.1	4.1 ± 8.4
$\Delta P_{di,sn}$, cmH_2O	149 36	127 45	121 37
$\Delta P_{oe,sn}$, cmH_2O	–74 20	–68 14	–64 15
$\Delta P_{ga,sn}$, cmH_2O	79 54	62 58	60 48
$EEP_{oe,sn}$, cmH_2O	–6.5 5.5	–6.8 5.6	7.2 5.1
$EEP_{ga,sn}$, cmH_2O	0.9 6.1	1.1 7.0	1.2 6.3

Data are mean ± *SD* for six participants. $\Delta P_{di,tw}$; twitch transdiaphragmatic pressure; $\Delta P_{oe,tw}$; twitch oesophageal pressure; $\Delta P_{ga,tw}$, twitch gastric pressure; $EEP_{oe,tw}$, end-expiratory oesophageal pressure for twitch; $EEP_{ga,tw}$ end-expiratory gastric pressure for twitch; $\Delta P_{di,sn,}$ sniff transdiaphragmatic pressure; $\Delta P_{oe,sn}$, sniff oesophageal pressure; $\Delta P_{ga,sn}$, sniff gastric pressure; $EEP_{oe,sn}$, end-expiratory oesophageal pressure for sniff; $EEP_{ga,sn}$, end-expiratory gastric pressure for sniff.

After VIH, the $\Delta P_{di,sn}$ declined by 8.1 ± 12.6% (range +5.1 to –26%) and 7.2 ± 9.0% (+5.1 to –15.9%) at POST$_{10}$ and POST$_{40}$, respectively. After IRL, the $\Delta P_{di,sn}$ declined by 3.1 ± 13% (+21.1 to –11.3% at POST$_{10}$, and then by 19.3 ± 8.9% (–8.7 to –30.6%) at POST$_{40}$ relative to PRE-IRL.

As in Chapter 7, it was not feasible to assess M-waves as cardiac artefacts and/or electrical artefacts owing to the triggering of the magnetic stimulators interfered with the EMG signal in most participants during both conditions. There was only one participant from which M-waves could be obtained at all three timepoints for both conditions, with the remaining five participants having ≤2 M-waves available for analysis at each timepoint. Thus, there were

insufficient data for presentation. For the participants with acceptable M-waves at baseline (*n* = 3), latency was measured to 8.44 ± 1.70 ms and peak-to-peak amplitude 1.21 ± 0.25 mV.

Diaphragm thickening

Ultrasound-derived diaphragm thickness and thickening (shortening) are shown in Table 8.3.4 (group mean data) and Figure 8.3.2 (individual data). At the peak of a twitch, costal diaphragm thickness was ~47-52% of maximal diaphragm thickness measured at TLC (during screening). After VIH, the thickening fraction in response to twitch declined by 9.1 ± 18.2% (range +14.7 to –32.1%) and 8.6 ± 12.1% (+8.7 to –19.2%) at $POST_{10}$ and $POST_{40}$, respectively. One participant did not exhibit any change in thickening after VIH, whereas remaining participants exhibited their greatest decline in diaphragm thickening at $POST_{10}$ (*n* = 3) or $POST_{40}$ (*n* = 2). After IRL, thickening fraction declined by 7.1 ± 19.2% (+24 to –28%) at $POST_{10}$, and then by 4.1 ± 8.3% (+4.1 to –8.8%) at $POST_{40}$.

At the peak of sniff contraction, diaphragm costal thickness was ~56-61% of maximal thickness measured at TLC. After VIH, diaphragm thickening fraction in response to sniffs declined by 32 ± 47% (range +31 to –64%) at $POST_{10}$, and by 58 ± 50% (–7 to –69%) at $POST_{40}$. After IRL, on the other hand, the relative thickening of diaphragm increased by 4.5 ± 37% (+69 to –21%) at $POST_{10}$, and then increased further to 27 ± 50% (+80 to –28%) at $POST_{40}$ relative to PRE.

It is worth noting that the relative changes in costal diaphragm thickening fraction did not exceed the normal variability shown in these exact participants in Chapter 4 in response to bilateral phrenic nerve stimulation (CV = 11 ± 8%; Table 4.3.10). Similarly, although the relative changes in diaphragm thickening fraction in response to sniffs were substantial, and even exceeded the normal variability by two- to three times (CV = 10 ± 7%; Table 4.3.11), the standard deviations and min-max ranges were extremely large, suggesting that the observed changes may not have been meaningful.

Table 8.3.4 Group mean ultrasound-derived diaphragm thickness and thickening in response to twitch contractions and maximal sniffs pre and post voluntary isocapnic hyperpnoea (VIH) and inspiratory resistive loading (IRL).

	PRE	**POST$_{10}$**	**POST$_{40}$**
VIH			
Twitch contraction			
Thickness at relaxation volume, mm	1.2 ± 0.2	1.3 ± 0.3	1.3 ± 0.3
Thickness at peak, mm	2.0 ± 0.3	2.0 ± 0.2	2.0 ± 0.2
Thickening fraction, %	67 ± 17	58 ± 25	58 ± 22
Thickening ratio	1.67 ± 0.17	1.58 ± 0.25	1.58 ± 0.22
Sniff contraction			
Thickness at relaxation volume, mm	1.2 ± 0.2	1.6 ± 0.4	1.7 ± 0.4
Thickness at peak, mm	2.4 ± 0.5	2.5 ± 0.6	2.4 ± 0.4
Thickening fraction, %	98 ± 57	67 ± 70	47 ± 48
Thickening ratio	1.98 ± 0.57	1.67 ± 0.70	1.47 ± 0.48
IRL			
Twitch contraction			
Thickness at relaxation volume, mm	1.3 ± 0.4	1.5 ± 0.3	1.4 ± 0.3
Thickness at peak, mm	2.0 ± 0.5	2.2 ± 0.4	2.0 ± 0.3
Thickening fraction, %	54 ± 27	47 ± 23	50 ± 33
Thickening ratio	1.54 ± 0.27	1.47 ± 0.23	1.50 ± 0.33
Sniff contraction			
Thickness at relaxation volume, mm	1.5 ± 0.3	1.6 ± 0.3	1.5 ± 0.3
Thickness at peak, mm	2.5 ± 0.7	2.5 ± 0.5	2.6 ± 0.9
Thickening fraction, %	65 ± 25	69 ± 60	78 ± 70
Thickening ratio	1.65 ± 0.25	1.69 ± 0.60	1.92 ± 1.08

Data are mean ± *SD* for six participants.

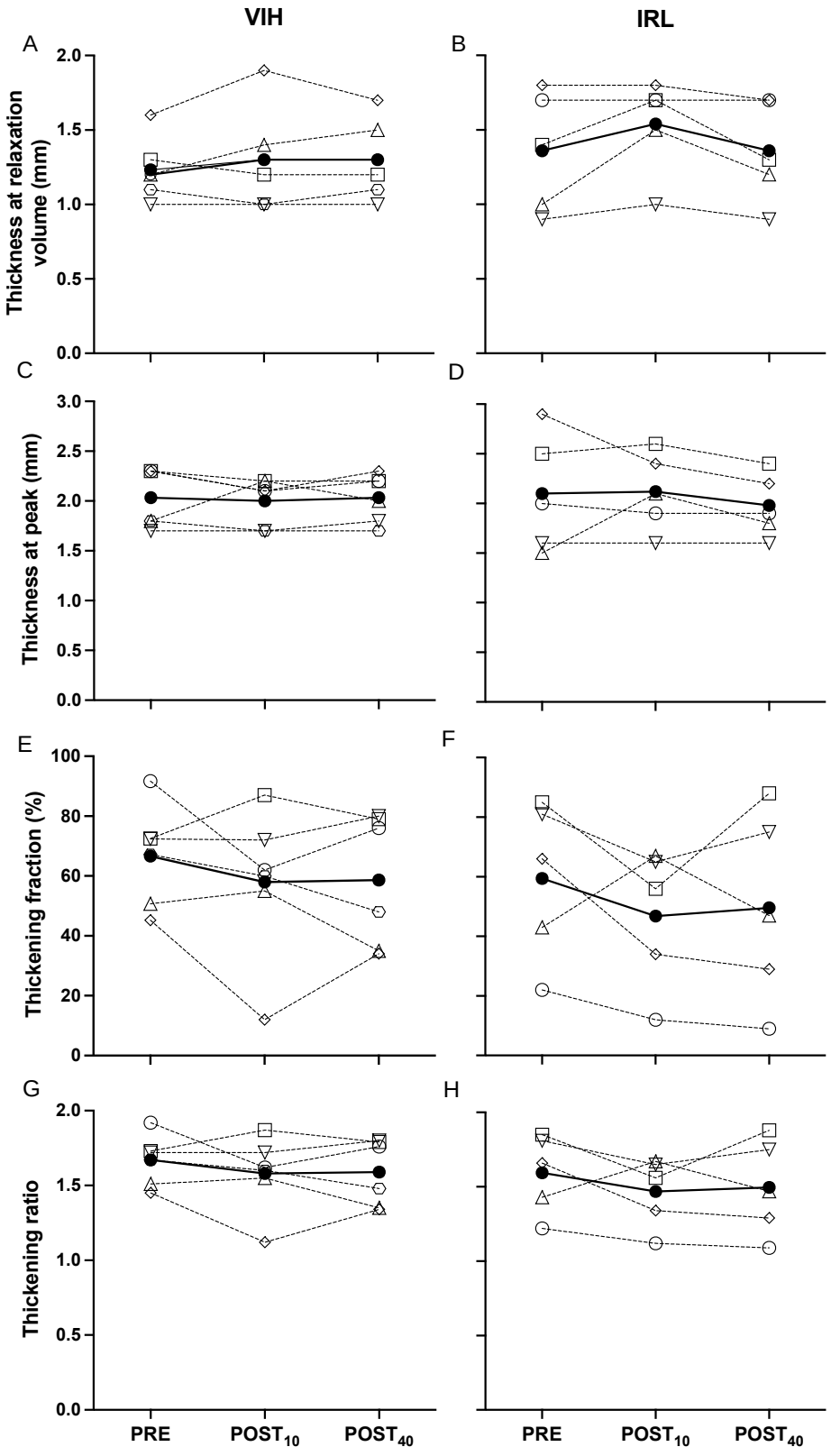

Figure 8.3.2 Individual responses (---) and group mean (—) ultrasound-derived diaphragm thickness and thickening in response to twitch contraction pre and post loading. Data are for six participants.

8.3.15 Hypercapnic hyperpnoea

Participants completed all CO_2-rebreathe tests without untoward events. Mean $P_{ET}CO_2$ at rest was 40.2 ± 0.9 mmHg and 40.6 ± 1.3 mmHg for VIH and IRL trials, respectively. Mean duration of CO_2-rebreathe was 2.21 ± 0.19 min (range 1.48 – 2.42 min; VIH) and 2.34 ± 0.8 min (range 1.77 – 3.18 min; IRL). Figure 8.3.3 shows the mean ventilatory slope responses ($\dot{V}_I$ vs. $P_{ET}CO_2$) during VIH and IRL trials. All participants exhibited a linear ventilatory response to CO_2, with slope responses ranging from 0.28 L/min/mmHg to 5.83 L/min/mmHg.

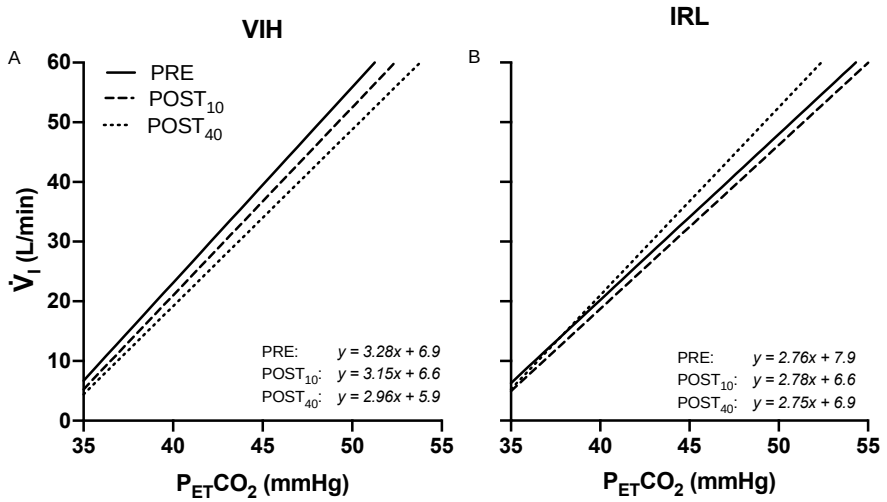

Figure 8.3.3 Slope responses for inspiratory minute ventilation ($\dot{V}_I$) at PRE (—), $POST_{10}$ (---) and $POST_{30}$ (⋯) loading for six participants. Equations of linear regression are shown in lower right corner.

Upon evaluating within-subject ventilatory responses, it was evident that one participant exhibited markedly lower ventilatory response at $POST_{10}$ after VIH (1.46 L/mmHg to 0.36 L/mmHg; $p < 0.001$). This participant also exhibited altered breathing pattern following VIH; manifested as reduced V_{TI} ($p < 0.001$), increased f_R ($p = 0.017$) and reduced inspiratory duty cycle ($p = 0.013$). The remaining participants ($n = 5$) did not show a clear pattern of response after VIH. Moreover, none of the participants exhibited altered intrathoracic pressure responses to hyperpnoea after VIH.

After IRL, there was also one participant who exhibited reduced ventilatory response at $POST_{10}$ (3.70 L/mmHg to 2.76 L/mmHg; $p = 0.03$). This participant, alongside three other participants (total $n = 4$), adopted a breathing pattern after IRL manifested as lower V_{TI} and higher f_R at a given $P_{ET}CO_2$ (tachypnoeic breathing pattern). The remaining two participants showed no clear pattern of response. Three of the participants with altered breathing pattern also exhibited a decline in $\overline{P}_{di,a}$ (–54 ± 12%), in $\overline{P}_{oe,a}$ ($n = 2$; –61 ± 11%,), and in $\overline{P}_{ga,a}$ ($n = 3$; –62 ± 12%) after IRL.

Table 8.3.5 Ventilatory and intrathoracic pressure *slope* responses to hyperpnoea pre and post voluntary isocapnic hyperpnoea (VIH) and inspiratory resistive loading (IRL).

	PRE	**POST$_{10}$**	**POST$_{40}$**
VIH			
$\dot{V}_I$ vs. $P_{ET}CO_2$, L/min/mmHg	3.28 ± 1.64	3.15 ± 1.65	2.96 ± 1.25
V_{TI} vs. $P_{ET}CO_2$, mL/mmHg	150 ± 92	134 ± 128	144 ± 86
f_R vs. $P_{ET}CO_2$, breaths/mmHg	0.52 ± 0.30	0.71 ± 0.59	0.51 ± 0.40
T_I vs. $P_{ET}CO_2$, s/mmHg	–0.18 ± 0.24	–0.12 ± 0.16	–0.13 ± 0.17
T_I/T_{TOT} vs. $P_{ET}CO_2$	–0.012 ± 0.024	–0.043 ± 0.095	–0.005 ± 0.006
$\overline{P}_{di,a}$ vs. $P_{ET}CO_2$, cmH_2O/mmHg	0.54 ± 0.31	0.47 ± 0.40	0.52 ± 0.43
$\overline{P}_{oe,a}$ vs. $P_{ET}CO_2$, cmH_2O/mmHg	–0.55 ± 0.32	–0.50 ± 0.24	–0.52 ± 0.41
$\overline{P}_{ga,a}$ vs. $P_{ET}CO_2$, cmH_2O/mmHg	0.20 ± 0.15	0.21 ± 0.21	0.19 ± 0.17
IRL			
$\dot{V}_I$ vs. $P_{ET}CO_2$, L/min/mmHg	2.76 ± 2.35	2.78 ± 1.59	2.75 ± 1.34
V_{TI} vs. $P_{ET}CO_2$, mL/mmHg	148 ± 142	125 ± 74	153 ± 84
f_R vs. $P_{ET}CO_2$, breaths/mmHg	0.42 ± 0.58	0.72 ± 0.27	0.64 ± 0.37
T_I vs. $P_{ET}CO_2$, s/mmHg	–0.013 ± 0.027	–0.17 ± 0.18	–0.21 ± 0.27
T_I/T_{TOT} vs. $P_{ET}CO_2$	0.039 ± 0.063	–0.004 ± 0.011	–0.0081 ± 0.013
$\overline{P}_{di,a}$ vs. $P_{ET}CO_2$, cmH_2O/mmHg	0.57 ± 0.44	0.74 ± 0.18	0.84 ± 0.66
$\overline{P}_{oe,a}$ vs. $P_{ET}CO_2$, cmH_2O/mmHg	–0.36 ± 0.23	–0.39 ± 0.22	–0.60 ± 0.57
$\overline{P}_{ga,a}$ vs. $P_{ET}CO_2$, cmH_2O/mmHg	0.42 ± 0.39	0.32 ± 0.19	0.43 ± 0.41

Data are mean ± *SD* for six participants. $\dot{V}_I$, inspiratory minute ventilation; V_{TI}, inspiratory tidal volume; f_R, respiratory frequency; T_I, inspiratory time; T_I/T_{TOT}, inspiratory duty cycle; $\overline{P}_{di,a}$, active component of mean inspiratory transdiaphragmatic pressure; $\overline{P}_{oe,a}$, active component of mean inspiratory oesophageal pressure; $\overline{P}_{ga,a}$, active component of mean inspiratory gastric pressure.

Peak responses to hyperpnoea

Group mean peak responses in ventilation, breathing pattern and intrathoracic pressures are shown in Table 8.3.6. Over the course of hyperpnoea, mean $\dot{V}_I$ increased progressively from rest (8.1 ± 1.7 L/min) to 34 ± 14 L/min (range 15 – 59 L/min), which was equal to 15-19% of MVV_{12}. Although some participants exhibited altered ventilatory response and breathing pattern post-loading (i.e., slopes), group mean ventilatory indices appeared to be well-preserved at the peak of hyperpnoea after both loading conditions. For intrathoracic pressures, peak responses were slightly more variable: after VIH the $\overline{P}_{di,a}$ increased by 10.1 ± 25.6% (+40.0 to –26.6%) at $POST_{10}$, and remained elevated at $POST_{40}$ (+10.3 ± 25.1%) relative to PRE. After IRL, mean $\overline{P}_{di,a}$ remained virtually unchanged (+0.7 ± 29.1%; range +31 to –42%) at $POST_{10}$ relative to PRE-IRL, before increasing by 24 ± 60% (+109 to – 42%) at $POST_{40}$ relative to PRE-IRL.

Table 8.3.6 Ventilatory and intrathoracic pressure *peak* responses to hyperpnoea pre and post voluntary isocapnic hyperpnoea (VIH) and inspiratory resistive loading (IRL).

	PRE	**$POST_{10}$**	**$POST_{40}$**
VIH			
$\dot{V}_I$, L/min	35.8 ± 13.5	35.0 ± 16.8	33.3 ± 15.4
$V_{TI,}$ L	2.29 ± 0.64	2.27 ± 1.27	2.13 ± 0.81
$f_{R,}$ breaths/min	16.6 ± 5.0	17.4 ± 5.4	19.6 ± 4.8
$T_{I,}$ s	1.86 ± 0.61	1.86 ± 0.65	1.59 ± 0.27
T_I/T_{TOT}	0.47 ± 0.06	0.46 ± 0.05	0.47 ± 0.07
$P_{ET}CO_2$, kPa	7.31 ± 0.01	7.32 ± 0.08	7.33 ± 0.01
$\overline{P}_{di,a,}$ cmH_2O	10.4 ± 3.2	11.2 ± 3.9	11.5 ± 4.6
$\overline{P}_{oe,a,}$ cmH_2O	–7.4 ± 3.1	–7.2 ± 4.3	–7.6 ± 5.1
$\overline{P}_{ga,a,}$ cmH_2O	4.0 ± 1.5	4.2 ± 1.3	4.3 ± 1.9
IRL			
$\dot{V}_I$, L/min	32.8 ± 12.0	36.3 ± 17.3	37.1 ± 16.0
$V_{TI,}$ L	2.29 ± 0.81	2.37 ± 0.94	2.42 ± 0.74
$f_{R,}$ breaths/min	14.0 ± 4.06	15.6 ± 4.61	15.6 ± 3.64
$T_{I,}$ s	2.47 ± 1.79	2.09 ± 0.80	1.81 ± 0.36
T_I/T_{TOT}	0.49 ± 0.09	0.48 ± 0.06	0.44 ± 0.05
$P_{ET}CO_2$, kPa	7.34 ± 0.03	7.32 ± 0.01	7.30 ± 0.06
$\overline{P}_{di,a,}$ cmH_2O	12.8 ± 2.5	12.8 ± 4.6	15.4 ± 6.6
$\overline{P}_{oe,a,}$ cmH_2O	–5.8 ± 2.4	–6.8 ± 1.8	–10.2 ± 6.9
$\overline{P}_{ga,a,}$ cmH_2O	6.9 ± 3.7	6.3 ± 4.4	6.4 ± 5.1

Data are mean ± *SD* for six participants. $\dot{V}_I$, inspiratory minute ventilation; V_{TI}, inspiratory tidal volume; f_R, respiratory frequency; Ti, peak inspiratory time; Ti/Ttot, peak inspiratory duty cycle; $\bar{P}_{di,a}$, active component of mean inspiratory transdiaphragmatic pressure; $\bar{P}_{oe,a}$, active component of mean inspiratory oesophageal pressure; $\bar{P}_{ga,a}$, active component of mean inspiratory gastric pressure.

Again, it is worth noting that the observed changes in ventilatory indices and intrathoracic pressures did not exceed the normal variability for these measures, as assessed in Chapter 5 (see Table 5.3.7). For instance, the CV for peak $\overline{P}_{di,a}$ during hypercapnic hyperpnoea was 33% (95% CI 18-48%). Given the large variation in the responses, as well as the extremely wide ranges, the observed changes were likely not meaningful in the present context.

Diaphragm thickening

Ultrasound-derived diaphragm thickness and thickening at the peak of hyperpnoea are shown in Table 8.3.7 (group mean responses) and Figure 8.3.4 (individual responses). After VIH, diaphragm thickening fraction at peak hyperpnoea increased by 33 ± 61% (range +94 to –32%) at $POST_{10}$, and remained elevated at $POST_{40}$ (+12 ± 51%; +57 to –49%) relative to PRE. Contrarily, after IRL thickening fraction decreased by 24 ± 27% (+12 to –60%) at $POST_{10}$, and remained low at $POST_{40}$ (–21 ± 28%; +3.1 to –63%) relative to PRE.

Table 8.3.7 Ultrasound-derived diaphragm thickness and thickening *peak* responses to hyperpnoea pre and post voluntary isocapnic hyperpnoea (VIH) and inspiratory resistive loading (IRL).

	PRE	**$POST_{10}$**	**$POST_{40}$**
VIH			
Thickness at EELV, mm	1.4 ± 0.4	1.5 ± 0.3	1.5 ± 0.4
Thickness at EILV, mm	2.6 ± 0.7	2.8 ± 0.4	2.6 ± 0.5
Thickening fraction, %	87 ± 36	102 ± 49	89 ± 51
Thickening ratio	1.87 ± 0.36	2.02 ± 0.49	1.89 ± 0.51
IRL			
Thickness at EELV, mm	1.4 ± 0.3	1.6 ± 0.3	1.4 ± 0.3
Thickness at EILV, mm	3.0 ± 0.7	2.8 ± 0.8	2.6 ± 0.8
Thickening fraction, %	130 ± 55	86 ± 22	93 ± 29
Thickening ratio	2.30 ± 0.55	2.05 ± 0.27	1.93 ± 0.29

Data are mean ± *SD* for six participants. EELV, end-expiratory lung volume, EILV, end-inspiratory lung volume.

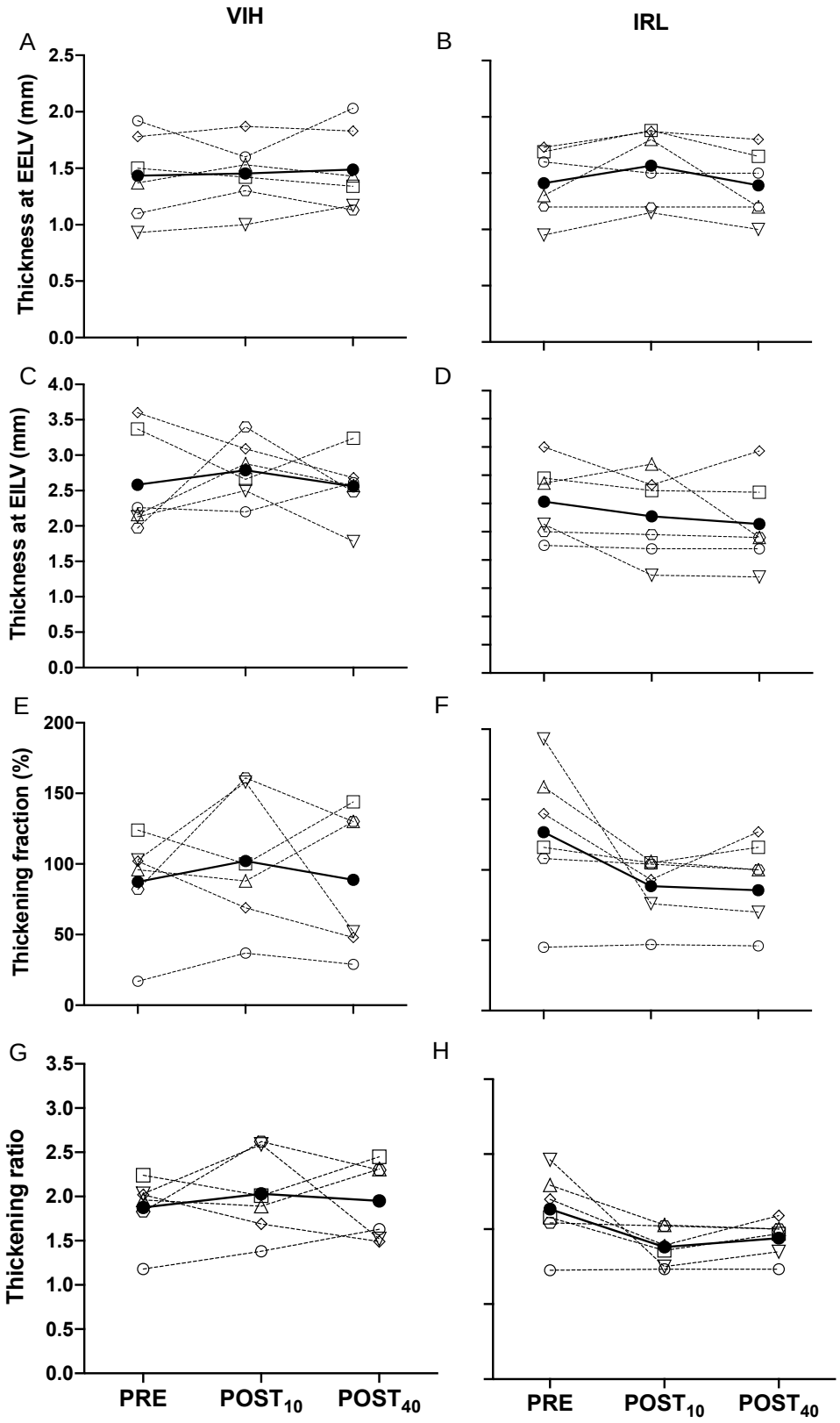

Figure 8.3.4 Individual (---) and group mean (—) peak responses in ultrasound-derived diaphragm thickness and thickening pre- and post-loading. Data are for six participants.

8.4 Discussion

This is the first study to attempt to use *intercostal* ultrasonography to evaluate the effect of external loading on ultrasound-derived costal diaphragm thickening. The main finding was that despite the presence of diaphragm fatigue after pressure-loading (IRL), costal diaphragm thickening in response to twitch contractions and sniffs remained well-preserved. Also after pressure-loading, the majority participants adopted a tachypnoeic breathing pattern that coincided with reduced diaphragm force. However, ultrasound-derived diaphragm thickening during hyperpnoea was highly variable. Two-dimensional, intercostal ultrasonography of costal diaphragm during hyperpnoea may, therefore, be more variable than originally expected (see Chapter 4 and 5, *Parts 2*), and the technique may be unsuited to evaluate the acute effect of external loading on diaphragm dynamic contractile properties.

It is important to emphasize that few of the observed changes in this study exceeded the normal variability expected (i.e., two- to three-fold the CV as established in Chapter 4 and 5). Moreover, some responses (e.g., intrathoracic pressures at peak hyperpnoea) exhibited extremely large standard deviations and ranges. Combined, this suggests that the changes observed in this study were not necessarily clinically meaningful. Due to the low sample size in this study, and because the data was not normally distributed, it was decided that inferential statistical analysis should not be performed in this study in order to promote data transparency and reduce the probability of type II error due to a 'underpowered' study (Zar, 2014). Therefore, results of this study should only be considered hypothesis-generating data and the object of further investigations.

To promote further investigations into the use of ultrasonography for the assessment of costal diaphragm thickening, the following sections will first aim to discuss the physiological mechanisms that would underpin a decline in *in vivo* diaphragm shortening after external loading and fatigue. Next, there will be a discussion regarding the methodological limitations in this study. Finally, there will be a brief presentation of new technological advances in diaphragm imaging that may provide the means to answer some of the questions left unanswered in this thesis.

8.4.16 The effect of fatigue on diaphragm shortening

As in Chapter 7, external loading of the diaphragm was performed using a pressure-loading task (IRL) and a flow-loaded task (VIH); each targeting the two extremes of the force-velocity spectrum. However, the purpose of this study was to evaluate if either, or both, of the tasks

would adversely affect costal diaphragm shortening; quantified as thickening using intercostal ultrasonography. It is known that muscle fatigue is characterised by a loss of force and/or slowing of shortening velocity that results in a substantial loss of power (Jones, 2010). In Chapter 4 it was shown that external loading of human diaphragm may impair contractile (excursion) velocity as assessed using subcostal ultrasonography. Conversely, this study used intercostal ultrasonography to better understand the effect of loading on the diaphragm's ability to shorten, and whether pressure- and flow-loading would impair diaphragm shortening to varying degrees.

Muscle fibre shortening is the result of cross-bridge cycling, whereby myosin heads bind and release from actin myofilaments by utilising available ATP during a concentric contraction (i.e., cross-bridge cycling). Although the focus of former research has mainly been on the loss of force and/or slowing of shortening velocity in fatigue, there is evidence that fatigue may also impair absolute fibre shortening. For instance, Mardini et al. (1987) showed that fatigue by prolonged isometric contractions (8 s trains at 40 Hz every 30 s for 5 min) in rat diaphragm elicited a reduction in maximal fibre shortening that was equal to the loss of tension relative to the fresh state (~65% decline in both). Because the principal role of the mammalian diaphragm is to shorten under load to meet the ventilatory demand, the authors urged that the definition of diaphragm fatigue should be expanded to include a failure of the muscle to sustain a given level of shortening.

The cellular mechanisms that underpin the impairment of fibre shortening in fatigue are not fully understood. In a series of studies, Hortemo & Munkvik et al. (2013; 2009) showed that maximal fibre shortening of rat soleus muscle was impaired after a series of fatiguing concentric contractions (100 ms on/off stimulations at 30 Hz for 15 min) of rat soleus muscle. The authors concluded that that the reduction in maximal fibre shortening (~40%) was likely the result of dynamic contractions (i.e., task-dependency); not isometric contractions, as commonly used for *in vitro* and *in situ* studies. The authors further concluded that the impairment of fibre shortening in fatigue may be attributed to the dephosphorylation of the RLCs of myosin filaments. Specifically, phosphorylation of RLC modulates the movement of the myosin heads to promote actin attachment upon Ca^{2+} binding to the troponin-tropomyosin complex (Hortemo et al., 2013; Yu et al., 2016). Thus, dephosphorylation of RLC may decrease the probability of an actin-myosin attachment, and thereby reduce absolute shortening of the fibres (Yu et al., 2016). It is not known, however, to what extent these mechanisms would also impair diaphragm shortening in humans.

Although the anatomical features of intact human diaphragm are unique, the muscle's contractile properties are like those seen in other striated skeletal muscles (see Literature Review, section 2.3). For instance, active fibre shortening (concentric contraction) reduces the overall length of the belly of a muscle. For the diaphragm *in vivo,* fibre shortening reduces the overall surface area of the muscle sheet, and, because muscle volume remains constant throughout a contraction, the diaphragm thickens upon shortening (Wait et al., 1989). Consequently, any fatigue-induced decline in active fibre shortening of diaphragm should – at least in theory – be detectable as a decline in diaphragm thickening. To our knowledge, intercostal ultrasonography at the zone of apposition is the only means to quantify thickening of the diaphragm in humans (Cohn et al., 1997; Wait et al., 1989). Nonetheless, given the small sample size and highly variable results found in this study, it is evident that further investigations are needed to evaluate the usefulness of this ultrasonography approach.

8.4.17 Methodological considerations

Because the relative thickening of diaphragm is calculated using absolute measures of diaphragm thickness, it is necessary to discuss the potential effect of prior activity on resting muscle thickness. In pennate limb locomotor muscles (e.g., vastus lateralis and quadriceps femoris), some have reported that fatigue by dynamic contractions acutely reduces fascicle length (~2-5%) and increases pennation angle (~10-12%), which ultimately increases thickness of the resting muscle (Brancaccio et al., 2008; Csapo et al., 2011). The diaphragm is, of course, not a pennate muscle, and exact parallels cannot be drawn. However, given the substantial increases in muscle thickness seen in pennate muscles after fatigue, the phenomenon cannot be entirely excluded for the human diaphragm.

Muscle swelling may also increase thickness of the intact muscle. More specifically, exhaustive muscle contractions increase vascular perfusion and, if associated with exercise-induced muscle damage, muscle swelling secondary to inflammatory responses (Csapo et al., 2011). In fact, muscle swelling may increase thickness of limb locomotor muscles by up to 11-14% after bouts of dynamic contractions (Vieira et al., 2018). It is, however, not known to what extent the diaphragm is susceptible to swelling after strenuous activity. It is worth noting that muscle swelling usually occurs at a later phase of recovery (24-48 h post-exercise), thereby making it unlikely to have affected the post-loading measurements in the current study (Allen et al., 2005).

Lastly, there is a strong relationship between lung volume and costal diaphragm thickness *in vivo*; whether this relationship is measured using sonomicrometry in canines (Newman et al., 1984), in human autopsy samples (Cohn et al., 1997), or by intercostal ultrasonography in living humans (Wait et al., 1989). Similar to limb locomotor muscles, diaphragm contractile properties are determined by length-tension relations (McCully & Faulkner, 1983). For the human diaphragm, however, the length-tension relationship is analogous to the volume-pressure relationship (Braun et al., 1982; Smith & Bellemare, 1987). It was therefore ensured that all stimulation-evoked twitch contractions and sniffs were performed at the same lung volume as to ensure similar muscle mechanical responses and diaphragm thickness across all loading conditions and timepoints. Although lung volumes were not measured during twitch contractions and sniffs, it was ensured that EEP_{oe} was kept similar before and after loading tasks as well as between experimental visits (Table 8.3.3).

8.4.18 The future of costal diaphragm ultrasonography

Based on the above considerations, it is intuitive and likely that acute architectural and/or structural changes may occur within the fatigued human diaphragm. The findings of Chapter 4 and 5 in this thesis suggest that intercostal ultrasonography produces reliable measures of diaphragm shortening. However, results from this study suggest that the two-dimensional, intercostal ultrasonography may not have the necessary resolution and sensitivity to capture the acute contractile changes induced by fatigue. For instance, unlike the high-frequency ultrasound transducers used to assess muscle architecture in limb locomotor muscles, ultrasound transducers used to image the human diaphragm generate low-frequency beams and are intended to reach deeper tissues with acceptable lateral resolution (Ng & Swanevelder, 2011). However, low-frequency transducers may not offer adequate resolution to capture structural changes within the costal diaphragm. Afterall, the average diaphragm thickness measures only 1.2-1.8 mm in healthy adults, depending on lung volume, sex, stature and training status (Carrillo-Esper et al., 2016; McCool, Benditt, et al., 1997). The utilised ultrasound system must, therefore, have the features to image small tissues with high resolution.

Thus, it may be necessary for future investigations to explore the use of alternative imaging techniques, such as speckle-tracking algorithms (Oppersma et al., 2017; Orde et al., 2016a), ultrasound shear-wave elastography (Bachasson et al., 2018; Morel et al., 2019) and ultrafast ultrasound (Poulard et al., 2020; Tanter & Fink, 2014). Although these techniques have not yet been adequately validated for the human diaphragm, these recent

advances in imaging technology may offer improved resolution as well as software packages (e.g., analysis algorithms) that may answer some of the questions left unanswered in this thesis. An in-depth discussion concerning future perspectives of diaphragm imaging is provided in Chapter 9 (General Discussion).

8.4.19 Conclusions

Theoretically, diaphragm fatigue should impair fibre shortening, and should be compromised to a similar extent as force. However, despite diaphragm fatigue after pressure-loading, costal diaphragm shortening was not adversely affected in response to twitch contractions, maximal sniffs or hypercapnic hyperpnoea. Thus, two-dimensional, intercostal ultrasonography of costal diaphragm may not provide the necessary resolution or be adequately sensitive to capture acute contractile changes within the costal diaphragm. Future studies should therefore consider using alternative imaging technologies, such as speckle-tracking algorithms, shear-wave elastography or ultrafast ultrasound in order to fill current knowledge gaps concerning the effect of external loading on shortening (thickening) of *in vivo* human diaphragm.

Chapter 9

General Discussion

9.1 Introduction

The overarching aim of this thesis was to evaluate the usefulness of ultrasonography for the assessment of contractile properties of fresh and fatigued diaphragm in healthy humans. Specifically, this thesis explored the feasibility, validity and reliability of ultrasonography for the assessment of diaphragm kinetics and shortening *in vivo* in response to evoked contractions, sniffs and hyperpnoea. Moreover, ultrasonography was used to quantify diaphragm kinetic responses to various modes of reflexively-driven hyperpnoea, and to assess the effect of external loading on dynamic contractile properties of the human diaphragm *in vivo*. These aims were addressed in five experimental chapters (Chapters 4 to 8). In the following section, the main findings will be summarised, after which there will be a discussion of their functional implications and how they may inform future research. Finally, there will be an explorative discussion about the future respiratory muscle imaging, and how technological advances in medical imaging may answer some of the questions left unanswered in this thesis.

9.2 Summary of main findings

Chapter 4: *Feasibility, Validity and Reliability of Ultrasonography for the Assessment of Diaphragm Kinetics and Thickening in Response to Non-Volitional and Volitional Perturbations in Healthy Adults*

The aim of this study was to determine the feasibility, concurrent validity and within-day reliability of ultrasound-derived diaphragm kinetics and shortening in response to evoked twitch contractions and maximal sniffs. It was hypothesised that assessment of diaphragm kinetics and shortening would be feasible, that ultrasound-derived diaphragm kinetics and shortening would be strongly related to conventional measures of contractile properties, and that the measures would exhibit acceptable within-day, intra-observer reliability.

Measuring crural diaphragm kinetics (*Part 1*) was feasible with M-mode and AM-mode ultrasound, regardless of stimulation frequency, post-activation potentiation and the volitional nature of maximal sniffs. Speckle-tracking algorithms for diaphragm kinetics exhibited poor feasibility and were excluded from further analysis. It was feasible to measure costal diaphragm shortening (*Part 2*) in response to non-potentiated twitch contractions and maximal sniffs. Measures of diaphragm kinetics were strongly correlated with $\Delta P_{di,tw}$ and mean rate of pressure development ($r^2 \geq 0.802$), thereby addressing the concurrent validity of the ultrasound-derived measures. The variance unaccounted for by this relationship (~20%) may be explained by the

inability of two-dimensional ultrasound to capture fully diaphragm descent and lateral distortion evoked by unilateral stimulation. Diaphragm shortening was not related to $\Delta P_{di,tw}$ nor $\Delta P_{di,sn}$, suggesting limited activation of costal diaphragm during anterolateral phrenic nerve stimulation. Diaphragm kinetics and shortening exhibited moderate-to excellent within-day, intra-observer reliability. These findings informed the use of ultrasonography for the assessment of diaphragm contractile properties in response to external loading in Chapter 7 and 8.

Chapter 5: *Feasibility, Validity and Reliability of Ultrasonography for the Assessment of Diaphragm Kinetics and Thickening During Hypercapnic Hyperpnoea in Healthy Men*

The aim of this study was to determine the feasibility, concurrent validity and within-day reliability of ultrasound-derived diaphragm kinetics and shortening during hypercapnic hyperpnoea. It was hypothesised that the assessment of diaphragm kinetics and shortening would be feasible during hyperpnoea, but that feasibility may be adversely affected by progressively increasing tidal volume, that ultrasound-derived measures of diaphragm kinetics and shortening would be strongly related to conventional measures of diaphragm contractile properties and ventilatory indices, and that the measures would exhibit acceptable within-day, intra-observer reliability.

The assessments of crural diaphragm kinetics (*Part 1*) and costal diaphragm shortening (*Part 2*) were feasible during hypercapnic hyperpnoea, and were not adversely affected by increasing tidal volume. For diaphragm kinetics, AM-mode ultrasound appeared to capture more closely crural diaphragm excursion compared to M-mode. Expectedly, ultrasound-derived diaphragm kinetics and shortening increased as a function of ventilatory drive and were strongly related to conventional measures of diaphragm contractile properties, thereby addressing the concurrent validity of the ultrasound-derived measures. Except for excursion time, which exhibited poor reliability, ultrasound-derived diaphragm kinetics and shortening exhibited good- to excellent within-day, intra-observer reliability even at the peak of hyperpnoea. These findings informed the use of ultrasonography for the assessment of diaphragm contractile properties in response to external loading in Chapter 7 and 8.

Chapter 6: *Application of Subcostal Ultrasonography for the Assessment of Diaphragm Kinetics During Exercise- and CO_2-Induced Hyperpnoea in Healthy Adults*

The aims of this study were to evaluate the feasibility of subcostal ultrasonography for the assessment of crural diaphragm kinetics during exercise- and non-exercise-induced hyperpnoea, and to compare diaphragm kinetics across the two modes of hyperpnoea to explore the mechanisms underpinning postural-ventilatory modulation of the diaphragm. It was hypothesised that diaphragm ultrasonography would be feasible during both modes of hyperpnoea, but that motion artefacts associated with exercise would adversely affect feasibility. Due to the proposed inhibition of postural drive to the diaphragm during hyperpnoea (Hodges et al., 2001), it was also hypothesised that diaphragm kinetic behaviour would be similar during exercise-induced hyperpnoea relative to non-exercise-induced hyperpnoea.

Ultrasonography of crural diaphragm was feasible during the two modes of reflexively-driven hyperpnoea, regardless of motion artefacts associated with semi-recumbent cycling exercise. At similar levels of ventilation, the diaphragm generated higher pressure ($\overline{P}_{di}$) during exercise compared to CO_2-rebreathe, despite moving significantly less. Upon partitioning inspiratory pressures into active and passive components during exercise, it was evident that the elevated $\overline{P}_{di}$ was due only to the passive component ($\overline{P}_{di,p}$), suggesting that significant 'bracing' occurred (i.e., quasi-isometric diaphragm contraction for postural support). Accordingly, these findings did not align with the original hypothesis, but instead suggest that the diaphragm is constrained during exercise due to the quasi-isometric contractions required for the modulation of postural and ventilatory tasks.

Chapter 7: *Application of Subcostal Ultrasonography for the Assessment of Pressure-Flow Specificity of Diaphragm Fatigue in Healthy Men*

The aim of this study was to assess the effect of pressure- and flow-loading on diaphragm kinetics and force output to elucidate the mechanisms that underpin fatigue task-dependency of human diaphragm. In line with our current understanding of fatigue task-dependency (Enoka, 1995; Hunter, 2018), it was hypothesised that a *high force-low velocity* task (pressure-loading) would impair diaphragm force, with negligible effect on ultrasound-derived diaphragm excursion velocity. Conversely, a *low force-high velocity* task (flow-loading) would primarily impair diaphragm excursion velocity, with negligible effect on force.

The study showed that pressure-loading of the diaphragm, but not flow-loading, impaired $\Delta P_{di,tw}$ and excursion velocity, resulting in a considerable decline in stimulation-evoked diaphragm power (–46%; p = 0.03). Despite the presence of fatigue, diaphragm contractile properties were relatively well-preserved during hyperpnoea. These findings suggest that, in line with studies of diaphragm muscle fatigue *in vitro* and *in situ* (Ameredes et al., 2006; Coirault et al., 1995), both diaphragm twitch force and contractile velocity appear to be impaired in the fatigued human diaphragm.

> **Chapter 8:** *Application of Intercostal Ultrasonography for the Assessment of Pressure-Flow Specificity of Diaphragm Fatigue in Healthy Men*

The aim of this exploratory study was to assess the effect of pressure- and flow-loading on diaphragm force and ultrasound-derived shortening. It was hypothesised that diaphragm fatigue by pressure- and flow-loading would equally reduce diaphragm force output and shortening with similar magnitude.

Despite the presence of diaphragm fatigue after pressure-loading, diaphragm shortening in response to twitch contractions and sniffs remained well-preserved. Ultrasound-derived diaphragm shortening during hyperpnoea was highly variable, suggesting that intercostal ultrasonography of costal diaphragm during hyperpnoea may be more variable than originally expected (Chapter 5, *Part 2*). Thus, the technique may be unsuited to evaluate the acute effect of external loading on diaphragm dynamic contractile properties.

9.3 Methodological considerations

It must be acknowledged that the investigator (CI) was not blinded to the assessment of diaphragm function using ultrasound in the above studies. Although this may be considered a methodological limitation, it was not logistically feasible to blind the investigator due to the complex procedure of acquiring, exporting and analysing ultrasound cine-loops with the equipment available. This being said, the procedures associated with ultrasound acquisition (e.g., choice of ultrasound transducer, anatomical landmarks and marking of the skin) have been described in great detail in each experimental chapter and in Chapter 3 (General Methods) in an attempt to standardise our approaches. We refer the reader to the works of Testa et al. (2011), Carrillo-Esper et al. (2016) and Laursen et al. (2021) for the assessment of inter-observer reliability of diaphragm function using ultrasound.

9.4 Implications of findings and recommendations for future research

Stimulation-evoked $\Delta P_{di,tw}$ is known as the 'gold standard' for assessing diaphragm contractile properties (Green et al., 2002). However, a major limitation of this technique is that quasi-isometric twitch pressure is a relatively poor index of diaphragm function *in vivo*, providing little to no information concerning the muscle's ability to shorten and generate power. With the ultrasonography techniques assessed in this thesis, however, it was possible not only to *visualise* dynamic properties of the human diaphragm but also to *quantify* them. It was also shown that ultrasonography can be applied to the study of diaphragm kinetics during various modes of hyperpnoea (e.g., CO_2-rebreathe and exercise). Moreover, subcostal ultrasonography can be used to identify slowing of contractile velocity and reduction in power after external loading, thereby elucidating the mechanisms that underpin fatigue task-dependency of the human diaphragm. Accordingly, the following sections will discuss the implications of these findings, and how they may inform future research.

9.4.1 Task-dependency of exercise-induced diaphragm fatigue

Respiratory muscle fatigue is defined as "a loss in the capacity for developing force and/or velocity of a muscle, resulting from muscle activity under load and which is reversible by rest" (Respiratory Muscle Fatigue Workshop Group, 1990, p. 474). For the diaphragm, external loading via whole-body exercise has been shown to elicit an acute decrement in evoked $\Delta P_{di,tw}$ (Johnson et al., 1993). As discussed in the Literature Review (section 2.3.5), shortening velocity of the human diaphragm has invariably been ignored due to the absence of accurate and reliable methods for assessing this variable for the intact muscle (Green et al., 2002). This thesis established that ultrasound can be used to provide reliable measures of diaphragm contractile velocity that complements conventional measures of intrathoracic pressure and EMG_{di}. Moreover, ultrasound-derived crural diaphragm excursion and excursion velocity can be used to estimate diaphragm work (force × distance) and power (force × distance / time), providing a comprehensive understanding of the dynamic contractile properties of human diaphragm *in vivo*.

In Chapter 7, fatigue task-dependency of diaphragm was assessed using two pressure- and flow-loading tasks that targeted the extremes of the force-velocity spectrum. Whole-body exercise, on the other hand, is typically considered a combination of pressure- *and* flow-loading, with intense exercise eliciting inspiratory pressures of 80-90% of maximal dynamic capacity in highly-trained endurance athletes (Johnson et al., 1992). In line with our current understanding

of fatigue task-dependency, and of diaphragm fatigue specifically, it is intuitive that exercise-induced inspiratory muscle fatigue elicits a decline in both diaphragm force *and* shortening velocity – although the latter has not been adequately addressed in humans. Future studies should, therefore, consider applying the ultrasonography techniques outlined in this thesis to better understand the effect of dynamic, whole-body exercise on diaphragm contractile properties across a range of exercise modalities. Indeed, techniques like AM-mode ultrasound for diaphragm kinetics can provide a methodological framework to address the many unknowns regarding how exercise modalities affect diaphragm contractile properties, and how a potential decline in these properties may impair 'real-world performance' (Enoka & Duchateau, 2016).

For instance, sustained, whole-body endurance exercise in known to induce fatigue of inspiratory muscles (Romer & Polkey, 2008). Moreover, the severity of this fatigue is determined by cumulative inspiratory muscle work and the competition with locomotor muscles for available blood flow (Archiza et al., 2018; Sheel et al., 2018). During whole-body endurance exercise, the diaphragm shortens and descends with elements of 'tonic activity' (i.e., quasi-isometric contractions) for postural support (Gandevia et al., 2002; Hodges & Gandevia, 2000, see Chapter 6), with a force that is usually substantially lower than maximal dynamic capacity (Johnson et al., 1992). The mechanisms that underpin diaphragm fatigue during whole-body endurance exercise are, therefore, markedly different from the mechanisms that underpin diaphragm fatigue during intense, explosive resistance exercises: during resistance exercises, the athlete is repeatedly required to generate extremely high intraabdominal pressures (>300 cmH_2O), particularly when exercises like squats and clean-and-jerk exceed 75% of one-repetition maximum (Blazek et al., 2019). Given the explosive nature of some weightlifting exercises, the diaphragm must contract rapidly to increase intraabdominal pressure in a postural response to increase stiffness of the lumbar spine and protect from injury (Hodges et al., 2005; Panjabi et al., 1989). This postural response involves a rapid rate of pressure development with negligible fibre shortening that is initiated prior to the lift and then sustained until the lift is completed (Harman et al., 1988; Hemborg et al., 1985). The proposed ultrasonography techniques from this thesis could, therefore, be used to characterise how various modes of exercise, and their particular physiological and mechanical demands, may impinge on the force-velocity relationship of the human diaphragm (not only force). In turn, future research may address the many gaps in knowledge of how a decline in dynamic contractile properties may ultimately impair of 'real-world' performance.

9.4.2 Inspiratory muscle training (IMT)

Respiratory muscle training is the specific and targeted training of respiratory muscles for the purpose of neuromuscular adaptation to enhance respiratory muscle strength or endurance. Respiratory muscle training can facilitate weaning from mechanical ventilation in critically ill patients (Elkins & Dentice, 2015), improve quality of life in patients with chronic heart failure (Dall'Ago et al., 2006), and potentially improve athletic performance in well-trained individuals (HajBhanbari et al., 2013). The effect of inspiratory muscle training (IMT) on athletic performance is, however, controversial (Sheel, 2002). For example, well-trained athletes may experience a performance-enhancing effect of IMT, involving increased MIP, reduced rating of perceived breathlessness and exertion, and/or improved time trial performance (HajBhanbari et al., 2013). Nonetheless, as pointed out by Sheel (2002), the controlled laboratory conditions under which exercise performance has been assessed in these studies may lack in ecological validity, ignoring environmental conditions and external factors that usually influence 'real-life' athletic performance. Another limitation is that most studies have used MIP as primary outcome measure; that is, a maximal static manoeuvre generated against occluded airways, and does not provide objective data regarding the muscle's ability to shorten and generate power. Afterall, skeletal muscle function is characterised by the ability to shorten, generate force, produce power and perform work. Accordingly, with the methodological framework provided in this thesis, ultrasonography may help inform IMT programmes and interventions.

For instance, swimming is an endurance sport characterised by whole-body immersion with a pronounced respiratory-locomotor coupling whereby the athlete can only inhale when the face is above water. Thus, the athlete must inhale rapidly against elevated hydrostatic pressure around the chest wall (Holmer, 1992), increasing the inspiratory work of breathing compared to upright, dry-land exercise (Leahy et al., 2019). IMT has a considerable ergogenic effect on performance in other endurance sports (e.g., cycling and rowing) (e.g., Romer et al., 2002; Volianitis et al., 2001); however, it remains a curious observation that IMT has little or no effect on swimming performance (Cunha et al., 2019; HajBhanbari et al., 2013; Kilding et al., 2010; Lemaitre et al., 2013).

A possible explanation for this discrepancy is that these training programmes have not been tailored to the nuances of high-performance swimming. For instance, the majority of IMT programmes involve inhaling against a moderate resistance (~50% of MIP) until a threshold is reached (pressure-threshold loading) (Cunha et al., 2019; Kilding et al., 2010; Wylegala et al.,

2007). However, given the physiological and biomechanical demands of swimming, shortening velocity may be a more important component of inspiratory muscle function for swimmers than force itself. Accordingly, inspiratory muscle training programmes for swimmers may need to emphasise shortening velocity of inspiratory muscles, thereby reducing T_I while maintaining similar V_{TI} (i.e., increase peak inspiratory flow). For swimmers, this adaptation will result in less time spent with head above water during which the swimmer opposes the highest frontal resistance in most competitive swim strokes (Holmer, 1992). In turn, swimmers would reduce the variation in swimming velocity within a stroke (intra-cyclic variation), and reduce the work needed to proceed at a certain velocity and, thus, enhance performance (Zamparo et al., 2020). Diaphragm ultrasonography could, therefore, be used to accurately determine the effect of these training programmes on the diaphragm's ability to shorten rapidly under load. Afterall, the acute overload (fatigue) necessary for neuromuscular adaptation is dependent on specificity of the task performed (Hunter, 2018), and contractions during IMT must, therefore, mirror closely the contractile pattern during the sport-specific exercise performance. Diaphragm ultrasonography offers a means to ensure that IMT elicits shortening of diaphragm fibres, and that the rate of this shortening mirrors the shortening elicited by sport-specific performance.

9.4.3 The effect of ageing on diaphragm contractile properties

Ageing causes marked changes in physical function. For the respiratory system, even healthy ageing is associated with an accelerated decline in most lung volumes and capacities owing to a decrease in chest wall compliance (i.e., increased stiffness) resulting from osteoporotic changes within the rib cage and spine (Lowery et al., 2013; Mittman et al., 1965). Conversely, lung compliance increases with ageing owing to changes to the configuration of lung elastin (Roman et al., 2016). Consequently, the ageing airways are more collapsible because there is less 'tethering' of the airways by lung parenchyma, ultimately reducing peak expiratory flow. For the musculoskeletal system, age-related impairments include altered neuromuscular function (e.g., nerve denervation), declining muscle mass (primary sarcopenia), changes in muscle fibre composition, and a reduction in muscle quality (Elliott et al., 2016; Reid & Fielding, 2012). These factors are not independent phenomena within the ageing muscle, but rather a complex set of mechanisms that gradually impair skeletal muscle contractile properties over time. Interestingly, however, diaphragm mass (volume) and cross-sectional area appear to be well-preserved in ageing compared to other skeletal muscles (Arora & Rochester, 1982; Mizuno, 1991). However, maximal respiratory muscle force generally (Watsford et al., 2007), and diaphragm force specifically (Polkey, Harris, et al., 1997), decline gradually with age.

Albeit a controversial area of research with conflicting data, it is generally thought that age-related loss of diaphragm force is attributed to a histochemical shift in muscle fibre type. In rodent diaphragm, there are reports suggesting an age-related, selective atrophy of fibre type IIX and IIB, while fibre type I and IIA remain well-preserved (Elliott et al., 2016). It is not entirely known why or how age-related selective atrophy occurs, although some have suggested that an age-related loss of type IIB and IIX motor neurons may denervate muscle fibres, causing remaining IIA motor neurons to reinnervate IIB and IIX fibres (Greising et al., 2015). Thus, motor units end up as 'clusters' of different muscle fibre types, which ultimately can reduce type IIB and IIX cross-sectional area and specific force (Elliott et al., 2016; Greising et al., 2015).

A shift from fast-twitch type IIB and IIX fibres to IIA fibres (i.e., a shift from fast to slow MHC isoforms) implies that maximal shortening velocity also declines with age (Zierath & Hawley, 2004). Some still claim, however, that shortening velocity increases in the ageing rat diaphragm (Powers et al., 1996), while others have found the opposite in human limb locomotor muscles (D'Antona et al., 2003; Larsson et al., 1997). As such, little is known about the effect of ageing on respiratory muscle shortening velocity in humans. Because power is the dot product of force and shortening velocity, any physiological mechanism that impairs one or both of these factors will contribute to a significant loss of muscle power. The methodological framework presented in this thesis may, therefore, be used as a tool to help better understand dynamic properties of diaphragm with ageing. This thesis showed that diaphragm ultrasonography is feasible and reliable in young adults in response to a range of perturbation. These perturbation are equally feasible in older adults (Gibson et al., 2002), and future research should expand the use of diaphragm ultrasonography to bridge the gap between current knowledge and a better understanding of the implications of healthy ageing on dynamic diaphragm function.

It is important to better understand the effect of ageing on dynamic diaphragm contractile properties because of the inherent loss of balance function with age. Indeed, ageing is associated with a loss of sensory organs as well as an impaired ability to process information and to issue motor commands (Konrad et al., 1999). Combined, these age-related changes reduce balance function, which increases risk of falls and injury (Cuevas-Trisan, 2017). Although the underlying mechanisms of balance function are complex, the diaphragm plays a significant role in spinal stability when maintaining balance (Kocjan et al., 2018). When the centre of gravity shifts (e.g., during walking), or limbs are moved in relation to the trunk, the diaphragm contracts 'tonically' to increase intraabdominal pressure (Hodges et al., 1997, 2004). So, during rapid

postural adjustments, the diaphragm's ability to contract rapidly becomes pivotal. Accordingly, it is evident that an age-related slowing of maximal shortening velocity of the human diaphragm may have severe implications. Future research is therefore needed to better understand the relationships between physical function (i.e., ability to perform daily tasks, maintaining balance and avoiding falls) and the dynamic contractile properties of the human diaphragm in an ageing population.

9.5 The future of respiratory muscle imaging

Finally, it is worth discussing some contemporary technological advances within the area of ultrasound imaging that have only recently been applied to the human diaphragm. In turn, these technological advances may be used to overcome some of the limitations identified in this thesis.

Ultrasonography of inspiratory and expiratory muscles

First, it is interesting to discuss briefly the use of ultrasonography to assess contractile properties of *other respiratory muscles*. In fact, it was only recently that the European Respiratory Society (2021) included ultrasound of the intercostals as an independent section in their official statement on thoracic ultrasound. Like diaphragm ultrasound, imaging of parasternal intercostals (Dres et al., 2020; Wallbridge et al., 2018) and external intercostals (Nakanishi et al., 2019) are used to monitor muscle atrophy during mechanical ventilation and to predict weaning success. However, because ultrasound of intercostals has only been implemented in the clinical setting recently, feasibility, validity and reliability of these techniques have not been adequately addressed in healthy individuals. Similarly, the use of ultrasound of sternocleidomastoids has not been adequately addressed in healthy individuals, but has been limited to diagnosis of muscular torticollis in infants and children (e.g., Hong et al., 2013).

There is an abundance of literature pertaining to expiratory muscle ultrasound. The expiratory muscles include the transverse abdominis, internal and external obliques and rectus abdominis (of abdominal wall), and internal intercostals and triangularis sterni (of rib cage); all of which can be imaged with ultrasound (Shi et al., 2019). Unlike ultrasound of inspiratory muscles, which is used almost exclusively in the ICU, imaging of expiratory muscles is well-established in the area of biomechanics and physiotherapy, particularly in patients with chronic lower-back pain (Koppenhaver et al., 2009). As such, feasibility, validity and reliability of abdominal muscle ultrasonography have been thoroughly assessed over recent decades (e.g., Arab et al.,

2013; Koppenhaver et al., 2009; Pirri et al., 2019). It is worth noting, however, that none of the abovementioned ultrasound techniques have been used to determine the effect of external loading on muscle contractile properties, as attempted for the diaphragm in this thesis. Moreover, these ultrasound techniques have only been applied at rest. Thus, little is known about the dynamic contractile properties of these muscles during 'real-life' scenarios, such as reflexively-driven hyperpnoea.

Ultrasound shear-wave elastography

For the diaphragm specifically, Chino et al. (2018) were the first to introduce *ultrasound shear-wave elastography* to measure real-time muscle shear modulus (stiffness). Briefly, ultrasound shear-wave elastography quantifies the velocity with which shear waves propagate through tissue. The propagation velocity of shear-waves is directly related to the stiffness of the tissue: the stiffer the tissue, the faster the propagation (Hug et al., 2015). Moreover, propagation velocity is determined by the density of the target tissue. So, in a contracting muscle in which both stiffness and density are elevated, propagation velocity is higher compared to in the relaxed muscle. Consequently, muscle stiffness has been strongly correlated with passive tension (stretching) and active tension during dynamic contractions (Hug et al., 2015).

Only recently has ultrasound shear-wave elastography been used to measure human diaphragm stiffness. As mentioned, Chino et al. (2018) first attempted to quantify diaphragm shear modulus, and found a strong, linear relationship between P_{mo} and diaphragm stiffness during inspiratory resistive loading ($r^2 = 0.99$). Later, Bachasson et al. (2018) extended these findings by showing that P_{di} swing during inspiratory pressure-threshold loading correlated strongly with diaphragm stiffness ($r = 0.77–0.96$; $p < 0.001$). Accordingly, only stiffness of *fresh* diaphragm has been determined with shear-wave elastography, and it is still unknown whether acute changes in muscle contractile properties (e.g., fatigue) can be quantified with the technique. There is evidence from limb locomotor muscle studies (e.g., vastus lateralis and rectus femoris) that shear-wave elastography can be used to quantify fatigue-induced changes in muscle stiffness (Cè et al., 2020). However, although muscle stiffness appears to correlate with force (pressure) output of a muscle, shear-wave elastography does not offer information concerning the muscle's ability to shorten, produce power and perform work (i.e., dynamic properties of a muscle contraction). It is therefore questionable to what extent ultrasound shear-wave elastography can provide novel information about the dynamic contractile properties of diaphragm muscle.

Ultrafast ultrasound

Another recent advance in diaphragm imaging is *ultrafast ultrasound*; first introduced in the early 2000s (Tanter & Fink, 2014). In contrast to conventional ultrasound (as used in this thesis) and ultrasound shear-wave elastography, ultrafast ultrasound has the ability to capture cine-loops with frame rates up to 20,000 FPS by utilising speckle-tracking algorithms to measure the velocity with which image pixels move when the muscle contracts (Tanter & Fink, 2014). It is also possible to derive the dislocation of image pixels, which is considered an *in vivo* estimate of muscle deformation (strain) (Sheng et al., 2020). It was only recently that Poulard et al. (2020) showed that ultrafast ultrasound can be used to assess costal diaphragm axial velocity in response to cervical magnetic stimulation. Although this study has later been criticised for the interpretation of their statistical tests (Beltrami, 2021), the study clearly demonstrated the feasibility of ultrafast ultrasound of the human costal diaphragm in response to evoked twitch contraction. Indeed, one of the strengths of ultrafast ultrasound is the sampling rate of image acquisition: a feature particularly useful during the rapid contractions evoked by nerve stimulation, maximal sniffs or even rapid postural adjustments.

Nonetheless, the technique has not yet been adequately validated or evaluated for reliability. Moreover, the technique has not been used to assess the effect of external loading on costal diaphragm contractile properties (i.e., axial velocity or strain). There is evidence that ultrafast ultrasound may be used to detect fatigue in human limb locomotor muscles, as shown by Sheng et al. (2020) who induced fatigue of quadriceps by electrical stimulation, and found that stimulation-evoked peak strain rate was markedly lower in fatigued muscles. Because the study only included four participants, no statistical tests were performed. It is worth noting that, unlike conventional ultrasound, ultrafast ultrasound is not yet readily available in most medical and research facilities, and the analysis technique is considered advanced and time-consuming (Sheng et al., 2020; Tanter & Fink, 2014). So, although the technique is a promising advance in the area of diaphragm imaging, future research is still necessary to assess its usefulness.

Tissue Doppler ultrasound

Finally, it is worth discussing the use of *tissue Doppler ultrasound* for the assessment of diaphragm contractile properties. Originally, the technique was developed in the 1970s for assessing systolic and diastolic cardiac function, with a particular emphasis on myocardial wall velocity during cardiac cycles. The technique resembles flow Doppler ultrasound by measuring the shift in ultrasound signal frequency reflected from the target tissue. However, whereas flow Doppler quantifies blood flow by measuring high-frequency, low-amplitude signals of moving

blood cells, tissue Doppler instead measures high-amplitude, low-velocity signals from tissue (Ho & Solomon, 2006). Accordingly, tissue Doppler can be used to quantify peak and mean tissue velocity (cm/s), velocity-time integral (cm/s/s) and relaxation velocity (cm/s), as well as to derive measures deformation (strain) of the tissue (Teske et al., 2007).

Although Doppler ultrasound has been thoroughly validated for myocardium analysis, it has only recently been applied to the human diaphragm (Fayssoil et al., 2019; Soilemezi et al., 2020). In fact, the technique is considered by some to hold much promise for the future of diaphragm imaging (McCool & Tzelepis, 2020). Fayssoil et al. (2019), for instance, used tissue Doppler ultrasound to measure crural diaphragm tissue velocity in response to maximal sniffs in healthy adults and in patients with muscular disorders. The authors found that diaphragm tissue velocity during maximal sniffs was significantly lower (–46%) in patients compared to healthy controls (median 6 vs. 13 cm/s; $p < 0.001$). In turn, this technique may provide useful information concerning inspiratory muscle function in patients with neuromuscular disorders beyond that provided by standard pulmonary function tests, ultimately speaking to the validity of the approach.

A limitation associated with tissue Doppler ultrasound is that tissue velocity can only be measured in one (vertical) direction and in a limited ROI. Thus, for a tissue moving diagonally or along multiple axes, such as crural diaphragm during increasing ventilatory load, the technique may be of limited use. Although Fayssoil et al. (2019) found it feasible to quantify crural diaphragm tissue velocity in response to maximal sniffs, evidence from this thesis suggests that a static, one-dimensional cursor may not capture the full extent of crural diaphragm excursion with a subcostal approach (see Chapter 5, section 5.3.9). Another concern is that tissue Doppler was originally intended and validated for myocardium analysis. Like speckle-tracking algorithms, which were found not to be feasible in Chapter 4, there may be reason for concern regarding the validity and reliability of the technique to capture diaphragm contractile properties. Nonetheless, tissue Doppler ultrasound is a well-established tool in echocardiography, and so, the equipment perform these analyses is readily available in most clinical and/or medical research institutions. Moreover, analysis of Doppler ultrasound is highly automated by specialty software (e.g., EchoPac from GE Medical), and therefore requires little training to perform.

9.6 Conclusion

Contractile function of the *in vivo* diaphragm is characterised by the ability to shorten, generate force and produce power. This thesis is the first to objectively measure these characteristics in humans. The overarching aim was to evaluate the usefulness of ultrasonography for the assessment of *in vivo* contractile properties of fresh and fatigue diaphragm in healthy adults. It was established that ultrasonography provides objective and reliable measures of crural diaphragm kinetics and costal diaphragm shortening in response to various non-volitional and volitional perturbations. In addition, ultrasonography can be used to compare diaphragm contractile properties (i.e., kinetics) across different modes of hyperpnoea as well as to quantify the effect of external loading (fatigue) on some of these contractile properties.

The methodological framework presented in this thesis has various applications. Ultrasonography can be used to further characterise the effect of external loading on fatigue task-dependency and respiratory muscle training in healthy adults and trained athletes. Moreover, these techniques can be applied to promote greater understanding the various roles of the respiratory muscles in healthy ageing, particularly in balance maintenance and fall prevention. Ideas for future research have been explored, and may include techniques such as shear-wave elastography, ultrafast ultrasound and tissue Doppler ultrasound. Imaging technology is under constant development, with imaging resolution, analysis algorithms and hardware exponentially improving. As innovative technologies emerge, it may be possible to overcome the methodological limitations identified in this thesis, leading to a more robust and comprehensive appreciation of the dynamic characteristics of respiratory muscles and their significance in health and disease. This thesis has drawn attention to the broad potential applications of imaging techniques in understanding respiratory mechanics, and it is important that investigators remain informed of contemporary developments in this rapidly emerging technological landscape.

References

Aaron, E. A., Seow, C. K., Johnson, B. D., & Dempsey, J. A. (1992). Oxygen cost of exercise hyperpnea: implications for performance. *Journal of Applied Physiology*, *72*(5), 1818–1825. https://doi.org/10.1152/jappl.1992.72.5.1818.

Abbate, F., Sargeant, A. J., Verdijk, P. W. L., & De Haan, A. (2000). Effects of high-frequency initial pulses and posttetanic potentiation on power output of skeletal muscle. *Journal of Applied Physiology*, *88*(1), 35–40. https://doi.org/10.1152/jappl.2000.88.1.35

Agostoni, E., & Fenn, W. O. (1960). Velocity of muscle shortening as a limiting factor in respiratory air flow. *Journal of Applied Physiology*, *15*, 349–353. https://doi.org/10.1152/jappl.1960.15.3.349

Agostoni, E., & Rahn, H. (1960). Abdominal at different and thoracic pressures lung volumes. *Journal of Applied Physiology*, *15*, 1087–1092. https://doi.org/10.1152/jappl.1960.15.6.1087

Alcazar, J., Csapo, R., Ara, I., & Alegre, L. M. (2019). On the shape of the force-velocity relationship in skeletal muscles: the linear, the hyperbolic, and the double-hyperbolic. *Frontiers in Physiology*, *10*(6), 1–21. https://doi.org/10.3389/fphys.2019.00769

Aldrich, T. K., Sinderby, C., McKenzie, D. K., Estenne, M., & Gandveia, S. C. (2005). Electrophysiologic techniques for the assessment of respiratory muscle function. In *ATS/ERS Statement on Respiratory Muscle Testing* (pp. 548–557). https://doi.org/10.1164/rccm.166.4.518

Aliverti, A., Cala, S. J., Duranti, R., Ferrigno, G., Kenyon, C. M., Pedotti, A., Scano, G., Sliwinski, P., Macklem, P. T., & Yan, S. (1997). Human respiratory muscle actions and control during exercise. *Journal of Applied Physiology*, *83*(4), 1256–1269. https://doi.org/10.1152/jappl.1997.83.4.1256

Allen, D. G., Lamb, G. D., & Westerblad, H. (2008). Skeletal muscle fatigue: cellular mechanisms. *Physiological Reviews*, *88*(1), 287–332. https://doi.org/10.1152/physrev.00015.2007

Allen, D. G., Whitehead, N. P., & Yeung, E. W. (2005). Mechanisms of stretch-induced muscle damage in normal and dystrophic muscle: Role of ionic changes. *Journal of Physiology*, *567*(3), 723–735. https://doi.org/10.1113/jphysiol.2005.091694

Ameredes, B. T., Zhan, W.-Z., Prakash, Y. S., Vandenboom, R., & Sieck, G. C. (2006). Power fatigue of the rat diaphragm muscle. *Journal of Applied Physiology*, *89*(6), 2215–2219. https://doi.org/10.1152/jappl.2000.89.6.2215

Andersen, P., & Saltin, B. (1985). Maximal perfusion of skeletal muscle in man. *Journal of Physiology*, *366*(1), 233–249. https://doi.org/10.1113/jphysiol.1985.sp015794

Arab, A. M., Rasouli, O., Amiri, M., & Tahan, N. (2013). Reliability of ultrasound measurement of automatic activity of the abdominal muscle in participants with and without chronic low back pain. *Chiropractic and Manual Therapies*, *21*(1), 1. https://doi.org/10.1186/2045-709X-21-37

Archiza, B., Welch, J. F., Geary, C. M., Allen, G. P., Borghi-Silva, A., & Sheel, A. W. (2018). Temporal characteristics of exercise-induced diaphragmatic fatigue. *Journal of Applied Physiology*, *124*(4), 906–914. https://doi.org/10.1152/japplphysiol.00942.2017

Arora, N. S., & Rochester, D. F. (1982). Effect of body weight and muscularity on human diaphragm muscle mass, thickness, and area. *Journal of Applied Physiology: Respiratory, Environmental and Exercise Physiology*, *52*(1), 64–70. https://doi.org/10.1152/jappl.1982.52.1.64

Aubier, M. (1986). Effect of theophylline on diaphragmatic and other skeletal muscle function. *The Journal of Allergy and Clinical Immunology*, *78*(4, pt 2), 787–792. https://doi.org/10.1016/0091-6749(86)90062-x

Aubier, M., Farkas, G., De Troyer, A., Mozes, R., & Roussos, C. (1981). Detection of diaphragmatic fatigue in man by phrenic stimulation. *Journal of Applied Physiology*, *50*(3), 538–544. https://doi.org/10.1152/jappl.1981.50.3.538

Ayoub, J., Cohendy, R., Dauzat, M., Targhetta, R., De La Coussaye, J. E., Bourgeois, J. M., Ramonatxo, M., Prefaut, C., & Pourcelot, L. (1997). Non-invasive quantification of diaphragm kinetics using m-mode sonography. *Canadian Journal of Anaesthesia*, *44*(7), 739–744. https://doi.org/10.1007/BF03013389

Babcock, M. A., Pegelow, D. F., Johnson, B. D., & Dempsey, J. A. (1996). Aerobic fitness effects on exercise-induced low-frequency diaphragm fatigue. *Journal of Applied Physiology*, *81*(5), 2156–2164. https://doi.org/10.1152/jappl.1996.81.5.2156

Babcock, M. A., Pegelow, D. F., McClaran, S. R., Suman, O. E., & Dempsey, J. A. (1995). Contribution of diaphragmatic power output to exercise-induced diaphragm fatigue. *J Appl Physiol*, *75*(5), 1710–1719. https://doi.org/10.1152/jappl.1995.78.5.1710

Babcock, M. A., Pegelow, D. F., Taha, B. H., & Dempsey, J. A. (1998). High frequency diaphragmatic fatigue detected with paired stimuli in humans. *Medicine & Science in Sports & Exercise*, *30*(4), 506–511. https://doi.org/10.1097/00005768-199804000-00006

Bachasson, D., Dres, M., Niérat, M. C., Gennisson, J. L., Hogrel, J. Y., Doorduin, J., & Similowski, T. (2018). Diaphragm shear modulus reflects transdiaphragmatic pressure during isovolumetric inspiratory efforts and ventilation against inspiratory loading. *Journal of Applied Physiology*, *126*(3), 699–707. https://doi.org/10.1152/japplphysiol.01060.2018

Baldwin, C. E., Paratz, J. D., & Bersten, A. D. (2011). Diaphragm and peripheral muscle thickness on ultrasound: Intra-rater reliability and variability of a methodology using non-standard recumbent positions. *Respirology*, *16*(7), 1136–1143. https://doi.org/10.1111/j.1440-1843.2011.02005.x

Bárány, K., Ledvora, R. F., Meulen, D. L. V, & Bárány, M. (1983). Myosin light chain phosphorylation during contraction of chicken fast and slow skeletal muscles. *Archives of Biochemistry and Biophysics*, *225*(2), 692–703. https://doi.org/10.1016/0003-9861(83)9008-2

Barnard, P. A., & Levine, S. (1986). Critique on application of diaphragmatic time-tension index to spontaneously breathing humans. *Journal of Applied Physiology*, *60*(3), 1067–1072. https://doi.org/10.1152/jappl.1986.60.3.1067

Baydur, A., Behrakis, P. K., Zin, W. A., Jaeger, M., & Milic-Emili, J. (1982). A simple method for assessing the validity of the esophageal balloon technique. *The American Review of Respiratory Disease*, *126*(5), 788–791. https://doi.org/10.1164/arrd.1982.126.5.788

Bellani, G., Mauri, T., Coppadoro, A., Grasselli, G., Patroniti, N., Spadaro, S., Sala, V., Foti, G., & Pesenti, A. (2013). Estimation of patient's inspiratory effort from the electrical

activity of the diaphragm. *Critical Care Medicine*, *41*(6), 1483–1491. https://doi.org/10.1097/CCM.0b013e31827caba0

Bellemare, F., & Bigland-Ritchie, B. (1984). Assessment of human diaphragm strength and activation using phrenic nerve stimulation. *Respiration Physiology*, *58*(3), 263–277. https://doi.org/10.1016/0034-5687(84)90003-3

Bellemare, F., & Bigland-Ritchie, B. (1987). Central components of diaphragmatic fatigue assessed by phrenic nerve stimulation. *Journal of Applied Physiology*, *62*(3), 1307–1316. https://doi.org/10.1152/jappl.1987.62.3.1307

Bellemare, F., & Grassino, A. (1982). Effect of pressure and timing of contraction on human diaphragm fatigue. *Journal of Applied Physiology: Respiratory, Environmental and Exercise Physiology*, *53*(5), 1190–1195. https://doi.org/10.1164/ajrccm/147.4.857

Bellemare, F., & Poirier, C. (2005). Diaphragm responses to stimulation. In Qutayba Hamid, J. Shannon, & J. Martin (Eds.), *Physiologic Basis of Respiratory Disease* (pp. 755–768). BC Decker Inc.

Bellemare, F., Wight, D., Lavigne, C. M., & Grassino, A. (1983). Effect of tension and timing of contraction on the blood flow of the diaphragm. *Journal of Applied Physiology Respiratory Environmental and Exercise Physiology*, *54*(6), 1597–1606. https://doi.org/10.1152/jappl.1983.54.6.1597

Beltrami, F. G. (2021). Is maximal diaphragm tissue velocity suited for assessment of diaphragm contractility? *Journal of Physiology*, *599*(8), 2341–2342. https://doi.org/10.1113/JP281149

Benowitz, N. L. (1990). Clinical pharmacology of caffeine. *Annual Review of Medicine*, *41*, 277–288. https://doi.org/10.1146/annurev.me.41.020190.001425

Bigland-Ritchie, B., & Woods, J. J. (1984). Changes in muscle contractile properties and neural control during human muscular fatigue. *Muscle & Nerve*, *7*(9), 691–699. https://doi.org/10.1002/mus.880070902

Bland, J. M. (2006). *How should I calculate a within-subject coefficient of variation?* https://www-users.york.ac.uk/~mb55/meas/cv.htm

Bland, J. M., & Altman, D. G. (1995a). Calculating correlation coefficients with repeated

observations: Part 1 — correlation within subjects. *British Medical Journal*, *310*(6977), 446. https://doi.org/10.1136/bmj.310.6977.446

Bland, J. M., & Altman, D. G. (1995b). Calculating correlation coefficients with repeated observations: Part 2 - correlation between subjects. *British Medical Journal*, *310*(6980), 633. https://doi.org/10.1136/bmj.310.6980.633

Blazek, D., Stastny, P., Maszczyk, A., Krawczyk, M., Matykiewicz, P., & Petr, M. (2019). Systematic review of intra-abdominal and intrathoracic pressures initiated by the Valsalva manoeuvre during high-intensity resistance exercises. *Biology of Sport*, *36*(4), 373–386. https://doi.org/10.5114/biolsport.2019.88759

Block, B. (2004). *Color atlas of ultrasound anatomy* (1st ed.). Georg Thieme Verlag, Stuttgart, Germany. www.thieme.com

Borg, G. (1998). *Borg´s Perceived Exertion and Pain Scales* (B. Lane, J. Rhoda, S. M. Bott, & C. Mitchell (eds.)). Human Kinetics; Leeds, United Kingdom. https://doi.org/10.1097/00005768-199809000-00018

Boussuges, A., Gole, Y., & Blanc, P. (2009). Diaphragmatic motion studied by M-Mode ultrasonography: methods, reproducibility, and normal values. *Chest*, *135*(2), 391–400. https://doi.org/10.1378/chest.08-1541

Boyas, S., & Guével, A. (2011). Neuromuscular fatigue in healthy muscle: underlying factors and adaptation mechanisms. *Annals of Physical and Rehabilitation Medicine*, *54*(2), 88–108. https://doi.org/10.1016/j.rehab.2011.01.001

Brancaccio, P., Limongelli, F. M., D'Aponte, A., Narici, M., & Maffulli, N. (2008). Changes in skeletal muscle architecture following a cycloergometer test to exhaustion in athletes. *Journal of Science and Medicine in Sport*, *11*(6), 538–541. https://doi.org/10.1016/j.jsams.2007.05.011

Braun, N. M., Arora, N. S., & Rochester, D. F. (1982). Force-length relationship of the normal human diaphragm. *Journal of Applied Physiology Respiratory Environmental and Exercise Physiology*, *53*(2), 405–412. https://doi.org/10.1152/jappl.1982.53.2.405

Buchfuhrer, M. J., Hansen, J. E., Robinson, T. E., Sue, D. Y., Wasserman, K., & Whipp, B. J. (1983). Optimizing the exercise protocol for cardiopulmonary assessment. *Journal of*

Applied Physiology Respiratory Environmental and Exercise Physiology, *55*(5), 1558–1564. https://doi.org/10.1152/jappl.1983.55.5.1558

Buchler, B., Magder, S., Katsardis, H., Jammes, Y., & Roussos, C. (1985). Effects of pleural pressure and abdominal pressure on diaphragmatic blood flow. *Journal of Applied Physiology*, *58*(3), 691–697. https://doi.org/10.1152/jappl.1985.58.3.691

Bunnell, A., Ney, J., Gellhorn, A., & Hough, C. L. (2015). Quantitative neuromuscular ultrasound in intensive care unit-acquired weakness: A systematic review. *Muscle and Nerve*, *52*(5), 701–708. https://doi.org/10.1002/mus.24728

Butler, J. E. (2007). Drive to the human respiratory muscles. *Respiratory Physiology and Neurobiology*, *159*(2), 115–126. https://doi.org/10.1016/j.resp.2007.06.006

Butler, J. E., & Gandevia, S. C. (2008). The output from human inspiratory motoneurone pools. *Journal of Physiology*, *586*(5), 1257–1264. https://doi.org/10.1113/jphysiol.2007.145789

Butler, J. E., McKenzie, D. K., & Gandevia, S. C. (2001). Discharge frequencies of single motor units in human diaphragm and parasternal muscles in lying and standing. *Journal of Applied Physiology*, *90*(1), 147–154. https://doi.org/10.1152/jappl.2001.90.1.147

Cala, S. J., Edyvean, J., & Engel, L. A. (1992). Chest wall and trunk muscle activity during inspiratory loading. *Journal of Applied Physiology*, *73*(6), 2373–2381. https://doi.org/10.1152/jappl.1992.73.6.2373

Calderón, J. C., Bolaños, P., & Caputo, C. (2014). The excitation-contraction coupling mechanism in skeletal muscle. *Biophysical Reviews*, *6*(1), 133–160. https://doi.org/10.1007/s12551-013-0135-x

Canepari, M., Pellegrino, M. A., D'Antona, G., & Bottinelli, R. (2010). Single muscle fiber properties in aging and disuse. *Scandinavian Journal of Medicine and Science in Sports*, *20*(1), 10–19. https://doi.org/10.1111/j.1600-0838.2009.00965.x

Carrillo-Esper, R., Perez-Calatayud, A. A., Arch-Tirado, E., Diaz-Carrillo, M. A., Garrido-Aguirre, E., Tapia-Velazco, R., Pena-Perez, C. A., Espinoza-de los Monteros, I., Meza-Marquez, J. M., Flores-Rivera, O. I., Zepeda-Mendoza, A. D., & de la Torre-Leon, T. (2016). Standardization of sonographic diaphragm thickness evaluations in healthy volunteers. *Respiratory Care*, *61*(7), 920–924. https://doi.org/10.4187/respcare.03999

Carroll, T. J., Taylor, J. L., & Gandevia, S. C. (2017). Recovery of central and peripheral neuromuscular fatigue after exercise. *Journal of Applied Physiology*, *122*(5), 1068–1076. https://doi.org/10.1152/japplphysiol.00775.2016

Cè, E., Longo, S., Limonta, E., Coratella, G., Rampichini, S., & Esposito, F. (2020). Peripheral fatigue: new mechanistic insights from recent technologies. *European Journal of Applied Physiology*, *120*(1), 17–39. https://doi.org/10.1007/s00421-019-04264-w

Chino, K., Ohya, T., Katayama, K., & Suzuki, Y. (2018). Diaphragmatic shear modulus at various submaximal inspiratory mouth pressure levels. *Respiratory Physiology and Neurobiology*, *252–253*, 52–57. https://doi.org/10.1016/j.resp.2018.03.009

Clausen, T. (2003). Na+ -K+ pump regulation and skeletal muscle contractility. *Physiological Reviews*, *83*(4), 1269–1324. https://doi.org/10.1152/physrev.00011.2003

Cohn, D., Benditt, J. O., Eveloff, S., & McCool, F. D. (1997). Diaphragm thickening during inspiration. *Journal of Applied Physiology*, *83*(1), 291–296. https://doi.org/10.1152/jappl.1997.83.1.291

Coirault, C., Chemla, D., Pery-Man, N., Suard, I., & Lecarpentier, Y. (1995). Effects of fatigue on force-velocity relation of diaphragm: Energetic implications. *American Journal of Respiratory and Critical Care Medicine*, *151*(1), 123–128. https://doi.org/10.1164/ajrccm.151.1.7812541

Coirault, C., Chemla, D., Pourny, J. C., Lambert, F., & Lecarpentier, Y. (1997). Instantaneous force-velocity-length relationship in diaphragmatic sarcomere. *Journal of Applied Physiology*, *82*(2), 404–412. https://doi.org/10.1152/jappl.1997.82.2.404

Collett, P. W., Perry, C., & Engel, L. A. (1985). Pressure-time product, flow, and oxygen cost of resistive breathing in humans. *Journal of Applied Physiology*, *58*(4), 1263–1272. https://doi.org/10.1152/jappl.1985.58.4.1263

Cooke, R., Franks, K., Luciani, G. B., & Pate, E. (1988). The inhibition of rabbit skeletal muscle contraction by hydrogen ions and phosphate. *The Journal of Physiology*, *395*, 77–97. https://doi.org/10.1113/jphysiol.1988.sp016909

Cooper, S., & Eccles, J. C. (1930). The isometric responses of mammalian muscles. *The Journal of Physiology*, *69*(4), 377–385. https://doi.org/10.1113/jphysiol.1930.sp002657

Corbellini, C., Boussuges, A., Villafañe, J. H., & Zocchi, L. (2018). Diaphragmatic mobility loss in subjects with moderate to very severe COPD may improve after in-patient pulmonary rehabilitation. *Respiratory Care*, *63*(10), 1271–1280. https://doi.org/10.4187/respcare.06101

Cory, J. M., Schaeffer, M. R., Wilkie, S. S., Ramsook, A. H., Puyat, J. H., Arbour, B., Basran, R., Lam, M., Les, C., MacDonald, B., Jensen, D., & Guenette, J. A. (2015). Sex differences in the intensity and qualitative dimensions of exertional dyspnea in physically active young adults. *Journal of Applied Physiology*, *119*(9), 998–1006. https://doi.org/10.1152/japplphysiol.00520.2015

Criée, C. P., Sorichter, S., Smith, H. J., Kardos, P., Merget, R., Heise, D., Berdel, D., Köhler, D., Magnussen, H., Marek, W., Mitfessel, H., Rasche, K., Rolke, M., Worth, H., & Jörres, R. A. (2011). Body plethysmography - its principles and clinical use. *Respiratory Medicine*, *105*(7), 959–971. https://doi.org/10.1016/j.rmed.2011.02.006

Cronin, N. J., & Lichtwark, G. (2013). The use of ultrasound to study muscle-tendon function in human posture and locomotion. *Gait and Posture*, *37*(3), 305–312. https://doi.org/10.1016/j.gaitpost.2012.07.024

Cross, T. J., Lalande, S., Hyatt, R. E., & Johnson, B. D. (2015). Response characteristics of esophageal balloon catheters handmade using latex and nonlatex materials. *Physiological Reports*, *3*(6), e12426. https://doi.org/10.14814/phy2.12426

Csapo, R., Alegre, L. M., & Baron, R. (2011). Time kinetics of acute changes in muscle architecture in response to resistance exercise. *Journal of Science and Medicine in Sport*, *14*(3), 270–274. https://doi.org/10.1016/j.jsams.2011.02.003

Cuevas-Trisan, R. (2017). Balance problems and fall risks in the elderly. *Physical Medicine and Rehabilitation Clinics of North America*, *28*(4), 727–737. https://doi.org/10.1016/j.pmr.2017.06.006

Cunha, M., Mendes, F., Paciência, I., Rodolfo, A., Carneiro-Leão, L., Rama, T., Rufo, J., Delgado, L., & Moreira, A. (2019). The effect of inspiratory muscle training on swimming performance, inspiratory muscle strength, lung function, and perceived breathlessness in elite swimmers. *Porto Biomedical Journal*, *4*(6), e49. https://doi.org/10.1097/j.pbj.0000000000000049

D'Angelo, E., & Milic-Emili, J. (2005). Statics of the respiratory system. In Qutayba Hamid, J. Shannon, & J. Martin (Eds.), *Physiological Basis of Respiratory Disease* (pp. 15–25). BC Decker Inc.

D'Antona, G., Pellegrino, M. A., Adami, R., Rossi, R., Naccari Carlizzi, C., Canepari, M., Saltin, B., & Bottinelli, R. (2003). The effect of ageing and immobilization on structure and function of human skeletal muscle fibres. *Journal of Physiology*, *552*(2), 499–511. https://doi.org/10.1113/jphysiol.2003.046276

D'Urzo, A. D., Jhirad, R., Jenne, H., Avendano, M. A., Rubenstein, I., D'Costa, M., & Goldstein, R. S. (1990). Effect of caffeine on ventilatory responses to hypercapnia, hypoxia, and exercise in humans. *Journal of Applied Physiology*, *68*(1), 322–328. https://doi.org/10.1152/jappl.1990.68.1.322

Dall'Ago, P., Chiappa, G. R. S., Guths, H., Stein, R., & Ribeiro, J. P. (2006). Inspiratory muscle training in patients with heart failure and inspiratory muscle weakness: A randomized trial. *Journal of the American College of Cardiology*, *47*(4), 757–763. https://doi.org/10.1016/j.jacc.2005.09.052

de Jongh, F. (2008). Spirometers. *Breathe*, *4*(3), 251–254. https://doi.org/10.3109/03091908109042435

De Troyer, A., & Boriek, A. M. (2011). Mechanics of the respiratory muscles. *Comprehensive Physiology*, *1*(3), 1273–1300. https://doi.org/10.1002/cphy.c100009

De Troyer, A., Cappello, M., & Brichant, J. F. (1994). Do canine scalene and sternomastoid muscles play a role in breathing? *Journal of Applied Physiology*, *76*(1), 242–252. https://doi.org/10.1152/jappl.1994.76.1.242

De Troyer, A., Cappello, M., Meurant, N., & Scillia, P. (2003). Synergism between the canine left and right hemidiaphragms. *Journal of Applied Physiology*, *94*(5), 1757–1765. https://doi.org/10.1152/japplphysiol.01013.2002

De Troyer, A., Sampson, M., Sigrist, S., & Macklem, P. T. (1982). Action of costal and crural parts of the diaphragm on the rib cage in dogs. *Journal of Applied Physiology*, *53*(1), 30–39. https://doi.org/10.1152/jappl.1982.53.1.30

Dempsey, J. A., Romer, L. M., Rodman, J., Miller, J., & Smith, C. (2006). Consequences of

exercise-induced respiratory muscle work. *Respiratory Physiology and Neurobiology*, *151*(2–3), 242–250. https://doi.org/10.1016/j.resp.2005.12.015

Dick, T. E., & Van Lunteren, E. (1990). Fiber subtype distribution of pharyngeal dilator muscles and diaphragm in the cat. *Journal of Applied Physiology*, *68*(5), 2237–2240. https://doi.org/10.1152/jappl.1990.68.5.2237

Dominelli, P. B., Archiza, B., Ramsook, A. H., Mitchell, R. A., Peters, C. M., Molgat-Seon, Y., Henderson, W. R., Koehle, M. S., Boushel, R., & Sheel, A. W. (2017). Effects of respiratory muscle work on respiratory and locomotor blood flow during exercise. *Experimental Physiology*, *102*(11), 1535–1547. https://doi.org/10.1113/EP086566

Dominelli, P. B., & Sheel, A. W. (2012). Experimental approaches to the study of the mechanics of breathing during exercise. *Respiratory Physiology & Neurobiology*, *180*, 147–161. https://doi.org/http://dx.doi.org/10.1016/j.resp.2011.10.005

Dres, M., Dubé, B. P., Goligher, E., Vorona, S., Demiri, S., Morawiec, E., Mayaux, J., Brochard, L., Similowski, T., & Demoule, A. (2020). Usefulness of Parasternal Intercostal Muscle Ultrasound during Weaning from Mechanical Ventilation. *Anesthesiology*, *132*(5), 1114–1125. https://doi.org/10.1097/ALN.0000000000003191

Dres, M., Dube, B. P., Mayaux, J., Delemazure, J., Reuter, D., Brochard, L., Similowski, T., & Demoule, A. (2017). Coexistence and impact of limb muscle and diaphragm weakness at time of liberation from mechanical ventilation in medical intensive care unit patients. *American Journal of Respiratory and Critical Care Medicine*, *195*(1), 57–66. https://doi.org/10.1164/rccm.201602-0367OC

Dres, M., Goligher, E. C., Dubé, B. P., Morawiec, E., Dangers, L., Reuter, D., Mayaux, J., Similowski, T., & Demoule, A. (2018). Diaphragm function and weaning from mechanical ventilation: an ultrasound and phrenic nerve stimulation clinical study. *Annals of Intensive Care*, *8*(1). https://doi.org/10.1186/s13613-018-0401-y

Dubé, B. P., Dres, M., Mayaux, J., Demiri, S., Similowski, T., & Demoule, A. (2017). Ultrasound evaluation of diaphragm function in mechanically ventilated patients: Comparison to phrenic stimulation and prognostic implications. *Thorax*, *72*(9), 811–818. https://doi.org/10.1136/thoraxjnl-2016-209459

Duffin, J. (2011). Measuring the respiratory chemoreflexes in humans. *Respiratory Physiology*

and Neurobiology, *177*(2), 71–79. https://doi.org/10.1016/j.resp.2011.04.009

Dutton, K., Blanksby, B. A., & Morton, A. R. (1989). CO2 sensitivity changes during the menstrual cycle. *Journal of Applied Physiology*, *67*(2), 517–522. https://doi.org/10.1152/jappl.1989.67.2.517

Easton, P. A., Abe, T., Smith, J., Fitting, J. W., Guerraty, A., & Grassino, A. E. (1995). Activity of costal and crural diaphragm during progressive hypoxia or hypercapnia. *Journal of Applied Physiology*, *78*(5), 1985–1992. https://doi.org/10.1152/jappl.1995.78.5.1985

Easton, P. A., Fitting, J. W., Arnoux, R., Guerraty, A., & Grassino, A. E. (1993). Costal and crural diaphragm functioning during CO2 rebreathing in awake dogs. *Journal of Applied Physiology*, *74*(3), 1406–1418. https://doi.org/10.1152/jappl.1993.74.3.1406

Elkins, M., & Dentice, R. (2015). Inspiratory muscle training facilitates weaning from mechanical ventilation among patients in the intensive care unit: A systematic review. *Journal of Physiotherapy*, *61*(3), 125–134. https://doi.org/10.1016/j.jphys.2015.05.016

Elliott, J. E., Greising, S. M., Mantilla, C. B., & Sieck, G. C. (2016). Functional impact of sarcopenia in respiratory muscles. *Respiratory Physiology & Neurobiology*, *226*(Jun), 137–146. https://doi.org/doi:10.1016/j.resp.2015.10.001

Enoka, R. M. (1995). Mechanisms of muscle fatigue: Central factors and task dependency. *Journal of Electromyography and Kinesiology*, *5*(3), 141–149. https://doi.org/10.1016/1050-6411(95)00010-W

Enoka, R. M., & Duchateau, J. (2016). Translating fatigue to human performance. *Medicine and Science in Sports and Exercise*, *48*(11), 2228–2238. https://doi.org/10.1249/MSS.0000000000000929

Enoka, R. M., & Stuart, D. G. (1992). Neurobiology of muscle fatigue. *Journal of Applied Physiology*, *72*(5), 1631–1648. https://doi.org/10.1152/jappl.1992.72.5.1631

Estenne, M., Yernault, J. C., & De Troyer, A. (1985). Rib cage and diaphragm-abdomen compliance in humans: effects of age and posture. *Journal of Applied Physiology*, *59*(6), 1842–1848. https://doi.org/10.1152/jappl.1985.59.6.1842

European Respiratory Society. (2018). *European Respiratory Society Monograph: thoracic ultrasound* (C. B. Laursen, N. M. Rahman, & G. Volpicelli (eds.)). European Respiratory

Society. https://doi.org/10.1183/2312508X.erm7918

Evans, J., & Whitelaw, W. (2009). The assessment of maximal respiratory mouth pressures in adults. *Respiratory Care*, *54*(10), 1348–1359. https://doi.org/10.1111/j.1365-2036.2011.04905.x

Farkas, G. A., & Rochester, D. F. (1988). Functional characteristics of canine costal and crural diaphragm. *Journal of Applied Physiology*, *65*(5), 2253–2260. https://doi.org/10.1152/jappl.1988.65.5.2253

Fayssoil, A., Nguyen, L. S., Ogna, A., Stojkovic, T., Meng, P., Mompoint, D., Carlier, R., Prigent, H., Clair, B., Behin, A., Laforet, P., Bassez, G., Crenn, P., Orlikowski, D., Annane, D., Eymard, B., & Lofaso, F. (2019). Diaphragm sniff ultrasound: normal values, relationship with sniff nasal pressure and accuracy for predicting respiratory involvement in patients with neuromuscular disorders. *PLoS ONE*, *14*(4), e0214288. https://doi.org/10.1371/journal.pone.0214288

Fenn, W. O., & Marsh, B. S. (1935). Muscular force at different speeds of shortening. *Journal of Physiology*, *85*(2), 277–297. https://doi.org/10.1113/jphysiol.1935.sp003318

Ferrari, G., Helbo Skaarup, S., Panero, F., & Wrightson, J. M. (2018). The diaphragm. In C. B. Laursen, N. M. Rahman, & G. Volpicelli (Eds.), *European Respiratory Society Monograph: Thoracic Ultrasound* (pp. 129–147). European Respiratory Society.

Finucane, K. E., & Singh, B. (2009). Human diaphragm efficiency estimated as power output relative to activation increases with hypercapnic hyperpnea. *Journal of Applied Physiology*, *107*(5), 1397–1405. https://doi.org/10.1152/japplphysiol.91465.2008

Fitting, J. W., Easton, P. A., & Grassino, A. E. (1985). Velocity of shortening of inspiratory muscles and inspiratory flow. *Journal of Applied Physiology*, *60*(2), 670–677. https://doi.org/doi: 10.1152/jappl.1986.60.2.670

Fitts, R. H. (1994). Cellular mechanisms of muscle fatigue. *Physiological Reviews*, *74*(1), 49–94. https://doi.org/10.1152/physrev.1994.74.1.49

Fitts, R. H. (2008). The cross-bridge cycle and skeletal muscle fatigue. *Journal of Applied Physiology*, *104*(2), 551–558. https://doi.org/10.1152/japplphysiol.01200.2007

Fitts, R. H., McDonald, K. S., & Schluter, J. M. (1991). The determinants of skeletal muscle

force and power: their adaptability with changes in activity pattern. *Journal of Biomechanics*, *24*(Suppl. 1), 111–122. https://doi.org/10.1016/0021-9290(91)90382-W

Fogarty, M. J., Mantilla, C. B., & Sieck, G. C. (2018). Breathing: motor control of diaphragm muscle. *Physiology*, *33*(2), 113–126. https://doi.org/10.1152/physiol.00002.2018

Forsha, D., Risum, N., Rajagopal, S., Dolgner, S., Hornik, C., Barnhart, H., Kisslo, J., & Barker, P. (2015). The influence of angle of insonation and target depth on speckle-tracking strain. *Journal of the American Society of Echocardiography*, *28*(5), 580–586. https://doi.org/10.1016/j.echo.2014.12.015

Gallagher, C. G., Hof, V. I., & Younes, M. (1985). Effect of inspiratory muscle fatigue on breathing pattern. *Journal of Applied Physiology*, *59*(4), 1152–1158. https://doi.org/10.1152/jappl.1985.59.4.1152

Gandevia, S. C. (2001). Spinal and supraspinal factors in human muscle fatigue. *Physiological Reviews*, *81*(4), 1725–1789. https://doi.org/10.1152/physrev.2001.81.4.1725

Gandevia, S. C., Butler, J. E., Hodges, P. W., & Taylor, J. L. (2002). Balancing acts: respiratory sensations, motor control and human posture. *Clinical and Experimental Pharmacology and Physiology*, *29*(1–2), 118–121. https://doi.org/10.1046/j.1440-1681.2002.03611.x

Gandevia, S. C., Killian, K. J., & Campbell, E. J. M. (1981). The effect of respiratory muscle fatigue on respiratory sensations. *Clinical Science*, *60*(4), 463–466. https://doi.org/10.1042/cs0600463

Gea, J., Zhu, E., Gáldiz, J. B., Comtois, N., Salazkin, I., Fiz, A., & Grassino, A. (2009). Functional consequences of eccentric contractions of the diaphragm. *Archivos De Bronchoneumologia*, *45*(2), 68–74. https://doi.org/10.1016/S1579-2129(09)70777-3

Geary, C. M., Welch, J. F., McDonald, M. R., Peters, C. M., Leahy, M. G., Reinhard, P. A., & Sheel, A. W. (2019). Diaphragm fatigue and inspiratory muscle metaboreflex in men and women matched for absolute diaphragmatic work during pressure-threshold loading. *Journal of Physiology*, *597*(18), 4797–4808. https://doi.org/10.1113/JP278380

Gerscovich, E. O., Cronan, M., McGahan, J. P., Jain, K., Jones, C. D., & McDonald, C. (2001). Ultrasonographic evaluation of diaphragmatic motion. *Journal of Ultrasound in Medicine*, *20*(6), 597–604. https://doi.org/10.7863/jum.2001.20.6.597

Gibson, G. J., Whitelaw, W., Siafakas, N., Supinski, G. S., Fitting, J. W., Bellemare, F., Loring, S. H., Troyer, A. de, & Grassino, A. E. (2002). ATS/ERS statement on respiratory muscle testing. *American Journal of American Critical Care Medicine*, *166*(4), 518–624. https://doi.org/10.1164/rccm.166.4.518

Gierada, D. S., Curtin, J. J., Erickson, S. J., Prost, R. W., Strandt, J. A., & Goodman, L. R. (1995). Diaphragmatic motion: fast gradient-recalled-echo MR imaging in healthy subjects. *Radiology*, *194*(3), 879–884. https://doi.org/10.1148/radiology.194.3.7862995

Goldman, M. D., Grassino, A., Mead, J., Sears, T. A., Mean, J., & Sears, T. A. (1978). Mechanics of the human diaphragm during voluntary contraction: dynamics. *Journal of Applied Physiology*, *44*(6), 840–848. https://doi.org/10.1152/jappl.1978.44.6.829

Goldman, M. D., Grimby, G., & Mead, J. (1976). Mechanical work of breathing derived from rib cage and abdominal V-P partitioning. *Journal of Applied Physiology*, *41*(5 (pt 1)), 752–763. https://doi.org/10.1152/jappl.1976.41.5.752

Goldman, M. D., Smith, H. J., & Ulmer, W. T. (2005). Whole-body plethysmography. In R. Gosselink & H. Stam (Eds.), *Lung Function Testing* (pp. 15–43). European Respiratory Society. https://doi.org/10.1183/1025448x.erm3105

Goligher, E. C., Dres, M., Fan, E., Rubenfeld, G. D., Scales, D. C., Herridge, M., Vorona, S., Sklar, M. C., Rittayamai, N., Lanys, A., Murray, A., Brace, D., Urrea, C., Reid, W. D., Tomlinson, G., Slutsky, A. S., Kavanagh, B., Brochard, L. J., & Ferguson, N. D. (2018). Mechanical ventilation-induced diaphragm atrophy strongly impacts clinical outcomes. *American Journal of Respiratory and Critical Care Medicine*, *197*(2), 204–213. https://doi.org/10.1164/rccm.201703-0536OC

Goligher, E. C., Fan, E., Herridge, M. S., Murray, A., Vorona, S., Brace, D., Rittayamai, N., Lanys, A., Tomlinson, G., Singh, J. M., Bolz, S. S., Rubenfeld, G. D., Kavanagh, B. P., Brochard, L. J., & Ferguson, N. D. (2015). Evolution of diaphragm thickness during mechanical ventilation: impact of inspiratory effort. *American Journal of Respiratory and Critical Care Medicine*, *192*(9), 1080–1088. https://doi.org/10.1164/rccm.201503-0620OC

Goligher, E. C., Laghi, F., Detsky, M. E., Farias, P., Murray, A., Brace, D., Brochard, L. J., Sebastien-Bolz, S., Rubenfeld, G. D., Kavanagh, B. P., & Ferguson, N. D. (2015).

Measuring diaphragm thickness with ultrasound in mechanically ventilated patients: feasibility, reproducibility and validity. *Intensive Care Medicine*, *41*(4), 642–649. https://doi.org/10.1007/s00134-015-3687-3

Gordon, A. M., Huxley, A. F., & Julian, F. J. (1966). The variation in isometric tension with sarcomere length in vertebrate muscle fibres. *Journal of Physiology*, *184*(1), 170–192. https://doi.org/10.1113/jphysiol.1966.sp007909

Gorman, R. B., McKenzie, D. K., & Gandevia, S. C. (1999). Task failure, breathing discomfort and CO2 accumulation without fatigue during inspiratory resistive loading in humans. *Respiration Physiology*, *115*(3), 273–286. https://doi.org/10.1016/S0034-5687(99)00010-9

Gottesman, E., & McCool, F. D. (1997). Ultrasound evaluation of the paralyzed diaphragm. *American Journal of Respiratory and Critical Care Medicine*, *155*(5), 1570–1574. https://doi.org/10.1164/ajrccm.155.5.9154859

Goutman, S. A., Hamilton, J. D., Swihart, B., Foerster, B., Feldman, E. L., & Rubin, J. M. (2017). Speckle tracking as a method to measure hemidiaphragm excursion. *Muscle & Nerve*, *55*(1), 125–127. https://doi.org/10.1002/mus.25380

Graham, B. L., Steenbruggen, I., Barjaktarevic, I. Z., Cooper, B. G., Hall, G. L., Hallstrand, T. S., Kaminsky, D. A., McCarthy, K., McCormack, M. C., Miller, M. R., Oropez, C. E., Rosenfeld, M., Stanojevic, S., Swanney, M. P., & Thompson, B. R. (2019). Standardization of Spirometry 2019 Update: An Official American Thoracic Society and European Respiratory Society Technical Statement. *American Journal of Respiratory and Critical Care Medicine*, *200*(8), e70–e88. https://doi.org/10.1164/rccm.201908-1590ST

Grassino, A., & Macklem, P. T. (1984). Respiratory muscle fatigue and ventilatory failure. *Annual Review of Medicine*, *35*, 625–647. https://doi.org/10.1146/annurev.me.35.020184.003205

Green, M., Road, J., Sieck, G. C., & Similowski, T. (2002). Tests of respiratory muscle strength. In *ATS/ERS Statement on Respiratory Muscle Testing* (pp. 528–542). American Thoracic Society/European Respiratory Society. https://doi.org/10.1164/rccm.166.4.518

Greising, S. M., Medina-Martinez, J. S., Vasdev, A. K., Sieck, G., & Mantilla, C. B. (2015). Analysis of muscle fiber clustering in the diaphragm muscle of sarcopenic mice. *Muscle*

and Nerve, *52*(1), 76–82. https://doi.org/10.1002/mus.24641.Analysis

Grimby, G., Goldman, M., & Mead, J. (1976). Respiratory muscle action inferred from rib cage and abdominal V-P partitioning. *Journal of Applied Physiology*, *41*(5), 739–751. https://doi.org/10.1152/jappl.1976.41.5.739

Guenette, J. A., Romer, L. M., Querido, J. S., Chua, R., Eves, N. D., Road, J. D., McKenzie, D. C., & Sheel, A. W. (2010). Sex differences in exercise-induced diaphragmatic fatigue in endurance-trained athletes. *Journal of Applied Physiology*, *109*(1), 35–46. https://doi.org/10.1152/japplphysiol.01341.2009

Guenette, J. A., Witt, J. D., McKenzie, D. C., Road, J. D., & Sheel, A. W. (2007). Respiratory mechanics during exercise in endurance-trained men and women. *Journal of Physiology*, *581*(pt 3), 1309–1322. https://doi.org/10.1113/jphysiol.2006.126466

HajBhanbari, B., Yamabayashi, C., Buna, T. R., Coelho, J. D., Freedman, K. D., Morton, T. A., Palmer, S. A., Toy, M. A., Walsh, C., Sheel, A. W., & Reid, W. D. (2013). Effects of respiratory muscle training on performance in athletes: a systematic review with meta-analyses. *Journal of Strength and Conditioning Research*, *27*(6), 1643–1663. https://doi.org/10.1519/JSC.0b013e318269f73f

Hansen, J. E., Sue, D. Y., & Wasserman, K. (1984). Predicted values for clinical exercise testing. *American Review of Respiratory Disease*, *129*(2 SUPPL.). https://doi.org/10.1164/arrd.1984.129.2p2.s49

Harman, E. A., Frykman, P. N., Clagett, E. R., & Kraemer, W. J. (1988). Intra-abdominal and intra-thoracic pressures during lifting and jumping. *Medicine & Science in Sports & Exercise*, *20*(2), 195–201. https://doi.org/10.1249/00005768-198820020-00015

Harms, C. A., Wetter, T. J., McClaran, S. R., Pegelow, D. F., Nickele, G. A., Nelson, W. B., Hanson, P., & Dempsey, J. A. (1998). Effects of respiratory muscle work on cardiac output and its distribution during maximal exercise. *Journal of Applied Physiology*, *85*(2), 609–618. https://doi.org/10.1152/jappl.1998.85.2.609

Harper, C. J., Shahgholi, L., Cieslak, K., Hellyer, N. J., Strommen, J. A., & Boon, A. J. (2013). Variability in diaphragm motion during normal breathing, assessed with B-mode ultrasound. *Journal of Ortopaedic & Sports Physical Therapy*, *43*(12), 927–931. https://doi.org/10.2519/jospt.2013.4931

Hart, N., Nickol, A. H., Cramer, D., Ward, S. P., Lofaso, F., Pride, N. B., Moxham, J., & Polkey, M. I. (2002). Effect of severe isolated unilateral and bilateral diaphragm weakness on exercise performance. *American Journal of Respiratory and Critical Care Medicine*, *165*(9), 1265–1270. https://doi.org/10.1164/rccm.2110016

Haverkamp, H. C., Dempsey, J. A., Miller, J. D., Romer, L. M., & Eldridge, M. W. (2005). Physiologic responses to exercise. In Qutayba Hamid, J. Shannon, & J. Martin (Eds.), *Physiological basis of respiratory disease* (pp. 525–540). BC Decker Inc.

Heidari, S., Babor, T. F., De Castro, P., Tort, S., & Curno, M. (2016). Sex and Gender Equity in Research: rationale for the SAGER guidelines and recommended use. *Research Integrity and Peer Review*, *1*(1), 1–9. https://doi.org/10.1186/s41073-016-0007-6

Hemborg, B., Moritz, U., & Löwing, H. (1985). Intra-abdominal pressure and trunk muscle activity during lifting. IV. The causal factors of the intra-abdominal pressure rise. *Scandinavian Journal of Rehabilitation Medicine*, *17*(1), 25–38. https://doi.org/10.2340/1650197785172538

Hill, J. M. (2000). Discharge of group IV phrenic afferent fibers increases during diaphragmatic fatigue. *Brain Research*, *856*(1–2), 240–244. https://doi.org/10.1016/S0006-8993(99)02366-5

Hill, A. V. (1938). The heat of shortening and the dynamic constants of muscle. *Proceedings of the Royal Society B: Biological Sciences*, *126*(843), 136–195. https://doi.org/10.1098/rspb.1938.0050

Hirschman, C. A., McCullough, R. E., & Weil, J. V. (1975). Normal values for hypoxic and hypercapnic ventilatory drives in man. *Journal of Applied Physiology*, *38*(6), 1095–1098. https://doi.org/10.1152/jappl.1975.38.6.1095

Ho, C. Y., & Solomon, S. D. (2006). A Clinician's Guide to Tissue Doppler Imaging. *Circulation*, *113*(10), e396-398. https://doi.org/10.1161/CIRCULATIONAHA.105.579268

Hodges, P. W., Butler, J. E., McKenzie, D. K., & Gandevia, S. C. (1997). Contraction of the human diaphragm during rapid postural adjustments. *Journal of Physiology*, *505*(2), 539–548. https://doi.org/10.1111/j.1469-7793.1997.539bb.x

Hodges, P. W., Cresswell, A. G., & Thorstensson, A. (2004). Intra-abdominal pressure response to multidirectional support-surface translation. *Gait and Posture*, *20*(2), 163–170. https://doi.org/10.1016/j.gaitpost.2003.08.008

Hodges, P. W., Eriksson, A. E. M., Shirley, D., & Gandevia, S. C. (2005). Intra-abdominal pressure increases stiffness of the lumbar spine. *Journal of Biomechanics*, *38*(9), 1873–1880. https://doi.org/10.1016/j.jbiomech.2004.08.016

Hodges, P. W., & Gandevia, S. C. (2000a). Activation of the human diaphragm during a repetitive postural task. *Journal of Physiology*, *522*(1), 165–175. https://doi.org/10.1111/j.1469-7793.2000.t01-1-00165.xm

Hodges, P. W., & Gandevia, S. C. (2000b). Changes in intra-abdominal pressure during postural and respiratory activation of the human diaphragm. *Journal of Applied Physiology*, *89*(3), 967–976. https://doi.org/10.1152/jappl.2000.89.3.967

Hodges, P. W., Heijnen, I., & Gandevia, S. C. (2001). Postural activity of the diaphragm is reduced in humans when respiratory demand increases. *Journal of Physiology*, *537*(3), 999–1008. https://doi.org/10.1113/jphysiol.2001.012648

Hodges, P. W., Pengel, L. H. M., Herbert, R. D., & Gandevia, S. C. (2003). Measurement of muscle contraction with ultrasound imaging. *Muscle & Nerve*, *27*(June), 682–692. https://doi.org/10.1002/mus.10375

Hodgson, M., Docherty, D., & Robbins, D. (2005). Post-activation potentiation: underlying physiology and implications for motor performance. *Sports Medicine*, *35*(7), 585–595. https://doi.org/10.2165/00007256-200535070-00004

Holmer, I. (1992). Swimming physiology. *Annals of Physiological Anthropology*, *11*(3), 269–276. https://doi.org/10.2114/ahs1983.11.269

Homma, I., & Masaoka, Y. (2008). Breathing rhythms and emotions. *Experimental Physiology*, *93*(9), 1011–1021. https://doi.org/10.1113/expphysiol.2008.042424

Hong, B. Y., Ko, Y. J., Kim, J. S., Ok, E. J., Hwang, Y., & Kim, H. W. (2013). Sternocleidomastoid ultrasonography data for muscular torticollis in infants. *Muscle and Nerve*, *48*(1), 100–104. https://doi.org/10.1002/mus.23712

Hooren, B. Van, & Teratsias, P. (2020). Ultrasound imaging to assess skeletal muscle

architecture during movements : a systematic review of methods, reliability, and challenges. *Journal of Applied Physiology*, *128*(4), 978–999. https://doi.org/10.1152/japplphysiol.00835.2019

Horseman, G. (2020a). *Record and analyse respiratory data*. Cambridge Electronic Design Limited. http://ced.co.uk/downloads/scriptspkanal?zoom_highlight=respiratory

Horseman, G. (2020b). *Remove ECG artefacts from EMG channels*. Cambridge Electronic Design Limited. http://ced.co.uk/downloads/scriptspkedit

Hortemo, K. H., Munkvik, M., Lunde, P. K., & Sejersted, O. M. (2013). Multiple causes of fatigue during shortening contractions in rat slow twitch skeletal muscle. *PLoS ONE*, *8*(8), e71700. https://doi.org/10.1371/journal.pone.0071700

Houston, J. G., Cowan, M. D., McMillan, N. C., Angus, R. M., & Thomson, N. C. (1994). Ultrasound assessment of normal hemidiaphragmatic movement: relation to inspiratory volume. *Thorax*, *49*(5), 500–503. https://doi.org/10.1136/thx.49.5.500

Houston, J. G., Fleet, M., Cowan, M. D., & McMillan, N. C. (1995). Comparison of ultrasound with fluoroscopy in the assessment of suspected hemidiaphragmatic movement abnormality. *Clinical Radiology*, *50*(2), 95–98. https://doi.org/10.1016/S0009-9260(05)82987-3

Houston, J. G., Morris, A. D., Howie, C. A., Reid, J. L., & McMillan, N. (1992). Technical report: Quantitative assessment of diaphragmatic movement - A reproducible method using ultrasound. *Clinical Radiology*, *46*(6), 405–407. https://doi.org/10.1016/S0009-9260(05)80688-9

Hubmayr, R. D., Litchy, W. J., Gay, P. C., & Nelson, S. B. (1989). Transdiaphragmatic twitch pressure: effects of lung volume and chest wall shape. *American Review of Respiratory Disease*, *139*(3), 647–652. https://doi.org/10.1164/ajrccm/139.3.647

Hug, F., Tucker, K., Gennisson, J. L., Tanter, M., & Nordez, A. (2015). Elastography for muscle biomechanics: toward the estimation of individual muscle force. *Exercise and Sport Sciences Reviews*, *43*(3), 125–133. https://doi.org/10.1249/JES.0000000000000049

Hunter, S. K. (2018). Performance fatigability: mechanisms and task specificity. *Cold Spring Harbor Perspectives in Medicine*, *8*(7), 1–22.

https://doi.org/10.1101/cshperspect.a029728

Huxley, A. F. (1957). Muscle structure and theories of contraction. *Progress in Biophysics and Biophysical Chemistry*, *7*, 257–318.

Huxley, A. F., & Niedergerke, R. (1954). Structural changes in muscle during contraction: interference microscopy of living muscle fibres. *Nature*, *173*(4412), 971–973. https://doi.org/10.1038/173971a0

Huxley, H. E., & Hanson, J. (1954). Changes in the cross-striations of muscle during contraction and stretch and their structural interpretation. *Nature*, *173*(4412), 973–976. https://doi.org/10.1038/173973a0

Hyatt, R. E., & Flath, R. E. (1966). Relationship of air flow to pressure during maximal respiratory effort in man. *Journal of Applied Physiology*, *21*(2), 477–482. https://doi.org/10.1002/jbm.b.33557

Hyslop, N. P., & White, W. H. (2009). Estimating precision using duplicate measurements. *Journal of the Air and Waste Management Association*, *59*(9), 1032–1039. https://doi.org/10.3155/1047-3289.59.9.1032

Jacobsen, J. A. (2018). *Fundamentals of musculoskeletal ultrasound* (3rd ed.). Elsevier Inc.

Jensen, D., Mask, G., & Tschakovsky, M. E. (2010). Variability of the ventilatory response to Duffin's modified hyperoxic and hypoxic rebreathing procedure in healthy awake humans. *Respiratory Physiology and Neurobiology*, *170*(2), 185–197. https://doi.org/10.1016/j.resp.2009.12.007

Jilani, T. N., Preuss, C. V, & Sharma, S. (2019). Theophylline. In *Europe PubMed Central*. StatPearls Publishing. https://www.ncbi.nlm.nih.gov/books/NBK519024/

Johnson, B. D., Babcock, M. A., Suman, O. E., & Dempsey, J. A. (1993). Exercise-induced diaphragm fatigue in healthy humans. *Journal of Physiology*, *460*, 385–405. https://doi.org/10.1113/jphysiol.1993.sp019477

Johnson, B. D., Saupe, K. W., & Dempsey, J. A. (1992). Mechanical constraints on exercise hyperpnea in endurance athletes. *Journal of Applied Physiology*, *73*(3), 874–886. https://doi.org/10.1152/jappl.1992.73.3.874

Jones, D. A. (1996). High- and low-frequency fatigue revisited. *Acta Physiologica Scandinavica*, *156*(3), 265–270. https://doi.org/10.1046/j.1365-201X.1996.192000.x

Jones, D. A. (2010). Changes in the force-velocity relationship of fatigued muscle: implications for power production and possible causes. *Journal of Physiology*, *588*(pt 16), 2977–2986. https://doi.org/10.1113/jphysiol.2010.190934

Jones, E. J., Bishop, P. A., Woods, A. K., & Green, J. M. (2008). Cross-sectional area and muscular strength. *Sports Medicine*, *38*(12), 987–994. https://doi.org/10.2165/00007256-200838120-00003

Katagiri, M., Abe, T., Yokoba, M., Dobashi, Y., Tomita, T., & Easton, P. A. (2003). Neck and abdominal muscle activity during a sniff. *Respiratory Medicine*, *97*(9), 1027–1035. https://doi.org/10.1016/S0954-6111(03)00133-1

Kido, T., Nakahara, K., Maeda, H., & Kawashima, Y. (1988). Experimental study on diaphragm fatigue during diaphragm pacing. *Journal of Surgical Research*, *45*(3), 304–313. https://doi.org/10.1016/0022-4804(88)90080-7

Kilding, A. E., Brown, S., & McConnell, A. K. (2010). Inspiratory muscle training improves 100 and 200 m swimming performance. *European Journal of Applied Physiology*, *108*(3), 505–511. https://doi.org/10.1007/s00421-009-1228-x

Kocis, K. C., Radell, P. J., Sternberger, W. I., Benson, J. E., Traystman, R. J., & Nichols, D. G. (1997). Ultrasound evaluation of piglet diaphragm function before and after fatigue. *Journal of Applied Physiology*, *83*(5), 1654–1659. https://doi.org/10.1152/jappl.1997.83.5.1654

Kocjan, J., Gzik-Zroska, B., Nowakowska, K., Burkacki, M., Suchoń, S., Michnik, R., Czyżewski, D., & Adamek, M. (2018). Impact of diaphragm function parameters on balance maintenance. *PLoS ONE*, *13*(12), e0208697. https://doi.org/10.1371/journal.pone.0208697

Konrad, H. R., Girardi, M., & Helfert, R. (1999). Balance and aging. *The Laryngoscope*, *109*(9), 1454–1460. https://doi.org/10.1097/00005537-199909000-00019

Koo, T. K., & Li, M. Y. (2016). A guideline of selecting and reporting intraclass correlation coefficients for reliability research. *Journal of Chiropractic Medicine*, *15*(2), 155–163.

https://doi.org/10.1016/j.jcm.2016.02.012

Koppenhaver, S. L., Hebert, J. J., Fritz, J. M., Parent, E. C., Teyhen, D. S., & Magel, J. S. (2009). Reliability of rehabilitative ultrasound imaging of the transversus abdominis and lumbar multifidus muscles. *Archives of Physical Medicine and Rehabilitation*, *90*(1), 87–94. https://doi.org/10.1016/j.apmr.2008.06.022

Koulouris, N., Mulvey, D. a, Laroche, C. M., Goldstone, J., Moxham, J., & Green, M. (1989). The effect of posture and abdominal binding on respiratory pressures. *The European Respiratory Journal*, *2*(10), 961–965. http://www.ncbi.nlm.nih.gov/pubmed/2606196

Koulouris, N., Vianna, L. G., Mulvey, D. A., Green, M., & Moxham, J. (1989). Maximal relaxation rates of esophageal, nose, and mouth pressures during a sniff reflect inspiratory muscle fatigue. *American Review of Respiratory Disease*, *139*(5), 1213–1217. https://doi.org/10.1164/ajrccm/139.5.1213

Kufel, T. J., Pineda, L. A., & Mador, M. J. (2002). Comparison of potentiated and unpotentiated twitches as an index of muscle fatigue. *Muscle and Nerve*, *25*(3), 438–444. https://doi.org/10.1002/mus.10047

Laghi, F., D'Alfonso, N., & Tobin, M. J. (1995). Pattern of recovery from diaphragmatic fatigue over 24 hours. *Journal of Applied Physiology*, *79*(2), 539–546. https://doi.org/10.1152/jappl.1995.79.2.539

Laghi, F., Topeli, A., & Tobin, M. J. (1998). Does resistive loading decrease diaphragmatic contractility before task failure? *Journal of Applied Physiology*, *85*(3), 1103–1012. https://doi.org/10.1152/jappl.1998.85.3.1103

Lakens, D. (2013). Calculating and reporting effect sizes to facilitate cumulative science: a practical primer for t-tests and ANOVAs. *Frontiers in Psychology*, *4*, 863. https://doi.org/10.3389/fpsyg.2013.00863

Laroche, C. M., Mier, A. K., Moxham, J., & Green, M. (1988). The value of sniff esophageal pressures in the assessment of global inspiratory muscle strenght. *American Review of Respiratory Disease*, *138*(3), 598–603. https://doi.org/10.1164/ajrccm/138.3.598

Larsson, L., Li, X., & Frontera, W. R. (1997). Effects of aging on shortening velocity and myosin isoform composition in single human skeletal muscle cells. *American Journal of*

Physiology, *272*(2 pt 1), 638–649. https://doi.org/10.1152/ajpcell.1997.272.2.c638

Larsson, L., Sjödin, B., & Karlsson, J. (1978). Histochemical and biochemical changes in human skeletal muscle with age in sedentary males, age 22–65 years. *Acta Physiologica Scandinavica*, *103*(1), 31–39. https://doi.org/10.1111/j.1748-1716.1978.tb06187.x

Laursen, C. B., Clive, A., Hallifax, R., Pietersen, P. I., Asciak, R., Davidsen, J. R., Bhatnagar, R., Bedawi, E. O., Jacobsen, N., Coleman, C., Edey, A., Via, G., Volpicelli, G., Massard, G., Raimondi, F., Evison, M., Konge, L., Annema, J., Rahman, N. M., & Maskell, N. (2021). European Respiratory Society statement on thoracic ultrasound. *European Respiratory Journal*, *57*, 2001519. https://doi.org/10.1183/13993003.01519-2020

Laveneziana, P., Albuquerque, A., Aliverti, A., Babb, T., Barreiro, E., Dres, M., Dubé, B. P., Fauroux, B., Gea, J., Guenette, J. A., Hudson, A. L., Kabitz, H. J., Laghi, F., Langer, D., Luo, Y. M., Neder, J. A., O'Donnell, D., Polkey, M. I., Rabinovich, R. A., … Verges, S. (2019). ERS statement on respiratory muscle testing at rest and during exercise. *European Respiratory Journal*, *53*(6). https://doi.org/10.1183/13993003.01214-2018

Leahy, M. G., Summers, M. N., Peters, C. M., Molgat-Seon, Y., Geary, C. M., & Sheel, A. W. (2019). The mechanics of breathing during swimming. *Medicine & Science in Sports & Exercise*, *51*(7), 1467–1476. https://doi.org/10.1249/MSS.0000000000001902

Lemaitre, F., Coquart, J. B., Chavallard, F., Castres, I., Mucci, P., Costalat, G., & Chollet, D. (2013). Effect of additional respiratory muscle endurance training in young well-trained swimmers. *Journal of Sports Science and Medicine*, *12*(4), 630–638.

Lomax, M. E., & McConnell, A. K. (2003). Inspiratory muscle fatigue in swimmers after a single 200 m swim. *Journal of Sports Sciences*, *21*(8), 659–664. https://doi.org/10.1080/0264041031000101999

Lowery, E. M., Brubaker, A. L., Kuhlmann, E., & Kovacs, E. J. (2013). The aging lung. *Clinical Interventions in Aging*, *8*, 1489–1496. https://doi.org/10.2147/CIA.S51152

Luo, Y. M., Hart, N., Mustfa, N., Lyall, R. A., Polkey, M. I., & Moxham, J. (2001). Effect of diaphragm fatigue on neural respiratory drive. *Journal of Applied Physiology*, *90*(5), 1691–1699. https://doi.org/10.1152/jappl.2001.90.5.1691

Luo, Y. M., Lyall, R. A., Harris, M. L., Rafferty, G. F., Polkey, M. I., & Moxham, J. (1999).

Quantification of the esophageal diaphragm electromyogram with magnetic phrenic nerve stimulation. *American Journal of Respiratory and Critical Care Medicine*, *160*(5), 1629–1634. https://doi.org/10.1164/ajrccm.160.5.9809068

Luo, Y. M., Moxham, J., & Polkey, M. I. (2008). Diaphragm electromyography using an oesophageal catheter: current concepts. *Clinical Science (London)*, *115*(8), 233–244. https://doi.org/10.1042/cs20070348

Luo, Y. M., Polkey, M. I., Johnson, L. C., Lyall, R. A., Harris, M. L., Green, M., & Moxham, J. (1998). Diaphragm EMG measured by cervical magnetic and electrical phrenic nerve stimulation. *Journal of Applied Physiology*, *85*(6), 2089–2099. https://doi.org/10.1152/jappl.1998.85.6.2089

MacIntosh, B. R., & Bryan, S. N. (2002). Potentiation of shortening and velocity of shortening during repeated isotonic tetanic contractions in mammalian skeletal muscle. *Pflügers Archiv - European Journal of Physiology*, *443*(5–6), 804–812. https://doi.org/10.1007/s00424-001-0746-0

MacIntosh, B. R., & Willis, J. C. (2000). Force-frequency relationship and potentiation in mammalian skeletal muscle. *Journal of Applied Physiology*, *88*(6), 2088–2096. https://doi.org/10.1152/jappl.2000.88.6.2088

MacKay, C. M., Skow, R. J., Tymko, M. M., Boulet, L. M., Davenport, M. H., Steinback, C. D., Ainslie, P. N., Lemieux, C. C. M., & Day, T. A. (2016). Central respiratory chemosensitivity and cerebrovascular CO2 reactivity: a rebreathing demonstration illustrating integrative human physiology. *Advances in Physiology Education*, *40*(1), 79–92. https://doi.org/10.1152/advan.00048.2015

MacNutt, M. J., De Souza, M. J., Tomczak, S. E., Homer, J. L., & Sheel, A. W. (2012). Resting and exercise ventilatory chemosensitivity across the menstrual cycle. *Journal of Applied Physiology*, *112*(5), 737–747. https://doi.org/10.1152/japplphysiol.00727.2011

Mademli, L., & Arampatzis, A. (2005). Behaviour of the human gastrocnemius muscle architecture during submaximal isometric fatigue. *European Journal of Applied Physiology*, *94*(5–6), 611–617. https://doi.org/10.1007/s00421-005-1366-8

Mador, M. J., & Acevedo, F. A. (1991). Effect of respiratory muscle fatigue on breathing pattern during incremental exercise. *American Review of Respiratory Disease*, *143*(3),

462–468. https://doi.org/10.1164/ajrccm/143.3.462

Mador, M. J., Kufel, T. J., Pineda, L. A., & Sharma, G. K. (2000). Diaphragmatic fatigue and high-intensity exercise in patients with chronic obstructive pulmonary disease. *American Journal of Respiratory and Critical Care Medicine*, *161*(1), 118–123. https://doi.org/10.1164/ajrccm.161.1.9903010

Mador, M. J., Magalang, U. J., & Kufel, T. J. (2000). Twitch potentiation following voluntary diaphragmatic contraction. *American Journal of Respiratory and Critical Care Medicine*, *161*(1), 118–123. https://doi.org/10.1164/ajrccm.161.1.9903010

Mador, M. J., & Tobin, M. J. (1992). The effect of inspiratory muscle fatigue on breathing pattern and ventilatory response to CO2. *Journal of Physiology*, *455*, 17–32. https://doi.org/10.1113/jphysiol.1992.sp019288

Man, W. D. C., Luo, Y. M., Mustfa, N., Rafferty, G. F., Glerant, J. C., Polkey, M. I., & Moxham, J. (2002). Postprandial effects on twitch transdiaphragmatic pressure. *European Respiratory Journal*, *20*(3), 577–580. https://doi.org/10.1183/09031936.02.00302702

Man, W. D. C., Moxham, J., & Polkey, M. I. (2004). Magnetic stimulation for the measurement of respiratory and skeletal muscle function. *European Respiratory Journal*, *24*(5), 846–860. https://doi.org/10.1183/09031936.04.00029004

Mardini, I. A., & McCarter, R. J. (1987). Contractile properties of the shortening rat diaphragm in vitro. *Journal of Applied Physiology*, *62*(3), 1111–1116. https://doi.org/10.1152/jappl.1987.62.3.1111

Matamis, D., Soilemezi, E., Tsagourias, M., Akoumianaki, E., Dimassi, S., Boroli, F., Richard, J. M., & Brochard, L. (2013). Sonographic evaluation of the diaphragm in critically ill patients. Technique and clinical applications. *Intensive Care Medicine*, *39*(5), 801–810. https://doi.org/10.1007/s00134-013-2823-1

Matsumoto, H., Hanajima, R., Terao, Y., & Ugawa, Y. (2013). Magnetic-motor-root stimulation: Review. *Clinical Neurophysiology*, *124*(6), 1055–1067. https://doi.org/10.1016/j.clinph.2012.12.049

McCool, F. D., Benditt, J. O., Conomos, P., Anderson, L., Sherman, C. B., & Hoppin, F. G. (1997). Variability of diaphragm structure among healthy individuals. *American Journal*

of Respiratory and Critical Care Medicine, *155*(4), 1323–1328. https://doi.org/10.1164/ajrccm.155.4.9105074

McCool, F. D., Conomos, P., Benditt, J. O., Cohn, D., Sherman, C. B., & Hoppin Jr, F. G. (1997). Maximal inspiratory pressures and dimensions of the diaphragm. *American Journal of Respiratory and Critical Care Medicine*, *155*(4), 1329–1334. https://doi.org/doi: 10.1164/ajrccm.155.4.9105075

McCool, F. D., Hershenson, M. B., Tzelepis, G. E., Kikuchi, Y., & Leith, D. E. (1992). Effect of fatigue on maximal inspiratory pressure-flow capacity. *Journal of Applied Physiology*, *73*(1), 36–43. https://doi.org/10.1152/jappl.1992.73.1.36

McCool, F. D., & Tzelepis, G. E. (2020). Tissue doppler imaging of the diaphragm: a new kid on the block? *American Journal of Respiratory and Critical Care Medicine*, *202*(7), 921–922. https://doi.org/10.1164/rccm.202007-2771ED

McCully, K. K., & Faulkner, J. A. (1983). Length-tension relationship of mammaliam diaphragm muscles. *Journal of Applied Physiology*, *54*(6), 1681–1686. https://doi.org/10.1152/jappl.1983.54.6.1681

McKenzie, D. K., Allen, G. M., Butler, J. E., & Gandevia, S. C. (1997). Task failure with lack of diaphragm fatigue during inspiratory resistive loading in human subjects. *Journal of Applied Physiology*, *82*(6), 2011–2019. https://doi.org/10.1152/jappl.1997.82.6.2011

McKenzie, D. K., & Gandevia, S. C. (1985). Phrenic nerve conduction times and twitch pressures of the human diaphragm. *Journal of Applied Physiology*, *58*(5), 1496–1504. https://doi.org/10.1152/jappl.1985.58.5.1496

Menezes, M. A., & Herbella, F. A. M. (2017). Pathophysiology of gastroesophageal reflux disease. *World Journal of Surgery*, *41*(7), 1666–1671. https://doi.org/10.1007/s00268-017-3952-4

Meznaric, M., & Cvetko, E. (2016). Size and Proportions of Slow-Twitch and Fast-Twitch Muscle Fibers in Human Costal Diaphragm. *BioMed Research International*, *2016*, e5946520. https://doi.org/10.1155/2016/5946520

Mier-Jedrzejowicz, A., Brophy, C., Moxham, J., & Green, M. (1988). Assessment of diaphragm weakness. *American Review of Respiratory Disease*, *137*(4), 877–883.

https://doi.org/10.1164/ajrccm/137.4.877

Milanzi, E. B., Koppelman, G. H., Oldenwening, M., Augustijn, S., Aalders-De Ruijter, B., Farenhorst, M., Vonk, J. M., Tewis, M., Brunekreef, B., & Gehring, U. (2019). Considerations in the use of different spirometers in epidemiological studies. *Environmental Health*, *18*(1), 39. https://doi.org/10.1186/s12940-019-0478-2

Miller, A. D. (1990). Respiratory muscle control during vomiting. *Canadian Journal of Physiology and Pharmacology*, *68*(2), 237–241. https://doi.org/10.1139/y90-037

Miller, A. D., Lakos, S. F., & Tan, L. K. (1988). Central motor program for relaxation of periesophageal diaphragm during the expulsive phase of vomiting. *Brain Research*, *456*(2), 367–370. https://doi.org/10.1016/0006-8993(88)90241-7

Miller, J. M., Moxham, J., & Green, M. (1985). The maximal sniff in the assessment of diaphragm function in man. *Clinical Science*, *69*(1), 91–96. https://doi.org/10.1042/cs0690091

Miller, M., Hankinson, J., Brusasco, V., Burgos, F., Casaburi, R., Coates, A., Crapo, R., Enright, P., van der Grinten, C. P. M., Gustafsson, P., Jensen, R., Johnson, D. C., MacIntyre, N., McKay, R., Navajas, D., Pedersen, O. F., Pellegrino, R., Viegi, G., & Wanger, J. (2005). Standardisation of spirometry. *European Respiratory Journal*, *26*(2), 319–338. https://doi.org/10.1183/09031936.05.00034805

Mills, G. H., Kyroussis, D., Hamnegard, C. H., Polkey, M. I., Green, M., & Moxham, J. (1996). Bilateral magnetic stimulation of the phrenic nerves from an anterolateral approach. *American Journal of Respiratory and Critical Care Medicine*, *154*(4, pt 1), 1099–1105. https://doi.org/10.1164/ajrccm.154.4.8887614

Mills, G. H., Kyroussis, D., Hamnegard, C. H., Wragg, S., Moxham, J., & Green, M. (1995). Unilateral magnetic stimulation of the phrenic nerve. *Thorax*, *50*(11), 1162–1172. https://doi.org/10.1136/thx.50.11.1162

Mittman, C., Edelman, N. H., Norris, A. H., & Shock, N. W. (1965). Relationship between chest wall and pulmonary compliance and age. *Journal of Applied Physiology*, *20*(6), 1211–1216. https://doi.org/10.1152/jappl.1965.20.6.1211

Mizuno, M. (1991). Human respiratory muscles: fibre morphology and capillary supply.

European Respiratory Journal, *4*(5), 587–601.

Mizuno, M., & Secher, N. H. (1989a). Histochemical characteristics of human expiratory and inspiratory intercostal muscles. *Journal of Applied Physiology*, *67*(2), 592–598. https://doi.org/10.1152/jappl.1989.67.2.592

Mizuno, M., & Secher, N. H. (1989b). Histochemical characteristics of human expiratory and inspiratory intercostal muscles. *Journal of Applied Physiology*, *67*(2), 592–598. https://doi.org/10.1152/jappl.1989.67.2.592

Moosavi, S. H., Golestanian, E., Binks, A. P., Lansing, R. W., Brown, R., & Banzett, R. B. (2003). Hypoxic and hypercapnic drives to breathe generate equivalent levels of air hunger in humans. *Journal of Applied Physiology*, *94*(1), 141–154. https://doi.org/10.1152/japplphysiol.00594.2002

Morel, B., Hug, F., Nordez, A., Pournot, H., Besson, T., Mathevon, L., & Lapole, T. (2019). Reduced active muscle stiffness after intermittent submaximal isometric contractions. *Medicine and Science in Sports and Exercise*, *51*(12), 2603–2609. https://doi.org/10.1249/MSS.0000000000002080

Moxham, J., Morris, A. J. R., Spiro, S. G., Edwards, R. H., & Green, M. (1981). Contractile properties and fatigue of the diaphragm in man. *Thorax*, *36*(3), 164–168. https://doi.org/10.1136/thx.36.3.164

Moxham, J., Wiles, C. M., Newham, D., Spiro, S. G., & Edwards, R. H. T. (1982). Respiratory muscle fatigue reduces the ventilatory response to carbon dioxide. *Medical Research Society*, *62*(2), 40. https://doi.org/10.1042/cs062040p

Mulvey, D. A., Koulouris, N. G., Elliott, M. W., Laroche, C. M., Moxham, J., & Green, M. (1991). Inspiratory muscle relaxation rate after voluntary maximal isocapnic ventilation in humans. *Journal of Applied Physiology*, *70*(5), 2173–2180. https://doi.org/10.1152/jappl.1991.70.5.2173

Munkvik, M., Lunde, P. K., & Sejersted, O. M. (2009). Causes of fatigue in slow-twitch rat skeletal muscle during dynamic activity. *American Journal of Physiology - Regulatory Integrative and Comparative Physiology*, *297*(3), 900–910. https://doi.org/10.1152/ajpregu.91043.2008

Murgiano, D., Aubier, M., Lecocguic, Y., & Pariente, R. (1984). Effects of theophylline on diaphragmatic strength and fatigue in patients with chronic obstructive pulmonary disease. *New England Journal of Medicine*, *311*(6), 349–535. https://doi.org/10.1056/nejm198408093110601

Nakanishi, N., Oto, J., Ueno, Y., Nakataki, E., Itagaki, T., & Nishimura, M. (2019). Change in diaphragm and intercostal muscle thickness in mechanically ventilated patients: A prospective observational ultrasonography study. *Journal of Intensive Care*, *7*(1), 1–10. https://doi.org/10.1186/s40560-019-0410-4

Nava, S., Ambrosino, N., Crotti, P., Fracchia, C., & Rampulla, C. (1993). Recruitment of some respiratory muscles during three maximal inspiratory manoeuvres. *Thorax*, *48*(7), 702–707. https://doi.org/10.1136/thx.48.7.702

Newman, S., Road, J., Bellemare, F., Lavigne, C. M., & Grassino, A. (1984). Respiratory muscle length measured by sonomicrometry. *Journal of Applied Physiology Respiratory, Environmental and Exercise Physiology*, *56*(3), 753–764. https://doi.org/10.1152/jappl.1984.56.3.753

Ng, A., & Swanevelder, J. (2011). Resolution in ultrasound imaging. *Continuing Education in Anaesthesia, Critical Care and Pain*, *11*(5), 186–192. https://doi.org/10.1093/bjaceaccp/mkr030

Noh, D. K., Lee, J. J., & You, J. H. (2014). Diaphragm breathing movement measurement using ultrasound and radiographic imaging: a concurrent validity. *Biomedical Materials and Engineering*, *24*(1), 947–952. https://doi.org/10.3233/BME-130889

O'Donoghue, P. (2012). *Statistics for sport and exercise studies: an introduction*. Routledge.

Oppersma, E., Hatam, N., Doorduin, J., van der Hoeven, J. G., Marx, G., Goetzenich, A., Fritsch, S., Heunks, L. M. A., & Bruells, C. S. (2017). Functional assessment of the diaphragm by speckle tracking ultrasound during inspiratory loading. *Journal of Applied Physiology*, *123*(5), 1063–1070. https://doi.org/10.1152/japplphysiol.00095.2017

Orde, S. R., Boon, A. J., Firth, D. G., Villarraga, H. R., & Sekiguchi, H. (2016a). Diaphragm assessment by two dimensional speckle tracking imaging in normal subjects. *BMC Anesthesiology*, *16*(1), 43. https://doi.org/10.1186/s12871-016-0201-6

Orde, S. R., Boon, A. J., Firth, D. G., Villarraga, H. R., & Sekiguchi, H. (2016b). Use of angle-independent M-mode sonography for assessment of diaphragm displacement. *Journal of Ultrasound in Medicine*, *35*(12), 2615–2621. https://doi.org/10.7863/ultra.15.11100

Otis, A. B. (1954). The work of breathing. *Physiological Reviews*, *34*(3), 449–458. https://doi.org/10.1152/physrev.1954.34.3.449

Panjabi, M., Abumi, K., Duranceau, J., & Oxland, T. (1989). Spinal stability and intersegmental muscle forces: a biomechanical model. *Spine (Philadelphia)*, *14*(2), 194–200. https://doi.org/10.1097/00007632-198902000-00008

Pellegrino, R., Viegi, G., Brusasco, V., Crapo, R. O., Burgos, F., Casaburi, R., Coates, A., van der Grinten, C. P. M., Gustafsson, P., Hankinson, J., Jensen, R., Johnson, D. C., MacIntyre, N., McKay, R., Miller, M. R., Navajas, D., Pedersen, O. F., & Wanger, J. (2005). Interpretative strategies for lung function tests. *European Respiratory Journal*, *26*(5), 948–968. https://doi.org/10.1183/09031936.05.00035205

Peters, R. M. (1969). The energy cost (work) of breathing. *Annals of Thoracic Surgery*, *7*(1), 51–67. https://doi.org/10.1016/S0003-4975(10)66146-2

Pette, D., & Staron, R. S. (2000). Myosin isoforms, muscle fiber types, and transitions. *Microscopy Research and Technique*, *50*(6), 500–509. https://doi.org/10.1002/1097-0029(20000915)50:6<500::AID-JEMT7>3.0.CO;2-7

Pillen, S. (2010). Skeletal muscle ultrasound. *European Journal Translational Myology*, *1*(4), 145–155. https://doi.org/10.1016/B978-0-444-53486-6.00042-9

Pirri, C., Todros, S., Fede, C., Pianigiani, S., Fan, C., Foti, C., Stecco, C., & Pavan, P. (2019). Inter-rater reliability and variability of ultrasound measurements of abdominal muscles and fasciae thickness. *Clinical Anatomy*, *32*(7), 948–960. https://doi.org/10.1002/ca.23435

Polkey, M. I., Harris, M. L., Hamnegård, C. H., Hughes, P. D., Lyons, D., Green, M., & Moxham, J. (1997). The contractile properties of the elderly human diaphragm. *American Journal of American Critical Care Medicine*, *155*(5), 1560–1564. https://doi.org/10.1164/ajrccm.155.5.9154857

Polkey, M. I., Kyroussis, D., Hamnegård, C. H., Hughes, P. D., Rafferty, G. F., Moxham, J., & Green, M. (1997). Paired phrenic nerve stimuli for the detection of diaphragm fatigue in

humans. *European Respiratory Journal*, *10*(8), 1859–1864. https://doi.org/10.1183/09031936.97.10081859

Poulard, T., Dres, M., Niérat, M. C., Rivals, I., Hogrel, J. Y., Similowski, T., Gennisson, J. L., & Bachasson, D. (2020). Ultrafast ultrasound coupled with cervical magnetic stimulation for non-invasive and non-volitional assessment of diaphragm contractility. *Journal of Physiology*, *598*(24), 5627–5638. https://doi.org/10.1113/JP280457

Powers, S. K., Criswell, D., Herb, R. A., Demirel, H., & Dodd, S. (1996). Age-related increases in diaphragmatic maximal shortening velocity. *Journal of Applied Physiology*, *80*(2), 445–451. https://doi.org/10.1152/jappl.1996.80.2.445

Quanjer, P. H., Stanojevic, S., Cole, T. J., Baur, X., Hall, G. L., Culver, B. H., Enright, P. L., Hankinson, J. L., Ip, M. S. M., Zheng, J., Stocks, J., & Schindler, C. (2012). Multi-ethnic reference values for spirometry for the 3-95-yr age range: The global lung function 2012 equations. *European Respiratory Journal*, *40*(6), 1324–1343. https://doi.org/10.1183/09031936.00080312

Ramsook, A. H., Koo, R., Molgat-Seon, Y., Dominelli, P. B., Syed, N., Ryerson, C. J., Sheel, A. W., & Guenette, J. A. (2016). Diaphragm recruitment increases during a bout of targeted inspiratory muscle training. *Medicine & Science in Sports & Exercise*, *48*(6), 1179–1186. https://doi.org/10.1249/MSS.0000000000000881

Ramsook, A. H., Molgat-Seon, Y., Boyle, K. G., Mitchell, R. A., Puyat, J. H., Koehle, M. S., Sheel, A. W., & Guenette, J. A. (2021). Reliability of diaphragm voluntary activation measurements in healthy adults. *Applied Physiology, Nutrition, and Metabolism*, *46*(3), 247–256. https://doi.org/10.1139/apnm-2020-0221

Read, D. J. (1966). A clinical method for assessing the ventilatory response to carbon dioxide. *Australasian Annals of Medicine*, *16*(1), 20–32. https://doi.org/10.1111/imj.1967.16.1.20

Read, D. J., & Leigh, J. (1967). Blood-brain tissue PCO2 relationships and ventilation during rebreathing. *Journal of Applied Physiology*, *23*(1), 53–70. https://doi.org/10.1152/jappl.1967.23.1.53

Read, D. J., Simon, H., Brandi, G., & Campbell, E. J. (1966). Regulation of ventilation during rebreathing at imposed respiratory frequencies. *Respiration Physiology*, *2*(1), 88–98. https://doi.org/10.1016/0034-5687(66)90040-5

Reid, K. F., & Fielding, R. A. (2012). Skeletal muscle power: a critical determinant of physical functioning in older adults. *Exercise and Sport Sciences Reviews*, *40*(1), 4–12. https://doi.org/10.1097/JES.0b013e31823b5f13

Renggli, A. S., Verges, S., Notter, D. A., & Spengler, C. M. (2008). Development of respiratory muscle contractile fatigue in the course of hyperpnoea. *Respiratory Physiology and Neurobiology*, *164*(3), 366–372. https://doi.org/10.1016/j.resp.2008.08.008

Respiratory Muscle Fatigue Workshop Group. (1990). Respiratory Muscle Fatigue. In *Critical Care Medicine* (Vol. 142, Issue 2). https://doi.org/10.1164/ajrccm/142.2.474

Road, J., Newman, S., Derenne, J. P., & Grassino, A. (1986). In vivo length-force relationship of canine diaphragm. *Journal of Applied Physiology*, *60*(1), 63–70. https://doi.org/10.1152/jappl.1986.60.1.63

Rodman, J. R., Henderson, K. S., Smith, C. A., & Dempsey, J. A. (2003). Cardiovascular effects of the respiratory muscle metaboreflexes in dogs: Rest and exercise. *Journal of Applied Physiology*, *95*(3), 1159–1169. https://doi.org/10.1152/japplphysiol.00258.2003

Rodriguez-Falces, J., & Place, N. (2018). Determinants, analysis and interpretation of the muscle compound action potential (M wave) in humans: implications for the study of muscle fatigue. *European Journal of Applied Physiology*, *118*(3), 501–521. https://doi.org/10.1007/s00421-017-3788-5

Rohrbach, M., Perret, C., Kayser, B., Boutellier, U., & Spengler, C. M. (2003). Task failure from inspiratory resistive loaded breathing: A role for inspiratory muscle fatigue? *European Journal of Applied Physiology*, *90*(3–4), 405–410. https://doi.org/10.1007/s00421-003-0871-x

Roman, M. A., Rossiter, H. B., & Casaburi, R. (2016). Exercise, ageing and the lung. *European Respiratory Journal*, *48*(5), 1471–1486. https://doi.org/10.1183/13993003.00347-2016

Romer, L. M., Mcconnell, A. K., & Jones, D. A. (2002). Effects of inspiratory muscle training on time-trial performance in trained cyclists. *Journal of Sports Sciences*, *20*(7), 547–590.

Romer, L. M., & Polkey, M. I. (2008). Exercise-induced respiratory muscle fatigue: implications for performance. *Journal of Applied Physiology*, *104*(3), 879–888. https://doi.org/10.1152/japplphysiol.01157.2007

Roussos, C., Fixley, M., Gross, D., & Macklem, P. T. (1979). Fatigue of inspiratory muscles and their synergic behavior. *Journal of Applied Physiology Respiratory Environmental and Exercise Physiology*, *46*(5), 897–904. https://doi.org/10.1152/jappl.1979.46.5.897

Roussos, C., & Macklem, P. T. (1977). Diaphragmatic fatigue in man. *Journal of Applied Physiology Respiratory Environmental and Exercise Physiology*, *43*(2), 189–197. https://doi.org/10.1152/jappl.1977.43.2.189

Sacco, P., McIntyre, D. B., & Jones, D. A. (1994). Effects of length and stimulation frequency of the human tibialis anterior muscle. *Journal of Applied Physiology*, *77*(3), 1148–1154. https://doi.org/10.1152/jappl.1994.77.3.1148

Sahn, S. A., Zwillich, C. W., Dick, N., McCullough, R. E., Lakshminarayan, S., & Weil, J. V. (1977). Variability of ventilatory responses to hypoxia and hypercapnia. *Journal of Applied Physiology Respiratory Environmental and Exercise Physiology*, *43*(6), 1019–1025. https://doi.org/10.1152/jappl.1977.43.6.1019

Sánchez, J., Medrano, G., Debesse, B., Riquet, M., & Derenne, J. P. (1985). Muscle fibre types in costal and crural diaphragm in normal men and in patients with moderate chronic respiratory disease. *Bulletin of European Respiratory Physiopathology*, *21*(4), 351–356.

Sandow, A. (1952). Excitation-contraction coupling in muscular response. *The Yale Journal of Biology and Medicine*, *25*(3), 176–201.

Santana, P. V., Prina, E., Albuquerque, A. L. P., Carvalho, C. R. R., & Caruso, P. (2016). Identifying decreased diaphragmatic mobility and diaphragm thickening in interstitial lung disease: The utility of ultrasound imaging. *Jornal Brasileiro de Pneumologia*, *42*(2), 88–94. https://doi.org/10.1590/S1806-37562015000000266

Scarlata, S., Mancini, D., Laudisio, A., Benigni, A., & Antonelli Incalzi, R. (2018). Reproducibility and clinical correlates of supine diaphragmatic motion measured by M-mode ultrasonography in healthy volunteers. *Respiration*, *96*(3), 259–266. https://doi.org/10.1159/000489229

Scatliff, J. H., & Morris, P. J. (2014). From röntgen to magnetic resonance imaging: the history of medical imaging. *North Carolina Medical Journal*, *75*(2), 111–113. https://doi.org/10.18043/ncm.75.2.111

Schweitzer, T. W., Fitzgerald, J. W., Bowden, J. A., & Lynne-Davies, P. (1979). Spectral analysis of human inspiratory diaphragmatic electromyograms. *Journal of Applied Physiology Respiratory Environmental and Exercise Physiology*, *46*(1), 152–165.

Scott, W., Stevens, J., & Binder-Macleod, S. A. (2001). Human skeletal muscle fiber type classifications. *Physical Therapy*, *81*(11), 1810–1816. https://doi.org/10.1093/ptj/81.11.1810

Seeley, R., VanPutte, C., Regan, J., & Russo, A. (2011). *Seeley's anatomy & physiology* (9th ed.). McGraw Hill Companies Inc.

Seven, Y. B., Mantilla, C. B., & Sieck, G. C. (2014). Recruitment of rat diaphragm motor units across motor behaviors with different levels of diaphragm activation. *Journal of Applied Physiology*, *117*(11), 1308–1316. https://doi.org/10.1152/japplphysiol.01395.2013

Sheel, A. W. (2002). Respiratory muscle training in healthy individuals: physiological rationale and implications for exercise performance. *Sports Medicine*, *32*(9), 567–581. https://doi.org/10.2165/00007256-200232090-00003

Sheel, A. W., Boushel, R., & Dempsey, J. A. (2018). Competition for blood flow distribution between respiratory and locomotor muscles: Implications for muscle fatigue. *Journal of Applied Physiology*, *125*(3), 820–831. https://doi.org/10.1152/japplphysiol.00189.2018

Sheng, Z., Sharma, N., & Kim, K. (2020). Quantitative assessment of changes in muscle contractility due to fatigue during NMES: an ultrasound imaging approach. *IEEE Transactions on Biomedical Engineering*, *67*(3), 832–841. https://doi.org/10.1109/TBME.2019.2921754

Shi, Z. H., Jonkman, A., de Vries, H., Jansen, D., Ottenheijm, C., Girbes, A., Spoelstra-de Man, A., Zhou, J. X., Brochard, L., & Heunks, L. (2019). Expiratory muscle dysfunction in critically ill patients: towards improved understanding. *Intensive Care Medicine*, *45*(8), 1061–1071. https://doi.org/10.1007/s00134-019-05664-4

Similowski, T., Fleury, B., Launois, S., Cathala, H. P., Bouche, P., & Derenne, J. P. (1989). Cervical magnetic stimulation: a new painless method for bilateral phrenic nerve stimulation in conscious humans. *Journal of Applied Physiology (Bethesda, Md. : 1985)*, *67*(4), 1311–1318. https://doi.org/10.1152/jappl.1989.67.4.1311 [doi]

Simon, P. M., Schwartzstein, R. M., Weiss, J. W., Fencl, V., Teghtsoonian, M., & Weinberger, S. E. (1990). Distinguishable types of dyspnea in patients with shortness of breath. *American Review of Respiratory Disease*, *142*(5), 1009–1014. https://doi.org/10.1164/ajrccm/142.5.1009

Sinderby, C., Beck, J., Spahija, J., Weinberg, J., & Grassino, A. (1998). Voluntary activation of the human diaphragm in health and disease. *Journal of Applied Physiology*, *85*(6), 2146–2158. https://doi.org/10.1152/jappl.1998.85.6.2146

Singh, B., Panizza, J. A., & Finucane, K. E. (2003). Breath-by-breath measurement of the volume displaced by diaphragm motion. *Journal of Applied Physiology*, *94*(3), 1084–1091. https://doi.org/10.1152/japplphysiol.00256.2002

Smith-Blair, N. (2002). Mechanisms of diaphragm fatigue. *AACN Clinical Issues*, *13*(2), 307–319. https://doi.org/10.1097/00044067-200205000-00014

Smith, J., & Bellemare, F. (1987). Effect of lung volume on in vivo contraction characteristics of the human diaphragm. *Journal of Applied Physiology*, *62*(5), 1893–1900. https://doi.org/10.1152/jappl.1987.62.5.1893

Soilemezi, E., Savvidou, S., Sotiriou, P., Smyrniotis, D., Tsagourias, M., & Matamis, D. (2020). Tissue doppler imaging of the diaphragm in healthy subjects and critically ill patients. *American Journal of Respiratory and Critical Care Medicine*, *202*(7), 1005–1012. https://doi.org/10.1164/rccm.201912-2341OC

Souza, H., Rocha, T., Pessoa, M., Rattes, C., Brandão, D., Fregonezi, G., Campos, S., Aliverti, A., & Dornelas, A. (2014). Effects of inspiratory muscle training in elderly women on respiratory muscle strength, diaphragm thickness and mobility. *Journals of Gerontology*, *69*(12), 1545–1553. https://doi.org/10.1093/gerona/glu182

Spengler, C. M., & Shea, S. A. (2001). Explained and unexplained variability of CO2 sensitivity in humans. *Advances in Experimental Medicine and Biology*, *499*, 483–488. https://doi.org/10.1007/978-1-4615-1375-9_78

Stell, I. M., Tompkins, S., Lovell, A. T., Goldstone, J. C., & Moxham, J. (1999). An in vivo comparison of a catheter mounted pressure transducer system with conventional balloon catheters. *European Respiratory Journal*, *13*(5), 1158–1163. https://doi.org/10.1034/j.1399-3003.1999.13e36.x

Stephenson, D. G., Lamb, G. D., Stephenson, G. M. M., & Fryer, M. W. (1995). Excitation-contraction coupling relevant to skeletal muscle. *Advanges in Experimental Medicine and Biology*, *384*, 45–56. https://doi.org/10.1007/978-1-4899-1016-5_4

Stocks, J., & Quanjer, P. H. (1995). Reference values for residual volume, functional residual capacity and total lung capacity: ATS Workshop on Lung Volume Measurements. Official statement of The European Respiratory Society. *European Respiratory Journal*, *8*(3), 492–506. https://doi.org/10.1183/09031936.95.08030492

Sundberg, C. W., & Fitts, R. H. (2019). Bioenergetic basis of skeletal muscle fatigue. *Current Opinion in Physiology*, *10*, 118–127. https://doi.org/10.1016/j.cophys.2019.05.004

Supinski, G. S., Clary, S. J., Bark, H., & Kelsen, S. G. (1987). Effect of inspiratory muscle fatigue on perception of effort during loaded breathing. *Journal of Applied Physiology*, *62*(1), 300–307. https://doi.org/10.1152/jappl.1987.62.1.300

Supinski, G. S., Levin, S., & Kelsen, S. G. (1986). Caffeine effect on respiratory muscle endurance and sense of effort during loaded breathing. *Journal of Applied Physiology*, *60*(6), 2040–2047. https://doi.org/10.1152/jappl.1986.60.6.2040

Tanter, M., & Fink, M. (2014). Ultrafast imaging in biomedical ultrasound. *IEEE Transactions on Ultrasonics, Ferroelectrics, and Frequency Control*, *61*(1), 102–119. https://doi.org/10.1109/TUFFC.2014.6689779

Teske, A. J., De Boeck, B. W. L., Melman, P. G., Sieswerda, G. T., Doevendans, P. A., & Cramer, M. J. M. (2007). Echocardiographic quantification of myocardial function using tissue deformation imaging, a guide to image acquisition and analysis using tissue Doppler and speckle tracking. *Cardiovascular Ultrasound*, *27*(5), 1–19. https://doi.org/10.1186/1476-7120-5-27

Testa, A., Soldati, G., Giannuzzi, R., Berardi, S., Portale, G., & Silveri, N. G. (2011). Ultrasound M-mode assessment of diaphragmatic kinetics by anterior transverse scanning in healthy subjects. *Ultrasound in Medicine & Biology*, *37*(1), 44–52. https://doi.org/10.1016/j.ultrasmedbio.2010.10.004

Tomczak, S. E., Guenette, J. A., Reid, W. D., McKenzie, D. C., & Sheel, A. W. (2011). Diaphragm fatigue after submaximal exercise with chest wall restriction. *Medicine and Science in Sports and Exercise*, *43*(3), 416–424.

https://doi.org/10.1249/MSS.0b013e3181ef5e67

Ueki, J., De Bruin, P. F., & Pride, N. B. (1995). In vivo assessment of diaphragm contraction by ultrasound in normal subjects. *Thorax*, *50*(11), 1157–1161. https://doi.org/10.1136/thx.50.11.1157

Umbrello, M., Formenti, P., Longhi, D., Galimberti, A., Piva, I., Pezzi, A., Mistraletti, G., Marini, J. J., & Iapichino, G. (2015). Diaphragm ultrasound as indicator of respiratory effort in critically ill patients undergoing assisted mechanical ventilation: a pilot clinical study. *Critical Care*, *19*(1), 161. https://doi.org/10.1186/s13054-015-0894-9

Validyne Engineering. (2020). *Very-low range differential pressure transducer variable reluctance*.

Van Lunteren, E., & Vafaie, H. (1993). Force potentiation in respiratory muscles: Comparison of diaphragm and sternohyoid. *American Journal of Physiology*, *264*(6 Pt 2), 1095–1100. https://doi.org/10.1152/ajpregu.1993.264.6.R1095

Verges, S., Bachasson, D., & Wuyam, B. (2010). Effect of acute hypoxia on respiratory muscle fatigue in healthy humans. *Respiratory Research*, *11*(1), 109. https://doi.org/10.1186/1465-9921-11-109

Verin, E., Delafosse, C., Straus, C., Morélot-Panzini, C., Avdeev, S., Derenne, J. P., & Similowski, T. (2001). Effects of muscle group recruitment on sniff transdiaphragmatic pressure and its components. *European Journal of Applied Physiology*, *85*(6), 593–598. https://doi.org/10.1007/s004210100469

Viasys Healthcare. (2004). *Oxycon Pro: technical report*. https://www.ntnu.edu/documents/221360533/221362168/oxypro.pdf/91b256f4-97d7-4408-8eec-53869132a03d

Vieira, A., Blazevich, A., Souza, N., Celes, R., Alex, S., Tufano, J. J., & Bottaro, M. (2018). Acute changes in muscle thickness and pennation angle in response to work-matched concentric and eccentric isokinetic exercise. *Applied Physiology, Nutrition and Metabolism*, *43*(10), 1069–1074. https://doi.org/doi:10.1139/apnm-2018-0055

Vivier, E., Dessap, A. M., Dimassi, S., Vargas, F., Lyazidi, A., Thille, A. W., & Brochard, L. (2012). Diaphragm ultrasonography to estimate the work of breathing during non-invasive

ventilation. *Intensive Care Medicine*, *38*(5), 796–803. https://doi.org/10.1007/s00134-012-2547-7

Vivier, E., Haudebourg, A. F., Le Corcoisier, P., Dessap, A. M., & Carteaux, G. (2020). Diagnostic accuracy of diaphragm ultrasound in detecting and characterizing patient-ventilator asynchronies during noninvasive ventilation. *Anesthesiology*, *132*(6), 1494–1502. https://doi.org/10.1097/ALN.0000000000003239

Volianitis, S., Mcconnell, A. K., Koutedakis, Y., Mcnaughton, L., Backx, K., & Jones, D. A. (2001). Inspiratory muscle training improves rowing performance. *Medicine & Science in Sports & Exercise*, *33*(5), 803–809. https://doi.org/10.1097/00005768-200105000-00020

Wait, L., Rochester, P., Juliette, L., Nahormek, P. A., William, T., Diaphragmatic, D. F. R., Wait, J. L., Nahormek, P. A., Yost, W. T., & Rochester, D. P. (1989). Diaphragmatic thickness-lung volume relationship in vivo. *Journal of Applied Physiology*, *67*(4), 1560–1568. https://doi.org/10.1152/jappl.1989.67.4.1560

Wallbridge, P., Parry, S. M., Das, S., Law, C., Hammerschlag, G., Irving, L., Hew, M., & Steinfort, D. (2018). Parasternal intercostal muscle ultrasound in chronic obstructive pulmonary disease correlates with spirometric severity. *Scientific Reports*, *8*(1), 1–9. https://doi.org/10.1038/s41598-018-33666-7

Wanger, J., Clausen, J. L., Coates, A., Pedersen, O. F., Brusasco, V., Burgos, F., Casaburi, R., Crapo, R., Enright, P., van der Grinten, C. P., Gustafsson, P., Hankinson, J., Jensen, R., Johnson, D., Macintyre, N., McKay, R., Miller, M. R., Navajas, D., Pellegrino, R., & Viegi, G. (2005). Standardisation of the measurement of lung volumes. *The European Respiratory Journal*, *26*(3), 511–522. https://doi.org/10.1183/09031936.05.00035005

Ward, M. E., Eidelman, D., Stubbing, D. G., Bellemare, F., & Macklem, P. T. (1988). Respiratory sensation and pattern of respiratory muscle activation during diaphragm fatigue. *Journal of Applied Physiology*, *65*(5), 2181–2189. https://doi.org/10.1152/jappl.1988.65.5.2181

Wasserman, K., Hansen, J. E., Sue, D. Y., Stringer, W. W., Sietsema, K. E., Sun, X., & Whipp, B. J. (2012). Principles of exercise testing and interpretation: including pathophysiology and clinical applications. In *Lippincott Williams & Wilkins* (Vol. 5). https://doi.org/10.1097/00024382-200014010-00017

Wasserman, K., & Whipp, B. J. (1975). Exercise physiology in health and disease. *American Review of Respiratory Disease*, *112*(2), 219–249. https://doi.org/10.1164/arrd.1975.112.2.219

Watsford, M. L., Murphy, A. J., & Pine, M. J. (2007). The effects of ageing on respiratory muscle function and performance in older adults. *Journal of Science and Medicine in Sport*, *10*(1), 36–44. https://doi.org/10.1016/j.jsams.2006.05.002

Wehrle, A., Waibel, S., Gollhofer, A., & Roecker, K. (2021). Power Output and Efficiency During Supine, Recumbent, and Upright Cycle Ergometry. *Frontiers in Sports and Active Living*, *3*(June), 1–9. https://doi.org/10.3389/fspor.2021.667564

Welch, J. F., Archiza, B., Guenette, J. A., West, C. R., & Sheel, A. W. (2018). Effect of diaphragm fatigue on subsequent exercise tolerance in healthy men and women. *Journal of Applied Physiology*, *125*(6), 1987–1996. https://doi.org/10.1152/japplphysiol.00630.2018

Westerblad, H., Allen, D. G., Bruton, J. D., Andrade, F. H., & Lännergren, J. (1998). Mechanisms underlying the reduction of isometric force in skeletal muscle fatigue. *Acta Physiologica Scandinavica*, *162*(3), 253–260. https://doi.org/10.1046/j.1365-201X.1998.0301f.x

Witte, R. S., Kim, K., Martin, B. J., & Donnell, M. O. (2006). Effect of fatigue on muscle elasticity in the human forearm using ultrasound strain imaging. *Annual International Conference of the IEEE Engineering in Medicine and Biology Society*, 4490–4493.

World Medical Association. (2013). World Medical Association Declaration of Helsinki: ethical principles for medical research involving human subjects. *Journal of the American Medical Association*, *310*(20), 2191–2194. https://doi.org/0.1001/jama.2013.281053

Wragg, S., Hamnegard, C., Kyroussis, D., Moxham, J., Green, M., Moran, J., Road, J., Kyroussis, D., Moran, J., Green, M., & Moxham, J. (1994). Potentiation of diaphragmatic twitch after voluntary contraction in normal subjects. *Thorax*, *49*(12), 1234–1237. https://doi.org/10.1136/thx.49.12.1234

Wylegala, J. A., Pendergast, D. R., Gosselin, L. E., Warkander, D. E., & Lundgren, C. E. G. (2007). Respiratory muscle training improves swimming endurance in divers. *European Journal of Applied Physiology*, *99*(4), 393–404. https://doi.org/10.1007/s00421-006-

0359-6

Yan, S., Lichros, I., Zakynthinos, S., & Macklem, P. T. (1993). Effect of diaphragmatic fatigue on control of respiratory muscles and ventilation during CO2 rebreathing. *Journal of Applied Physiology*, *75*(3), 1364–1370. https://doi.org/10.1152/jappl.1993.75.3.1364

Yan, S., Sliwinski, P., Gauthier, A. P., Lichros, I., Zakynthinos, S., & Macklem, P. T. (1993). Effect of global inspiratory muscle fatigue on ventilatory and respiratory muscle responses to CO2. *Journal of Applied Physiology*, *75*(3), 1371–1377. https://doi.org/10.1152/jappl.1993.75.3.1371

Ye, X., Xiao, H., Bai, W., Liang, Y., Chen, M., & Zhang, S. (2013). Two-dimensional strain ultrasound speckle tracking as a novel approach for the evaluation of right hemidiaphragmatic longitudinal deformation. *Experimental and Therapeutic Medicine*, *6*(2), 368–372. https://doi.org/10.3892/etm.2013.1133

Yu, H., Chakravorty, S., Song, W., & Ferenczi, M. A. (2016). Phosphorylation of the regulatory light chain of myosin in striated muscle: methodological perspectives. *European Biophysics Journal*, *45*(8), 779–805. https://doi.org/10.1007/s00249-016-1128-z

Zamparo, P., Cortesi, M., & Gatta, G. (2020). The energy cost of swimming and its determinants. *European Journal of Applied Physiology*, *120*(1), 41–66. https://doi.org/10.1007/s00421-019-04270-y

Zar, J. H. (2014). Comparing simple linear regression equations. In *Biostatistical Analysis* (5th ed., p. 387). Pearson Education Ltd.

Zierath, J. R., & Hawley, J. A. (2004). Skeletal muscle fiber type: influence on contractile and metabolic properties. *PLoS Biology*, *2*(10), e348. https://doi.org/10.1371/journal.pbio.0020348

Zin, W. A., & Milic-Emili, J. (2005). Esophageal pressure measurement. In Quatayba Hamid, J. Shannon, & J. Martin (Eds.), *Physiologic basis of respiratory disease* (pp. 639–647). BC Decker Inc.

Appendix 1

Ethical Approvals

College of Health and Life Sciences Research Ethics Committee (DLS)
Brunel University London
Kingston Lane
Uxbridge
UB8 3PH
United Kingdom

www.brunel.ac.uk

23 March 2018

LETTER OF APPROVAL

Applicant: Miss Camilla Rønn Illidi

Project Title: Validity and Reliability of Ultrasonography for the Objective Assessment of Diaphragm Function in Healthy Adults

Reference: 8404-MHR-Feb/2018- 11973-1

Dear Miss Camilla Rønn Illidi

The Research Ethics Committee has considered the above application recently submitted by you.

The Chair, acting under delegated authority has agreed that there is no objection on ethical grounds to the proposed study. Approval is given on the understanding that the conditions of approval set out below are followed:

- Please amend and state that the study is part of your PhD at Brunel University London and that it has been approved by the College of Health and Life Sciences Research Ethics Committee and the date.
- The agreed protocol must be followed. Any changes to the protocol will require prior approval from the Committee by way of an application for an amendment.

Please note that:

- Research Participant Information Sheets and (where relevant) flyers, posters, and consent forms should include a clear statement that research ethics approval has been obtained from the relevant Research Ethics Committee.
- The Research Participant Information Sheets should include a clear statement that queries should be directed, in the first instance, to the Supervisor (where relevant), or the researcher. Complaints, on the other hand, should be directed, in the first instance, to the Chair of the relevant Research Ethics Committee.
- Approval to proceed with the study is granted subject to receipt by the Committee of satisfactory responses to any conditions that may appear above, in addition to any subsequent changes to the protocol.
- The Research Ethics Committee reserves the right to sample and review documentation, including raw data, relevant to the study.
- You may not undertake any research activity if you are not a registered student of Brunel University or if you cease to become registered, including abeyance or temporary withdrawal. As a deregistered student you would not be insured to undertake research activity. Research activity includes the recruitment of participants, undertaking consent procedures and collection of data. Breach of this requirement constitutes research misconduct and is a disciplinary offence.

Professor Christina Victor

Chair

College of Health and Life Sciences Research Ethics Committee (DLS)
Brunel University London

College of Health and Life Sciences Research Ethics Committee (DLS)
Brunel University London
Kingston Lane
Uxbridge
UB8 3PH
United Kingdom

www.brunel.ac.uk

13 August 2018

LETTER OF APPROVAL

Applicant: Miss Camilla Rønn Illidi

Project Title: Validity and Reliability of Ultrasonography for the Objective Assessment of Diaphragm Function in Healthy Adults

Reference: 8404-A-Aug/2018- 13769-1

Dear Miss Camilla Rønn Illidi

The Research Ethics Committee has considered the above amendment application recently submitted by you.

The Chair, acting under delegated authority has agreed that there is no objection on ethical grounds to the proposed study. Approval is given on the understanding that the conditions of approval set out below are followed:

- The agreed protocol must be followed. Any changes to the protocol will require prior approval from the Committee by way of an application for an amendment.

Please note that:

- Research Participant Information Sheets and (where relevant) flyers, posters, and consent forms should include a clear statement that research ethics approval has been obtained from the relevant Research Ethics Committee.
- The Research Participant Information Sheets should include a clear statement that queries should be directed, in the first instance, to the Supervisor (where relevant), or the researcher. Complaints, on the other hand, should be directed, in the first instance, to the Chair of the relevant Research Ethics Committee.
- Approval to proceed with the study is granted subject to receipt by the Committee of satisfactory responses to any conditions that may appear above, in addition to any subsequent changes to the protocol.
- The Research Ethics Committee reserves the right to sample and review documentation, including raw data, relevant to the studyYou may not undertake any research activity if you are not a registered student of Brunel University or if you cease to become registered, including abeyance or temporary withdrawal. As a deregistered student you would not be insured to undertake research activity. Research activity includes the recruitment of participants, undertaking consent procedures and collection of data. Breach of this requirement constitutes research misconduct and is a disciplinary offence.

Professor Christina Victor

Chair

College of Health and Life Sciences Research Ethics Committee (DLS)
Brunel University London

College of Health and Life Sciences Research Ethics Committee (DLS)
Brunel University London
Kingston Lane
Uxbridge
UB8 3PH
United Kingdom

www.brunel.ac.uk

21 June 2019

LETTER OF APPROVAL

Applicant: Miss Camilla Illidi

Project Title: Pressure-flow specificity of diaphragm fatigue assessed using ultrasonography

Reference: 16371-MHR-Jun/2019- 19444-2

Dear Miss Camilla Illidi

The Research Ethics Committee has considered the above application recently submitted by you.

The Chair, acting under delegated authority has agreed that there is no objection on ethical grounds to the proposed study. Approval is given on the understanding that the conditions of approval set out below are followed:

- Advert/ PIS - The study has been reviewed by the College of Health and Life Sciences Research Ethics Committee – please amend.
- The agreed protocol must be followed. Any changes to the protocol will require prior approval from the Committee by way of an application for an amendment.

Please note that:

- Research Participant Information Sheets and (where relevant) flyers, posters, and consent forms should include a clear statement that research ethics approval has been obtained from the relevant Research Ethics Committee.
- The Research Participant Information Sheets should include a clear statement that queries should be directed, in the first instance, to the Supervisor (where relevant), or the researcher. Complaints, on the other hand, should be directed, in the first instance, to the Chair of the relevant Research Ethics Committee.
- The Research Ethics Committee reserves the right to sample and review documentation, including raw data, relevant to the study.
- You may not undertake any research activity if you are not a registered student of Brunel University or if you cease to become registered, including abeyance or temporary withdrawal. As a deregistered student you would not be insured to undertake research activity. Research activity includes the recruitment of participants, undertaking consent procedures and collection of data. Breach of this requirement constitutes research misconduct and is a disciplinary offence.

Professor Christina Victor

Chair of the College of Health and Life Sciences Research Ethics Committee (DLS)

Brunel University London

College of Health and Life Sciences Research Ethics Committee (DLS)
Brunel University London
Kingston Lane
Uxbridge
UB8 3PH
United Kingdom

www.brunel.ac.uk

25 July 2019

LETTER OF APPROVAL

Applicant: Miss Camilla Illidi

Project Title: Pressure-flow specificity of diaphragm fatigue assessed using ultrasonography

Reference: 16371-A-Jul/2019- 19984-1

Dear Miss Camilla Illidi

The Research Ethics Committee has considered the above application recently submitted by you.

The Chair, acting under delegated authority has agreed that there is no objection on ethical grounds to the proposed study. Approval is given on the understanding that the conditions of approval set out below are followed:

- As you have received funding from CHPER, you should mention this under who is organising and funding the research.
- You were asked to amend the following in your previous approval letter; 'Advert/ PIS - The study has been reviewed by the College of Health and Life Sciences Research Ethics Committee – please amend.' I can see you have changed the advert but you have not updated the PIS under the section 'who has reviewed the study' you have still got the Brunel university London research ethics committee.
- The agreed protocol must be followed. Any changes to the protocol will require prior approval from the Committee by way of an application for an amendment.

Please note that:

- Research Participant Information Sheets and (where relevant) flyers, posters, and consent forms should include a clear statement that research ethics approval has been obtained from the relevant Research Ethics Committee.
- The Research Participant Information Sheets should include a clear statement that queries should be directed, in the first instance, to the Supervisor (where relevant), or the researcher. Complaints, on the other hand, should be directed, in the first instance, to the Chair of the relevant Research Ethics Committee.
- The Research Ethics Committee reserves the right to sample and review documentation, including raw data, relevant to the study.
- You may not undertake any research activity if you are not a registered student of Brunel University or if you cease to become registered, including abeyance or temporary withdrawal. As a deregistered student you would not be insured to undertake research activity. Research activity includes the recruitment of participants, undertaking consent procedures and collection of data. Breach of this requirement constitutes research misconduct and is a disciplinary offence.

Professor Christina Victor

Chair of the College of Health and Life Sciences Research Ethics Committee (DLS)

Brunel University London

Appendix 2

Health Questionnaire and Consent Form

College of Health and Life Sciences
Department of Life Sciences

PRE-PARTICIPATION HEALTH CHECK QUESTIONNAIRE

Health and safety is of paramount importance. For this reason, we need to be aware of your current health status before you begin any testing procedures. The questions below are designed to identify whether you are able to participate now or should obtain medical advice before undertaking this investigation. Whilst every care will be taken to the best of the investigator's ability, an individual must know his/her limitations.

Subject name: …… DOB: …….. AGE……
Doctors Surgery Address: ……..
Emergency Contact Name & Number: ……

	YES	NO
1. Has your doctor ever diagnosed a heart condition or recommend only medically supervised exercise?	☐	☐
2. Do you suffer from chest pains, heart palpitations or tightness of the chest?	☐	☐
3. Do you have known high blood pressure? If yes, please give details (e.g. medication)	☐	☐
4. Do you have low blood pressure or often feel faint or have dizzy spells?	☐	☐
5. Do you have known hypercholesteremia?	☐	☐
6. Have you ever had any bone or joint problems, which could be aggravated by physical activity?	☐	☐
7. Do you suffer from diabetes? If yes, are you insulin dependent?	☐	☐
8. Do you suffer from any lung/chest problem? (e.g. asthma, bronchitis, emphysema)	☐	☐
9. Do you suffer from epilepsy? If yes, when was the last incident?	☐	☐
10. Do you have any history of infectious diseases (e.g. HIV, Heb B)	☐	☐
11. Are you taking any medication?	☐	☐
12. Have you had any injuries in the last year? (e.g. muscle strains, back problems)	☐	☐
13. Are you currently enrolled in any other studies?	☐	☐
14. Have you recently participated in a blood donation program?	☐	☐
15. Are you a smoker?	☐	☐
16. Do you exercise on a regular basis (at least 60 min a week)?	☐	☐

17. Describe your exercise routines (mode, frequency, intensity/speed, race times):

18. Provide detail of any other reasons that would affect your ability to take part in this experiment:

19. Do you have a known allergy for		
Latex?	☐	☐
Local anaesthesia?	☐	☐

If you feel at all unwell because of a temporary illness such as a cold or fever please inform the investigator. Please note if your health status changes so that you would subsequently answer YES to any of the above questions, please notify the investigator immediately.

College of Health and Life Sciences
Department of Life Sciences

I have read and fully understand this questionnaire. I confirm that to the best of my knowledge; the answers are correct and accurate. I know of no reasons why I should not participate in physical activity and this investigation and I understand I will be taking part at my own risk.

PARTICIPANT'S NAME AND SIGNATURE _____DATE:_____

INVESTIGATOR'S NAME AND SIGNATURE_____DATE:_____

CONSENT FORM

	YES	NO
1. Have you read the participant information sheet?	☐	☐
2. Have you read and completed the health questionnaire?	☐	☐
3. Have you had an opportunity to ask questions and discuss this study?	☐	☐
4. Have you received satisfactory answers to all your questions?	☐	☐
5. Who have you spoken to?	☐	
6. Do you understand that you will not be referred to by name in any report concerning the study?	☐	☐
7. Do you understand that you are free to withdraw from the study		
At any time?	☐	☐
Without having to give a reason for withdrawing?	☐	☐
8. Do you agree to take part in this study?	☐	☐

Signature of research participant:…….

Date: ……..

Name in capital letters: ……

Appendix 3

Example Participant Information Sheet

College of Health and Life Sciences
Department of Life Sciences

PARTICIPANT INFORMATION SHEET

Study title
Task-dependency of diaphragm fatigue assessed using ultrasonography

We invite you to take part in a research study. Before you decide whether to take part, we would like to tell you more about the study and what it would involve for you.

Why have I been invited to participate?
You have been invited to take part in this research study as you are a young, physically active, healthy volunteer. Inclusion criteria include: non-smoker; age 18-40 years; body mass index 18-39 kg/m^2; no history or current symptoms of respiratory, cardiovascular, metabolic or neuromuscular disorders; and normal lung function (to be assessed during a screening visit). In total, we will invite 16 volunteers to participate.

What is the purpose of the study?
The purpose of this study is to assess the task-dependency of inspiratory loading on the contractile properties of human diaphragm muscle. The diaphragm is the principle muscle of breathing. It is a thin, dome-shaped muscle that separates the lungs and chest from the abdomen. When the diaphragm muscle contracts, it descends and the lungs are inflated with air. Like other skeletal muscles, the diaphragm muscle can also fatigue when the load exceeds the muscle's capacity. In the present study, we will induce diaphragm muscle fatigue using protocols characterised by high-force or high-velocity. The high-force protocol involves maximal voluntary efforts against a high external load. The high-velocity protocol involves maximal voluntary ventilation with minimal external load. The specific objective is to evaluate the influence of these different loading tasks on the dynamic function of diaphragm muscle. Diaphragm function will be assessed on the basis of traditional measures (e.g., respiratory pressures in response to nerve stimulation) in combination with novel ultrasound-derived measures (e.g., diaphragm movement during volitional and non-volitional manoeuvres).

Do I have to take part?
Your decision to participate in this research study is entirely voluntary. You may withdraw from the study at any time, without reason, without subsequent penalty or prejudice, without affecting your future care, and without affecting your university grades (if applicable). You will be notified of any new findings or changes in the testing protocol that may affect your willingness to continue.

What will happen to me if I take part?
If you decide to participate, you will visit the laboratory on three separate days. The first visit will last approximately 1.5 hours. The two remaining visits will last up to 3 hours. At the initial visit, you will have an opportunity to ask any questions you might have about the project. In addition, you will complete a health questionnaire and sign an informed consent form. Next, we will measure your height, weight, chest dimensions, diaphragm thickness and lung function. To facilitate measurement, we ask that you wear light clothing (e.g., shorts/leggings and t-shirt) during all visits. Finally, we will familiarise you with the remaining procedures. At the second and third visits, you will perform (in random order) a diaphragm fatigue protocol consisting of inspiratory resistive loading (high-force) or maximal voluntary ventilation (high-velocity). A rebreathe test that uses carbon-dioxide as a respiratory stimulant will be performed 15 min before and at 15 and 45 min after each of the fatigue protocols. Traditional nerve-stimulation techniques will be performed immediately before and at 10 and 40 min after each protocol. Neuromuscular responses to carbon-dioxide and nerve-stimulation will be assessed using a catheter positioned in your food pipe (oesophagus). Contractile properties of the diaphragm will be assessed non-invasively using ultrasound.

Before the Visit 2 and Visit 3, you will need to refrain from strenuous exercise and alcohol for at least 24 h, caffeine for 12 h, and eating for 3 h in order to reduce the likelihood of external factors affecting your results.

What do I have to do?

Screening and familiarisation visit (Visit 1):

- Participant characteristics: Height, weight and chest dimensions will be assessed using standard "anthropometric" techniques. Diaphragm thickness will be assessed using ultrasound, which involves placing an ultrasound transducer on the right side of your ribcage. The transducer sends ultrasound waves into the body and receives the echoes produced by the waves when it is placed on or over the body part being imaged. There is no ionizing radiation exposure associated with ultrasound imaging.

- Lung function: While wearing a nose-clip, you will perform the following manoeuvres. First, you will sit in an airtight box for one minute (to allow the temperature inside the box to adjust) then breathe normally into a mouthpiece for a further minute. A shutter will then close transiently against the mouthpiece, and you will be instructed to breathe normally against the shutter. Once the shutter opens, you will perform a slow full inhalation followed by a slow full exhalation. Three repeatable manoeuvres will be completed. You will remain in the box for no longer than 10 minutes at a time. Next, you will exhale as forcefully and rapidly as possible after a maximal inhalation; this manoeuvre will be repeated 3 to 8 times, with 30 seconds of recovery between each effort. You will then be asked to ventilate hard and fast for 12 seconds; this manoeuvre will be performed twice, with 5 minutes between efforts. Finally, you will perform maximal inspiratory and expiratory efforts against a closed airway for the determination of maximum inspiratory and expiratory mouth pressures. Each manoeuvre will be repeated 3 to 8 times, with 30 seconds of recovery between efforts.

Experimental visits (Visit 2 and Visit 3):

- Neuromechanical measurements: you will be instrumented with an oesophageal catheter for the determination of respiratory pressures and electrical activation of the diaphragm muscle. The oesophageal catheter is a thin, flexible silicone tube with integrated transducers to measure pressures and pairs of electrodes to measure electrical activity. The catheter will be passed through one nostril and swallowed into the stomach. To facilitate placement of the catheter, we will apply a small amount of local anaesthetic numbing gel (less than 1 millilitre of 2% lidocaine hydrochloride; trade name: Instillagel Sterile Gel) to the nostril. To verify the catheter is in the correct position, you will produce a series of graded inspiratory and expiratory efforts. When the catheter is satisfactorily positioned, it will be securely taped at the nose.

- Nerve stimulation: two magnetic coils will be positioned on each side of your neck. The magnetic coils are insulated, twisted copper wires in the shape of a figure-of-eight. When triggered, a magnetic field is created in the coil. This magnetic field, when placed over a nerve, generates a muscle contraction. The area of stimulation that evokes the greatest diaphragm muscle response will be located, marked with a water-soluble pen, and used for all subsequent stimulations. A series of single stimulations will be obtained at different percentages of the stimulator's maximum power output. All subsequent twitches will be performed at 100% of the stimulator's maximum power output. Approximately 5 single stimulations will be delivered at the end of a normal expiration with the mouth closed.

- Carbon dioxide re-breathe test: while adopting a reclined position, you will be fitted with a mouthpiece and nose-clip before taking five to six deep breaths from a bag containing a certified gas mixture (95% oxygen, 5% carbon dioxide). You will then relax and breathe on an "as-needed" basis. Re-breathing will continue until: 1) a specific level of carbon dioxide is detected in the air you exhale, 2) you feel that you cannot continue, 3) re-breathing lasts longer than 15 minutes (normally 4 to 6 minutes), or 4) the re-breathe bag is deflated. During rest, test and recovery periods we will monitor your cardiorespiratory and perceptual responses. Briefly, ventilatory parameters will be assessed with a gas-analysis system connected to the mouthpiece. Heart rate will be measured using a chest strap. Arterial oxygen concentration will be estimated using an earlobe sensor. You will also be asked to rate your intensity of breathing using a standard rating scale. Respiratory pressures will be measured throughout the test using the catheter described above. Diaphragm movement will be assessed every minute using a commercially available ultrasound system and transducer. The transducer will be covered in gel prior to measurement and will be held on the right side of your body, either below or directly over the lower ribs.

- Inspiratory resistive loading: while seated upright, you will be fitted with a mouthpiece and nose-clip. Then, you will breathe normally from room air without added resistance. When the test

starts, you will feel a resistance when breathing in (but no resistance when breathing out). During the test you will be encouraged to perform maximal inspiratory efforts against the resistance for 3 bouts, each lasting 5 minutes and separated by 10 min of rest.

- Maximal voluntary ventilation: while seated upright, you will be fitted with a mouthpiece and nose-clip. Then, you will breathe normally from room air without any resistance. When the test starts, you will be asked to breathe as hard and fast as you can for 2 minutes.

What are the benefits of taking part?
You will be taking part in novel research aimed at increasing our understanding of how the respiratory muscles function at rest and in response to fatigue. Upon request, we will provide an individualised report of your lung function data and a copy of any publications that stem from the research. In addition, you will have an opportunity to experience first-hand how scientific research is conducted; if you are a student, this might be helpful for your wider understanding of the scientific process. Upon completion of the full study (three visits to the laboratory) you will be compensated for your time and effort with £75 Amazon vouchers.

What are the possible disadvantages and risks of taking part?
We will perform only standardised procedures. Thus, there are few disadvantages and risks of taking part in this study. However, some side effects may occur during the research:

- Lung function testing: to safeguard against infection, you will be issued with a new disposable filter at each visit and equipment will be washed, disinfected and sterilised in line with laboratory and manufacturer guidelines. There is a small risk of injury from falling as a result of fainting during maximal breathing manoeuvres. This is a rare occurrence, but to protect you from any harm we will ensure that all lung function tests are conducted in a seated position.

- Catheter placement: during placement and removal of the oesophageal catheter there might be some mild irritation or soreness in the nostrils and upper airway, and you may experience a gag reflex when swallowing the catheter. Both sensations should disappear once the catheter is in position. Before swallowing the catheter, a small amount of local anaesthetic numbing gel (less than 1 millilitre of 2% lidocaine hydrochloride; Instillagel Sterile Gel) will be applied to one nostril in order to minimise any irritation. Adverse effects of using Instillagel are extremely rare, but if you are allergic or hypersensitive to local anaesthetics then you will not be allowed to participate.

- Nerve stimulation: diaphragm contraction induced by magnetic stimulation is often perceived as a mild and non-disturbing hiccup. Compared to other methods of inducing involuntary contraction of the diaphragm (e.g., needle electrodes or electrical stimulation), magnetic stimulation is well tolerated and painless, with only mild discomfort.

- Carbon dioxide re-breathing: this test is considered low-risk, but may cause some discomfort and anxiety as ventilation increases. These are normal responses and you will be able to terminate the test when the respiratory response becomes intolerable.

- Ultrasound assessment: ultrasound is painless, and the waves produced by the transducer are considered safe by the British Medical Ultrasound Society. The ultrasound transducer needs to be placed directly below or over your lower ribs. This particular skin surface area will need to be free from clothing. If you are uncomfortable performing the ultrasound examination bare-chested, then the examination can be completed with a t-shirt folded-up immediately under the chest. Due to the nature of the technique, the person performing the ultrasound scans (Ms Camilla Illidi) will be inclined to touch the skin surface area around the ultrasound transducer to stabilise the transducer position during the examination. The physical contact will be kept to a minimum, and you are encouraged to notify the investigator in the event of any uncomfortableness.

Inspiratory resistive loaded and maximal voluntary ventilation: these tests are considered low-risk, but may cause some discomfort as the tests progress. These are normal responses and you will be able to terminate the test when the respiratory responses become intolerable. Maximal voluntary ventilation can cause you to feel faint. To prevent this from happening, we will monitor your expired carbon dioxide levels and introduce additional carbon dioxide into the breathing circuit if needed. In

addition, you may experience mild levels of “delayed-onset muscle soreness” (DOMS) of the ribcage muscles. DOMS is a normal response to unfamiliar "exercise" that usually disappears after a few days. To minimise any discomfort, we will schedule the two experimental visits approximately one week apart.

What if something goes wrong?
The investigator conducting the experiment is qualified in first aid, and an individual with immediate life support training will be onsite at all times. In addition, an emergency name and contact telephone number must be provided during the initial visit. In case of a problem or complaint, contact details for the investigators and the Research Ethics Committee can be found at the bottom of this document.

Will my taking part in this study be kept confidential?
No personal information will be used or referred to in the study. Instead, you will be issued with an anonymous identification number. All data will be stored securely in an on-campus, locked filing cabinet and computers, all of which are password protected. The data will be saved for a maximum of 10 years at Brunel University London, and will not be released without written permission from yourself or unless required by law.

What will happen to the results of the research study?
The researchers hope to publish data collected from this study in scientific journal articles and/or present the research findings at scientific conferences. However, your personal information will remain confidential and we will always refer to you using an anonymous identification number.

Who is organising and funding the research?
The research will form part of Ms Camilla Illidi’s PhD thesis. The research supervisors are Dr Lee Romer (1st Supervisor) and Dr Sian MacRae (2nd Supervisor). The research is funded by the College of Health and Life Sciences, Brunel University London.

What are the indemnity arrangements?
Brunel University London holds insurance policies which apply to this study. If you can demonstrate that you experienced harm as a result of your participation in this study, you may be able to claim compensation. Please contact Prof Peter Hobson, the Chair of the University Research Ethics committee (Peter.hobson@brunel.ac.uk) if you would like further information about the insurance arrangements which apply to this study.

Who has reviewed the study?
This study has been reviewed, signed and approved by the Brunel University London Research Ethics Committee.

Passage on the University’s commitment to the UK Concordat on Research Integrity
Brunel University London is committed to compliance with the Universities UK Research Integrity Concordat. You are entitled to expect the highest level of integrity from our researchers during the course of their research.

Contact for further information and complaints
For general information
Ms Camilla Illidi (PhD research student): camilla.illidi@brunel.ac.uk
Dr Lee Romer (1st Supervisor): lee.romer@brunel.ac.uk

For complaints and questions about the conduct of the research
Professor Christina Victor, Chair College of Health and Life Sciences Research Ethics Committee: christina.victor@brunel.ac.uk